ISAS - INTERNATIONAL SCHOOL
FOR ADVANCED STUDIES

Structure-Function Analysis of Cyclic Nucleotide-Gated Channels

Thesis submitted for the degree of "Doctor Philosophiae"

CANDIDATE
Katia Gamel

SUPERVISOR
Prof. Vincent Torre

SISSA - SCUOLA
INTERNAZIONALE
SUPERIORE
DI STUDI AVANZATI
TRIESTE
Via Beirut 2-4

TRIESTE

To my grand-mother Irma Gamel (1921-1997)

Declaration

The work described in this dissertation was carried out at the International School for Advanced Studies, Trieste, between December 1996 and June 1999. All work reported, with the exceptions listed below, arise solely from my own experiments and this work has not been submitted in whole or in part to any other University.

The electrophysiological part regarding the functional analysis of the cysteine mutants as well as the measurement of their accessibility (Sections III.A.1. and III.A.2.) were carried out in collaboration with Andrea Becchetti.

Katia Gamel
August 1999

Acknowledgements

I am particularly grateful to my colleague Andrea Becchetti, for his helpfulness and for all the work he has done and to Pr. Vincent Torre, for all he taught me in electrophysiology.

I would also like to address many thanks to Dr. Anna Rosati, for her very precious help and advice. Thanks also to Gabriella Rossi, Mr. Becciani, Laura Giovanelli, Dr. Andrew Bradbury, Pr. Roberto Marzari, Jessica Franzot, Giada Pastore, Leonardo Guidoni, Marco Punta, Alessandro Laio and Paola Roncaglia : all these persons gave me either precious support or technical help.

This thesis is also the fruit of a constant interaction with my husband Frédéric Didelon, who supported me during all this work with encouragements and precious advice. Special thanks to him, to all the members of my family and to my friends.

Table of Contents

ABBREVIATIONS USED IN THE TEXT

CNG=cyclic nucleotide-gated
LG=ligand-gated
VG=voltage-gated
eag=ether-à-gogo
BRET=bovine retinal rod
cyto=C-terminal part of BRET CNG channel
CNS=central nervous system
cGMP=cyclic 3', 5'-guanosine monophosphate
cAMP=cyclic 3',5'-adenosine monophosphate
GDP=3', 5'-guanosine diphosphate
GTP=3', 5'-guanosine triphosphate
GMP=3', 5'-guanosine monophosphate
ATP=adenosine triphosphate
dNTP=desoxyribonucleotide triphosphate
PDE=phosphodiesterase
IRBP=interphotoreceptor retinol-binding protein
RPE=retinal pigment epithelium
IP3=inositol 1, 4, 5-triphosphate
PKA=protein kinase A
PLC=phospholipase C
DAG=diacylglycerol
GARP=glutamic-acid-rich protein
CAP=catabolite activator protein
CaM1 and CaM2=Ca^{2+}-calmodulin binding sites 1 and 2
PIP_2=phosphatidylinositol-4, 5-biphosphate
cDNA=complementary DNA
SCAM=substituted-cysteine accessibility method
PCR=polymerase chain reaction
PAGE=polyacrylamide gel electrophoresis
MTS=methane thiosulfonate
MTSEA=2-aminoethylmethane thiosulfonate
MTSET=2-trimethylammonioethylmethane thiosulfonate
CO=carbon monoxide
NO=nitric oxide
TE=Tris-EDTA=tris-ethylenediamine tetraacetate
DEPC=diethyl pyrocarbonate
HEPES=(N-2-hydroxyethyl)piperazine-N'-(2-ethanesulphonic acid)
TMAOH=tetramethylammonium hydroxide
SDS=sodium dodecylsulphate
IPTG=isopropyl-β-D-thiogalactoside
DTT=dithiotreithol

NP40=non ionic polyglycol ether type 40
BOG=octyl-βD-glucopyranoside
PMSF=phenylmethylsulfonylfluoride
PEG=polyethyleneglycol
HRP=horseradish peroxidase
BSA=bovine serumalbumine
PCM=pulse code modulation
VCR=video cassette recorder
DAT=digital audio tape
SEM=standard error of the mean
Vrev=reversal potential
Po=open probability
tKdc=transient K^+-dependent current
NMR=nuclear magnetic resonance
EPR=electron paramagnetic resonance
MDM=molecular dynamics and modelling

INTRODUCTION

Recently, significant progress has been made in the field of protein structure. Using a combination of different powerful techniques of molecular biology, physiology, biophysics and computer science, major findings have been successfully achieved in the resolution of protein structure. Such important discoveries are the basis necessary to understand functional properties of proteins. Hence, the study of the relationship linking structure and function of particular protein domains or protein molecules such as ion channels represent a major scientific area in constant expansion. An important finding of structural biology was achieved last year with the successful crystallisation of an ion channel, the KcsA potassium channel (Doyle *et al.*, 1998). The structural description of this ion channel by X-ray analysis represents a basis for the resolution of functional features of the superfamily of voltage-gated (VG) channels. The scientific interest in ion channels comes from the fundamental role played by these membrane proteins involved in principal cellular properties such as cell to cell communication, sensory and signal transduction and information processing in the nervous system. These basic features are usually mediated by transient changes in ion conductance. This process occurs through the channel pore in response to either electrical or chemical signals. Ion channels mediating cellular communication using electrical signals, i.e. voltage changes, are called VG channels, whereas the channels involved in cellular communication via chemical signals are termed ligand-gated (LG) channels. A direct consequence of the fundamental role played by ion channels is that many biological disorders are associated with defects in their structure. Hence, many diseases such as cystic fibrosis, cardiac arrhythmia, long Q-T syndrome, are due to defectuous ion channels. Therefore, understanding the relationship between ion channels structure and function represents a major scientific challenge. The first step in the study of ion channels is to obtain the primary sequence of the protein. Indeed, the amino acid sequence is characteristic of each protein and represents a fundamental key for the comprehension of the functional links between different proteins then classified in distinct families. Moreover, many genetic disorders such as the ones mentioned above were shown to be due to changes in the amino acids sequence of ion channels. Thus, the correct determination of the primary structure of channels together with the interpretation of the functional significance of particular motifs or residues, are of high interest for basic research as well as for clinical applications. The second step in the study of ion channels consists in preliminary approaches useful to draw conclusions regarding their secondary and tertiary organisation. Many techniques of molecular

biology and biotechnology (site-directed mutagenesis, antibody mapping) as well as physiology (pharmacology, electrophysiology) are useful tools in that sense. The final step in the study of ion channels consists in the resolution of their tridimensional structure. These tertiary and quaternary levels in the structural organisation of ion channels can be solved by a variety of spectroscopic techniques such as Nuclear Magnetic Resonance (NMR) and X-ray diffraction and also by techniques providing structural information at a lower resolution such as Electron Paramagnetic Resonance (EPR) and Molecular Dynamics and Modelling (MDM) simulations. The bi- and tri-dimensional structures of ion channels are of primary interest for applied research. Indeed, information drawn from those studies are for example at the basis of drug design and therapeutic applications.

In this thesis, techniques of molecular biology and biotechnology were combined with electrophysiology in the aim of understanding the relationships between structure and function of cyclic nucleotide-gated (CNG) channels. These channels play a fundamental role in visual and olfactory sensory transduction. The CNG channel studied in this thesis is present in the rod photoreceptors which are sensory cells localised in the retina. Its gating is mainly regulated by the binding of its ligand, the guanosine 3', 5'-cyclic monophosphate (cGMP) in function of light intensity. A complete pathway involving ion permeation through this particular channel is then at the origin of the mechanism of phototransduction which consists in the conversion of a physical stimulus into electrical and chemical signals.

Two major findings have been obtained during my thesis :

1 - the structure of the pore of CNG channels is homologous to that of usual K^+ channels.

2 – Na^+ and K^+ do not permeate in the same way in the pore of CNG channels.

These results are interesting because the model of the structure of the CNG channel pore proposed here is in contradiction with a previous one (Sun *et al.*, 1996) but resembles the structural organisation of the KcsA channel pore. Our finding is in accordance with the fact that CNG channels belong to the superfamily of VG channels. Therefore, some structural homologies can be expected in particular in domains which are functionally fundamental not only at the level of the primary sequence but also at higher levels of organisation. The fact that Na^+ and K^+ seem to permeate in a different and complex way is also a novelty in the knowledge of CNG channels. Usually, CNG channels are thought to be non selective channels, i.e. channels which do not discriminate significantly the nature of ions and thus are able to be permeant to many different ions. Concerning Na^+ and K^+, previous interpretations of the values

obtained from the reversal potentials of these two ions were in accordance with similar mechanisms of permeation. The comprehension of the mechanisms of permeation of these two cations in particular is of significant importance because they are both physiologically involved in the mechanisms of sensory transduction. The results described in this thesis suggest a complex interaction of these two fundamental ions in the pore of CNG channels which is at the origin of altered gating properties.

This thesis is organised in five major chapters. Chapter I is an introduction to the field of CNG channels presenting : a brief history of the major scientific findings regarding these channels, a description of their physiological role in sensory transduction, a detailed presentation of their molecular cloning and structural organisation, and finally a complete picture of their functional features. Chapter II describes the material and the methods used in the experiments conducted during this thesis. Chapter III describes the results obtained and is divided in two major sections. The first one concerns the study of the relationship between structure and function of the channel pore. It is dedicated to a complete substituted-cysteine accessibility method (SCAM) applied to the CNG channel pore. To this aim, residues forming the pore region of the cGMP-gated channel from bovine retinal (BRET) were replaced in turn by cysteines. The properties of the cysteine mutants were analysed and their accessibility to thiol-specific reagents were subsequently tested. The measure of cysteine accessibility constitutes a powerful tool for assessing the position of the residues replaced by this particular amino acid in the channel pore. Then, ionic permeation and in particular Na^+ and K^+ permeation through CNG channels is analysed. Site-directed mutagenesis combined to patch-clamp techniques of electrophysiology allowed to identify a particular portion of the channel pore which is involved in ionic permeation as well as gating properties in CNG channels. In addition, the results of this study are in accordance with the model of the pore obtained by SCAM. The second section of the results describes a protocol for cloning, expression and purification of the C-terminal cytoplasmic domain of the CNG channel from BRET which contains the ligand binding-site for CNG channels activation. Such a binding domain for cyclic nucleotides is found in different proteins such as the *Escherichia coli* catabolite activator protein (CAP) and the regulatory subunits of cAMP-dependent or cGMP-dependent protein kinases. The resolution of the structural organisation of this ligand binding domain is fundamental for the comprehension of the coupling of cyclic-nucleotide binding to channel gating. Considering that the tridimensional structure of the CAP is already available, the resolution of this structure for CNG channels can represent a mean of comparison of two apparently different functional processes. This last part of the thesis represents a preliminary study in the aim of crystallisation. Chapter IV discusses the

results obtained. In particular a new model for the structure of the pore of CNG channels is described and compared to the structural organisation of VG K^+ channels. Then a new concept of ionic permeation and gating in CNG channels is proposed underlining the role played by a particular motif consisting in three successive prolines characteristic of CNG channels. The thesis finishes with chapter V which draws conclusions from the work achieved and proposes some future scientific prospects that may be envisaged after the results obtained in this thesis.

I. BACKGROUND

I.A. BRIEF HISTORY

The history of CNG channels is relatively recent and started with the discovery in the mid-1980s that phototransduction in retinal rod photoreceptors consists in a cation conductance directly activated by intracellular cGMP (Fesenko *et al.*, 1985). Until that time, it was generally thought that cyclic-nucleotides had only indirect effects on ion channels by acting on cyclic-nucleotide dependent protein kinases which in turn modulated channels functions (for review see Levitan, 1985, 1994). The finding that the channel involved in phototransduction was directly activated by cGMP was further confirmed by the discovery of similar channels involved in cone photoreceptor transduction (Cobbs *et al.*, 1985; Haynes and Yau, 1985) and in olfactory transduction (Nakamura and Gold, 1987). The physiological findings were then confirmed when, using the powerful tools provided by molecular biology, Kaupp *et al.* (1989) cloned the first cGMP-gated channel from a complementary DNA (cDNA) library from bovine retina. Similar channels were then cloned from olfactory epithelium (Dhallan *et al.*, 1990; Ludwig *et al.*, 1990; Goulding *et al.*, 1992), from cone photoreceptors (Bönigk *et al.*, 1993) and also from tissues different from retina or olfactory epithelium such as aorta (Biel *et al.*, 1993), kidney (Biel *et al.*, 1994), testis (Weyand, 1994), keratinocytes (Oda *et al.*, 1997). Widespread expression of these channels throughout the body were also described, for example in heart and kidney (Ahmad *et al.* 1990), in the central nervous system (CNS) (Leinders-Zufall *et al.* 1995; Bradley *et al.* 1997) but also in molluscan neurons (Sudlow, 1993) or more recently in the lizard parietal eye (Finn *et al.*, 1997), suggesting that the family of CNG channels is likely to expand further with future research work. In addition, clones for a separate β-subunit have been isolated from both the rod (Chen *et al.*, 1993) and the olfactory (Bradley *et al.*, 1994; Liman and Buck, 1994) CNG channels. These β subunits do not lead to functional channels but when coexpressed together with the corresponding α-subunit they bear features reminiscent from those of the native channel suggesting that CNG channels are heteromultimers of both the α and β subunits. One might also include in this family some channels which are modulated by cyclic-nucleotides such as the renal cGMP-modulated channel (Light *et al.*, 1988), the cardiac cyclic nucleotide-modulated pacemaker channels (DiFrancesco, 1993; Ludwig *et al.*, 1999), the fruit-fly *ether-à-gogo* K^+ channel (Kaplan and Trout, 1969). In this thesis, the different aspects regarding these channels will not be developed.

I.B. ROLE OF CNG CHANNELS

I.B.1. PHOTOTRANSDUCTION

I.B.1.1. FUNCTIONAL ORGANISATION OF PHOTORECEPTORS

The electrical signal generated by the absorption of light originates in rods and cones photoreceptor cells. These cells are organised in two principal parts : the outer segment and the inner segment. The outer segment is the site where the phototransduction takes place. Its structure consists in a stack of a series of membranous disks containing the visual pigment rhodopsin; in a rod cell, the discs are enclosed by the surface membrane whereas they consists in infoldings of the surface membrane in a cone (Fig. 1a). A rhodopsin molecule is made of a chromophore, the retinal, and a protein component, the opsin. The outer segment also houses the cGMP-gated channels and the Na^+/Ca^{2+} exchangers. The inner segment contains the nucleus as well as mitochondria and the endoplasmic reticulum. In addition to the cellular organelles, the inner segment includes Na^+/K^+ pumps in its membrane. The photoreceptor cells end with the synaptic terminals which are connected to bipolar and horizontal cells. The synaptic endings houses glutamate containing vesicles. Although it was usually thought that cGMP-gated channels were exclusively present in the photoreceptor cells outer segment, it is now admitted that they are also found in the inner segment as well as in the terminals (Watanabe and Matthews, 1988, Rieke and Schwartz, 1994).

I.B.1.2. THE MECHANISM OF PHOTOTRANSDUCTION

In darkness, the cGMP-gated channels in the outer segment are open and allow a steady "dark-current" to enter the photoreceptor cells (Hagins *et al.*, 1970; Baylor *et al.*, 1979): Ca^{2+} and Na^+ ions are entering the cells through the cGMP-gated channels and Ca^{2+} ions are leaving the outer segment via the Na^+/Ca^{2+} exchangers. As a consequence, intracellular Ca^{2+} concentration in darkness is around 550 nM (Gray-Keller and Detwiler, 1994). The cell in dark is kept slightly depolarised with a membrane potential of -40 mV and glutamate is continuously released from the synaptic endings. The absorption of a photon by a rhodopsin molecule causes the conversion of the retinal chromophore from its 11-*cis* stereoisomer to its all-*trans* form (Yoshizawa and Wald, 1963, Baylor, 1996). The opsin component of the rhodopsin is subsequently converted to metharhodopsin II (Emeis, 1982). This form of

phosphorylated rhodopsin converts the GDP which is bound to the α subunit of a G protein called transducin into GTP. In parallel, metharhodopsin II binds to arrestin, a protein which competitively inhibits the binding of transducin to rhodopsin in order to let the transducin free to bind GTP. The GDP -> GTP conversion leads to the transfer of the GTP-α to one of the inhibitory γ subunit of the phosphodiesterase (PDE), an enzyme which is then able to hydrolyse cGMP into GMP. This enzymatic reaction is at the origin of the closure of the cGMP-gated channels and thus causes a decrease in the intracellular Ca^{2+} concentration (Yau and Nakatani, 1984). In saturating light, intracellular Ca^{2+} concentration declines to a minimum value of about 50 nM (Gray-Keller and Detwiler, 1994). The membrane is hyperpolarized and the rate of glutamate release is reduced (Fig. 1b). In order for a bleached rhodopsin molecule to be able to absorb an eventual other photon, the response to light has to terminate and this involves several steps. The majority of the metarhodopsin II is first converted to metarhodopsin III and the chromophore part of the rhodopsin molecule separates from the opsin component and is converted into retinol. The arrestin which was bound to the metarhodopsin II is removed as well as the phosphate groups. The chromophore is also regenerated. It is transported by an interphotoreceptor retinol-binding protein (IRBP) to the retinal pigment epithelium (RPE) where the retinol after various enzymatic steps is finally converted into 11-*cis* retinal. The chromophore is transported back to the photoreceptor where it associates with the dephosphorylated form of opsin to give the functional rhodopsin (Fig. 1c). The transducin molecule regenerates also thanks to an endogenous GTPase activity of the α subunit which subsequently permits the reunion of the α subunit to the βγ complex. Without the GTP-α transducin the PDE inactivates and the guanylate cyclase can transform GMP in cGMP and restore the cGMP concentration present in the dark, before the light-triggered cGMP cascade (see Yau and Baylor, 1989; Fain et al, 1996). Recently, glutamic-acid-rich proteins (GARP) which exist as two soluble forms (GARP1 and GARP2) and as a cytoplasmic domain of the rod CNG channel β subunit were shown to interact with the cGMP signalling pathway. GARP2 was shown to potently inhibit PDE (Körschen *et al.*, 1999).

To fulfil their function, the photoreceptor cells have to be able to register small changes in light intensity. In this aim it is important for vision to prevent the closure of all cGMP-gated channels when moderate changes of the background light occur. This role is played by Ca^{2+} ions which are involved in a fairly complex mechanism of feedback (Koutalos and Yau, 1996; Baylor, 1996). First guanylate cyclase is inhibited by Ca^{2+} so that, when the intracellular Ca^{2+} concentration falls down in the presence of light, the hydrolysis of cGMP by PDE is counterbalanced (Lolley and Racz, 1982;

Koch and Stryer, 1988). The same role is played by a Ca^{2+}-binding protein termed GCAP for guanylate cyclase-activating protein (Koch and Stryer, 1988, Gorczyca, 1994). Second, at low Ca^{2+} concentration, the shut-off of rhodopsin by phosphorylation is favoured by recoverin (another Ca^{2+}-binding protein) which prevents inhibition of phosphorylation (see Gray-Keller *et al.*, 1993). This action may have an influence on the different steps occurring downstream in the light-triggered cascade (Lagnado and Baylor, 1994). Finally the cGMP-gated channel is itself a target for Ca^{2+}-dependent feedback through the action of calmodulin (for review see Molday, 1996). Indeed, activated by Ca^{2+}, calmodulin binds to the N-terminal part of the cGMP-gated channel β-subunit (Weitz *et al.*, 1999) and the apparent affinity of the CNG channel for its ligand decreases. Thus when intracellular Ca^{2+} concentration decreases in the presence of light, some of the cGMP-gated channels tend to reopen. Despite the complexity of Ca^{2+}-dependent channel modulation, the contribution of this feedback process to the overall light adaptation is thought to be rather small (Nakatani *et al.*, 1995).

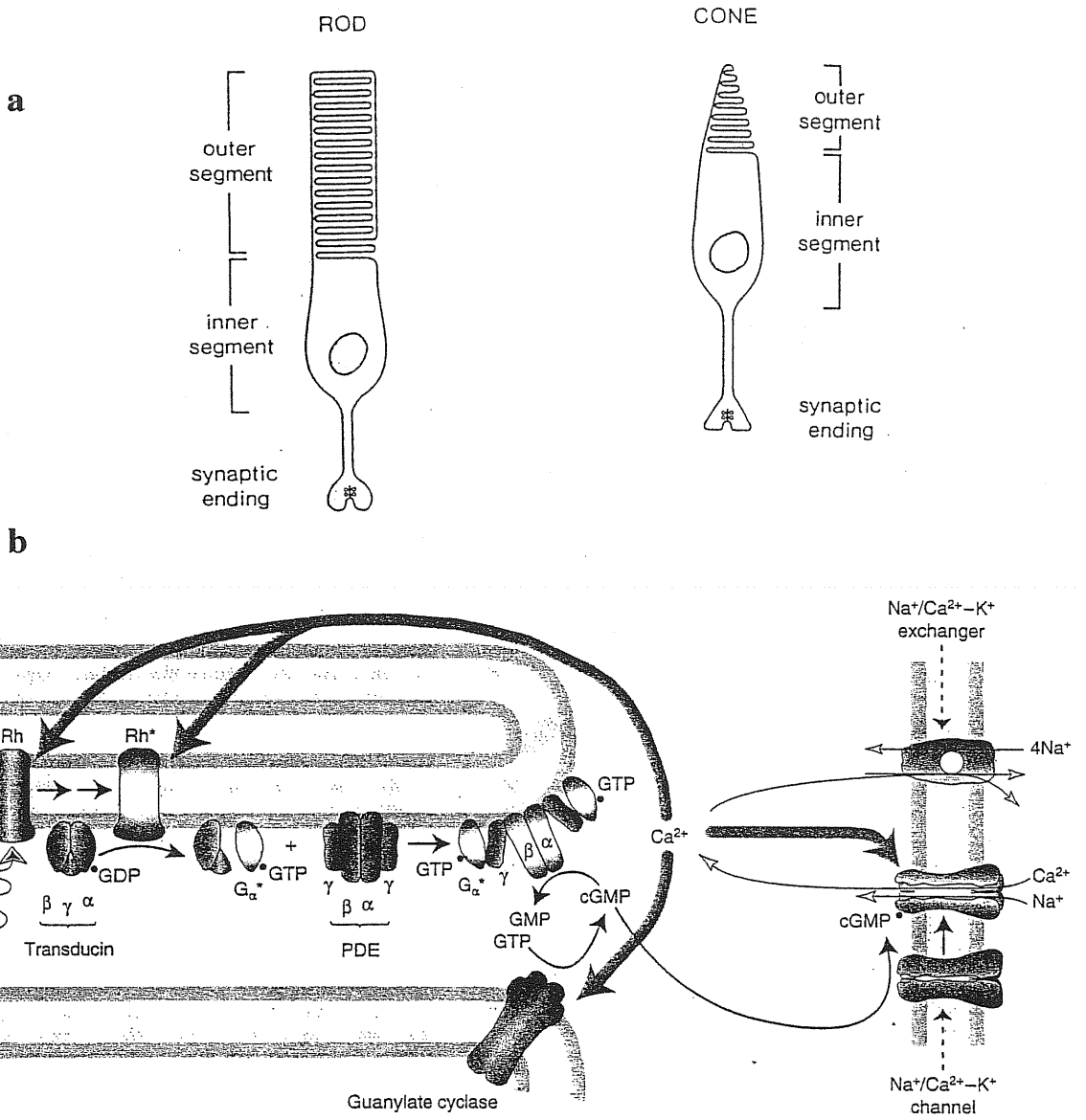

Fig. 1 : Photoreceptors and Phototransduction

a) Schematic diagrams of rods and cones (taken from Yau and Baylor, 1989).
b) Scheme of vertebrate phototransduction (taken from Fain *et al.*, 1996).
c) The visual cycle (taken from Fain *et al.*,1996).

For detailed comments regarding this figure, see the text.

I.B.2. OLFACTORY TRANSDUCTION

I.B.2.1. FUNCTIONAL ORGANISATION OF OLFACTORY RECEPTORS

The olfactory epithelium is made of three different cell types : supporting cells, basal cells and olfactory receptor cells. The supporting cells are involved in the so-called secretion transduction, a mechanism stimulated by odorants and that generates a field potential before the large response occurring in the olfactory receptors. The supporting cells are also involved in the oxidation of odorant molecules in order to render them less membrane permeable. The basal cells are dividing cells that upon differentiation lead to the receptor cells. Finally, the olfactory receptor cells function is to transduce odorant molecules into membrane depolarisation. Olfactory receptor cells are bipolar neurons having a single dendrite extending to the apical surface of the olfactory epithelium. The tip of the dendrite is the olfactory knob from which numerous (10-30) cilia extend into the mucus that covers the olfactory epithelium. The cell body is physically not clearly separated from the dendrite and contains the nucleus. It is then prolonged by a single axon that projects into the olfactory bulb (Fig. 2a; for review see Gold, 1999).

I.B.2.2. THE MECHANISM OF OLFACTORY TRANSDUCTION

Olfactory transduction in vertebrates occurs in the olfactory cilia, which extend in a thin layer of mucus covering the olfactory epithelium and that is exposed to the environment i.e. to the odorant molecules. It is generally thought that olfactory transduction occurs via two different second-messenger pathways (Sklar *et al.*, 1986; for review see Ache and Zhainazarov, 1995). The cyclic 3', 5'-adenosine monophosphate (cAMP) transduction pathway and the inositol 1, 4, 5-triphosphate (IP3) pathway (Fig. 2b). According to the cAMP-second messenger model (Buck and Axel, 1991), a subset of odorants activate a subset of receptor proteins which are coupled to a G-protein (G_{olf}; a G_s like G protein) which is itself coupled to adenylate cyclase. The activation of adenylate cyclase leads to a rise in cAMP concentration and to the subsequent activation of CNG channels. Through the open CNG channels flows a current of Na^+ and Ca^{2+} ions. The entry of Ca^{2+} in the olfactory cells results in the activation of a Ca^{2+}-dependent chloride current. This Cl^- current amplifies the primary odour-induced cations current. Mechanisms of odorant adaptation and inactivation in the olfactory receptor cells were first studied *in vitro* and several possible mechanisms

were proposed : phosphorylation of the odour-receptor by protein kinase A (PKA) (Boekhoff and Breer, 1992; Boekhoff *et al.*, 1992), activation of a phosphodiesterase to reduce the cAMP concentration (Borisy, 1992), ion channel regulation (Kramer and Siegelbaum, 1992; Chen and Yau, 1994; Lynch and Lindermann, 1994; Balasubramanian *et al.*, 1996). The nature of the olfactory adaptation was investigated later in intact olfactory cells of the newt (Kurahashi and Menini, 1997) and the principal mechanism of adaptation was identified as being a regulation of the cAMP-gated channels by a Ca^{2+}-feedback via Ca^{2+}-calmodulin. According to the IP3 hypothesis (Sklar *et al.*, 1986; Boekhoff *et al.*, 1990; Breer and Boekhoff, 1991), a different subset of odorant molecules would activate a different subset of receptors that couple to phospholipase C (PLC) via a different G-protein (Gα like G protein); PLC then cleaves the membrane phospholipid phosphatidyl inositol leading to diacylglycerol (DAG) and IP3. IP3 which is water soluble would then activate IP3-gated Ca^{2+} channels in the ciliary membrane that subsequently mediate Ca^{2+} influx and membrane depolarisation. A recent review (Gold, 1999) favours the cAMP-triggered cascade and propose that the cAMP-cascade is the only transduction mechanism in olfactory cells. Gold criticises the sensitivity of the biochemical assays and cilia preparations used when the IP3 second possible pathway was postulated. A study made by the group of Gold (Lowe *et al.*, 1989) showed that differences observed by Sklar *et al.* in the magnitude of cyclase activity was simply reflecting the number of cells activated by each odour. In addition, knockout mice have been bred for both the cAMP-gated channels (Brunet *et al.*, 1996) and for G_{olf} (Belluscio *et al.*, 1998). Knockout mice for the CNG channel showed that both the cAMP and IP3 responses were abolished suggesting that olfactory transduction in any case depend on the activation of the cAMP-gated channel. In the new born G_{olf} knockout mice, Gs could substitute the lacking G_{olf} but G_S expression declines after birth and by 3 weeks of age, the responses induced by both cAMP and IP3 odorants were only 2.5% of the wild-type responses, arguing for the cAMP-cascade as a majoritary transduction pathway. It has been also proposed that gaseous second messenger such as carbon monoxide (CO; Zufall and Leinders-Zufall, 1997) and nitric oxide (NO; Broillet and Firestein, 1997) produce cGMP and prolong the responses to odorants triggered by cAMP. However the data obtained for CO were obtained for the salamander and the generality to humans is controversial; regarding the NO pathway, the way of activation of NO synthase is still unclear (Gold, 1999). In brief, the mechanism of olfactory transduction and its modulation are still matter of debate.

a

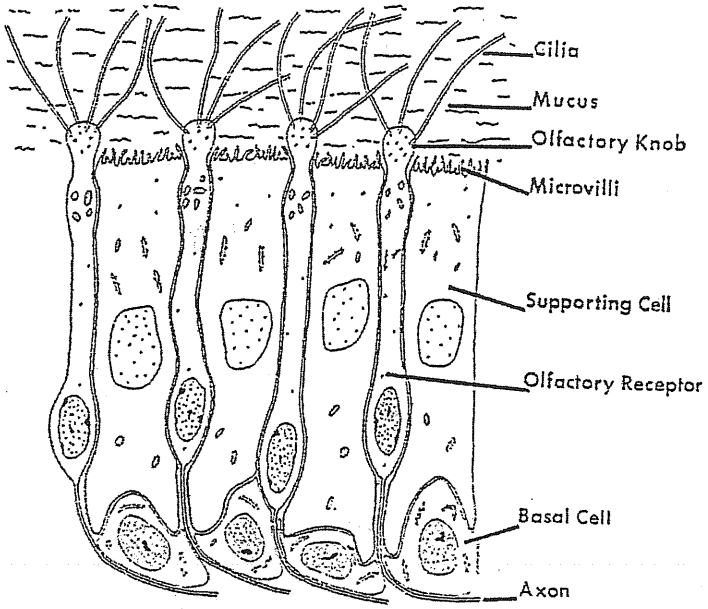

b

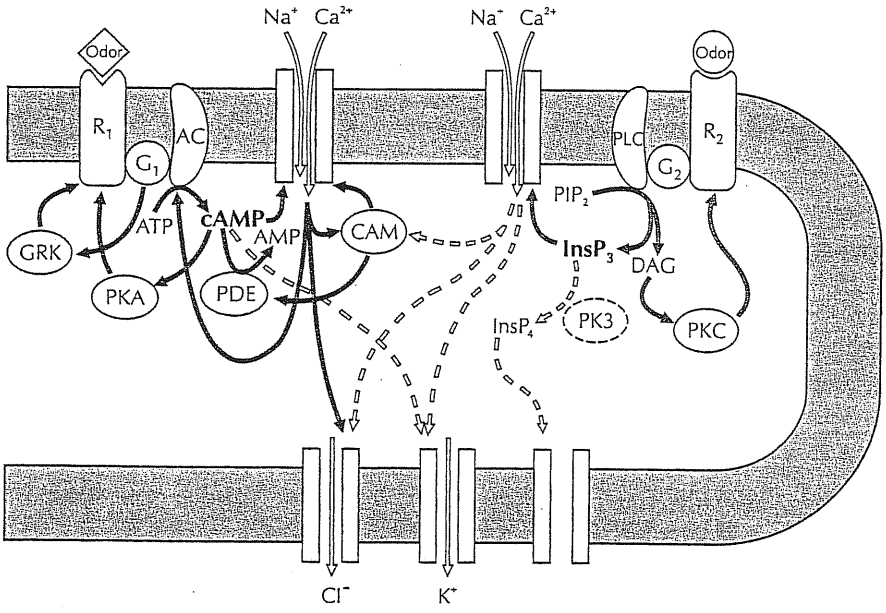

Fig. 2 : Olfactory sensory neurons and olfactory transduction

a) Diagram showing the olfactory epithelium and the cells found there, including the olfatory receptors (taken from Gold, 1999).

b) Schematic representation summarizing olfactory transduction (taken from Ache and Zhainarov, 1995). See the text for detailed description of the mechanisms.

I.C. STRUCTURE OF CNG CHANNELS

I.C.1. MOLECULAR CLONING OF CNG CHANNELS

The physiological findings describing channels directly activated by cyclic nucleotides (Fesenko *et al.*, 1985; Yau and Nakatani, 1985a) were confirmed when molecular cloning of these channels became possible. The first CNG channel was identified through protein purification (Cook *et al.*, 1987; Kaupp *et al.* 1989) and subsequent cloning from a cDNA library from bovine retina (Kaupp *et al.* 1989). This cDNA encoded for a 63 kDa polypeptide and was termed α-subunit. Functional reconstitution of the purified channel into liposomes (Cook *et al.*, 1987) as well as heterologous expression of the cloned cDNA (Kaupp *et al.* 1989) confirmed that the purified protein and the related cDNA actually corresponded to a functional cGMP-gated channel. The structure of the protein consisted in six hydrophobic regions lately shown to span the membrane, a pore-forming region, two N- and C- cytoplasmic terminal parts (Henn *et al.*, 1995). Based on sequence homology to the α-subunit of the rod cGMP-gated channel a "second" subunit was cloned from the human rod (Chen *et al.*, 1993). This subunit appeared to exist in two different forms of respectively 70 and 102 kDa but none of these proteins was found in retinal rod channel preparations. Two years later, a polypeptide of 240 kDa was identified as the authentic β-subunit and was shown to have a bipartite structure (Körschen *et al.*, 1995). The two parts consisted in a cytoplasmic amino-terminal segment similar to a GARP, whereas the second part was homologous to the polypeptide previously described by Chen and coworkers. Similarly to the α-subunit, the second portion of the β-subunit consists in six transmembrane segments, a pore region, a calmodulin binding site and the cGMP-binding site. Recently, a third subunit was cloned from the rat olfactory epithelium (Sautter *et al.*, 1998). This subunit represents an alternative splice form of the β-subunit of the rod CNG channel. To date more than 20 genes encoding for different subtypes of CNG channels were cloned from a variety of invertebrates and vertebrates, from different species and tissues. Table 1 shows a recapitulative from the CNG channels cloned so far.

I.C.2. STRUCTURAL ORGANISATION AND STOICHIOMETRY

Most ionic channels belong to two classes : ligand-gated (LG) and voltage-gated (VG) channels. The membership of one class or the other depends on the transmembrane

structure, the quaternary organisation and on the functional characteristics. CNG channels are directly activated by the binding of either cGMP (Fesenko *et al.*, 1985; Yau and Nakatani, 1985a) or cAMP (Nakamura and Gold, 1987) and thus can functionally fall into the class of LG channels. Each subunit in LG channels is composed of four transmembrane segments (Barnard, 1992) whereas each subunit of a CNG channel is made of six membrane-spanning domains (Henn *et al.*, 1995), a topology shared with VG channels. Moreover, VG channels either form homotetramers (K^+ channels) or adopt a pseudotetrameric organisation (Na^+ and Ca^{2+} channels are made of a single polypeptidique chain with four repetition of a motif constituted by six transmembrane domains) (for review, see Guy and Durell, 1995). The stoichiometry of the native rod channel has yet to be rigorously determined. Nevertheless it was shown that the expressed α-subunit assembles into a homotetrameric channel (Liu *et al.*, 1996; Varnum and Zagotta, 1996) whereas β-subunits alone do not lead to functional homomeric channels (Liman and Buck, 1994; Bradley *et al.*, 1994). In reality β-subunits only were described for the vomeronasal organ (Berghard *et al.*, 1996). The cooperativity observed for calmodulin modulation of the channel suggests that the native rod channel consists of two α-subunits and two β-subunits (Bauer, 1996); the same conclusion was drawn from studies using tandem dimers combining α and β subunits of the olfactory CNG channel (Shapiro and Zagotta, 1998; Liu *et al.*, 1998). In addition, the analysis of the dose-response relations of the macroscopic currents for CNG channels suggests that a multiple binding event is at the origin of channel activation : the Hill coefficient which represents a measure of apparent cooperativity, usually falls between 1.7 and 3.5 (Zimmerman and Baylor, 1986; Yau and Baylor, 1989). Analysis of channel gating made by Ruiz and Karpen (1997) using photoaffinity cGMP analogue that covalently bind to cGMP-activated channels led to the conclusion that these channels open maximally with four ligand bound. This result is also consistent with a tetrameric organisation of CNG channels. Thus, it is generally assumed that, similarly to VG channels, CNG channels are organised in tetramers. As a consequence, because of their transmembrane topography and their quaternary organisation, CNG channels belong to the superfamily of VG channels (Jan and Jan, 1990; Jan and Jan, 1992).

Nature of the CNG channel	References
bovine rod α	Kaupp *et al.*, 1989
bovine olf α	Ludwig *et al.*, 1990
rat olf α	Dhallan *et al.*, 1990
human rod α	Dhallan *et al.*, 1992 – Pittler *et al.*, 1992
mouse rod α	Pittler *et al.*, 1992
catfish olf α	Goulding *et al.*, 1992
chick rod α	Bonïgk *et al.*, 1993
human rod β	Chen *et al.*, 1993
bovine cone α	Weyand *et al.*, 1994 – Biel *et al.*, 1994
rat olf β	Bradley *et al.*, 1994 – Liman and Buck, 1994
Drosophila CNGC1	Baumann *et al.*, 1994
rabbit aorta	Biel *et al.*, 1994
rat rod α	Barnstable and Wei, 1995
bovine rod β	Korschen *et al.*, 1995
mouse olf α	Ruiz *et al.*, 1996
human cone α	Yu *et al.*, 1996
C. elegans TAX-2	Coburn and Bargmann, 1996
C. elegans TAX-4	Komatsu *et al.*, 1996
rat gust α	Misaka *et al.*, 1997
rat pineal gland	Sautter *et al.*, 1997
lizard parietal eye	Finn *et al.*, 1997
dog rod α	Zhang *et al.*, 1997
human fetal heart CNGC	Gong *et al.*, 1998
Limulus CNG channel	Chen *et al.*, 1999

Table 1 : CNG channel subunits cloned so far

I.C.3. STRUCTURAL SIMILARITIES WITH THE VG CHANNELS

The primary structure of CNG channels is shown in Fig. 3 where it is compared to voltage-dependent K^+, Na^+ and Ca^{2+} channels. The sequence homology suggests that the transmembrane topology may be similar to the one of VG channels. Similarly to these channels, CNG channels contain six transmembrane segments and two intracellular N- and C- termini. In addition, CNG channels bear two regions presenting striking sequence similarities with two particular portions of the VG channels : the S4 segment and the pore region.

I.C.3.1. THE S4 SEGMENT

The fourth transmembrane segment in VG channels is characterised by repeated positively charged residues (R or K) at every third position interspersed with mainly hydrophobic amino acids. CNG channels bear between the third and the fifth transmembrane domains a segment reminiscent of the S4 segment of VG channels. Indeed, the fourth transmembrane domain of CNG channels also contains regular repetition of positively charged residues but the net charge of the motif is reduced by the presence of additional negative amino acids. The presence of this peculiar segment is intriguing because it is thought to constitute the major component of the voltage sensor in VG channels. Indeed activation of the VG channels is thought to result from a voltage-driven movement of the S4 motif that leads to a conformational change that propagate in order to consequently open the pore of the channel. Models have been proposed to describe the activation of VG channels (Guy and Conti, 1990; Durell and Guy, 1992) and in recent publications many evidences demonstrate that the S4 segment of the VG channels effectively moves inside the membrane of VG channels, mainly thanks to studies using site-directed mutagenesis (Yang and Horn, 1995; Aggarwal and Mac Kinnon, 1996; Yang *et al.*, 1996; Yusaf *et al.*, 1996). The presence of the S4 motif in CNG channels is particularly intriguing considering that CNG channels are almost completely insensitive to voltage changes but open through the binding of cyclic-nucleotides. Two principal questions arise from these observations. First, is the presence of the S4 motif a residual portion that originates from a common ancestor of CNG- and VG- channels? Second, is the S4 segment of CNG-channels still functional but its functionality impaired by some surrounding sequences? The presence of the S4 motif in CNG-channels effectively served as one of the bases of the classification of those channels into the superfamily of VG-channels (see North, 1995). Concerning the second question, some insights have been recently brought but no

definite answer has still been given. Indeed, Tang and Papazian recently showed that the S4 motif of the rat olfactory CNG channel when transferred into the fruit-fly *ether-à-gogo* (eag) VG-channel sequence was able to retain significant sensitivity to voltage changes (Tang and Papazian, 1997). They additionally proposed that the S3-S4 loop of the rat olfactory CNG channel increases the stability of the open conformation of the eag channel converting it into a voltage-independent channel. Nevertheless, if the work of Tang and Papazian is of great interest, also because it is unique in the concept of functional chimeras between CNG- and VG- channels, it remains a study made on a sequence backbone having the property of voltage-dependency, a property which is in a certain way only conserved, but to date no one ever conferred the property of voltage-sensitivity to CNG channels.

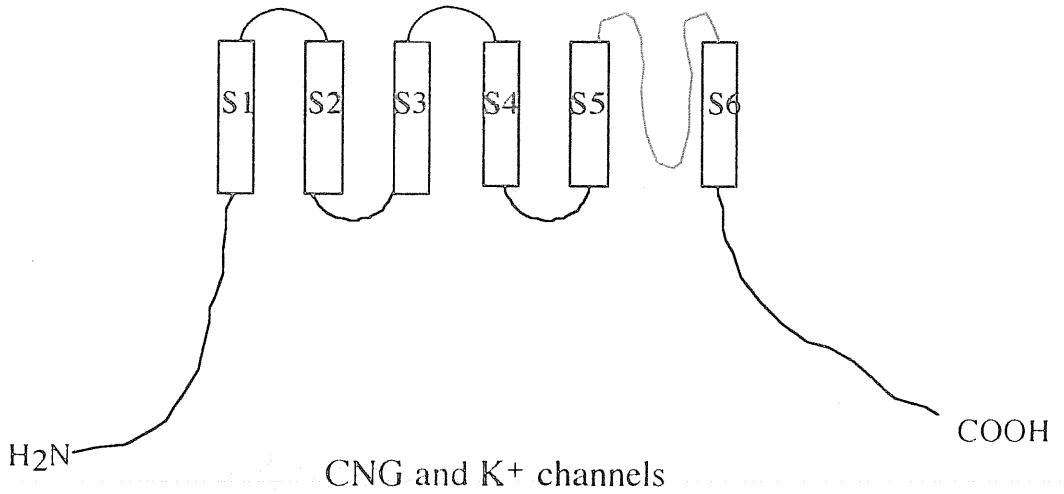

CNG and K^+ channels

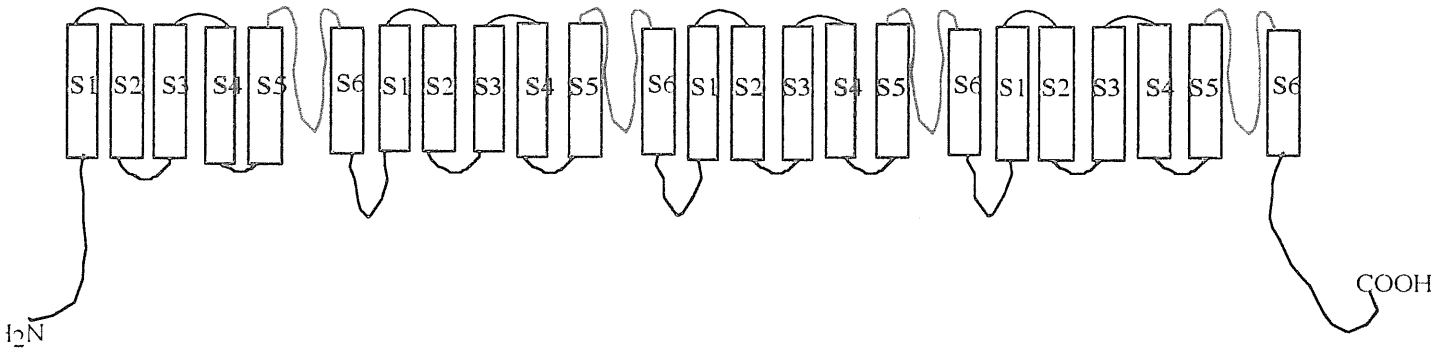

Na^+ and Ca^{2+} channels

Fig. 3 : Structure of CNG and VG channels

A motif constituted by six transmembrane domains is conserved in CNG and VG channels. In Na^+ and Ca^{2+} channels this motif is repeated four times in a single polypeptidique chain. At the contrary, in CNG and K^+ channels, each motif is a separate gene product and the functional channel is formed by homo- or hetero-tetramers.

I.C.3.2. **THE PORE REGION**

A second motif shared by CNG- and VG- channels is the putative pore forming region (P region). This region which links the extracellular ends of the fifth and the sixth membrane spanning regions was initially believed to line the wall of the aqueous pore by forming a hairpin that spans the membrane twice (Eismann *et al.*, 1993). Recently, another structural organisation has been proposed for the pore of CNG channels. Indeed, according to Sun and coworkers who applied substituted-cysteine accessibility method (SCAM), the P region loops of the CNG tetramer would organise such as extending towards the central axis of the pore, forming the blades of an iris-like structure (Sun *et al.*, 1996). In 1998, the crystal structure of a related K^+ channel was finally obtained and described the pore organisation like an inverted teepee or cone made of the different P loops of the four subunits that form the channel (Doyle *et al.*, 1998). The pore region consists in a stretch of about 20 amino acids and exhibits approximately 30% sequence identity between CNG- and VG- channels. It has still to be assessed whether their structural organisation is similar or not. In the pore region of all Shaker-like K^+ channels and of several other K^+ selective ion channels two residues, a tyrosine and a glycine (the YG motif), are always present. The YG motif is absent in CNG channels and VG Ca^{2+} channels. Interestingly, when these conserved residues are deleted from the Shaker pore region, the channel is converted into a non selective ion channel (Heginbotham *et al.*, 1994) suggesting that the YG motif belongs to the selectivity filter. To date, no YG addition in the pore of the CNG channels has been reported.

I.C.4. **THE C-TERMINAL PORTION**

The observation that phototransduction in retinal rod photoreceptors consists in a cation conductance directly activated by intracellular cGMP (Fesenko *et al.*, 1985; Yau and Nakatani, 1985a) suggested the existence of a binding site for cyclic-nucleotide on retinal ionic channels. Indeed, such a site was later identified in the C-terminal cytoplasmic portion of the BRET sequence (Kaupp *et al.*, 1989) as well as on the one of the olfactory CNG channels (Dhallan *et al.*, 1990; Ludwig *et al.*, 1990). The cyclic-nucleotide binding site of CNG channels consists on a stretch of about 120 residues presenting a sequence homology with corresponding regions of the *E. coli* CAP (Shabb and Corbin, 1992) and with the regulatory subunits of cAMP-dependent or cGMP-dependent protein kinases. Crystal structures of CAP and a regulatory subunit

of bovine protein kinase A (PKA) were solved (McKay and Steitz, 1981; Weber and Steitz, 1987; Su *et al.*, 1995) and, because most of the residues forming the nucleotide-binding pocket of CAP are conserved in the cyclic-nucleotide binding site of CNG channels, the tertiary structure might be similar. The cGMP-binding site for the α-subunit of BRET was subsequently identified more precisely (Brown *et al.*, 1995) and was localised to residues 515 to 580. The conformation of the ligand binding site, its function in cyclic-nucleotide selectivity and the way the binding of the ligand is then coupled to the gating will be described further in this thesis. The C-terminal portion of CNG channels also bears another interesting domain which is called C-linker because it is joining the cyclic-nucleotide binding site to the sixth transmembrane domain. This fragment is about 90 amino acids long and shows a high sequence conservation between the different CNG channels. The C-linker and in particular some of its residues were shown to play an important role in coupling the binding of the ligand to the gating of the channel (Zong *et al.*, 1998; Paoletti *et al.*, 1999). In addition a histidine residue in the C-linker (H420 in the BRET) was shown to be a site of binding for Ni^{2+}. A mechanism of potentiation by Ni^{2+} was proposed suggesting that this histidine residue in the C-linker of the rod photoreceptor was involved in gating mechanisms (Gordon and Zagotta, 1995a). The C-linker is also involved in a direct interaction between the N- and C- terminal domains of CNG channels through a cysteine residue (C481 in the BRET) localised at the C-terminus of the C-linker (Gordon *et al.*, 1997).

I.D. FUNCTIONAL PROPERTIES OF CNG CHANNELS

I.D.1. EFFECTS OF SUBUNIT COMPOSITION

Heterologous expression of the α-subunit of the BRET CNG channel results in channel activity largely resembling the one of the native channel. However, the native rod channels display a rapid flickering behaviour indicating very brief open and closed times (Haynes *et al.*, 1986; Zimmerman and Baylor, 1986; Matthews and Watanabe, 1988; Quandt *et al.*,1991; Torre *et al.*, 1992) contrary to the expression of the cloned α-subunit that gives rise to distinct rectangular currents (Kaupp *et al.*, 1989; Nizzari *et al.*, 1993). An additional difference between the native and the cloned BRET CNG channel lies in their distinct sensitivity to *l-cis*-diltiazem. Indeed, the native channel is more sensitive to this ion channel blocker (Stern *et al.*, 1986; Quandt *et al.*, 1991;

Haynes, 1992). These discrepancies suggested that α-subunits required additional(s) factors or subunits in order to form the native channel. As it was already mentioned in this thesis, the first "second" subunit of a CNG channel was reported by Chen and coworkers who cloned the β-subunit of the human rod CNG channel (Chen *et al.*, 1993). This subunit appeared to exist in two different forms of respectively 70 and 102 kDa but none of these proteins was found in retinal rod channel preparations. Two years later, a polypeptide of 240 kDa was identified as the authentic β-subunit and was shown to have a bipartite structure (Körschen *et al.*, 1995). Although the β-subunit does not lead to functional CNG-channels when expressed on its own, when co-expressed with the corresponding human α-subunit (Dhallan *et al.*, 1992; Körschen *et al.*, 1995), it introduced rapid flickers to the channel openings reminiscent from the ones observed in the native channel (Torre *et al.*, 1992; Sesti *et al.*, 1994). In addition, the heteromeric channel was shown to be highly sensitive to *l-cis*-diltiazem, similarly to the native channel (McLatchie and Matthews, 1992). Coexpression of the β subunit also led to a reduced sensitivity to external divalent cations (Körschen *et al.*, 1995) analogue to the level reported for the native channel and contrary to the block observed for the α-subunit homomeric channels (Root and MacKinnon, 1993; Eismann *et al.*, 1994). This result is consistent with the presence of a glycine residue in the β-subunit at a position corresponding to the glutamate 363 in the bovine rod α-subunit which was reported to be involved in divalent cations block (Root and MacKinnon, 1993; Eismann *et al.*, 1994). The currents carried by hetero-oligomeric channels were also diminished by Ca^{2+}/Calmodulin (Körschen *et al.*, 1995) whereas this feature in common with the native channel was not observed for the homomeric channels formed with α-subunits only (Chen *et al.*, 1994). In addition to the olfactory α-subunit (often termed CNCα3) discovered in 1990 (Dhallan *et al.*, 1990; Ludwig *et al.*, 1990), a second subunit was found to be expressed in the olfactory epithelium (Bradley *et al.*, 1994; Liman and Buck, 1994). This second subunit had a shorter N-terminus as the one of the rod β-subunit and is phylogenetically more related to the α-subunits than to the rod β-subunit (Kaupp, 1995). Coexpressing this second subunit of the olfactory channel with the corresponding α-subunit conferred increased sensitivity to cAMP. Nevertheless, this sensitivity to cAMP was still twofold lower than the one observed for native channels. Another caveat concerning the block by external divalent cations was still remaining after the finding of the second olfactory subunit. Indeed, a glutamate present in the pore of α-subunits was found to be involved in this blockade (Root and MacKinnon, 1993; Eismann *et al.*, 1994) so that for accounting for the decreased sensitivity to divalent cations of the native channel a totally different

amino acid residue should have been present in the second subunit at the position of the α-subunit glutamate. But the second olfactory subunit contains an aspartate which was shown to allow divalent cations block (Root and MacKinnon, 1993) in place of the glutamate residue of the α-subunit. As a consequence either other residues had to be involved in the blockade of the channel pore by divalent cations or an additional agent was still lacking in order to explain the behaviour of the native channels regarding divalent cations but also sensitivity to cAMP. Recently, a third subunit was cloned from the rat olfactory epithelium (Sautter *et al.*, 1998). This subunit represents an alternative splice form of the β-subunit of the rod CNG channel. Coexpression of this olfactory β-subunit (CNCβ1b) together with the first olfactory α-subunit (CNCα3) and with the second olfactory α-subunit (CNCα4) produced channels displaying a sensitivity for cAMP similar to the native channels (Bönigk *et al.*, 1999). Moreover, in situ hybridisation and RNase protection assays confirmed the presence of all three subunits mRNAs in the olfactory epithelium and subsequent immunoprecipitation experiments made on preparations of solubilized olfactory cilia suggested that all three subunits co-assemble in the cilia to form the native channels. Macroscopic currents as well as single channel analysis were finally performed on patches excised from rat olfactory neurons and confirmed that the best match with respect to functional characteristics of the native channels were obtained when all three subunits were present (Bönigk *et al.*, 1999). In cone photoreceptors, only one α-subunit (CNCα2; Bönigk *et al.*, 1993) was described so far.

I.D.2. FUNCTIONAL PROPERTIES OF THE PORE REGION

I.D.2.1. IONIC PERMEATION

The pore forming region is known to be the major determinant of ion permeation in VG- (Heginbotham *et al.*, 1994; Heinemann *et al.*, 1992, Yang *et al.*, 1993) as well as in CNG- channels (Goulding *et al.*, 1993). Despite the sequence homologies displayed by the pores of VG-K^+ channels and CNG channels, ions surprisingly do not permeate in the same manner in both groups of channels. Indeed, while VG-K^+ channels, like VG-Na^+ channels, are highly selective, CNG channels do not discriminate well between the different monovalent alkali cations (Picco and Menini, 1993). This peculiarity of CNG channels was early demonstrated both in intact retinal rods (Capovilla *et al.*, 1983; Nakatani and Yau, 1988, Menini *et al.*, 1988) as well as in excised patches (Fesenko *et al.*, 1985; Nunn, 1987; Furman and Tanaka, 1990;

Menini, 1990). Nevertheless, a small difference in the permeability for monovalent alkali cations is observed between the native CNG channel and the α-subunit : contrary to the native channel, the α-subunit is more selective for Na^+ than for Li^+ (Kaupp *et al.*, 1989). Surprisingly, CNG channels share many permeation properties with VG Ca^{2+} channels, despite different amino acid sequences in their pore regions. Indeed, both channels are permeable to Ca^{2+} and monovalent cations (Yau and Nakatani, 1985b). But in addition to permeating through the pore of both channels, Ca^{2+} also blocks the flow of current carried by monovalent ions (for photoreceptors, see Yau and Baylor, 1989; Zimmerman and Baylor, 1992; for olfactory receptors, see Zufall *et al.*, 1994; for Ca^{2+} channels, see Almers and McCleskey, 1984; Hess and Tsien, 1984). In CNG channels Ca^{2+} permeation is very subtile since, depending on the cyclic nucleotide concentration, Ca^{2+} ions either permeate or block the channel (Colamartino *et al.*, 1991). The ratio of Na^+ and Ca^{2+} ions crossing the pore is then determinant for the sensitivity of the visual and olfactory systems (Picones and Korenbrot, 1995a; Kolesnikov *et al.*, 1990). Similarly to Ca^{2+} channels, CNG channels are also sensitive to external proton concentration in that a subconductance state due to a blocking effect is observed when the pH is decreased (for CNG channels, see Goulding *et al.*, 1992; Zufall and Firestein, 1993). Ionic selectivity of CNG channels to non physiological cations has also been investigated in order to understand the permeability rules at the molecular level and to give an estimate of the pore size (Picco and Menini, 1993). The study of permeation of ammonium and guanidinium derivatives indicate that the pore of CNG channels is permeable to at least thirteen organic cations. Whereas Na^+ and K^+ VG channels exclude all methylated cations, the cGMP-gated channel is permeable to many cations containing a methyl group. Following this study of ionic permeation an estimate of the size of the pore was given : the cross section of the narrowest part of the pore must be at least as large as 0.38 x 0.5 nm. This estimated size suggests that the pore of CNG channels is bigger than the ones of Na^+ and K^+ channels but smaller than the one of the Ca^{2+} channel of skeletal muscle. This conclusion is in accordance with the estimation obtained by Laio and Torre after a study of statistical mechanics (Laio and Torre, 1999). In this study, the physical origins of ionic selectivity were investigated and it was concluded that the selectivity for monovalent cations depends on geometrical properties of the inner core of the channel without any critical contribution from charged or polar groups that would interact electrostatically with the permeant ions. This hypothesis may explain the differences in ionic selectivity between channels having similar pore residues and *vice-versa* the similarities in ionic selectivity between channels having

different pore residues.

I.D.2.2. THE FUNCTIONAL ROLE OF A CONSERVED GLUTAMATE

Some residues in the pore region of CNG channels might be more important than others in controlling the flow of ions. Indeed, a conserved glutamate which is found at position 363 in the BRET sequence appeared to be involved in the block by external Mg^{2+}, Ca^{2+} (Root and MacKinnon, 1993; Eismann *et al.*, 1994) and protons (Root and MacKinnon, 1993). Because substitution of E363 by a neutral amino acid reduced external divalent cations block but maintained the channel sensitivity to internal blockade, it was suggested that this glutamate was localised inside the pore, close to the external surface. The β subunit bears a glycine residue at the position corresponding to the glutamate 363. Interestingly, coexpression of α and β subunits led to a reduced sensitivity to external divalent cations (Körschen *et al.*, 1995) analogue to the level reported for the native channel. This result is consistent with the role played by E363 in divalent cations block. Indeed, it has been proposed that in homotetrameric channels the four glutamate residues form the high affinity Ca^{2+} binding site. Various homomeric CNG channels differ in their sensitivity to external Ca^{2+} ions (Frings *et al.*, 1995). Since the glutamate residue is conserved in all CNG channels α-subunits known so far, additional residues or factors must participate in the binding of divalent cations and account for the different sensitivity to Ca^{2+} blockade. Indeed, it was recently shown that the S5-P-S6 region defines a particular dielectric environment that sets the state of protonation of the glutamate residues and consequently determines the affinity of the Ca^{2+} binding site inside the pore (Seifert *et al.*, 1999). This glutamate was also shown to be responsible for the multi-ion nature of the pore of CNG channels (Sesti *et al.*, 1995). Sesti and coworkers tested the anomalous mole fraction effect with mixtures of Li^{+} and Cs^{+}. This effect is characteristic of a pore containing multi ion-binding sites and was observed for the native channel as well as for the homomeric channels. At the contrary, the anomalous mole fraction was not observed when the glutamate 363 was replaced by a neutral amino acid and was only reduced when it was mutated into an aspartate. These results suggest that the coordination of several negative residues is necessary to form the molecular structure that can bind one or two monovalent cations. This structural organisation is reminiscent from the coordination of four glutamate residues in the four different repeats of Ca^{2+} channels that constitutes a binding site for one or two small cations (Armstrong and Neyton, 1992). Another interesting observation regarding

E363 of the BRET was made regarding channel gating (Bucossi *et al.*, 1996). By mutating E363 into an alanine, a serine or an asparagine, a current decline reminiscent of the desensitisation of LG channels was observed for the BRET CNG channel suggesting that glutamate 363 was involved in gating properties in addition to be part of the selectivity filter. In the same study, it was demonstrated that, contrary to the wild type channel, the mutant E363S was permeable to dimethylammonium. The fact that replacing the glutamate by a smaller residue led larger organic cations to permeate suggested that E363 was located close to the narrowest part of the pore.

I.D.3. FUNCTION OF THE CYCLIC-NUCLEOTIDE BINDING SITE

The apparent ligand sensitivity of the cyclic nucleotide binding sites differs depending on the channel considered. Nevertheless, all CNG channels are more sensitive for cGMP than for cAMP. The constant for half activation, $K_{1/2}$ for the native and for the cloned bovine rod are similar : 10-50 μM for cGMP and 1.2-1.5 mM for cAMP. For the native salamander photoreceptor $K_{1/2}$ is 4 μM for cGMP and 20 μM for cAMP (for review, see Eisman *et al.*, 1993). For the cone photoreceptor, $K_{1/2}$ is around 34-70 μM for cGMP and 1 mM for cAMP. For the olfactory CNG channels, the $K_{1/2}$ values for both cyclic nucleotides are in general closer : for the cloned bovine olfactory receptor, $K_{1/2}$ is 1.4 μM for cGMP and 54 μM for cAMP; for the native rat olfactory receptor, $K_{1/2}$ is 1 μM for cGMP and 2.5 μM for cAMP. Although the olfactory CNG channel is slightly more sensitive for cGMP than for cAMP, its physiological ligand is cAMP.

The binding site is formed by eight-stranded antiparallel β-rolls flanked by a short amino-terminal α-helix (A helix) and two C-terminal α-helices (B and C helices). Based on sequence comparison between the different cyclic-nucleotide binding protein, a model of binding was proposed (Fig. 4, taken from Kumar and Weber, 1992). Some residues were identified as key residues in the interaction with the cyclic-nucleotides. A set of highly conserved glycines in the β-rolls are important for the proper folding of the binding pocket. Using a photoaffinity radioactive analogue of the cGMP able to label specifically both subunits of the BRET CNG channel, Brown and coworkers localised more precisely the cGMP binding site and identified the residues lining the binding pocket (Brown *et al.*, 1995). Indeed, the specific labelling of the BRET α-subunit was localised to a 66 amino acid region (Tyr 515-Met 580) entirely contained into the 120 amino acids previously supposed to form the binding site for cyclic-

nucleotides. Moreover, within this fragment, residues Val 524, 525 and Ala 526 were found to contain label and thus to line the binding pocket. The specific labelling was also confirmed repeating these experiments on the β-subunit of the BRET. Conserved residues of the β7 strand were also subjected to investigation. Molecular modelling on cGMP-dependent protein kinase suggested that the hydroxyl group of the threonine residue of the β7 strand formed a hydrogen bond with the amino group attached to the C2 of cGMP (Weber *et al.*, 1989). Based on the fact that this amino group is absent from the cAMP molecule, this residue might have accounted for ligand discrimination. Mutation of the first alanine of the β7 roll into a threonine in the cAMP dependent kinase indeed increased the binding of cGMP but this mutation had little effects on the cAMP binding (Shabb *et al.*, 1990). This alanine/threonine hypothesis was subsequently studied by Altenhofen and coworkers who concluded that the hydroxyl group of Thr 560 (rod) and Thr 537 (olf) form an hydrogen bond with cGMP but not cAMP (Altenhofen *et al.*, 1991). However this threonine could not account for the molecular basis of ligand discrimination between the retinal and olfactory channels since all CNG channels contain a threonine at this position. Moreover the hydrogen bond can only be formed when the cGMP is in a syn conformation whereas for the CAP the binding is known to occur in the anti conformation (see the review of Zagotta and Siegelbaum, 1996). Based on the observation that the C-helix of the CAP (Thr 127- Ser 128) makes two hydrogen bonds with the C6-amino group of cAMP (Weber and Steitz, 1987), the group of Siegelbaum performed a study of chimeras between the BRET and the catfish olfactory channel and concluded that the C-helix is both necessary and sufficient to account for ligand specificity (Goulding *et al.*, 1994). By comparing the sequences of the CAP and the BRET C-helices, the residue D604 of the BRET, which corresponds to T127 in the CAP sequence, was mutated (Varnum *et al.*, 1995). The nucleotide selectivity of the BRET (cGMP > cIMP >> cAMP) was significantly altered when the aspartate was mutated into a glutamine (corresponding residue in the fish olfactory channel) (cGMP >> cAMP > cIMP). Substitution of D604 by a methionine completely inverted the initial selectivity sequence (cAMP >> cIMP ≥ cGMP). Varnum and coworkers concluded that these changes were due to an alteration in the relative ability of the bound agonist to trigger the allosteric conformational changes necessary to the channel opening. In addition, they proposed that D604 forms two hydrogen bonds with N1 and N2 of the guanine ring in anti configuration. Recently, the functional role of aromatic residues in the ligand-binding domain of CNG channels was analysed (Li and Lester, 1999). By replacing Tyr 565 of the rat olfactory CNG channel into an alanine, a 10 fold increase in sensitivity to both cAMP and cGMP was observed. This

tyrosine lies in the hinge between helices B and C and is thought to facilitate gating transitions that occur after ligand binding.

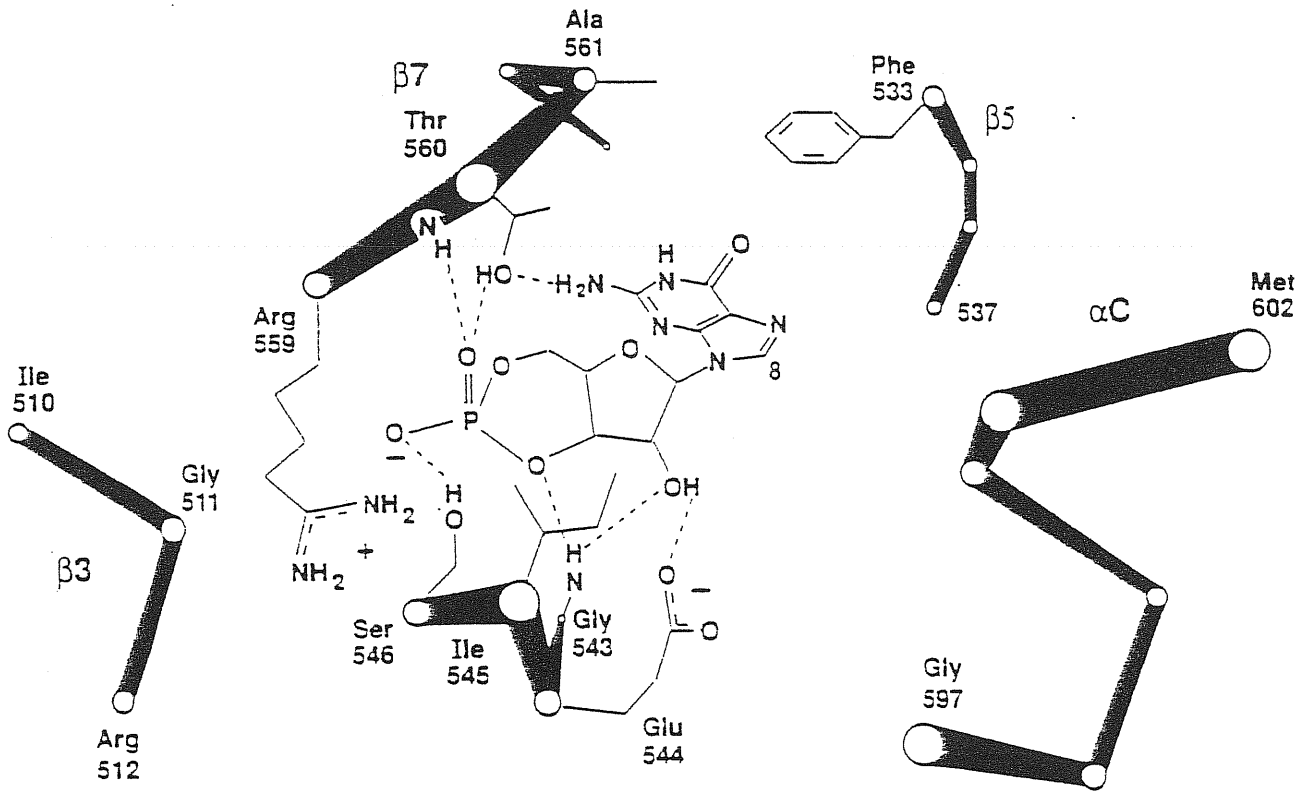

Fig. 4 : Schematic representation of the cGMP-binding site of the BRET CNG channel.

The side chains that are conserved between cyclic nucleotide binding sites or interact with the ligand are shown. Hydrogen bonds and ionic interactions are indicated (taken from Kumar and Weber, 1992).

I.D.4. GATING PROPERTIES

I.D.4.1. PROPERTIES OF THE MACROSCOPIC CURRENTS

The macroscopic properties of CNG channels are usually studied using the patch-clamp technique, excising membrane patches either from photoreceptors or from *Xenopus* oocytes or cultured cells expressing the heterologous channel of interest. When an inside-out patch excised from the membrane of the system expressing CNG channels, is exposed to micromolar concentrations of cyclic-nucleotide, many channels are activated and macroscopic currents are recorded. Fig. 5a shows the macroscopic current obtained from an inside-out patch excised from the outer segment membrane of a photoreceptor, at +60 mV and in the presence of different cGMP concentrations. The current observed is dependent on the cGMP concentration : at saturating concentrations of cGMP (100 μM) currents as large as 1-2 nA can be obtained whereas very small currents (some pA) are measured at low cGMP concentration. As a consequence, the relationship between the current and the cGMP concentration can be described as : $I = I_{max} [g^n / (g^n + K^n)]$

where Imax is the maximal current activated by cGMP, g is the cGMP concentration, K the cGMP concentration activating half of the maximal current and n the Hill coefficient. Experimentally, n is between 1.7 and 3.5 (Zimmerman and Baylor, 1986; Yau and Baylor, 1989) and K has a value of 10 μM or 50 μM (for CNG channels of salamander photoreceptors; see Zimmerman and Baylor, 1986; Colamartino *et al.*, 1991; for CNG channels of bovine rods; see Luehring *et al.*, 1990). CNG channel activation also present evidence for a slight voltage-dependence : hyperpolarisation appears to increase the rate constant of channel closing (Karpen *et al.*, 1988). According to Sesti and coworkers (1994), analysis of single channel activity at positive and negative voltages indicates that the outward rectification observed in the presence of low cGMP concentration is primarily due to an increase in the open probability at positive voltages. Similarly to the CNG channel from photoreceptors, the ones from olfactory receptors physiologically respond to the binding of an agonist, cAMP. For the cloned channel, the half saturating concentration value (at +40 mV) is higher in the case of cAMP (38-68 μM) than for cGMP (1.2-2.4 μM) (Dhallan *et al.*, 1990); for the native channel, Nakamura and Gold (1987) found a bimodal value (K = 2 and 40 mM for cAMP). The Hill coefficient is around 1.9, similar to the one of the cGMP-activated channel from photoreceptor (Dhallan *et al.*, 1990). Similarly to the CNG channels involved in phototransduction, the currents activated by cAMP in olfactory receptors

also present a very small outward rectification (Dhallan *et al.*, 1990; Goulding *et al.*, 1992).

I.D.4.2. SINGLE CHANNEL PROPERTIES

The first attempts to record cGMP-induced single channel current were unsuccessful (Fesenko *et al.*, 1985; Nakamura and Gold, 1987). Noise measurements revealed a very small single channel conductance of less than 0.1 pS that was inconsistent with an aqueous pore but fitted more to the conduction observed in case of membrane carriers (Fesenko *et al.*, 1985). An other explanation for a so small unitary current was that the effective conductance of the channel pore was reduced because of a blockade. Indeed, the first measurements of single channels were obtained in excised rod membrane patches using solutions free in divalent cations (Zimmerman and Baylor, 1986; Haynes *et al.*, 1986; Matthews and Watanabe, 1987, 1988). The reduction in single-channel conductance by divalent cations was proposed to be physiologically important in reducing the signal-to-noise ratio of sensory transduction (Yau and Baylor, 1989). A great variability in the mean open time ranging from 0.1 to 1 msec and a single-channel conductance between 20 and 60 pS were obtained (Yau and Baylor, 1989; Torre *et al.*, 1992; Zufall *et al.*, 1994; Sesti *et al.*, 1994). The typical traces for single-channel recordings from excised patches of rod outer segments reveal a continuous flickering between the closed and the open states (Fig. 5b). Theoretical analysis of the experimental amplitude histograms gives an estimate of the mean open time of maximally 35 μsec (Torre and Menini, 1994). The density of cGMP-activated channels in the membrane of the rod outer segment is high (126 μm^{-2}, Karpen *et al.*, 1992) and single channels openings can only be obtained using very small concentrations of cGMP. However, cGMP-gated channels are not so dense in the inner segment simplifying single-channel recordings (Matthews and Watanabe, 1988). Inner segment recordings also exhibited in majority the flickering behaviour. Surprisingly, in some rare recordings the application of cGMP induced well defined openings without flickering behaviour (Torre *et al.*, 1992; Sesti *et al.*, 1994). The properties of these single-channel recordings in terms of conductance (25-30 pS) and open probability (half activation of this channel occurred at about 18 μM cGMP) were reminiscent from the ones observed when expressing the α-subunit of the BRET (Kaupp *et al.*, 1989). Depending on the nature of the preparations, the properties of CNG channels were quite different. It has been just mentioned that the α-subunit of the BRET displays a single open state with a conductance around 28 pS (Kaupp *et al.*, 1989). In contrast, the α-subunit of the CNG channels from catfish olfactory sensory

neurons were found to be characterised by three different open states with respective conductances of 25, 50 and 80 pS (Goulding *et al.*, 1992; Root and Mac Kinnon, 1994). The α-subunit of the CNG channel from rat olfactory neurons has a conductance of about 40 pS and is characterised by the absence of subconductance states (Li and Lester, 1999). On the whole, the sum of the collected data are consistent with the existence of different conducting levels in the CNG channel, leading to the appearance of well resolved open states in homomeric channels and to flickering behaviour in heteromeric channels (Bucossi *et al.*, 1997).

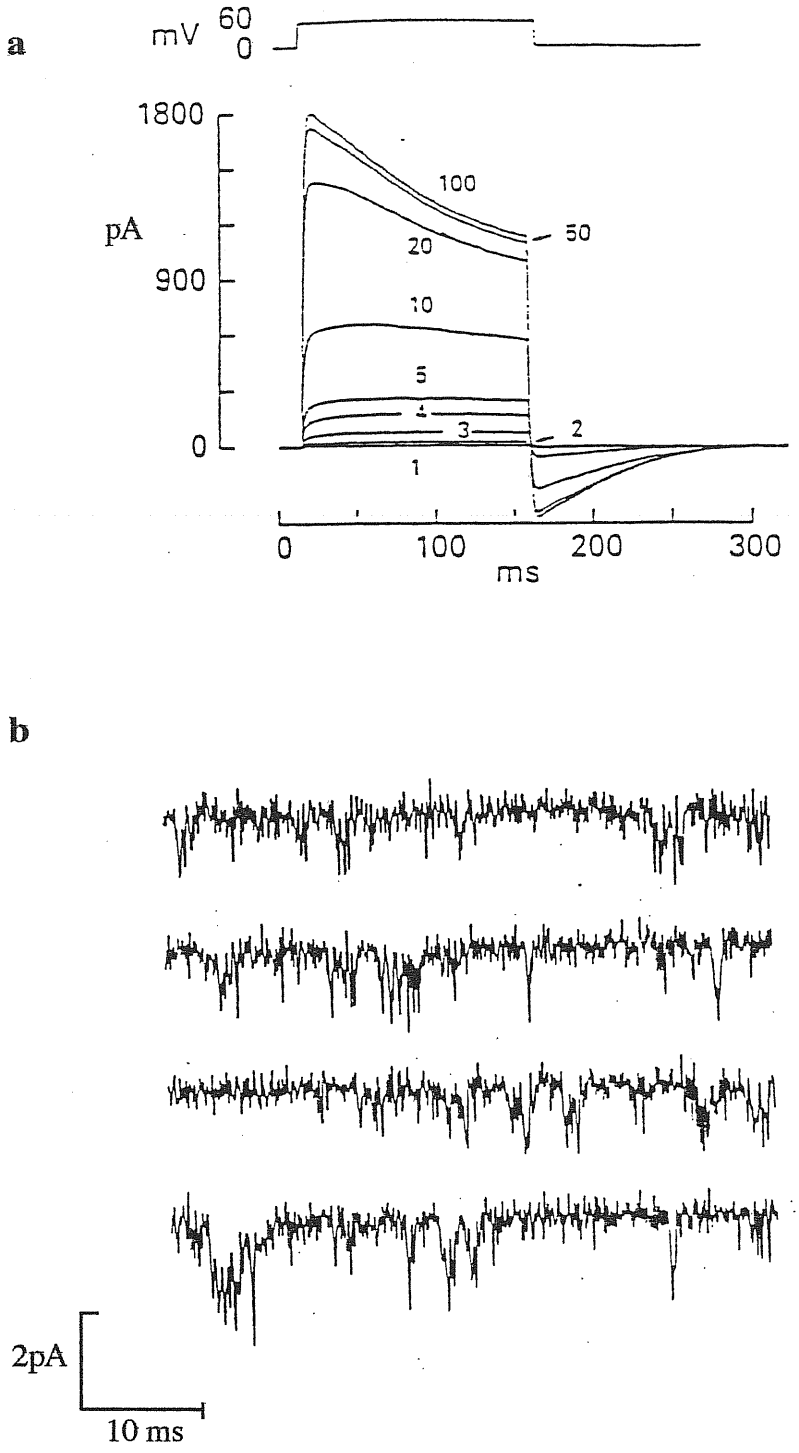

Fig. 5 : Macroscopic currents and single-channel properties of the cGMP-gated channel obtained from membrane patches excised from photoreceptors of the tiger salamander.

a) cGMP stoichiometry of the activation of the Na^+ current measured at +60 mV (taken from Torre and Menini, 1994). b) Single channel currents recorded with 2 μM cGMP at -60 mV and filtered at 4 kHz (taken from Torre and Menini, 1994).

I.D.4.3. COUPLING OF LIGAND BINDING TO CHANNEL GATING : ROLE OF THE C-LINKER

The molecular mechanisms underlying the coupling of ligand binding to channel opening have been recently investigated. One of the first insights were given by Gordon and Zagotta, who identified a histidine residue in the C-linker of the BRET CNG channel responsible for potentiation by internal Ni^{2+} ions (a phenomenon previously described by Idefonse *et al.*, 1992) by stabilisation of the open conformation (Gordon and Zagotta, 1995a). Another histidine was found by the same researchers in the rat olfactory CNG channel but this histidine accounted for channel inhibition by preferential binding of the Ni^{2+} to the closed states, stabilising them and thus reducing the efficiency of channel activation (Gordon and Zagotta, 1995b). A conserved cysteine residue in the C-linker L2 region was then identified as a site of potentiation through the modification by sulfhydryl-reactive chemicals (Broillet and Firestein, 1996; Brown *et al.*, 1998). Based on their results, Brown *et al.* suggested that the C-linker undergoes a movement during channel activation which is essential for coupling ligand binding to channel gating. The same year, Zong *et al.* investigated chimeric channels between the cone photoreceptor and the olfactory receptor and identified three amino acids in the C-linker that account for the differences in cAMP efficacy and are major determinants in channel gating (Zong *et al.*, 1998). Three other residues in the C-linker L2 region were found to be involved in gating processes after another study of chimeras. Indeed, the group of Siegelbaum conferred the very high cAMP efficacy of a *Caenorbitis elegans* sensory neuron channel (TAX-4) to the BRET CNG channel which is usually poorly activated by cAMP (Paoletti *et al.*, 1999). The exchange of the two different C-linker L2 regions did not alter the spontaneous open probability of the channel, despite a large effect on gating. This result inferred the possibility of a gate-like function for the C-linker but suggested a possible role for the C-linker in determining the differences in agonist interaction between the closed and the open states. Indeed, they found that the C-linker favours the stability of the ligand-binding to the open state, stabilising the interactions between the ligand and its binding site. This stabilisation occurring in the same way for both cGMP and cAMP, the C-linker must interact with the cyclic nucleotide in a part of the molecule which is common to both cGMP and cAMP. They proposed that the C-linker would act as a rigid arm that couples a change in the structure of the core of the channels to a movement of the ligand-binding site, which favours the binding of the cyclic-nucleotide in the open conformation, intersubunits interactions and consequently stabilises the open state. The cyclic nucleotide-binding site itself has been proposed to play an

important role in coupling ligand-binding to channel allosteric conformational change (see in this thesis the section I.D.3.).

I.D.4.4. KINETIC MODELS OF GATING

The gating kinetics of CNG channels were studied by Karpen and coworkers (1988). As previously mentioned, they showed the cGMP-dependence of channel activation, the saturation of the opening rate at high cGMP levels and mentioned also the slight voltage sensitivity of CNG channels whose opening can be increased by depolarisation. From their results, they proposed a model with three ligand-binding steps followed by a closed to open transition which is favoured by depolarisation and occurs when the channel is fully liganded. This model accounts for the nearly linear current-voltage (I/V) relation observed at saturating concentration of cGMP, i.e. when almost all channels are open even at negative voltages. At low concentration of cGMP, the open probability is low so that the role of voltage changes in the C4 to O equilibrium is major for increasing the open probability.

I.D.4.5. ALLOSTERIC MODELS

Spontaneous openings of CNG channels in the absence of ligand have been reported (Picones and Korenbrot, 1995b; Tibbs *et al.*, 1995). Taking this observation into account, an allosteric model has been proposed by Stryer (1987). In this model, the affinity of cGMP is higher for the open conformation than for the closed one, the change of conformation is concerted between the different subunits, the binding of the ligand to each subunit is independent from the other bound subunits and the greater the number of cGMP molecules that bind, the more stable the conformational change. By constructing chimeras between the BRET and the rat olfactory channels, Goulding and coworkers identified two distinct domains, the N-S2 domain of the N-terminal region and the C-helix of the C-terminal domain, which are important for channel opening. They propose that the N-S2 region is a portion of intersubunit contact. These contacts are enhanced during channel activation, these modifications lead to changes in subunit orientation, that, combined to a movement of the C-helix leads to channel opening (Goulding *et al.*, 1994). This interpretation is based on a simple tetrameric allosteric model that, similarly to the model proposed by Stryer, supposes that the ligand prefers the open conformation. The N-terminal region of the olfactory channels seems to be of particular importance (Chen and Yau, 1994; Gordon and Zagotta, 1995b). This feature has been exploited by Sunderman and Zagotta, who analysed the

kinetic behaviour of single BRET CNG channels in which mutations in the binding domain (D604, see section I.D.3. in this thesis and Varnum *et al.*, 1995) have been introduced and/or the rat olfactory N-terminal domain substituted to the original one of the BRET (Sunderman and Zagotta, 1999a). They refined the previously proposed model (Gordon and Zagotta, 1995b; Varnum *et al.*, 1995) in which the cyclic nucleotide is supposed to bind to the closed state through interactions with the β-roll of the binding site, this binding leads to a movement of the β-roll relative to the C helix and to a subsequent strenghtening of the cGMP binding through hydrogen bonds with D604. The formation of the hydrogen bonds has been shown to be important for the allosteric transition leading to channel opening whereas the closure of the channels requires their dissolution. The stabilisation exerted by the N-terminal portion occurs just before the allosteric transition and then after for stabilising the interactions between the aspartate residue of binding domain and the ligand. The same authors studied in details the mechanisms of allosteric transition performing single-channels analysis of the BRET α-subunit expressed in *Xenopus* oocytes (Sunderman and Zagotta, 1999b). They determined that two closed and one open states are required to explain the gating at saturating ligand-concentration. Two kinds of models were then possible : C <--> C <--> O or C <--> O <--> C. The first hypothetical model could describe the activation of a channel composed of two functional dimers which would have to enter both in the activated conformation to allow the channel to open (concerted transition). A scheme similar to this C <--> C <--> O model was previously proposed by Liu *et al.* (1998). For the second possible model, a single concerted allosteric conformational change could underly the C <--> O transition, while the O <--> C being cyclic nucleotide independent would depend on an open-channel block or closing of a secondary gate (multiple conformational changes). While the real mechanism is undoubtedly more complex than two closed and one open state, they favoured the second model. Sunderman and Zagotta also studied the effect of Ni^{2+} and concluded that Ni^{2+} induces and stabilises the allosteric transition of liganded channels. This hypothesis also implies that the conformational changes occurring spontaneously are based on a different mechanism that does not involve the movement of H420. This is in accordance with the recent findings of Paoletti *et al.* (1999) who showed that alterations in the C-linker does not affect spontaneous openings. Opening mechanisms have been recently studied by Ruiz and Karpen (1999) who performed analysis of single channels locked in each liganded state. Usually, studies of kinetics have always been impaired by the fact that the ligand binds and unbinds continuously from the binding site. In 1997, Ruiz and Karpen overcame these problems by using a photoaffinity cGMP analogue that binds covalently to CNG

channels. From this study, these researchers found that CNG channels can be locked in four liganded states and that in each state, channels opened to two or three different conductance states. Now, Ruiz and Karpen refined their studies and concluded that the channels exhibit at least nine different states for each doubly, triply and fully liganded channel. This observation supposes that the channels exhibits the same series of conformational changes at each possible liganded state. Such complex behaviour can not be explained with simple concerted or sequential allosteric models. A general allosteric model is proposed in this study : channels with zero and one activated subunits are closed, channels with two adjacent subunits activated lead to an open state (O1), channels with diagonally activated subunits are closed, channels with three or four activated subunits are open (states O2 and O3). In the four liganded channels, additional states are required : an additional conformational change can be added for a change in the interaction between two liganded subunits that are adjacent. There are some evidence for such a conformational change that occurs between pairs of subunits : Gordon and Zagotta (1995c) showed that the open state is stabilised by such intersubunits interactions through Ni^{2+} coordination; Varnum and Zagotta (1996) showed that activation properties were different for adjacent subunits than for diagonally opposed ones; Liu *et al.* (1998) also proposed a mechanism based on interaction between adjacent subunits.

I.D.5. MODULATION OF CNG CHANNELS

For review see Wei *et al.*, 1998

I.D.5.1. MODULATION BY Ca^{2+}-CALMODULIN

Functions of ion channels are known to be modulated by various factors and structural modifications that alter their voltage- or ligand-sensitivity or their gating properties. Among those modulations one involves Ca^{2+}-calmodulin. Channels that are modulated by this protein include Ca^{2+}-dependent sodium and potassium channels in *Paramecium*, the ryanodine receptor channel in muscle, a potassium channel in kidney and also CNG channels (Liu *et al.*, 1994). Modulation of CNG channels by Ca^{2+}-calmodulin was first reported for the rod photoreceptor by Hsu and Molday (1993). In this study, the effect of Ca^{2+}-calmodulin was investigated using in particular a calcium ion flux assay with a calcium-sensitive dye. The results of this work allowed to conclude that Ca^{2+}-calmodulin increases the apparent Michaelis constant of the

channel for cGMP. This effect leads to a decrease by two- to six- fold in the rate of cations influx, including Ca^{2+}, through CNG channels activated by low cGMP concentrations. The Ca^{2+}-calmodulin effect can be incorporated into the process of phototransduction. In the dark, cGMP-activated channels are open and the cytoplasmic Ca^{2+} concentration is maintained at relatively high levels (around 0.3 μM). In this situation, the guanylate cyclase is at its basal level, the cGMP-gated channels are in a low affinity state for cGMP binding and Ca^{2+}-calmodulin is bound to the channel. In the presence of light, cGMP-gated channels are closed, cytoplasmic Ca^{2+} level decreases, guanylate cyclase is activated, Ca^{2+}-calmodulin dissociates from the channel that consequently switches to its high affinity state for cGMP. This causes the reopening of cGMP-activated channels in the presence of low cGMP facilitating the photorecovery of the system. By performing calmodulin affinity chromatography and Western blots, Hsu and Molday also found that the site of binding of Ca^{2+}-calmodulin is located on the 240 kDa channel subunit. The modulation is thus thought to effect by allosteric interaction between the 63 and the 240 kDa subunits. This hypothesis which involves 240 kDa, i.e. the β-subunit, of the rod photoreceptor was further confirmed by Chen *et al.* (1994). An action of Ca^{2+}-calmodulin was also described for CNG channels of olfactory receptors using the cloned rat olfactory channel expressed in cell lines (Chen and Yau, 1994). In this study, Ca^{2+} was shown to reduce the apparent affinity of the channel for cAMP by up to 20-fold in the presence of Ca^{2+}-calmodulin. This action involves a direct interaction between the calmodulin and the 63 kDa channel protein as expression of the cloned olfactory CNG channel (i.e., α subunit) is enough to observe Ca^{2+}-calmodulin modulation. The group of Yau went on studying the modulation of CNG channels by Ca^{2+}-calmodulin and succeeded in the identification of the Ca^{2+}-calmodulin binding site on the α subunit of the olfactory CNG channel (Liu *et al.*, 1994). They used chimeras between the rat olfactory channel and the human rod channel N-terminal parts. The cDNAs encoding for these chimeras were then transfected into HEK293 cells and tested for Ca^{2+}-calmodulin sensitivity. These experiments showed that the N-terminal portion of the olfactory channel contains a putative Ca^{2+}-calmodulin binding domain that is a peptidic sequence characterised by two aromatic or long chain residues (aromatic residues at position 1 and 14; other hydrophobic residues at position 5 and 8) separated by 12 amino acids which are often positively charged (the amphipathic α-helical model). In the case of the rat olfactory channel, this calmodulin binding sequence is located from residues Arg62 to Arg87 on the α-subunit and constitutes the only Ca^{2+}-calmodulin binding domain.

In order to quantify the interaction of the Ca^{2+}-calmodulin and its binding site, they performed the synthesis of a peptide made of the residues comprised between Arg62 and Arg87 and performed experiments of gel-shift assays and fluorescence. They concluded in a one-to-one stoichiometry with a dissociation constant of 3.4 nM. Experiments using cAMP indicated that Ca^{2+}-calmodulin in addition to change ligand affinity affects channel gating in that the current activated by high cAMP concentration is reduced in the presence of calmodulin. In addition to the Ca^{2+}/calmodulin mediated feedback, another mechanism of CNG channel inhibition in olfactory neurons that involves high intracellular Ca^{2+} concentration and an unknown Ca^{2+} binding protein has been suggested (Kramer and Siegelbaum, 1992). The presence of such an additional Ca^{2+} binding protein has also been proposed for photoreceptors. Indeed, the binding site for calmodulin seems to be also a binding domain for an additional endogenous factor present in rods (Gordon *et al.*, 1995). CNG channels seem to be inhibited by this unknown endogenous factor most of the time in darkness and dim light. This is in accordance with the observation of Gray Keller *et al.* (1991) and Lagnado and Baylor (1994) who saw no effect of exogenous calmodulin applied to detached or truncated rods in the dark. When the cytoplasmic Ca^{2+} concentration is very low, i.e. in bright light, the endogenous inhibitory factor leaves the binding sites that can thus be occupied by calmodulin. The putative inhibitor seems to play a role in adaptation to strong bleaches. Recently, the binding domain for calmodulin on the rod photoreceptor CNG channel has been localised more precisely. Two Ca^{2+}-calmodulin binding sites (CaM1 and CaM2), one on the N-terminal and one on the C-terminal part of the β-subunit of the cGMP-gated channel were identified using surface plasmon resonance microscopy (Weitz *et al.*, 1998). In contrast to the Ca^{2+}-calmodulin binding domain found on the olfactory CNG channel, the CaM1 sequence does not fit to the amphipathic α-helical model and seem to be unique among calmodulin targets. Indeed, the motif comprises a positively charged amino acid at position 14 instead of a hydrophobic or aromatic residue and bears a large number of Glu/Asp. Thus, CaM1 resembles more an IQ motif, i.e. a motif generally recognised by Ca^{2+} free-calmodulin. Only CaM1 is necessary for channel modulation whereas the function of CaM2 is unknown.

I.D.5.2. MODULATION BY PHOSPHORYLATION/DEPHOSPHORYLATION

The response of cGMP-gated channel to the binding of cGMP is influenced by dephosphorylation. Just after excision of patches from the membrane of frog rod outer

segments, Gordon and coworkers observed a spontaneous increase in apparent agonist affinity. The conversion of the cGMP-activated channel from a low cGMP affinity state to a state of higher sensitivity was blocked by serine/threonine phosphatase inhibitor suggesting that an endogenous phosphatase was involved. In reality, two different phosphatases may play a role : an increase in apparent cGMP affinity was observed when phosphatase 1 was added whereas a decrease in ligand affinity appeared in the presence of phosphatase 2A. This dual action suggested that two sites of phosphorylation may regulate agonist affinity during phototransduction mechanism (Gordon *et al.*, 1992). CNG channels have been also shown to be modulated by protein kinases (Molokanova *et al.*, 1997; Muller *et al.*, 1998). Recently a site for tyrosine phosphorylation was identified on the C-terminal portion of the α-subunit of the BRET cGMP-gated channel (Molokanova *et al.*, 1999a). Because only CNG channels from photoreceptors display this modulation via phosphorylation, studies of chimeras between the α-subunits of the BRET and the rat olfactory channels allowed to localise the phosphorylation site on a specific tyrosine residue (Y498). Y498 is located in the C-linker, i.e. a region shown to be important in coupling ligand-binding to channel gating, and is highly conserved in proteins bearing a binding site for cyclic nucleotides. When this tyrosine is removed from the BRET channel, modulation is reduced by 75%; the residual modulation suggests the existence of additional phosphorylation sites. Considering that deletion of the C-terminal part of the channel totally abolishes the modulation by phosphorylation, the supplementary phosphorylation sites must be located on this cytoplasmic region. Molokanova and coworkers suggest a model for the mechanism of tyrosine phosphorylation/dephosphorylation : in presence of cGMP, the binding of the phosphatase leads to dephosphorylation and promotes channel opening by increasing the affinity for cGMP; at the contrary, when the channel is closed, the tyrosine kinase binds to the channel, phosphorylates it and stabilises the closed conformation by reducing the affinity for cGMP. Hence, modulation by changes in tyrosine phosphorylation is activity-dependent and is interpreted as a positive feedback, maybe present to counterbalance the Ca^{2+}-dependent negative feedback. In a recent work, the effect of genistein, a competitive inhibitor of the ATP binding site on protein kinases, was studied on inside out patches excised from the membrane of *Xenopus* oocytes expressing the α-subunit of the BRET CNG channel (Molokanova *et al.*, 1999b). Cytoplasmic application of genistein prevents changes in cGMP sensitivity that are attributed to tyrosine phosphorylation, slows activation kinetics and reduces the maximal current through CNG channels at saturating cGMP concentrations. These effect are ATP-independent and occur indirectly via the binding of genistein to the

protein tyrosine kinase. This interaction between genistein and the kinase induces a non catalytic interaction between the enzyme and the CNG channel. The consequence is an allosteric inhibition of channel gating. This study allows to confirm that protein kinase catalyses the phosphorylation of the cGMP-gated channel but in addition suggest a second effect of tyrosine kinase on the regulation of channel gating.

I.D.5.3. **OTHER TYPES OF MODULATORS**

I.D.5.3.a. Gaseous Messengers

In addition to its activation by cyclic nucleotides, the native olfactory CNG channel can be independently activated by NO in the form of nitrosonium (NO^+). This ion can interact with sulfhydryl groups. Consistent with this idea, the effect of NO was mimicked by SH-modifying reagents (Broillet and Firestein, 1996). The chemical reaction that leads to the formation of nitrosothiol has been shown to occur *in vivo* (Lander, 1997) thus, this chemical modification may play a role in modulating CNG channels activity in olfactory transduction. Indeed, it has been demonstrated that the native olfactory CNG channel is activated by such a mechanism (Broillet and Firestein, 1996). The target site for S-nitrosylation is a cysteine residue present in the C-linker and conserved in the α- and β-subunits. The report by Berghard *et al.* (1996) of β-subunits but not α-subunits in the vomeronasal organ (results of *in situ* hybridisations) suggested the possibility of homomeric channels constituted by β-subunits only. Broillet and Firestein (1997) tested this hypothesis and concluded that such channels exist, are not activated by cyclic-nucleotides but by NO, present common features with Ca^{2+}-activated channels and may play a role *in vivo*. Indeed, an important role for NO was described in cone photoreceptors (Savchenko *et al.*, 1997). CNG channels are numerous in cones synaptic terminals and endogenous NO was shown to modulate synapses between cones and horizontal cells in lizard retina by triggering neurotransmitter release. NO has been described as a retrograde messenger in brain (O'Dell *et al.*, 1991; Schuman and Madison, 1994) and the discovery of CNG channels in hippocampus (Kingston *et al.*, 1996; Bradley *et al.*, 1997) and elsewhere in the central nervous system (Finn *et al.*, 1996) raises the possibility of a mechanism involving in the brain the action of both NO and cGMP on CNG channels in order to modulate synaptic transmission. Another gaseous messenger, carbon monoxide (CO), was shown to act as a modulator of CNG channels action. Like NO, CO was shown to activate soluble guanylate cyclase (Brüne and Ullrich, 1987; Furchgott and Jothianandan, 1991; Kharitonov *et al.*, 1995), and was proposed to act on synaptic

strength in hippocampus (Stevens and Wang, 1993; Zhuo *et al.*, 1993). In addition a long-lasting form of odour adaptation dependent on a CO/cGMP messenger system was described (Zufall and Leinders-Zufall, 1997) but the way CO is acting (on CNG channels?) is not discussed in this paper.

I.D.5.3.b. Diacylglycerol

Light has been found to stimulate PLC to hydrolyse phosphatidylinositol-4,5-biphosphate (PIP_2) in IP3 and DAG. DAG analogs have been found to allosterically interfere with the rod cGMP-activated channel opening by reducing the apparent affinity of the channel for its ligand and by lowering the maximum current amplitude (Gordon *et al.*, 1995). The action of DAG has been shown to be phosphorylation-independent.

I.D.5.3.c. ATP and GTP

The light response is affected by both ATP and GTP *in vivo*. In rods, ATP has been shown to increase the response of cGMP-gated channels whereas GTP can abolish the action of ATP (Filatov *et al.*, 1989). The action of ATP in cones was shown to change in function of pH variation (ATP enhances the response of cGMP-gated channels at low pH and decreases their response at high pH). The mechanism of modulation by ATP/GTP seem to consist in a change in apparent agonist affinity of CNG channels (Watanabe and Shen, 1997).

I.D.5.3.d. Nickel

The effect of Ni^{2+} ions has been already described in this thesis (see sections I.C.4. and I.D.4.3.). Briefly, it has been shown that Ni^{2+} enhances, at low concentrations, bovine rod CNG channel responses but inhibits the olfactory CNG channel through the binding of two different histidines present respectively in the rod CNG channel (H420) and in the olfactory CNG channel (H396) (Gordon and Zagotta, 1995a,b,c). These histidine residues are located in the C-linker, a region found to play a role in coupling of ligand binding to channel gating. Ni^{2+} binding affects the conformational changes that lead to stabilisation of the open state in the cGMP-activated channel whereas it stabilises the closed state in the olfactory channel. At position 420 an histidine is effectively present in the α-subunits of the bovine and human rod CNG channels (Kaupp *et al.*, 1989; Dhallan *et al.*, 1992) but an asparagine is present in the sequences

of both mouse and rat homologues (Pittler *et al.*, 1992; Bärnstable and Wei, 1995) so that any physiological relevance of the interaction of Ni^{2+} with histidines is controversial.

I.D.5.3.e. Divalent Cations

This feature of divalent cations has already been mentioned in this thesis (see section I.D.2.). Under physiological conditions, with photoreceptor membrane potential around -45 mV, rod CNG channels are always blocked by external divalent cations (Mg^{2+}, Co^{2+}, Cd^{2+}, Ca^{2+}). Blockade by divalent cations occurs on both external and internal sites which are located in the pore of CNG channels. In particular, a highly conserved glutamate residue has been identified as the binding site for external divalent cations in rod, cone and olfactory CNG channels (Root and MacKinnon, 1993; Eismann *et al.*, 1994; Kramer and Siegelbaum, 1992; Kleene, 1995; Frings *et al.*, 1995; Biel *et al.*, 1995; Haynes, 1995). It is thought that the carboxyl group is important to form a high affinity binding site.

I.D.5.3.f. External Protons

A mechanism similar to the one that regulates the block by divalent cations involves external protons. In the catfish olfactory neurons, pH titration combined with mutagenesis studies of Glu 333 (the conserved glutamate involved in the block by divalent cations) have suggested that this pore residue is also involved in protons binding and subsequent channel block (Tanaka, 1993; Root and MacKinnon, 1994). In some cases, protons have been shown to activate CNG channels : protonation of D604 in the rod CNG channel may enhance the interaction between the binding site and the cyclic-nucleotide triggering the allosteric changes that lead to channel opening (Varnum *et al.*, 1995; Gordon *et al.*, 1996).

I.D.5.3.g. Peptide Blockers

The structural similarities between CNG- and VG-channels has been already analysed in this thesis (see section I.C.3.). Despite their totally distinct gating mechanisms, CNG- and VG- channels share features that reflect their structural homologies. Hence, the 20 amino acid "ball peptide" derived from the Shaker K^+ channel and responsible for its rapid inactivation has been transferred to CNG channels where it induced channel block (Kramer *et al.*, 1994). This channel blockade was characterised by a selective

action on open CNG channels and a consequent prevention of channel closure; the inactivation peptide interact with the pore forming region of CNG channels. Recently a peptide blocker that can be used as a pharmacological tool has been extracted from the venom of a snake and purified (Brown *et al.*, 1999). When applied to the extracellular face of membrane patches containing the α-subunit of the rat olfactory CNG channel, this peptide called pseudochetoxin, blocked the current carried by CNG channels in a very efficient way (one pseudochetoxin was enough). This blockade was found to be more efficient on the homomeric than on the heteromeric version of the olfactory CNG channel.

I.D.5.3.h. Tetracaine

Tetracaine is a local anaesthetic which has been shown to block the BRET but not the rat olfactory CNG channel (Fodor *et al.*, 1997). Studies of chimeras failed in identifying a specific sequence of interaction with tetracaine. The mechanism of this blockade is state-dependent because tetracaine binds more tightly to the closed channel. A single tetracaine molecule is enough to observe the block. In addition, this block has been shown to be voltage-dependent. A model for tetracaine block has been proposed : interactions between tetracaine and the inner mouth of the pore could lead to tighter binding to closed channels and stabilisation of the closed conformation. An increase in the width of the pore when the channel opens could lead to the disruption of these interactions. Alternatively, repulsion of the pore blocker by cations permeating through the open channel pore have been envisaged.

I.D.5.3.i. Calcium Channels Blockers

L-*cis*-diltiazem, the inactive isomer of a calcium channel blocker was the first blocker of CNG channels to be discovered (Koch and Kaupp, 1985). In the rod channel, the efficiency of this block depends on the β-subunit (Chen *et al.*, 1993). This drug is less effective for olfactory CNG channels (Frings *et al.*, 1992). Pimozide blocks the rod cGMP-gated channel (Nicol, 1993) whereas D-600 and nifedipine act on the olfactory CNG channels (Frings *et al.*, 1992; Zufall and Firestein, 1993)

I.D.5.3.j. Nicotine

Nicotine has been reported to stabilise the closed conformation of the rod CNG channel (McGeoch *et al.*, 1995).

I.D.5.3.k. Polyamines

Polyamines have been shown to block the pore of inward rectifiers K^+ channels as well as some glutamate-gated channels. They have thus been tested also on CNG channels and in particular on the retinal cGMP-gated channel which was shown to be blocked by polyamines from both sides of the membrane. Because polyamines are constituents of both intra- and extra-cellular media, they may play a physiological role of modulation of CNG channels, for example as suppressor of the noise in the phototransduction process (Lu and Ding, 1999).

II. MATERIALS AND METHODS

In order to study the relationship between structure and function in the pore of CNG channels, methods of molecular biology (site-directed mutagenesis, *in vitro* RNA synthesis) were combined to techniques of electrophysiology (patch-clamp). The corresponding protocols are given in the next section (II.A.). Then, the methods of molecular biology and protein biochemistry used for studying the C-terminal part of the BRET are described in section II.B.

II. A. THE PORE OF CNG CHANNELS

The technique of substituted-cysteine accessibility method (SCAM) was applied to the pore of CNG channels in order to determine its structure. In the α subunit from the bovine rod, the pore loop is formed by the residues R345-S371, here called R1-S27. The SCAM is a technique of site-directed mutagenesis which consists in mutating to cysteine one at a time every residue of a segment of interest in the sequence of an ionic channel, to express the mutants in heterologous cells and determine whether the cysteine react with small charged sulfhydryl-specific reagents. If the function of the channel is altered, the cysteine is accessible i.e. in the water-accessible surface of the membrane-embedded channel (Karlin and Akabas, 1998).

For the SCAM analysis the following series of 56 mutants were designed :

K2C, V4C, Y5C, S6C, L7C, Y8C, W9C, S10C, T11C, L12C, T13C, L14C, T15C, T16C, I17C, G18C, E19C, T20C, P21C, P22C, V24C, S27C

E19A, K2C+E19A, V4C+E19A, S6C+E19A, L7C+E19A, T15C+E19A, T16C+E19A, I17C+E19A, T20C+E19A, P22C+E19A, V24C+E19A, S27C+E19A

C505T, K2C+C505T, V4C+C505T, S6C+C505T, L7C+C505T, T15C+C505T, T16C+C505T, I17C+C505T, T20C+C505T, P22C+C505T, V24C+C505T, S27C+C505T

E19A+C505T, K2C+E19A+C505T, V4C+E19A+C505T, S6C+E19A+C505T, L7C+E19A+C505T, T15C+E19A+C505T, T16C+E19A+C505T, I17C+E19A+C505T, T20C+E19A+C505T, P22C+E19A+C505T,

V24C+E19A+C505T, S27C+E19A+C505T

I designed all the mutants except mutants Y5C, Y8C, W9C, S10C, T11C, L12C, T13C, L14C, G18C.
The different single mutants were designed in order to cover almost the entire pore region. Such a study was previously performed (Sun *et al.*, 1996) but a lower number of functional mutants were then reported. The different E19A-containing mutants were designed to assess their accessibility to Cd^{2+} ions and will be discussed elsewhere. The neutralization of the E19 removes the inhibition produced by low concentrations of cadmium on the w.t., thereby allowing the use of this ion to probe cysteine accessibility. The C505T mutation is necessary to the study of accessibility when the thiol reagents are applied from the intracellular side of the patch.

II.A.1. MOLECULAR BIOLOGY

II.A.1.1. DNA MATERIAL

The cDNA encoding for the α subunit of the BRET CNG channel (Kaupp *et al.*, 1989) was provided by the laboratory of Pr. U. B. Kaupp (Institut für Biologische Informationsverarbeitung, Forschungzentrum Jülich, Jülich, Germany), cloned into a pGEM-3Z (Pharmacia, Uppsala, Sweden) modified vector named pGEM-HE (Fig. 6). The pGEM-HEcG (stands for pGEM-HE containing the cGMP-gated α subunit of the BRET) plasmid was initially transformed into *E. coli* DH5αF' [F'*/endA1 hsdR17* (r_K^- m_K^+) *supE44 thi- 1 recA1 gyrA*(Nal^r) *relA1 Δ(lacIZYA-argF)U169 deoR* (ϕ80*dlacΔ(lacZ)M15*)] competent cells following a classical $CaCl_2$ method (Sambrook *et al.*, 1989). Medium scale DNA preparation was obtained using the Plasmid Midi Kit (Qiagen GmbH, Hilden, Germany).

II.A.1.2. SITE-DIRECTED MUTAGENESIS

Very few mutants, i.e. mutants (T15C, T16C, I17C, E19C, T20C, and the corresponding E19C double mutants) were designed using a classical method of site-directed mutagenesis which is described here below (section II.A.1.2.a.). All the other mutants designed for the SCAM (part III.A.1. and 2.) as well as the one studied in

"Interaction of Na^+ and K^+ in the pore of CNG channels" (part III.A.3.) were engineered using the QuikChange™ Site-Directed Mutagenesis method (Stratagene, La Jolla, CA) which will be described further (section II.A.1.2.b.).

II.A.1.2.a. Classical Method

Cloning and Mutagenesis

In order to prepare the cloning vector the pGEM-HEcG plasmid was digested by *SnaB* I (Promega Corporation, Madison, WI) and *SgrA* I (Boehringer Mannheim, GmbH, Mannheim, Germany). The digestion sample was run on a preparative 1% agarose (FMC® BioProducts, Rockland, MF) gel and the 4.5 kb expected band was then purified by Geneclean (Bio101, Vista, CA). For the insert preparation, the pGEM-HEcG vector was first linearised with *Hind* III (Promega). The linearised DNA was then extracted using the phenol-chloroform method, precipitated with 3 M sodium-acetate, washed with 70% ethanol (for all this method, see Sambrook *et al.*, 1989) and resuspended in Tris-EDTA (TE) 10:1 at a final concentration of 100 ng/µl.
Mutation were then introduced by Polymerase Chain Reaction (PCR) starting from 100 ng of *Hind* III - linearised DNA, 100 ng of the primer forward (5' AGA ACC CCC ACG CAA GGG 3') and 250 ng of the primer back which was the one that introduced the *SgrA* I site (which serves as a checking point - 5' AGA ATC CCT CAC CGG TGG TGG TGT TTC GCC AAT AGT GGT C 3') as well as the desired mutation. The reaction mix additionally contained 250 µM of dNTPs, the Perking Elmer buffer as well as 2 units (U) of the Perkin-Elmer *Taq* Polymerase (Perkin-Elmer Applied Biosystems, Forest City, CA) in a total volume of 100 µl overlaid with mineral oil (Sigma, St Louis, MO). The PCR was performed using a PTC-100™ Programmable Thermal Controller (MJ Research Inc., Waltham, MA) and the following PCR-programme : 94°C, 2 min (denaturation step) followed by 30 cycles at 94°C, 50 sec; 50 °C, 50 sec; 72°C, 30 sec. and finally by an extension step at 72°C, 10 min.
The PCR products were digested by both *SgrA* I and *SnaB* I and the 0.6 kb expected band containing the mutated sequence was purified (Geneclean).
50 ng of the mutated DNA insert was then ligated to 100 ng of the previously prepared vector using 2 U of T4 DNA ligase (New England Biolabs, Beverly, MA) and a 16°C o/n incubation.
E. coli DH5α F' competent cells were then transformed by $CaCl_2$ method with the

ligation products. Minipreps of DNA were obtained following the alkaline lysis protocol (Sambrook *et al.*, 1989).

Mutation Analysis

1 μg of DNA of the putative mutants was digested by *SgrA* I as a first control. Prior to sequencing, the DNA of the positive clones was purified through the Microspin S-400 HR columns (Pharmacia, Uppsala, Sweden). 1-2 μg of this DNA was then used for sequencing the region of interest (see Annex B for the primers) with the T7 sequencing kit (Pharmacia). The sequencing reactions were ran using the CastAway™ Precast Sequencing System (Stratagene).

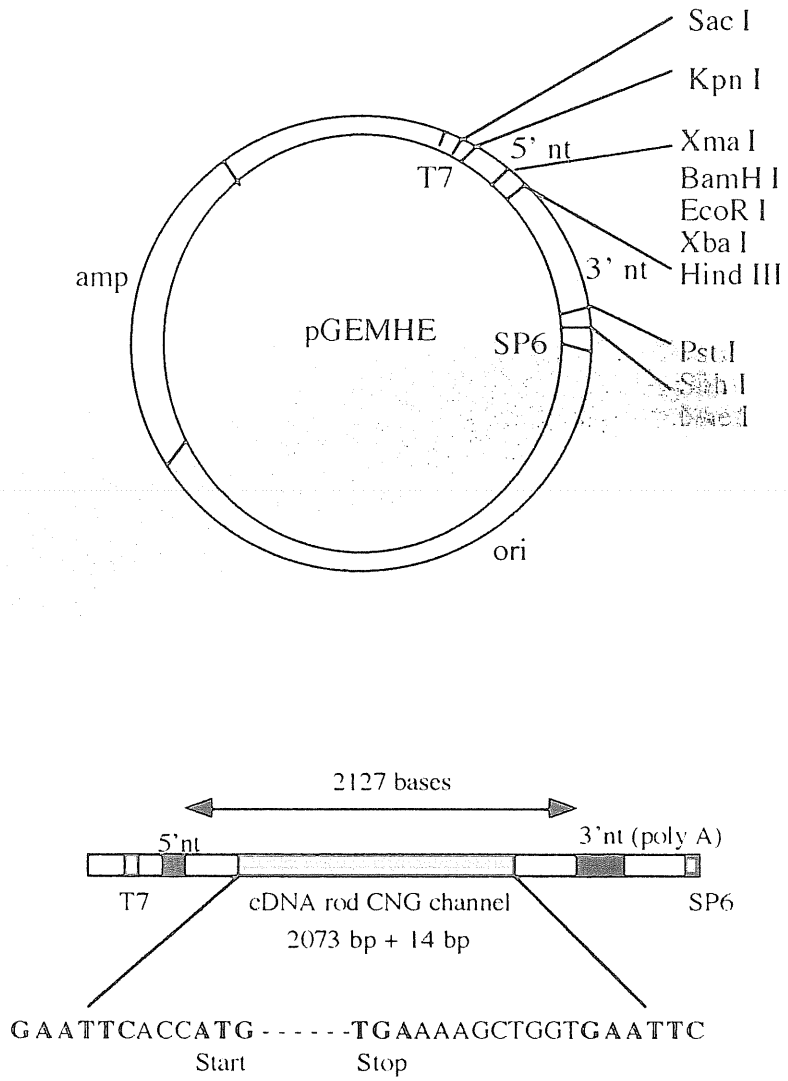

Fig. 6 : Plasmid map from pGEM-HE (Promega).

The cDNA from the bovine rod CNG channel was cloned EcoR I-EcoR I in this plasmid leading to pGEM-HEcG.

II.A.1.2.b. The QuikChange™ Site-Directed Mutagenesis Method

The time consuming "classical method" for mutagenesis was rapidly abandoned in favour of the QuikChange™ Site-Directed Mutagenesis kit (Stratagene). This rapid four step procedure allows to obtain mutants in 2-3 days with a minimal efficiency of 33% (the analysis of 3 putative clones only always allowed to identify a real positive clone). The efficiency of mutagenesis calculated for the pWhitscript™ positive control provided in the kit was of 62%.

The basic procedure is summarised in Fig. 7. The QuikChange™ Site-Directed Mutagenesis system uses the *Pfu* DNA polymerase, which replicates with a higher fidelity (estimated error rate of 1.3 x 10^{-6} compared to the 8 x 10^{-6} of the *Taq* polymerase) both strands of any supercoiled plasmid DNA template avoiding the step of linearisation classically required. The primers containing the mutation to be introduced are 2 overlapping primers ideally designed in the way to be 25-45 bases in length, with a minimal G-C content of 40% and a melting temperature of at least 70°C (recommended temperature : 78°C). The primers, complementary to each strand of the vector, extend during temperature cycling by means of *Pfu* polymerase. On incorporation of the oligonucleotide primers, a mutated plasmid containing 2 overlapping nicks is generated. Following temperature cycling, the product is treated with *Dpn* I, an endonuclease able to recognise methylated or hemimethylated DNA (target sequence: 5'-G^{m6}ATC-3') and therefore used to digest the parental DNA template (DNA isolated from almost all *E. coli* strains is *dam* methylated and can be recognised by *Dpn* I). The nicked DNA vector containing the desired mutation is then transformed into Epicurian Coli® XL1-Blue supercompetent cells by simple heat-shock.

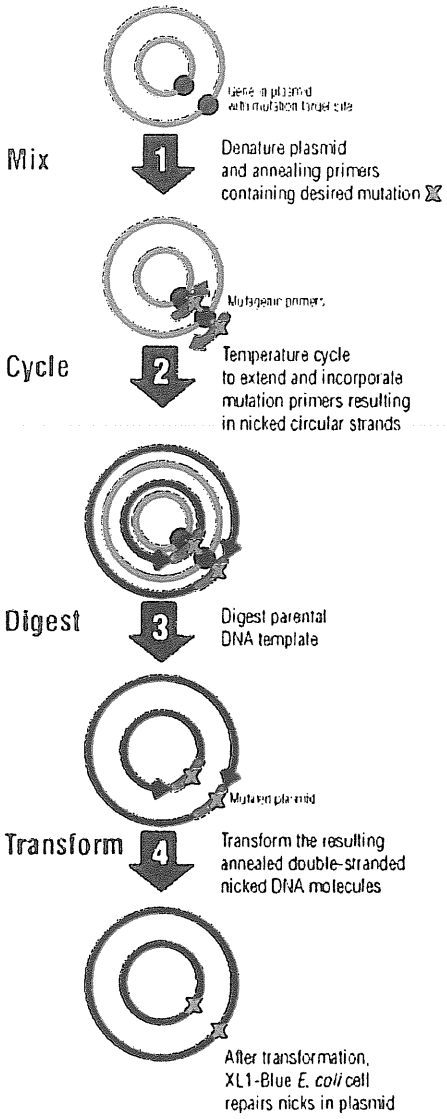

Fig. 7 : Overview of the QuikChange™ site-directed mutagenesis method.

The reaction mix for the QuikChange™ was done using 50 ng of the pGEM-HEcG plasmid containing the BRET cDNA and following the instructions of the manufacturer.

All the pipetting steps were done using small 10 µl ART® pipet tips with filter, which were sterile and RNase/DNase free (Molecular Bio-Products Inc., San Diego, CA). The tubes used for each reaction sample were the Thin-Wall Tubes (Stratagene). The cycling reactions were performed using a PTC-100™ thermo-cycler (MJ Research) and the following cycling parameters : 95°C, 30 sec. (denaturation step) followed by either 12 cycles (for single point mutations) or 16 cycles (for 2-3 bases change) at 95°C, 30 sec; 55 °C, 1 min; 68°C, 10 min (2min/kb of plasmid length). Following the cycling, the reactions were cooled down on ice and subsequently treated with *Dpn* I to digest the parental DNA. *Dpn* I-treated samples were transformed into Stratagene XL1-Blue supercompetent cells (30-50 µl) using a classical $CaCl_2$ method with a 42°C heat shock of 45 sec. Plating of the transformations were done on LB+amp Petri dishes.

For each putative mutant, 3 colonies were picked up from the plates and grown for subsequent DNA minipreps achieved using either the Qiagen Plasmid Mini Kit (Qiagen) or the Talent equivalent (Talent srl, Trieste, Italy).

For controlling the accuracy of mutagenesis, 1 µg of each putative mutant was sequenced using the *SequiTherm EXCEL* II *Long-Read* DNA Sequencing Kit-LC (Epicentre Technologies, Madison, WI) with 1 pmol of one of the following primers chosen depending on the region of interest: CNG-147, CNG-313 or CNG-481 (see Annex B). All the oligonucleotide primers were fluorescently modified (IRD41-labelling) to allow the automated DNA sequencing by the LI-COR automated DNA sequencer (4000L type) (LI-COR, Lincoln, NE).

One positive clone was chosen for each mutant in order to prepare its DNA in larger scale using the Qiagen Plasmid Midi Kit (Qiagen).

All mutants were sequenced completely with the LI-COR automated DNA sequencer (4000L type). In addition to the so called CNG-147, -313, -481 primers, the T7 primer (2 pmol) and a reverse primer termed CNG-reverse were needed to cover the entire BRET sequence (see Annex B). Depending on the quality of the sequencing gels four primers were often sufficient. The sequences obtained for all the mutants were of very high quality an reproducibility (with the exception of several sequences when the T7 primer was used). This allowed us to have a high confidence in the mutants nature and in the subsequent electrophysiological data.

II.A.1.3. **RNA SYNTHESIS**

5 to 10 µg of DNA coming from the midipreps were then used for synthetizing cRNAs for the w.t. and the mutant channels in the aim of injecting them into *Xenopus* oocytes.
The DNA was first linearised by *Nhe* I (New England Biolabs), extracted, precipitated, washed and finally resuspended in 5-10 µl DEPC-treated ddH_2O. From this step on, all the precautions for working in RNase-free conditions were taken.
In vitro transcription was performed using the T7 RNA polymerase and the mCAP™ RNA Capping Kit (Stratagene). Once the transcription completed, the remaining DNA was removed by *DNase* I treatment and the RNA was extracted following a classical phenol/chloroform method. After resuspension in DEPC-treated ddH_2O, RNAs were precipitated with sodium acetate (2M) for 1 hour at -20°C. Following this precipitation step a 50-60 min high speed centrifugation at 4°C was performed. These precipitation/centrifugation steps were repeated once for eliminating any residual impurity. RNAs were finally resuspended in DEPC-treated ddH_2O and aliquots suitable for microinjection were made (2µl aliquots at about 1 µg/µl).

II.A.2. **ELECTROPHYSIOLOGY**

The electrophysiological experiments carried out in this thesis consisted in recording the currents activated by cGMP in w.t. and mutant CNG channels heterologously expressed in *Xenopus laevis* oocytes. The recordings were performed in excised patches in inside-out and outside-out configuration.

II.A.2.1. **CHEMICALS**

Unless specified, all chemicals were purchased either from Sigma or from Merck (Darmstadt, Germany).

II.A.2.2. **ISOLATION AND PREPARATION OF XENOPUS OOCYTES**

The *Xenopus laevis* frogs were anaesthetised by immersion in a 0.2% solution of tricaine methanesulfonate for about half an hour. The anaesthetised animal was put on

its back above a bed of ice and a small incision of about 1 cm was performed with a scalpel laterally on its abdomen. Once the skin and the underneath abdominal muscles were incised, ovary lobes became visible. The follicles (oocytes and follicle cells) were surgically removed from frogs ovary and placed in Barth's solution (in mM : 88 NaCl, 1 KCl, 0,82 $MgSO_4$, 0,33 $Ca(NO_3)_2$, 0,41 $CaCl_2$, 2,4 $NaHCO_3$, 5 Tris-HCl, pH 7.4). Follicles were then separated in small groups containing about ten oocytes and incubated for 1h in Barth's solution without calcium but supplemented with 1mg/ml of collagenase. After the collagenase treatment, oocytes were washed extensively with Barth's solution and the residual follicle cells were removed manually with fine forceps. At this step the healthiest defolliculated oocytes presenting two clearly delineated hemispheres were selected. These oocytes were transferred in Barth's solution supplemented with gentamicin (50mg/ml) until microinjection.
Injection needles of about 10 μm of tip diameter were made from borosilicate glass capillaries (World Precision Instruments, Sarasota, FL) by using an horizontal puller (BB-CH-PC, Mecanex S.A., Geneva, Switzerland). Oocytes were injected under a binocular microscope at low magnification (Olympus, Japan) using a manual microinjector (CellTram Air, Eppendorf, Germany). About 100-200 nl of capped cRNA (at approximatively 1 μg/μl in DEPC-treated ddH_2O) were injected in each oocytes. Once injected, oocytes were maintained in Barth's solution with gentamicin (50mg/ml) and incubated at 19°C for 2-5 days. Just before patch-clamp experiments, the vitelline membrane was removed from the oocytes under visual control in a hyperosmotic medium. During the experiments, oocytes were kept in Ringer solution: (in mM) 110 NaCl, 2.5 KCl, 1 $CaCl_2$, 1.6 $MgCl_2$, 10 HEPES-NaOH, pH 7.4 (with NaOH).

II.A.2.3. **SOLUTIONS**

The patch pipette was filled with (in mM): 110 NaCl, 10 HEPES-tetramethylammonium hydroxide (TMAOH), 0.2 EDTA (titrated at pH 7.6 with TMAOH). Neutralising the solution with TMAOH did not significantly affect either the macroscopic or the single channel current (some experiments, as for example the ones described in section III.A.3.4., were done buffering the NaCl-based solutions with NaOH and the KCl-based solutions with KOH as a control). Solutions bathing the intracellular side of the membrane had the same composition as that filling the patch pipette, supplemented, when necessary, with cGMP. For ion selectivity experiments, the chloride salts of the different monovalent alkali cations were substituted in turn to NaCl in the bath solution (see below).

II.A.2.4. RECORDING APPARATUS

Currents from inside-out and outside-out patches (Hamill et al, 1981) were recorded with a patch-clamp amplifier (Axopatch 200B, Axon Instruments Inc., Foster City, CA, USA). Borosilicate glass pipettes (Brand GmbH, Wertheim, Germany) had resistances of 2-5 MΩ, in symmetrical NaCl solutions. For the SCAM study, patch currents were low-pass filtered at 10 kHz and stored on PCM\VCR. During the analysis, single-channel traces were low-pass filtered again at 2 kHz and sampled at 5 kHz (pClamp6 hardware and software, Axon Instruments). Macroscopic currents measured at constant membrane potential were digitised from PCM/VCR at 50 Hz. Currents for current-voltage relations were low-pass filtered at 1 kHz and acquired on-line (at 5kHz) with pClamp6. For the study of interaction of Na^+ and K^+ ions in the channel pore, the macroscopic currents were digitised using a DAT instead of a PCM/VCR system. In order to properly resolve the brief current transient shown in Fig. 24, currents were recorded at a bandwidth up to 10 kHz and were sampled at 30 kHz. If a lower bandwidth up to 2 kHz was used, current transients were significantly distorted. The perfusion system was as previously described (Menini et Nunn, 1990; Sesti *et al.*, 1996).

II.A.2.5. ANALYSIS OF CYSTEINE MUTANTS PROPERTIES

Macroscopic and single-channel currents were analysed with pClamp6 or SigmaPlot (Jandel). Single-channel conductance and Po were determined from the analysis of amplitude histograms of currents from patches containing a limited number of active cGMP-gated channels. Amplitude histograms were fitted as the sum of two or more gaussian functions, by using pClamp software. Data are usually given as mean SEM.
For cGMP dose-response experiments, the theoretical curve was a Hill equation of the form:

$$I/Imax = \{1 + (Kd /[cGMP])^n\}^{-1} \qquad (1)$$

where Imax = current produced by 1 mM cGMP, n = Hill coefficient, Kd = concentration of cGMP which yields 50% of the maximal current.

For the ionic selectivity experiments, permeability ratios relative to Na^+ (P_X/P_{Na}) were computed from the reversal potential Vrev obtained with experiments with 110 mM Na^+ in the patch pipette and 110 mM of ion X in the medium bathing the intracellular side of the membrane. The voltage offset between the extracellular and intracellular

sides of the membrane was routinely zeroed in the presence of a symmetrical solution on both sides of the membrane. The liquid junction potential between a patch pipette filled with 110 mM NaCl and the bath solution containing an equimolar amount of one of the other monovalent cations was about -2 mV in the case of LiCl and less than 1 mV in the other cases. Therefore, measured Vrev was not corrected for junction potentials (Menini, 1990). Px/PNa was calculated from the equation:

$$P_X / P_{Na} = ([Na]o/[X]i) \exp(-F\,Vrev / RT) \qquad (2)$$

where P_{Na} and P_X are the permeabilities to Na^+ and X^+; [X]i and [Na]o are, respectively, the concentrations of the ion X (either Li, Na, K, Rb or Cs) in the bath and sodium in the pipette, Vrev is the reversal potential of the cGMP-activated current, F is the Faraday constant, R is the gas constant and T is the absolute temperature.

II.A.2.6. **ACCESSIBILITY EXPERIMENTS**

Methane thiosulfonate (MTS) reagents were purchased from Toronto Research Chemicals Inc. (Ontario, Canada). They were always dissolved in the appropriate solution at 2.5 mM before the experiment, and applied to the patch within about 30 min. A relatively high concentration of MTS compounds is necessary when performing SCAM studies (Kurz *et al.*, 1995; Pascual *et al.*, 1995; Sun *et al.*, 1996; Kuner *et al.*, 1996; Wilson and Karlin, 1998), because the time course of the hydrolysis of thiosulfonates in saline solution at pH 7.6 is not known with precision (Karlin and Akabas; 1998). This time course, however, is similar for 2-aminoethylmethane thiosulfonate (MTSEA) and 2-trimethylammonioethylmethane thiosulfonate (MTSET) (Karlin and Akabas, 1998). Furthermore, control experiments performed on mutants sensitive to MTS compounds, like T20C and P22C, showed that in our experimental conditions MTSEA and MTSET were still completely effective 30 min after dissolvement (data not shown).

II.A.2.6.a. Accessibility to MTS Compounds from the Inner Side

Pipette contained (in mM): 110 NaCl, 10 HEPES, 0.2 EDTA (standard solution, buffered with tetramethylammonium hydroxide, at pH 7.6). Inside-out patches were perfused with the same solution supplemented, when necessary, with 0.5 mM cGMP and/or the appropriate MTS compound (2.5 mM). Current gated by cGMP was the difference between the currents in the presence and in the absence of cGMP. After

allowing current and baseline stabilisation, by applying cGMP several times, the MTS reagent was applied for 2-3 min. We followed the MTS effect continuously, at -40 mV, either in the presence (open state) or in the absence (closed state) of cGMP (Fig. 14). After washout, we measured the residual current for comparison with the initial current. At least once for each tested mutant, we also applied consecutive 200 ms voltage steps between -100 and +100 mV (20 mV increments; holding potential was 0 mV; Fig. 14), to study the I/V relations before, during and after MTS application. I/V relations potentially provide more information about mutant channel behaviour during gating. When the current inhibition was irreversible, as expected for a block due to covalent reaction of MTS with substituted cysteines, we perfused the inside face of the patch with Ringer solution. This procedure always activated oocyte's calcium-dependent chloride channels (Stuhmer, 1992), and reassured us that the absence of a cGMP-activated current was not caused by the formation of a vesicle preventing the perfusion solution from reaching channels contained within the membrane patch. In the absence of MTS compounds, all mutants (except I17C) showed stable currents for at least 10 min.

II.A.2.6.b. Accessibility to MTS Compounds from the Outer Side, in the Open State

The cGMP-activated current was measured from outside-out patches as the difference between the currents in the absence and in the presence of 5 mM external $MgCl_2$. Pipette (internal side) contained our standard solution supplemented with 0.5 mM cGMP, whereas $MgCl_2$ was added to the bath standard solution. Mg^{2+} ions completely block cGMP-gated currents from the extracellular side, at negative membrane potentials (Colamartino et. al., 1991; Ildefonse and Bennett, 1991; Karpen *et al.*, 1993; Root and MacKinnon, 1993; Sun *et al.*, 1996). The effect of 5 mM $MgCl_2$ on the basal - leak - current, i.e. in the absence of cGMP, was negligible (data not shown). MTS compounds were applied for 2-3 min in the bath. The time course of their effect was usually followed at -40 mV. As for the intracellular experiments, whenever possible I/V relations were obtained before and after the effect of MTSET. In this case, however, membrane potential was stepped from -100 to +40 mV, because the Mg^{2+} block is voltage dependent and complete only up to about +40 mV (Colamartino *et al.*, 1991; Root and McKinnon, 1993).

II.A.2.6.c. Accessibility to MTS Compounds from the Outer Side, in the Closed State

Inside-out experiments were carried out with MTSET in the pipette and, after measuring the initial current immediately after excision, followed the current kinetics at -40 mV, by sampling the residual current with brief applications of cGMP (Sun *et al.*, 1996). In these experiments, MTSET was constantly present on the outer side of the patch, from the moment of seal formation. Therefore, in mutants accessible from the outer side of the plasma membrane, we could follow the inhibition time course only when the procedure of seal formation and patch excision took about 20-30 sec. Otherwise, no cGMP-gated current was measurable in the presence of MTSET, even in patches excised from oocytes expressing high levels of CNG current (data not shown; see also Sun *et al.*, 1996).

II.B. CLONING EXPRESSION AND PURIFICATION OF THE C-TERMINAL PART OF THE BRET

This section describes a method to clone the C-terminal part of the α-subunit of the bovine rod CNG channel into a bacterial expression vector which provides a His-tag useful for purification purposes. The protocols for heterologous expression and protein purification are detailed here below. They represent a useful starting point to elaborate a more complete method for obtaining a pure protein solution necessary to envisage crystallisation trials.

II.B.1. CLONING

For cloning purposes a *Pst* I site was introduced in pGEM-HEcG using the QuikChange™ Site-Directed Mutagenesis procedure (see section II.A.1.2.b. for detailed description) by the means of the two following primers:

primer for	5' G GTG CGC ATT TCT GCA GAC TGT GAA GC 3'
primer back	5' GC TTC ACA GTC TGC AGA AAT GCG CAC C 3'

The mutation introduced consisted in changing the second base of the codon encoding for the amino acid 478 located in the hydrophobic segment of the cytoplasmic C-terminal part of the BRET. The T -> C conversion led to the 5' CTGCAG 3' *Pst* I recognition sequence (see Annex A).
After the mutagenesis, pGEM-HEcG was double digested with *Pst* I and *EcoR* I (New England Biolabs) for isolating the DNA fragment corresponding to the C-terminal part of the BRET starting at the amino acid 480 with a 3' protruding end and finishing at the last residue of the channel sequence, amino acid 690. The fragment of interest (0.6 kb) was purified by Geneclean (Bio101).
The expression vector chosen for cloning the C-terminal part of the BRET was the pTrcHis B vector of Invitrogen (Invitrogen Corporation, San Diego, CA). The pTrcHis vectors are pUC derived expression vectors designed for efficient and inducible expression of recombinant proteins in *E. coli*. In addition, these vectors contain a tag composed of six histidine residues at the N-terminal peptide. This tag has a high affinity for the nickel of the ProBond™ resin and is therefore a system of choice for rapid and limited-step protein purification.
Following pTrcHis B digestion by *Pst* I and *EcoR* I, the digest was purified on a low-

melting-agarose gel (Sambrook *et al.*, 1989). 50 ng of insert was ligated to the same quantity of vector o/n at 16°C using the T4 DNA ligase.
After DNA miniprep the nature of the ligation product was checked first by restriction analysis and subsequently the complete sequence of the cloned C-terminal part of BRET -termed "cyto"- was controlled using the LI-COR DNA sequencer.

II.B.2. **EXPRESSION**

For propagation of the pTrcHis B-cyto plasmid, the construct was transformed by a classical $CaCl_2$ method into *E. coli* TOP10 [F', *mcr*A Δ(*mrr-hsd*RMS-*mcr*BC) ϕ80*lac*ZΔM15 Δ*lac*X74 deoR recA1 *ara*D139 Δ(*ara-leu*)7697 *gal*U *gal*K *rps*L *end*A1 *nup*G].
In order to find the right conditions of expression, a pilot expression was performed and the content of several fractions of the bacterial membrane and cytoplasm were analysed on 10% SDS-polyacrylamide gels. The marker used for indicating the protein size was the Kaleidoscope from BioRad (BioRad, Hercules, CA). Transfert of the protein on nitrocellulose was done using the Western blot technique (Sambrook *et al.*, 1989) and the presence of the cyto recombinant protein was assessed by ECL detection (Amersham, Amersham, UK) using the AntiXpress™ antibody as a primary antibody (diluted 1/5000, Invitrogen) and the Antimouse-HRP (Pierce Chemical Company, Rockford, IL) as a secondary antibody (diluted 1/2000). The recombinant protein was essentially present in the membrane fraction.
Bacteria were grown at 37°C to an OD_{600} = 0.6. Once the mid-log phase was reached, the expression of the recombinant protein was induced by IPTG (final concentration of 0.5-1 mM) and the temperature was switched to 30°C. The expression was stopped after 2 hours of incubation.

II.B.3. **PURIFICATION**

The purification of the cyto recombinant protein was done under denaturing conditions using the solutions provided in the Xpress™ System kit of purification (Invitrogen) and following instructions of the manufacturer. Briefly, the bacterial culture was centrifuged and the bacterial pellet was resuspended in guanidium lysis buffer (6M guanidine hydrochloride, 20 mM sodium phosphate, 500 mM sodium chloride, pH7.8). Slow rocking was performed to assure the cell lysis. The subsequent

sonication steps were done on ice using an Ultraturax sonicator (Janke & Kunkel GmbH, Staufen Germany) on position 5 (3 x 5 sec pulses). After a RNase / DNase treatment of the lysate, the insoluble debris were removed by centrifugation (3000 g, 15 min). The sheared lysate was then batch bound to the preequilibrated ProBond™ resin (10 min on a rotative wheel, at 4°C). Column washings were performed in batch mode using a decreasing pH gradient as described in the Xpress™ System manual (8 M urea, 20 mM sodium phosphate, 500 mM sodium chloride - successive pH : 7.8, 6, 5.3). The elution was done by gravity applying the denaturing elution buffer of the kit (8M urea, 20 mM sodium phosphate, 500 mM sodium chloride, pH 4). Fractions of 1ml were manually collected and the elution was monitored measuring the OD_{280}. The fractions containing the peak of absorbency were submitted to the Bradford test (Sambrook *et al.*, 1989) for determining the amount of protein present. Aliquots of the fractions of interest were boiled, supplemented with 1% β-mercaptoethanol or 100 mM DTT and run on 10% SDS-polyacrylamide gels subsequently stained with Coomassie blue (Sambrook *et al.*, 1989). When run without β-mercaptoethanol or DTT cyto had the tendency of forming multimeres.

II.B.4. **BINDING EXPERIMENTS**

The radioactivity was purchased from NEN™ (NEN™ Life Science Products Inc, Boston, MA). The [^{3}H]cGMP specific activity was of 7.4-8.2Ci/mmol (variation from one confection to another) and its concentration 1mCi/ml. Before use, the radioactivity was diluted in Tris-HCl 20mM, pH7.5.

Unless otherwise specified, the chemicals were purchased either from Merck or from Sigma.

All the methods used were based on an incubation period of the radioligand together with the purified cyto protein. After this incubation time, the aim was to isolate the [^{3}H]cGMP-cyto complex and estimate the quantity of ligand bound by the protein counting the radioactivity using a Tri-Carb 2100 TR Liquid Scintillation Analyzer (Packard Instruments Company, Meriden, CT). Cold ligand was also used in excess in order to displace the radioligand eventually bound to the protein and in this way assess the specificity of the binding. A protein whose binding capability to cAMP and cGMP was previously checked was always used as a positive control (cAMP Binding Protein purchased from Sigma).

The methods tried were the following : precipitation of the [^{3}H]cGMP-cyto complex with polyethyleneglycol (PEG), precipitation with ammonium sulphate [$(NH_4)_2SO_4$],

separation of the [^{3}H]cGMP-cyto complex from the free ligand by centrifugation (using the Microcon 10 from Amicon Inc., Beverly, MA) or by filtration using the Whatman GF/B or nitrocellulose filters purchased from Sigma.

The experimental device used for the equilibrium dialysis experiments is represented in Fig. 8. The method consists of dialysing the protein against a large volume of buffer containing the radioligand. Aliquots of cyto protein were added to small bags made of dialysis tubing (Spectrum Laboratories Inc., Rancho Dominguez, CA). The bags were then tied and put in Pyrex tubes containing the buffer (Tris-HCl 20 mM pH7.5, 10 mM EDTA, 200 mM NaCl, 1 mM DTT) as well as the radioligand. A small magnetic stirrer was put in the tubes subsequently screw capped and put (unless otherwise specified) at 4°C for o/n incubation. The radioactivity was measured on aliquots of identical volumes taken from the external medium and from the bags. For counting the radioactivity, the samples were put in scintillation vials together with Filter Count or Ultima Gold scintillation liquids (Packard).

Experimental device :

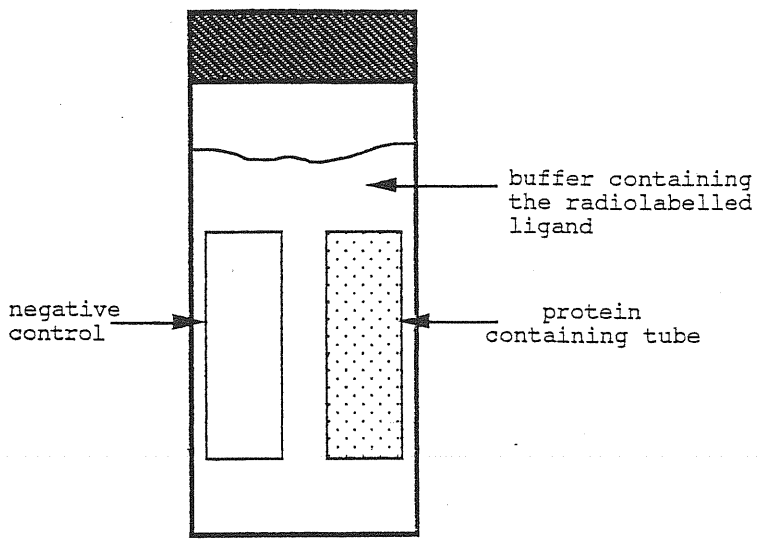

the principles of an equilibrium dialysis experiment

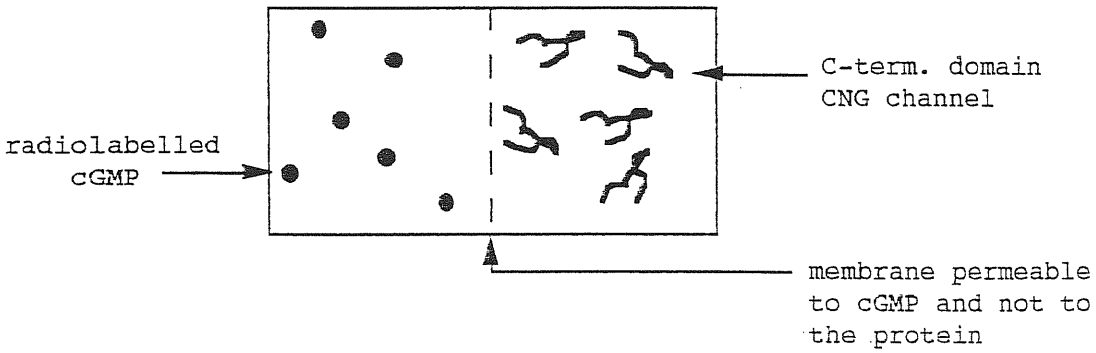

at the equilibrium, there are a concentration g_{free} of free cGMP and a concentration g_{tot} (g_{tot}= free cGMP + bound cGMP)

if g_{tot} is greater than g_{free} there is binding

Fig. 8 : The Equilibrium Dialysis : experimental device and principles.

III. RESULTS

III.A. STRUCTURE / FUNCTION OF THE CNG CHANNEL PORE

SCAM was applied to the α subunit of the bovine rod CNG channel (here called either w.t. or BRET; Kaupp *et al.*, 1989). When expressed in *Xenopus laevis* oocytes, w.t. channels form homomultimers (probably tetramers, Zagotta and Siegelbaum, 1996) with the main properties of native channels (Kaupp *et al.*, 1989).
SCAM consists in mutating to cysteine one at a time every residue of a segment of interest in the sequence of an ionic channel, to express the mutants in heterologous cells and determine whether the cysteine react with small charged sulfhydryl-specific reagents. If the function of the channel is altered, the cysteine is accessible i.e. in the water-accessible surface of the membrane-embedded channel (Karlin and Akabas, 1998).
This technique was applied to the pore residues of the bovine rod CNG channel in order to get some insights in the structure of the CNG channel pore. Before going into the details of the results of the substituted cysteines accessibility to methanethiosulfonate (MTS) sulfhydryl-specific compounds, the properties of the cysteine mutants are described.

III.A.1. PROPERTIES OF THE CYSTEINE MUTANTS

In CNG channels, the channel pore is thought to be formed by the loop which connects the S5 and S6 transmembrane domains of each subunit. This loop which is also termed P region plays fundamental roles as it determines ion selectivity and participates in gating. In the α subunit of CNG channels from bovine rod, the pore loop is formed by the residues R345-S371, here called R1-S27.
In this chapter of the thesis the characteristic features of the mutant P21C will only be briefly mentioned as the third part of the Results section is entirely dedicated to the replacement of this particular proline (see section III.A.3.).

III.A.1.1. EXPRESSION OF CYSTEINE MUTANTS

The following aminoacid residues were substituted with cysteines: K2, V4, S6, L7, Y8, W9, S10, T11, L12, T13, L14, T15, T16, I17, G18, T20, P21, P22, V24, S27. The experiments were carried out at room temperature, on inside-out patches excised from *Xenopus* oocytes, in symmetrical NaCl and in the absence of divalent cations. No current was measurable from mutants Y5C, Y8C, S10C, T11C and L14C. Mutants W9C, L12C, T13C, I17C and G18C had a consistent tendency to low expression. Macroscopic currents from these mutants were only measurable 4-6 days after injection, while w.t. macroscopic currents were always easily recorded 24-48 hours after injection. W.t. current properties remained stable for at least 6 days after injection. No major difference was found in the expression of the other mutants.

III.A.1.2. MACROSCOPIC I/V RELATIONS

Currents flowing through w.t. channels expressed in *Xenopus* oocytes (Kaupp *et al.*, 1989; Sesti *et al.*, 1996; Fodor *et al.*, 1997) outwardly rectify, to some extent. Current amplitude at +100 mV is 20-30 % larger than it is at -100 mV. Fig. 9 shows current traces and corresponding I/V curves for w.t. channels and for a number of cysteine mutants representative of the different observed behaviours (for P21C see Fig. 24a). Mutants K2C, V4C, S6C and L7C, located within the amino-terminal segment of the P region, had macroscopic currents indistinguishable from the w.t. ones, with the exception of L7C whose outward rectification was more pronounced (data not shown). I/V relation from S6C is shown for comparison with w.t. (Fig. 9). Mutants belonging to the carboxy-terminal portion of the P region, i.e. T20C to S27C, also had I/V curves similar to the w.t.'s except P21C which exhibited a significant outward rectification (see section III.A.3.1. and Fig. 24a). On the other hand, macroscopic currents from mutants within the central segment of the pore loop, i.e. between W9C and T16C, were altered. Mutant L12C was a strong outward rectifier, at the steady state (Fig. 9). In 8 experiments, the current at -100 mV was 16% ± 2% of the current at +100 mV. Moreover, the development of the steady-state current showed a time dependence absent in w.t. and in most of the other mutants (see Discussion). W9C (Fig. 9) and T13C (not shown) showed a similar, though less pronounced, behaviour. The steady state current at +100 mV was about twice the current at -100 mV. On the other hand, rectification in T16C was moderate and it was inwardly directed (Fig. 9). The steady state current at +100 mV was 46% ± 3% of the current at -100 mV (n = 12). In this case, too, we observed a time dependence in the activation of the cGMP-

activated current, showing that gating was affected in a complex way. Due to the low Po, only single channel currents activated by cGMP were measurable in patches containing G18C channels. Currents from I17C mutant progressively decayed during continuous recording in inside-out patches and will be described below.

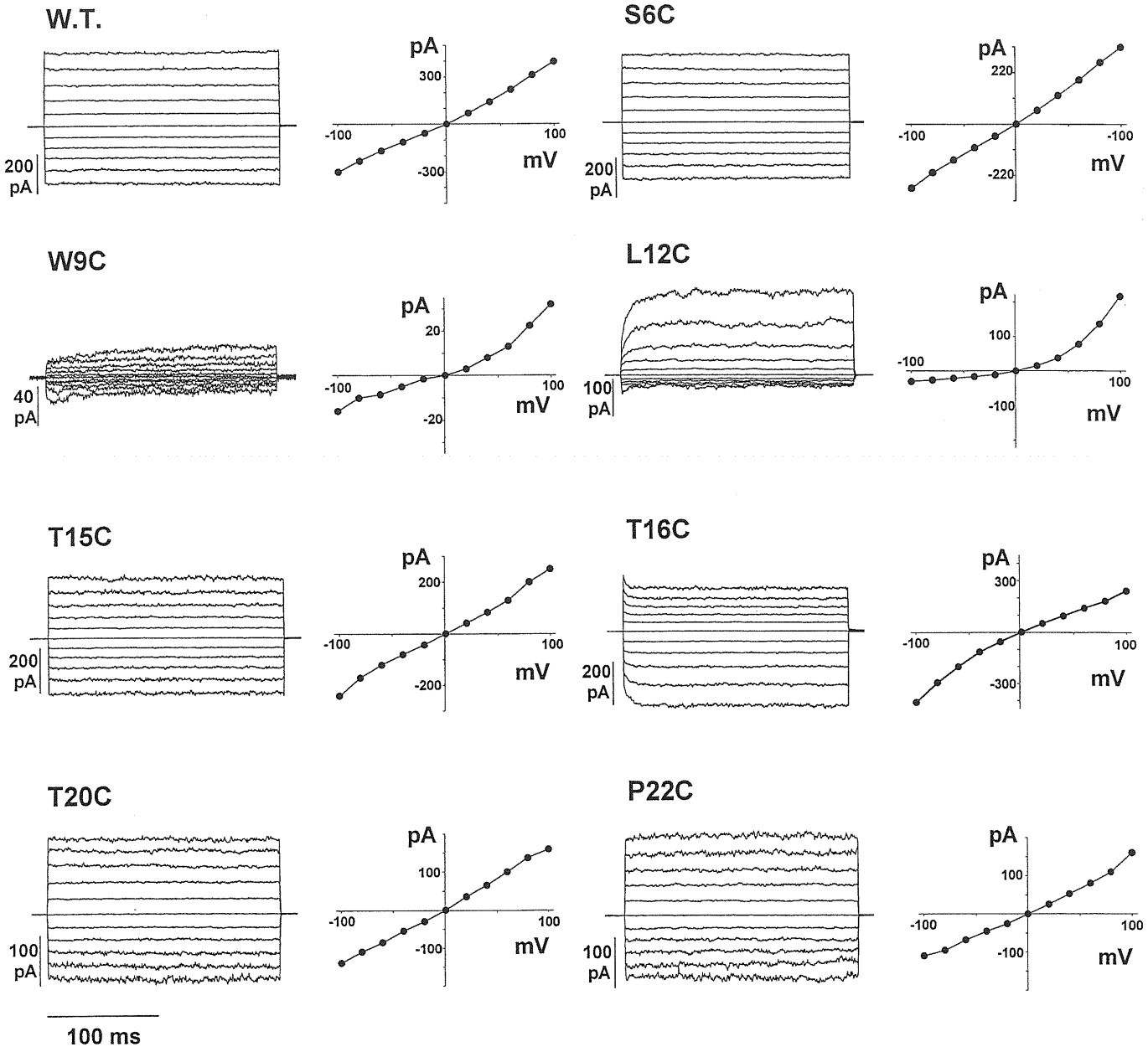

Fig. 9 : Macroscopic current traces and corresponding I/V relations for w.t. and mutant channels

Currents were elicited by applying consecutive 20 mV voltage steps, from -100 to + 100 mV, to inside-out patches containing the indicated mutant, in saturating cGMP. Holding potential between steps was 0 mV. Linear leak and capacitive currents were subtracted by plotting the difference between the currents in the presence and in the absence of cGMP. Traces are averages of 5-10 trials. Each I/V relation is representative of at least 5 measures on different patches.

III.A.1.3. DOSE-RESPONSE TO cGMP

The dose-response to cGMP was weakly affected by cysteine mutations, except marginally in T16C (Fig. 10 and Table 2). Fig. 10a shows typical dose-response curves for w.t. and P22C. A Hill equation was fitted to the experimental data obtained from the different mutants at +60 mV, giving Kd's around 100 μM (Table 2) and Hill coefficients around 2 (not shown). This is in agreement with data available in literature for w.t. channels expressed in *Xenopus* oocytes, with Kd's in the range 50-100 μM and Hill coefficients around 2 (Kaupp *et al.*, 1989; Goulding *et al.*, 1994; Fodor *et al.*, 1997). The dose-responses to cGMP of T16C mutant currents showed the maximal discrepancy with respect to the w.t.'s (Fig. 10b). The average Kd was in fact 0.294 mM. However, also in the case of T16C mutant, 1 mM cGMP was close to the saturating cGMP concentration. Current at 1 mM cGMP was 92% ± 3.8% (average of five experiments) of the current measured in the presence of 5 mM cGMP. In the case of the other mutants, the difference between current amplitudes in the presence of 1 mM and 5 mM cGMP was always negligible (data not shown). Thus, concentrations of cGMP between 0.5 and 1 mM are saturating for cysteine mutants.

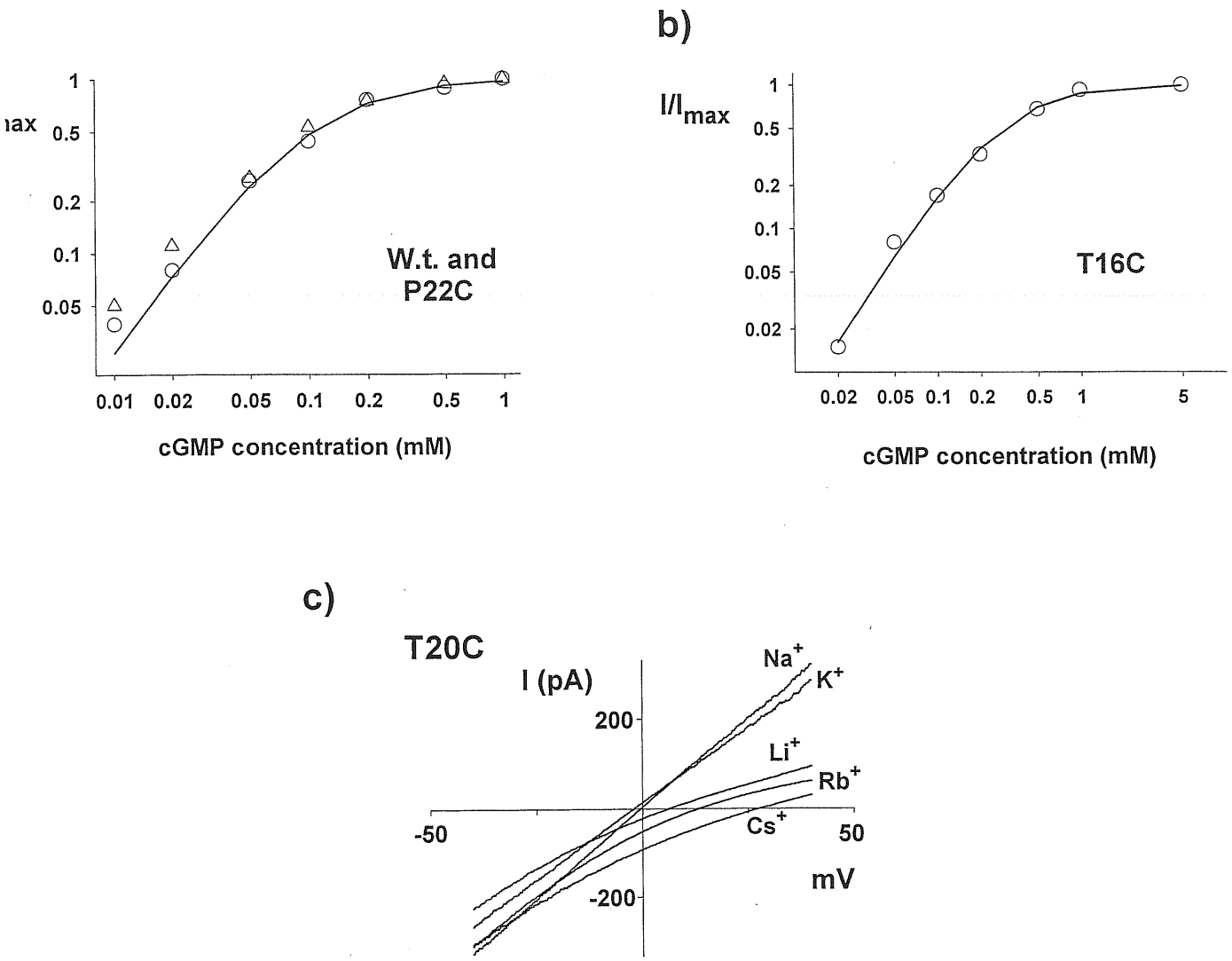

Fig. 10 : Dose-response curve for cGMP and selectivity to alkali monovalent cations

a) Representative cGMP dose-response curves for w.t. (triangles) or P22C (circles) channels. Currents from inside-out patches were measured at +60 mV and normalised to currents obtained in the presence of saturating (1 mM) cGMP. Current values are plotted as a function of cGMP concentration (mM), on a double logarithmic scale. Continuous line is fit to equation 1, for P22C data, with Kd = 0.11 mM. b) Dose-response to cGMP for T16C mutant currents. Experimental protocol was as in a. Currents were normalised to currents obtained in the presence of 5 mM cGMP. Data are averages of 5 experiments. Circles = experimental data; Continuous line = fit to equation 1, with Kd = 0.294 mM. c) Selectivity of T20C mutant channels to monovalent alkali cations. Currents were elicited by 1 s voltage ramps from -40 to +40 mV, applied to inside-out patches. Traces are differences between currents in the presence and in the absence of 1 mM cGMP. Each trace is the average of 3-5 trials, obtained in biionic conditions (NaCl inside the pipette, see section II.A.2.3.).

Mutant	K_d (μM)	Li^+		K^+		Rb^+		Cs^+	
		V_{rev} (mV)	P_{Li}/P_{Na}	V_{rev} (mV)	P_K/P_{Na}	V_{rev} (mV)	P_{Rb}/P_{Na}	V_{rev} (mV)	P_{Cs}/P_{Na}
Wild type	87 ± 7.3	7.5 ± 2.0	0.75	1.0 ± 0.6	0.96	8.2 ± 1.8	0.73	26.3 ± 4.0	0.36
K2C	90 ± 9.2	4.1 ± 2.0	0.86	-6.0 ± 1.5*	1.26	n.d.		n.d.	
V4C	94 ± 11	15.0 ± 1.8	0.56	-2.5 ± 0.9	1.10	13.7 ± 3.0	0.59	21.7 ± 1.8	0.43
S6C	95 ± 20	14.6 ± 2.6	0.57	-1.5 ± 1.0	1.06	12.8 ± 2.1	0.61	28.0 ± 2.0	0.34
L7C	88 ± 9	n.d.		-8.0 ± 2.1*	1.37	13.0 ± 1.8	0.60	n.d.	
L12C	102 ± 10	n.d.		-1.0 ± 1.1	1.04	n.d.		n.d.	
T13C	91 ± 18	n.d.		2.0 ± 2.0	0.93	n.d.		n.d.	
T15C	182 ± 20*	23.3 ± 1.2	0.40	-6.8 ± 2.6	1.30	1.3 ± 0.8	0.95	3.7 ± 1.1	0.87
T16C	294 ± 71*	12.9 ± 2.8	0.60	-6.5 ± 1.7*	1.29	3.6 ± 1.3	0.87	12.0 ± 1.3	0.63
T20C	150 ± 26	6.8 ± 1.4	0.77	-1.2 ± 1.0	1.05	14.2 ± 3.2	0.57	28.5 ± 2.6	0.33
P22C	106 ± 11	n.d.		-0.7 ± 2.2	1.03	n.d.		n.d.	
V24C	85 ± 18	7.5 ± 0.8	0.75	-3.0 ± 0.8	1.12	15.0 ± 1.8	0.56	26.0 ± 2.1	0.36
S27C	112 ± 14	17.5 ± 2.2	0.51	-6.1 ± 2.8	1.27	6.5 ± 2.0	0.78	21.4 ± 2.6	0.43

Table 2 : Summary of affinity for cGMP and reversal potentials for alkali monovalent cation

Average Kds (μM) for cGMP of different cysteine mutants were obtained from dose-response curves as explained in Fig. 10a. Reversal potentials were obtained in biionic conditions (NaCl inside the pipette) from patch currents elicited by voltage ramps as shown in Fig. 10b. Reversal potentials for L12C and T16C were estimated from steady-state current-voltage relations, instead of voltage ramps. Currents from W9C mutant were usually to small to allow a reliable estimate of Vrev. Data are averages of at least 3 determinations. N.d. = not determined. Wild type data are from Sesti *et al.*, 1996. * = significantly different from w.t. (for dose-response to cGMP) or significantly different from w.t. Vrev in the presence of potassium (for selectivity data). A Students t-test was applied, p value was less than 0.05.

III.A.1.4. IONIC SELECTIVITY TO MONOVALENT ALKALI CATIONS

The selectivity to monovalent alkali cations was estimated by measuring Vrev in biionic conditions, in saturating cGMP (see II.A.2.5.). Pipette always contained 110 mM NaCl. Currents were elicited by applying voltage ramps from -40 to +40 mV. An example is shown in Fig. 10c, for T20C mutant. For mutants L12C and T16C however, Vrev was estimated from steady state I/V curves obtained in the presence of the different monovalent cations. From Vrev values (Table 2), the P_X/P_{Na} permeability ratio can be calculated as explained in Methods. For instance, the permeability ratios calculated for S6C mutant are 1.06 (P_K/P_{Na}), 0.61 (P_{Rb}/P_{Na}), 0.57 (P_{Li}/P_{Na}), and 0.34 (P_{Cs}/P_{Na}). The corresponding selectivity sequence is: $K^+ \cong Na^+ > Rb^+ \geq Li^+ > Cs^+$. It was shared by most mutant channels and is identical to the w. t.'s (Sesti *et al.*, 1996). However, a few mutants were slightly more permeable to potassium than to sodium, compared to wild-type (Table 2).
Concerning the P21C mutant, its ionic selectivity is reported in details in section III.A.3.7. Briefly, its behaviour is very different from that of the w.t. and from that of all other cysteine mutants and its selectivity sequence for alkali monovalent cations is unclear because the V_{rev} for K^+, Rb^+, and Cs^+ can not be determined.

III.A.1.5. I17C MUTANT SHOWED CURRENT RUNDOWN

I17C channel activity progressively decayed, in inside out patches (Fig. 11a and 11c). This rundown was partially prevented by the reducing compound dithiotreitol (DTT, 1 mM), in the bath (Fig. 11b and 11c). DTT had no effect on w.t. currents (data not shown, cf. also Lynch, 1998). These results suggest that, in this mutant channel, disulphide bridges are formed between corresponding cysteines of the different subunits forming the channel, soon after patch excision.

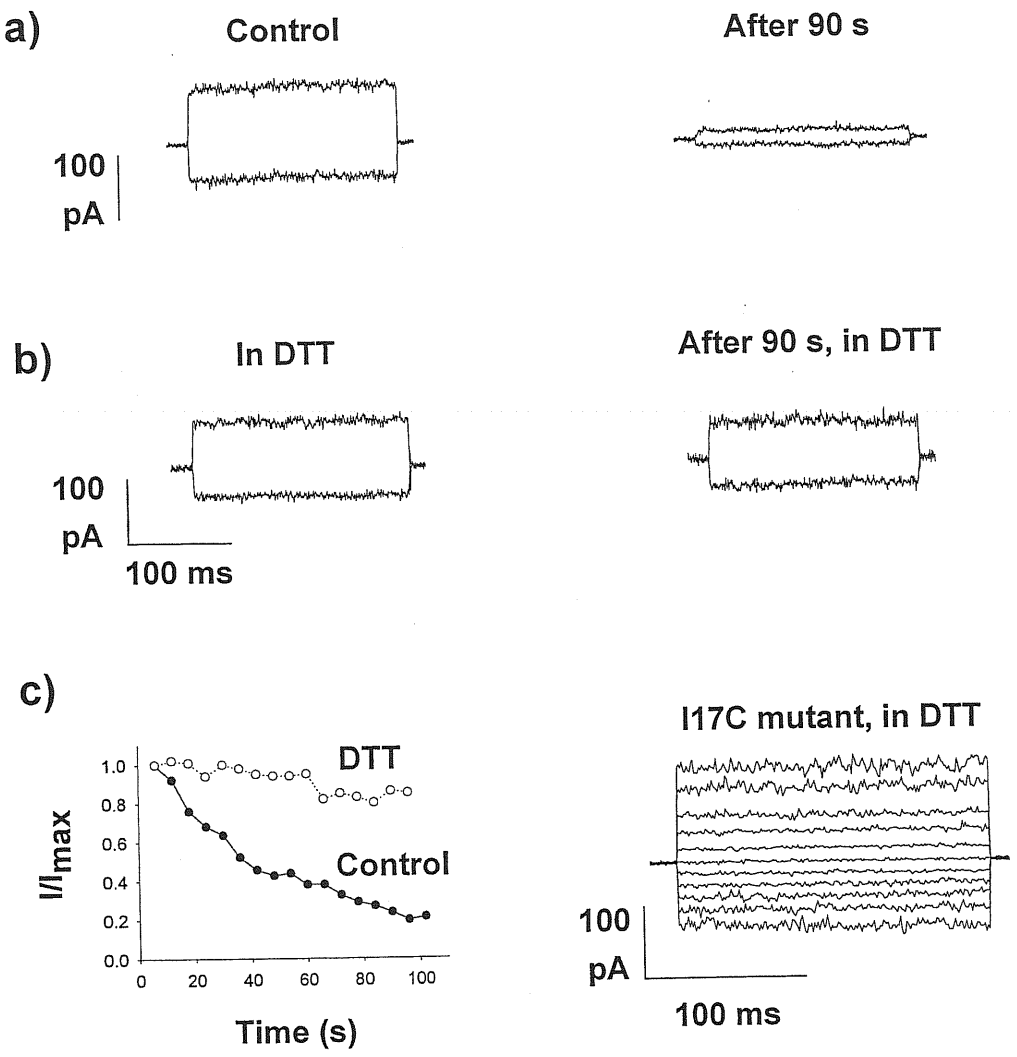

Fig. 11 : DTT prevents current rundown in mutant I17C

a) cGMP-gated current from mutant I17C, at +60 and -60 mV, immediately after patch excision (Control) and after 90 seconds. Holding potential was 0 mV. Current decline was about 80%. b) same as in a), but in the presence of 1 mM DTT. Current decline after 90 s was about 15%. c) time-course of I17C current rundown in the presence and in the absence of DTT, at +60 mV. Consecutive voltage steps at + 60 and -60 mV were applied to inside-out patches for about 2 min, in the continuous presence of saturating cGMP. Only data obtained at +60 mV are shown. Points are averages of three consecutive trials. d) Macroscopic I/V relation from I17C mutant, in the presence of DTT and 1 mM cGMP. No major difference was found with respect to w.t. currents. Data showing current rescue in DTT are representative of four similar experiments.

III.A.1.6. SINGLE-CHANNEL PROPERTIES

Figs. 12 and 13 summarise single-channel recordings from cysteine mutants belonging to different segments of the P loop. Traces and amplitude histograms give a concise picture of channel behaviour at saturating cGMP concentrations, at both polarities. W.t. channels expressed in *Xenopus* oocytes have single-channel conductance of 25-30 pS, independent of cGMP concentration and weakly voltage-dependent (Kaupp *et al.*, 1989; Nizzari *et al.*, 1993; Bucossi *et al.*, 1997). The cloned channel has well-resolved openings, especially at positive membrane potentials. Single-channel currents are somewhat noisier at negative membrane potentials (Bucossi *et al.*, 1997). At +100 mV, the Po in saturating cGMP is around 0.8 (Bucossi *et al.*, 1997). This allows to estimate reliably the number of active channels in patches containing a limited number of channels (Horn, 1991; Bucossi *et al.*, 1997).

Fig. 12a shows current traces from a patch expressing S6C channels, at +100 mV and -100 mV, in the presence of 1 mM cGMP. The amplitude histogram obtained at +100 mV was fitted by the sum of two Gaussian functions, showing one well resolved state. A clear open state was also observed at -100 mV. Continuous line were superimposed to the data points fitted as the sum of gaussian functions, with peaks at 0 and 2.8 pA. The average single-channel conductance was 28 pS ± 0.6 at +100 mV (1 mM cGMP, n=3) and 27 pS ± 0.7 at -100 mV (1 mM cGMP; n=3). I/V relations and dose-response to cGMP revealed that the single-channel conductance was scarcely dependent either on voltage or on ligand concentration (Fig. 12a and data not shown). Although the amplitude histogram at +100 mV represents about 10 s continuous recording, no double openings were detected during the whole experiment (lasting several minutes). We thus assumed that patch contained only one active channel. The Po was 0.82 at +100 mV and 0.85 at -100 mV, in the presence of 1 mM cGMP. Overall, conductance and Po values at different cGMP concentrations and at both polarities, were very similar to those measured in w.t. channels (Bucossi *et al.*, 1997) and consistent with dose-response curves and I/V relations obtained from mutant macroscopic currents (Fig. 9 and Table 2). Similar results were found for K2C and V4C mutants (data not shown). Since S6C channel properties closely approximated those of w.t. channels, we do not show w.t. single-channel traces (Nizzari *et al.*, 1993; Bucossi *et al.*, 1997).

On the other hand, W9C mutant had low single-channel activity at both polarities, in saturating cGMP (Fig. 12b). Channel conductance was about 26 pS. In general, a small Po prevents a reliable estimate of the number of active channels contained in a patch (N), whose knowledge is necessary to calculate Po (Horn, 1991). We could however estimate an upper limit to the Po value. In four experiments in which no double

opening was detected, the apparent Po (calculated assuming N = 1) in saturating cGMP was never higher than 0.15 at +100 mV, and 0.1 at -100 mV. Po might be smaller, if patch activity derived from multiple channels, but not larger. Low Po values were also observed in L12C (especially at negative membrane potentials) and T13C (data not shown). T15C and T16C mutant channels showed higher activity, consistent with the presence of large macroscopic currents. However, in this case too, single-channel recording revealed that Po was reduced compared to w.t. channels. Results from patches containing multiple channels allowed again an estimate of the maximum possible Po. Fig. 12c shows an example of single-channel recordings from T16C mutant. Assuming that only 3 independent channels were present in the patch (the number of detected open levels at +120 mV, in saturating cGMP), application of the binomial distribution gives an open probability around 0.2. Channel conductance was 31 pS. In this mutant, channel openings were shorter than in w.t. at both polarities. This was especially evident at negative potentials, where clear open levels were not resolved, as shown in Fig. 12c (bottom) for currents at -160 mV (at 0.05 mM cGMP, for better appreciation of the current baseline). Similar properties were observed in T15C mutant (data not shown). We conclude that cysteine mutations within the central segment of the P loop prevent channels from reaching Po's larger than about 0.2 (Table 3). The single-channel conductance in mutants within the W9-T16 segment, when measurable, was in the range 25-30 pS at both polarities, not different from w.t. values. G18C mutant channels had a very low Po at all membrane potentials. In five experiments, the maximal estimated Po at +100 mV was always less than 0.05, in saturating cGMP (data not shown).

Mutants within the segment T20-S27 showed different features. Fig. 13 summarises data collected from patches likely containing one active channel. With the exception of mutant P21C, all of the tested mutants within this stretch of residues had Po's similar to the w.t.'s, with weak outward rectification. Po in saturating cGMP was always larger than 0.7, at +100 mV. However, changes appeared in single-channel conductance. The amplitude histogram for T20C channels, at -100 mV, revealed at least two conductance states, with peaks at 22 and 37 pS (average of 3 experiments, Fig. 13a). The subconductance state is better resolved in current trace and amplitude histogram obtained from recording at -180 mV (Fig. 13a). At +100 mV only one open state at 28 ± 1.3 pS was present (n = 4, Fig. 13a). The lower panel of Fig. 13a shows the Po as a function of cGMP concentration (right), and the unitary I/V relation (left), for T20C mutant. Both are in agreement with data obtained from macroscopic currents (Fig. 9 and Table 2), with Kd for cGMP around 0.15 mM and nearly linear I/V curves. In P21C mutant the single channel conductance is around 18 pS; the origin

of its outward rectification of the macroscopic current was likely to be due to a voltage-dependent gating as the open probability at the level of single channel recordings increases with the voltage. Finally, the use of a potentiating agent allowed to conclude in a rectification due to the fact that cGMP acts as a partial agonist for this mutant (see the data of the P21T mutant which are similar in Fig. 25a). In P22C mutant (Fig. 13b), single-channel currents at +100 mV showed a well resolved conductance level around 30 pS. On the other hand, at -100 mV, the single-channel conductance was about 23 pS, somewhat smaller than it was at positive potentials and in w.t. channels. In S27C mutant (not shown), the single-channel conductance was 21 ± 0.9 pS at +100 mV and 22 ± 0.9 pS at -100 mV (n = 3), smaller than in w.t. channels. Po and single-channel conductance values for most of the tested mutants are summarised in Table 3.

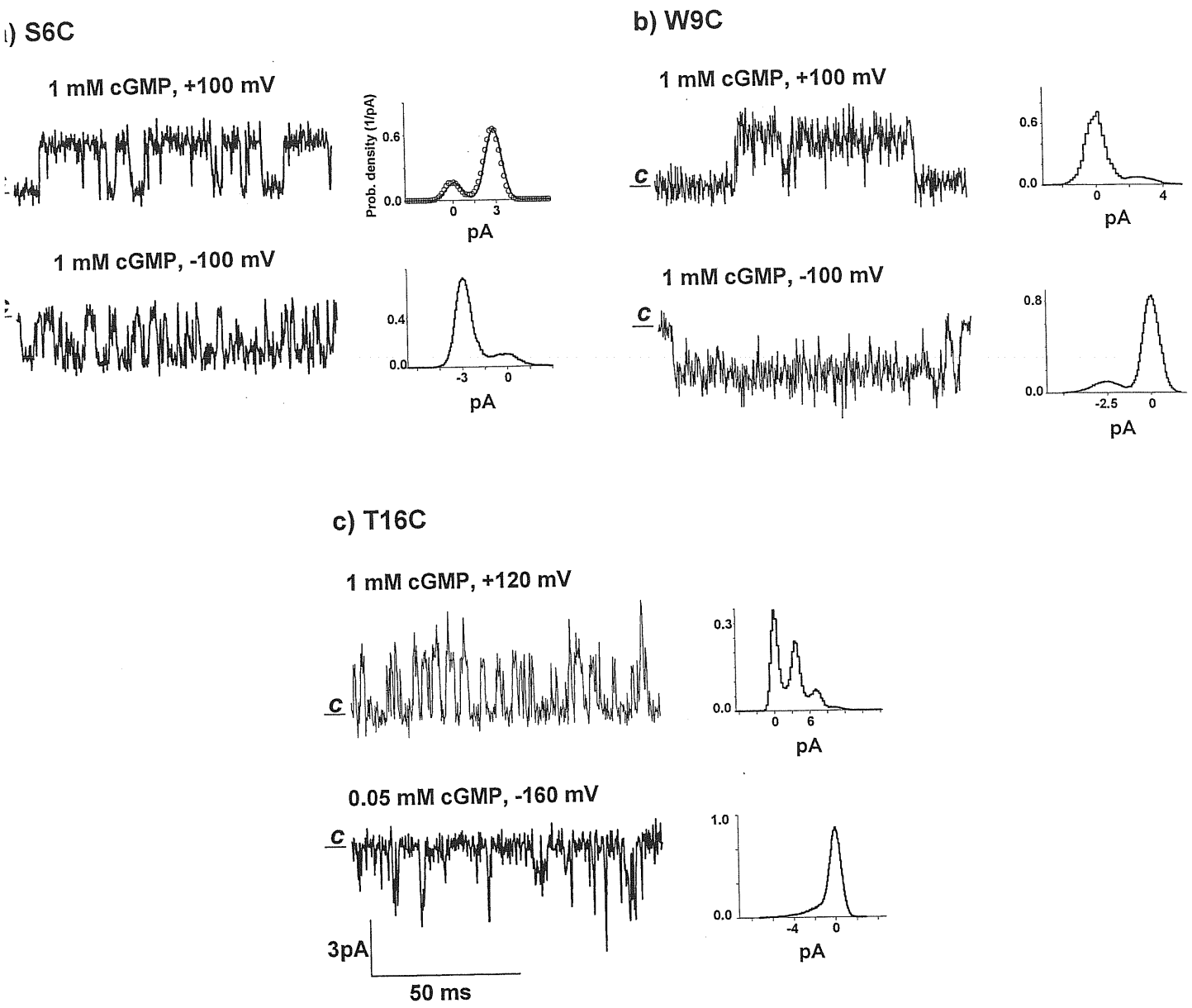

Fig. 12 : S6C, W9C and T16C single-channel currents

Current traces (left panels) were obtained from continuous recording at the indicated membrane potential and cGMP concentration. Data were filtered at 5 kHz and sampled at 20 kHz. The corresponding amplitude histograms (right panels) represent at least 10 sec continuous recording. C = closed level.

a) Currents from S6C mutant, at +100 mV in the presence of 1 mM cGMP (upper panel) and at -100 mV in the presence of 1 mM cGMP (lower panel). b) Currents from W9C mutant, at +100 (upper) and -100 mV (lower), in the presence of 1 mM cGMP.c) Currents from T16C mutant, at +120 mV (1 mM cGMP) and at -160 mV (0.05 mM cGMP, for better appreciation of current baseline).

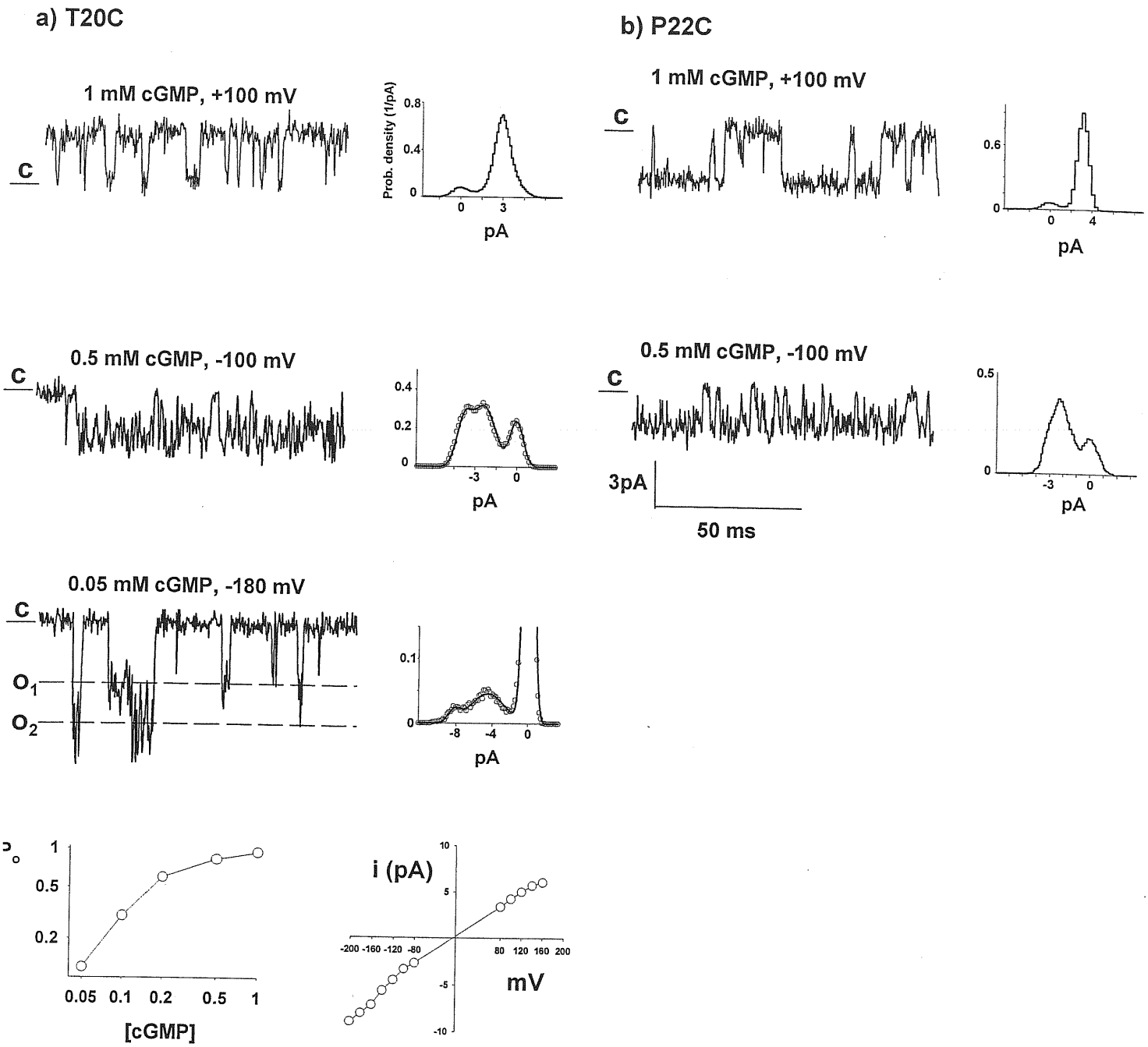

Fig. 13 : T20C and P22C single-channel currents

Current traces were obtained from continuous recording at the indicated membrane potential and cGMP concentration. Data were filtered at 5 kHz and sampled at 20 kHz. The corresponding amplitude histograms represent at least 10 sec continuous recording. C = closed level.

a) T20C single-channel currents. This patch likely contained a single active channel. Bottom panel (left) shows Po against cGMP concentration. Data are averages of three experiments, normalised to the value obtained at 1 mM cGMP. Bottom panel (right) shows unitary current/voltage relation for a representative patch. Data points represent unitary current at the indicated membrane potential, for the channel state showing the highest conductance. b) Single-channel currents from P22C mutant. Experimental procedures as for a). This patch, also, likely contained one active channel.

Mutant	P_o	γ_{+100} (pS)	γ_{-100} (pS)
w.t.	0.78±0.04	28±0.5	27±0.4
S6C	0.82±0.05	28±0.9	27±0.8
W9C	≤ 0.15	26±0.6	26±0.7
L12C	≤ 0.30	-	-
T13C	≤ 0.15	31±1.1	25±0.9
T15C	≤ 0.25	-	-
T16C	≤ 0.25	31±0.9	-
G18C	≤ 0.05	-	-
T20C	0.83±0.08	30±1.2	37±1.1*
P22C	0.75±0.09	32±1.3	21±1.2*
S27C	0.81±0.07	21±0.9*	22±0.9*

Table 3 : Single-channel properties of cysteine mutants

Open probabilities (at +100 mV, in saturating cGMP) and single-channel conductances (measured at + 100 and -100 mV, in saturating cGMP) are shown for w.t. and the indicated cysteine mutants. Po = open probability, γ +100 = single-channel conductance, at +100 mV, γ -100 = single-channel conductance, at -100 mV. Values are averages of at least three experiments. For T20C, the conductance of the higher current level is shown. For L12C, T15C, T16C (at negative potentials) and G18C mutant channels, measure was imprecise, and it was not reported, because the high frequency fluctuations prevented us from obtaining a clear peak in the amplitude histogram (e.g. see Fig. 13c, lower panel). However, the midpoint of the lobe corresponding to the open state was always within the range 20-30 pS. * = significantly different from w.t. (Students t-test, p 0.05).

III.A.2. STRUCTURE OF THE PORE REVEALED BY SCAM

The effect of MTS compounds on w.t. channels are shown in Fig. 14. Then, the accessibility of the different cysteine mutants to MTSEA and MTSET, from the outer and inner surface of excised membrane patches is examined (see Annex C for the formula of MTS compounds).
Experiments were done in symmetrical NaCl, in the absence of divalent cations and at saturating concentrations of cGMP (0.5-1 mM) as no major difference was found between cysteine mutants and w.t. channels, in the affinity for cGMP (see section III.A.1.3.). Since our results with MTSEA agree with those reported by Sun *et al.* (1996) data obtained with MTSET will be mostly shown. Due to experimental variability (see e.g. Karpen *et al.*, 1993), we assumed that only average MTSET effects larger than 20% inhibition or potentiation provided information on residue accessibility.

III.A.2.1. EFFECTS OF MTS REAGENTS ON W. T. CHANNEL

MTSET (Fig. 14a) and MTSEA (not shown) produced a voltage-dependent block of w.t. channels, when applied to the patch inner side, in the presence of cGMP (i.e. when the channels were open). This block resembled the one caused by other organic cations (Picco and Menini, 1993). Since the channel inhibition at positive membrane potentials was reversible, the interaction of MTS's with the open channel does not involve any covalent reaction with endogenous cysteines. On the contrary, when MTSET (Fig. 14c) or MTSEA (not shown) were applied in the absence of cGMP (i.e. when the channels were closed), the subsequent perfusion of cGMP, after MTS reagent had been shed out, revealed a partial (approximately 50%) irreversible current inhibition, independent of membrane potential. Sun *et al.* (1996) showed that MTSEA's irreversible block is removed by substituting the cysteine in position 505 with a threonine. The same result applies to MTSET, which had no effect on C505T mutant channels either in the presence or in the absence of cGMP (Fig. 14b and 14d). Therefore, when studying the MTS effect on CNG channels from the cytoplasmic side in the closed state, it is necessary to use cysteine mutants containing the supplementary mutation C505T. This mutation C505T did not cause any effect in addition to preventing irreversible block by MTS compounds (data not shown). Figs. 14b and 14d also exemplify our experimental procedure. Unless otherwise indicated, the MTS effect is shown for patches maintained at -40 mV. Usually, cGMP was applied 2-3 times before MTS application. The appropriate MTS reagent was then applied for 2-3 min.

After washout, cGMP was applied again for comparison with the initial current (see section II.A.2.6.).

Fig. 14 :

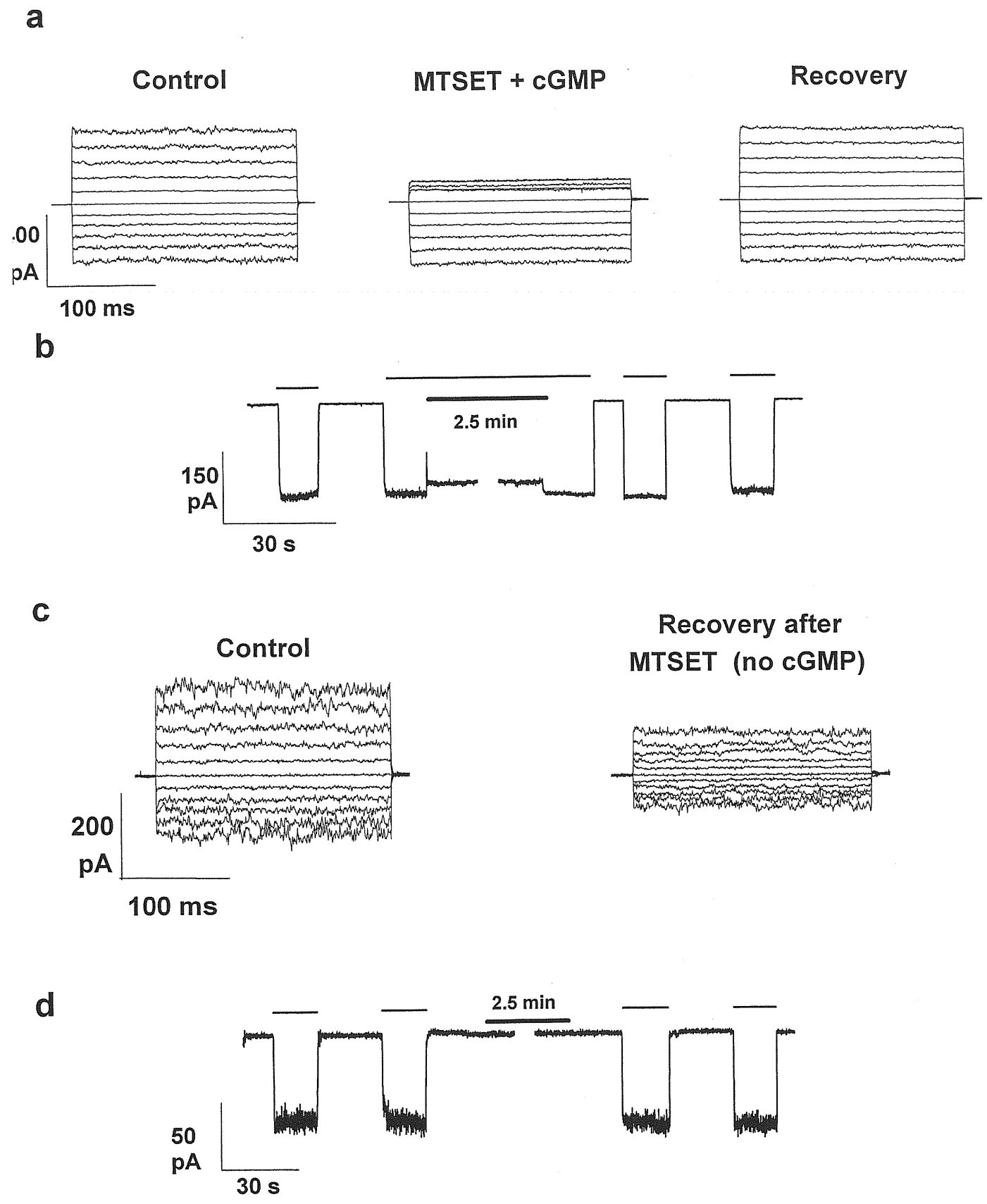
a
Control
MTSET + cGMP
Recovery
00
pA
100 ms
b
2.5 min
150
pA
30 s
c
Control
Recovery after
MTSET (no cGMP)
200
pA
100 ms
d
2.5 min
50
pA
30 s

Fig. 14 : MTSET effect on w.t. and C505T channels

a) I/V relations from w.t. CNG channels, in inside-out patches, before (Control), during (MTSET + cGMP) and after (Recovery) application of 2.5 mM MTSET, in the presence of 500 μM cGMP (open state). Recovery was measured about 1 min after MTSET washout. Currents were elicited by 200 ms voltage steps from -100 mV to 100 mV (20 mV increments). Holding potential was 0 mV. Traces are averages of 5 trials. b) MTSET had no irreversible effect on C505T channels, in the open state. MTSET was applied for about 2.5 min at -40 mV, in the presence of 500 μM cGMP. c) MTSET irreversibly inhibited w.t. channels. I/V relations before (Control) and after (Recovery) application of 2.5 mM MTSET, in the absence of cGMP. d) MTSET had no effect on C505T channels, in the closed state. MTSET was applied for about 2.5 min at -40 mV, in the absence of cGMP.
In Figs. 14, 15,16,17,19,20, and 21, the thick bar indicates the duration of MTS application, and the thin bar indicates either the application of 500 μM cGMP to the intracellular side of the membrane (for inside-out patches) or the time during which cGMP was present in the absence of Mg^{2+} (for outside-out patches). Unless otherwise indicated, membrane potential was always maintained at -40 mV.

III.A.2.2. ACCESSIBILITY OF K2C-L14C RESIDUES

Neither MTSEA nor MTSET had any effect on mutants K2C and S6C (Fig. 22). cGMP-activated currents from mutant V4C were not affected by MTSET application to the inner side of the plasma membrane, either in the closed or in the open state (Fig. 15a and Fig. 22). On the contrary, MTSET strongly inhibited cGMP-gated currents in mutant V4C, when applied to the outer side of membrane patches, both in the presence and in the absence of cGMP (Fig. 15b and Fig. 22). These results suggest that V4 is located extracellularly, possibly in the outer pore vestibule.

The segment formed by residues L7-L14 is very sensitive to cysteine mutation (see section III.A.1.1.). Indeed, whereas no current was measurable from Y8C, S10C, T11C and L14C channels the functional mutant channels -L7C, W9C, L12C and T13C- showed a reduced maximal open probability and an altered gating. cGMP-activated currents from L7C mutant were scarcely different from those observed in w.t. channels. They were not affected by external MTSET (Fig. 15b and Fig. 22). However, MTSET application to the inner side of membrane patches produced a partial but reproducible block: 60% (± 9.9%, n=4) in the closed state, and 25% (± 3.6%, n=5) in the open state (Fig. 15a, bottom panels). These results show that L7 residue is accessible from the internal side of the plasma membrane. The difference between MTSET effect in the open and closed state is statistically significant ($p < 0.01$; Student's t-test) and suggests that this residue changes its location during gating.

Mutant channels L12C and to a lesser extent W9C and T13C had altered gating with outwardly rectifying I/V relations (see section III.A.1.2.). External application of MTSET, in the presence of cGMP, had no effect on either W9C and L12C mutant channel (Fig. 16b). The accessibility to MTS compounds was not tested on T13C because this mutant never exhibited sufficient current. On the other hand, W9C mutant was inhibited, while L12C was potentiated by intracellular MTSET (Fig. 16a and Fig. 22). These data indicate that cysteines introduced in positions 9 and 12 are accessible from the inner side of the plasma membrane.

Fig. 15 :

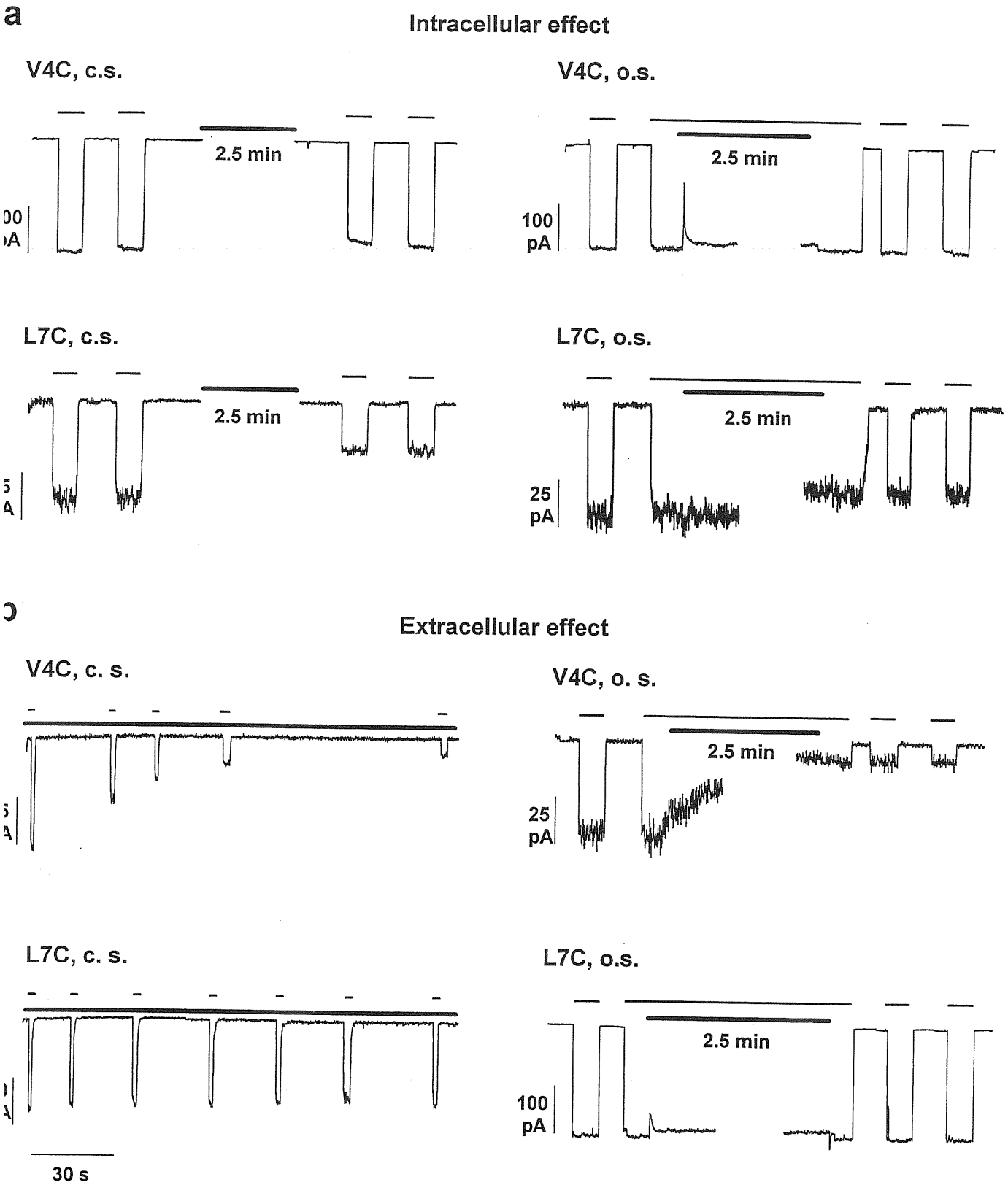
a
Intracellular effect
V4C, c.s.
2.5 min
V4C, o.s.
2.5 min
100
pA
L7C, c.s.
2.5 min
L7C, o.s.
2.5 min
25
pA
Extracellular effect
V4C, c. s.
V4C, o. s.
2.5 min
25
pA
L7C, c. s.
L7C, o.s.
2.5 min
100
pA
30 s

Fig. 15 : MTSET effect on V4C and L7C mutant channels

a) MTSET application on the inner side of membrane patches. Upper panel: MTSET effect on V4C mutant in the closed state (c.s.) and in the open state (o.s.). Lower panel: MTSET effect on L7C mutant in the closed state (c.s.) and in the open state (o.s.). b) MTSET application on the outer side of membrane patches. Upper panel: MTSET effect on V4C mutant in the closed state (c.s.) and in the open state (o.s.). Lower panel: MTSET effect on L7C mutant in the closed state (c.s.) and in the open state (o.s.).

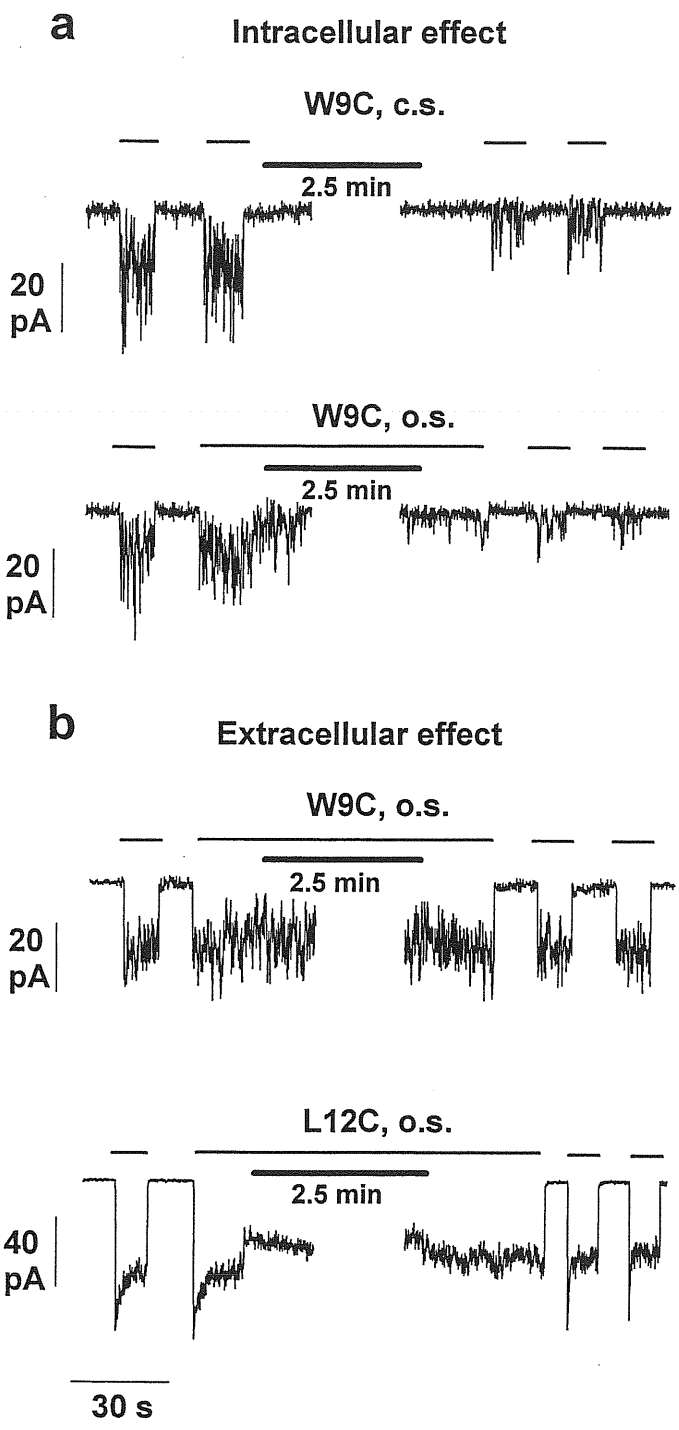

Fig. 16 : MTSET effect on W9C and L12C channels

a) MTSET application on the inner side of membrane patches. Upper panel: MTSET effect on W9C mutant in the closed state (c.s.). Lower panel: MTSET effect on W9C mutant in the open state (o.s.). b) MTSET application on the outer side of membrane patches. Upper panel: MTSET effect on W9C mutant in the open state (o.s.). Lower panel: MTSET effect on L12C mutant in the open state (o.s.).

III.A.2.3. ACCESSIBILITY OF T15C AND T16C RESIDUES

Mutant channels T15C and T16C showed large macroscopic currents (Fig. 9) but, compared to w.t. channels, single-channel recordings revealed a reduced Po (around 0.2) at both polarities (Figs. 12 + Fig. 18). Because mutants T15C and T16C had similar properties only data from T16C mutant will be presented. The cGMP-gated currents were strongly and rapidly potentiated by intracellular application of MTSET (and MTSEA, not shown), in the presence and in the absence of cGMP (Fig. 17a, 17b and 22). This potentiation varied from 50 to 200 % and was almost absent when MTSET was applied from the outer side (Fig. 17c). When MTSET was applied in the presence of cGMP, it was possible to follow the time-course of its effect. After the initial fast potentiation, we observed a slow partial irreversible current inhibition reaching the steady state about 2 min after addition (Fig. 17a). The partial inhibition with respect to the maximal current, measured shortly after MTSET addition, was 55% ± 8%. Fig. 22 only shows the net steady state potentiation, i.e. the potentiation of the current measured after MTSET washout with respect to the current before treatment. It should be noted that the I/V relations of T16C mutant exhibited a weak inward rectification, and current traces revealed a time dependency in the development of the steady state current (Fig. 17d, left panel). These features persisted after the MTSET effect (Fig. 17d, right panel). In addition, we followed the potentiation in a patch containing a low number of channels (Fig. 18). Before MTSET application, single-channel recording in the presence of 0.5 mM cGMP exhibited only two distinct current levels, corresponding to the closed state and to an open state of 2.3 pA. After MTSET application, the open state became more populated and it was often possible to observe current openings of 4.6 pA, corresponding to the simultaneous opening of two channels. This shows that no major change in channel conductance was produced by MTSET, and suggests that the potentiation produced by MTSET was caused by an increased open probability. A similar MTSET potentiation from the inner side of membrane patches was observed in mutant T15C. However, in this case, no inhibition was observed after the rapid initial potentiation (not shown). The potentiation produced by MTSET is a consequence of the low open probability of T15C and T16C channels, even in saturating cGMP (Fig. 18). Furthermore, we investigated whether, in T15C, a partial inhibition produced by MTSET was masked by the strong potentiation. To assess this point, the inner side of patches containing T15C channels was perfused with our standard solution supplemented with 10 μM Ni^{2+} to activate maximally the channels within the patch (Gordon and Zagotta, 1995). After potentiation by Ni^{2+}, MTSET did not produce any supplementary effect (data not shown). On the other

hand, MTSET application to the outer face of the plasma membrane produced negligible effects on both T15C and T16C mutants (Fig. 17c and 22). These results suggest that residues in position 15 and 16 are not accessible from the extracellular side, and that T16C is accessible to MTSET from the inner side of the plasma membrane and may be partially involved in channel gating.

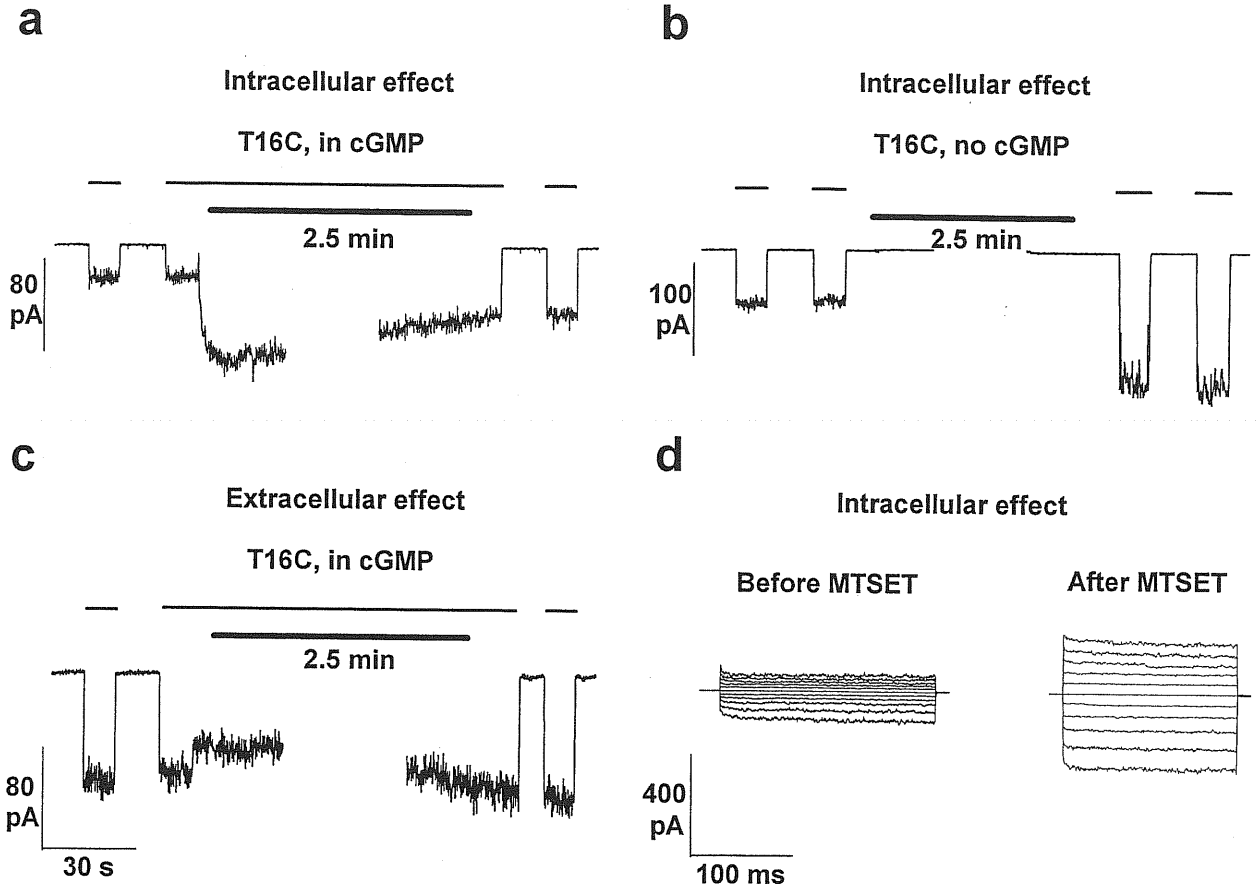

Fig. 17 : MTSET effect on T16C channels

a) MTSET effect on the inner side of membrane patches, in the presence of cGMP. b) MTSET effect on the inner side of membrane patches, in the absence of cGMP. c) MTSET effect on the outer side of membrane patches, in the presence of cGMP. d) I/V relations before and after the application of MTSET on the inner side of membrane patches, in the absence of cGMP. Membrane potential was stepped from -100 to +100 mV (20 mV increments). Holding potential was 0 mV. Currents are the difference between the patch current in the presence and in the absence of cGMP. Current traces were the average of five consecutive trials.

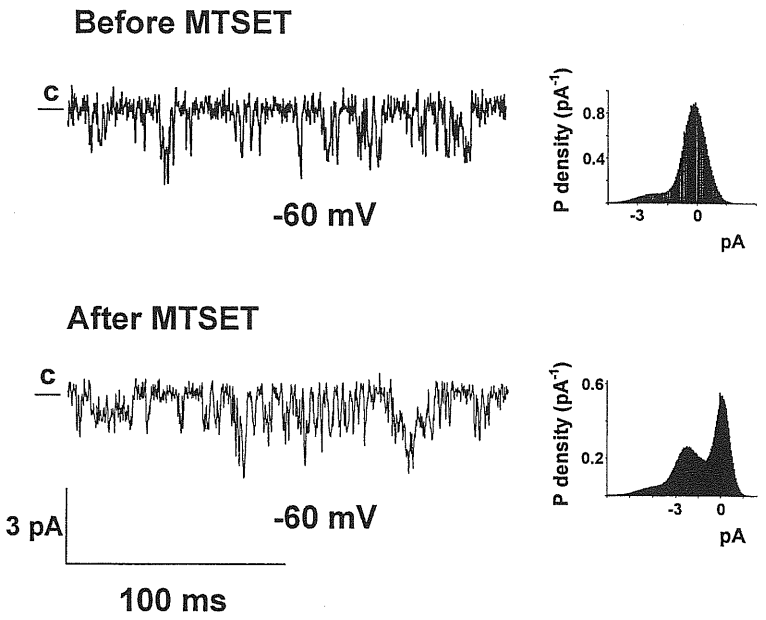

Fig. 18 : MTSET effect on single T16C channels

Upper panel: representative single channel traces before the application of MTSET (left) and corresponding amplitude histogram from 1 min continuous recording at -60 mV (right). Lower panel: representative single channel traces after the application of MTSET to the inner side of membrane patches, in the absence of cGMP (left) and corresponding amplitude histogram from 1 min continuous recording, at -60 mV (right). C = closed level.

III.A.2.4. ACCESSIBILITY OF I17C RESIDUES

Contrary to what was observed in all other cysteine mutants in the CNG channel pore, cGMP-activated currents recorded from the mutant channel I17C rapidly decayed in inside-out patches (see section III.A.1.5. and Fig. 11a and 11c). Current did not recover even when patches were maintained several minutes in the absence of cGMP (data not shown + see Lynch, 1998). The current lifetime was prolonged by adding the reducing agent DTT to the medium bathing the intracellular side of the plasma membrane (Fig. 11b and 11c). These results are reminiscent of those obtained in Na^+ channels, when mutants containing two substituted cysteines in the pore region are expressed in *Xenopus* oocytes (Benitah *et al.*, 1997). As proposed for sodium channels, a possible explanation for these results is that cysteines in close proximity form disulphide bridges. In this view, cysteines in position 17 of neighbouring subunits should be in closer contiguity than cysteines in the other functional mutants. The half-time (t1/2) of the I17C current decay was 45.8 ± 5.2 s in the presence of 0.5 mM cGMP (Fig. 19a, lower panel) and 80.1 ± 12.1 s in the absence of cGMP (Fig. 19a, upper panel). The difference is statistically significant ($0.01 < p < 0.05$, Student's t-test). Application of MTS compounds to the inner side of membrane patches strongly reduced the t1/2 in the presence of cGMP, the average value being 20.4 ± 2.5 s (comparison with control value gave $p < 0.001$, from Student's t-test; Fig. 19b). The presence of MTS compounds also reduced the data scatter (Fig. 19b). These results argue that residue in position 17 is accessible from the inner side of the patch membrane. Furthermore, we propose that I17 is located near the narrowest section of the channel pore, at its intracellular side (see Discussion). The faster decay in the presence of cGMP suggests also that I17 residues of different subunits are closer to each other in the open state.

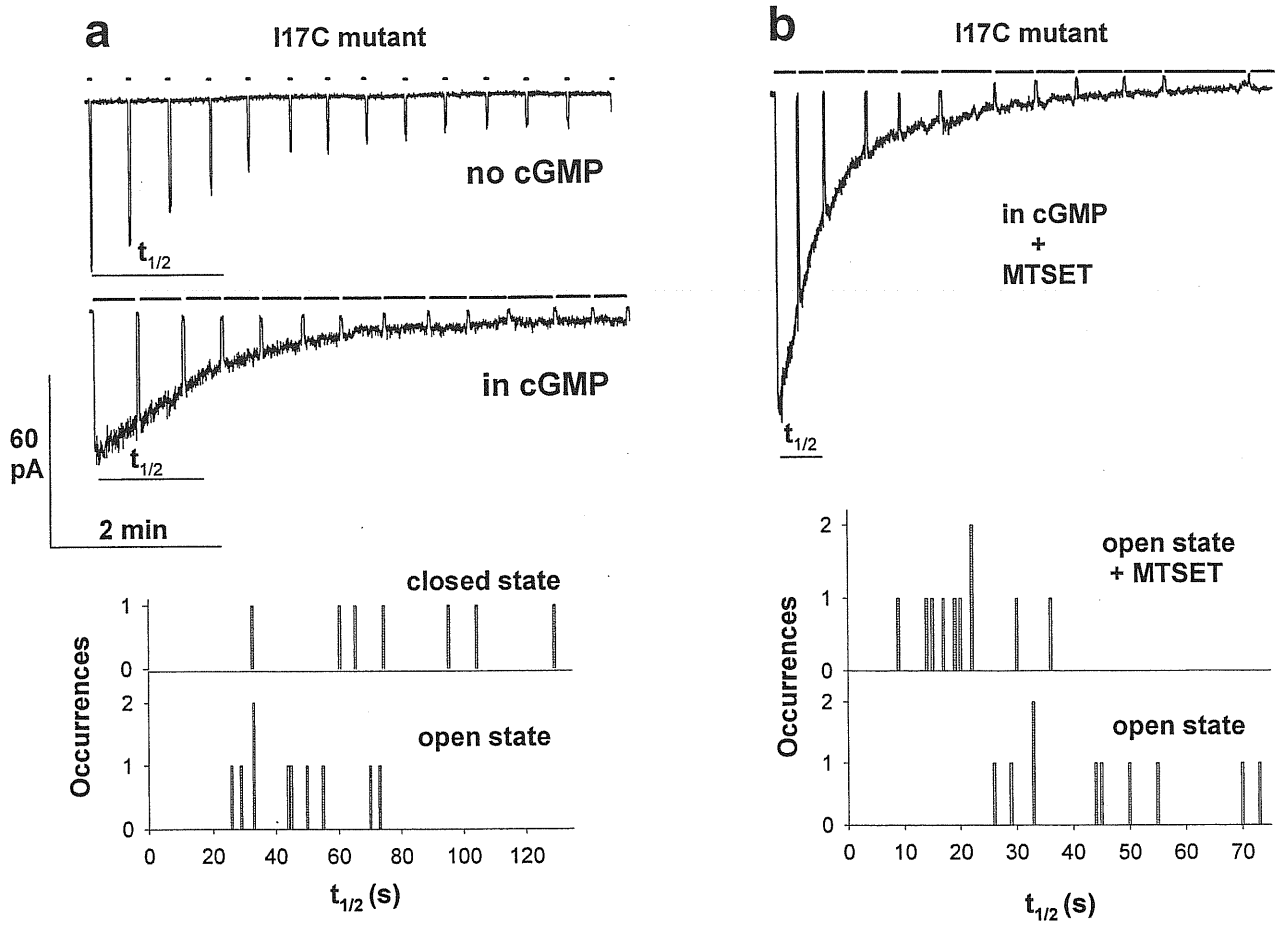

Fig. 19 : MTSET effect on I17C mutant

a) I17C current decay in inside-out membrane patches, during continuous recording at -40 mV. Upper panel: current rundown in the absence of cGMP. Residual current was sampled every 30 s by brief application of cGMP (short bars). Middle panel: current rundown in the presence of cGMP. Baseline level was checked every 30 s by briefly applying solution without cGMP. Lower panel: current half-time (t1/2) from 17 experiments in the absence (closed state) or in the presence (open state) of cGMP. Experimental procedure was as exemplified in upper and middle panels. b) I17C current decay in inside-out membrane patches, during continuous recording at -40 mV, in the presence of MTSET. Upper panel: current rundown in the presence of cGMP. Lower panel: current half-time (t1/2) from 20 experiments in the presence of cGMP. Open state + MTSET = in the presence of MTSET. Open state = in the absence of MTSET.

III.A.2.5. ACCESSIBILITY OF T20C-S27C RESIDUES

Glutamate in position 19 is known to be accessible to both intracellular and extracellular cations (Root and MacKinnon, 1993; Eismann *et al.*, 1994; Sesti *et al.*, 1995) and is believed to be close to the narrowest section of the channel pore (Sesti *et al.*, 1995). When E19 was mutated to a cysteine no functional channels were observed, thus the accessibility of this residue cannot be studied with SCAM. Therefore, it is particularly important to analyse in details both properties and accessibility of residues in position 20, 21 and 22.

All the mutants within the stretch of residues T20-S27 and thus including the mutants T20C, and P22C had Po's similar to the w.t.'s, with weak outward rectification (see section III.A.1.2. and Fig. 13).

Both MTS reagents strongly blocked T20C currents, extracellularly, both in the closed and in the open state (Figs. 20b and 22). However, MTSEA and MTSET gave different results when applied to T20C channels from the inner side of the plasma membrane. MTSEA inhibited T20C current in both the open and closed state (Figs. 21b, 21c and 22; see also Sun *et al.*, 1996), whereas MTSET was not effective in either condition (Fig. 20a). Similar results were found for P22C channels. In the latter however, at variance with w.t. and the other cysteine mutants, the reversible MTSET block was also present at negative membrane potentials. Furthermore, the inhibition of this mutant channel required several minutes washout to be completely reversed. This suggests that the affinity of the channel pore for MTSET is increased in P22C mutant.

As shown in Figs. 20, 21 and 22, MTSEA applied to the inner and outer side of membrane patches irreversibly inhibited T20C and P22C channels, while MTSET was only effective when applied to the external side. This suggests that the internal MTSEA inhibition, in these cases, is due to permeation of this compound through the lipid bilayer (Holmgren *et al.*, 1996). To verify this possibility, MTSEA was applied to the inner side of inside-out patches containing either T20C or P22C, when the patch pipette contained 10 mM cysteine, thereby used as a thiol scavenger on the outer side of inside-out patches (Holmgren *et al.*, 1996; Wilson and Karlin, 1998). The presence of cysteine in the pipette solution did not affect the cGMP-gated current appreciably (Fig. 21a). In the presence of cysteine, the inhibition produced by MTSEA was always incomplete and partially reversible after washout (Fig. 21b, c, d), although washout needed to be prolonged for several minutes, indicating again that cysteine mutation in residues T20 and P22 somewhat alters the channel affinity for MTS compounds. In the presence of external cysteine, MTSEA produced 48% ± 8.6% block on T20C channels (n=6), and 23% ± 12% (n=3) block on P22C channels, whereas the inhibition

in the absence of cysteine was always complete and irreversible even after 10-15 min washout, for both mutants. In this case, experiments in which MTSEA was applied in the presence and in the absence of cGMP were pooled, since no difference was found between the two conditions. Cysteine rescue of MTSEA internal block on T20C and P22C currents reinforces the conclusion that T20 and P22 are extracellular residues. Finally, MTSET had no effect on P21C currents when applied from the inner side of the patch and produced a small block (about 25%, Fig. 22) when applied externally. Finally, negligible effects were produced by MTSET on V24C and S27C mutant channels (Fig. 22). These results lead to conclude that T20, P21 and P22 are extracellular residues. The weak effect on P21C indicates that the side chain of this residue does not line the channel pore lumen, after cysteine mutation at least.

For summarising the effects produced by the application of MTSET on the different cysteine mutants : residues L7, W9, L12, T15, T16, I17 were accessible intracellularly; residues V4, T20, P21, P22 were accessible extracellularly. For L7 the effects of MTSET was more pronounced in the closed state than in the open state.

Fig. 20 :

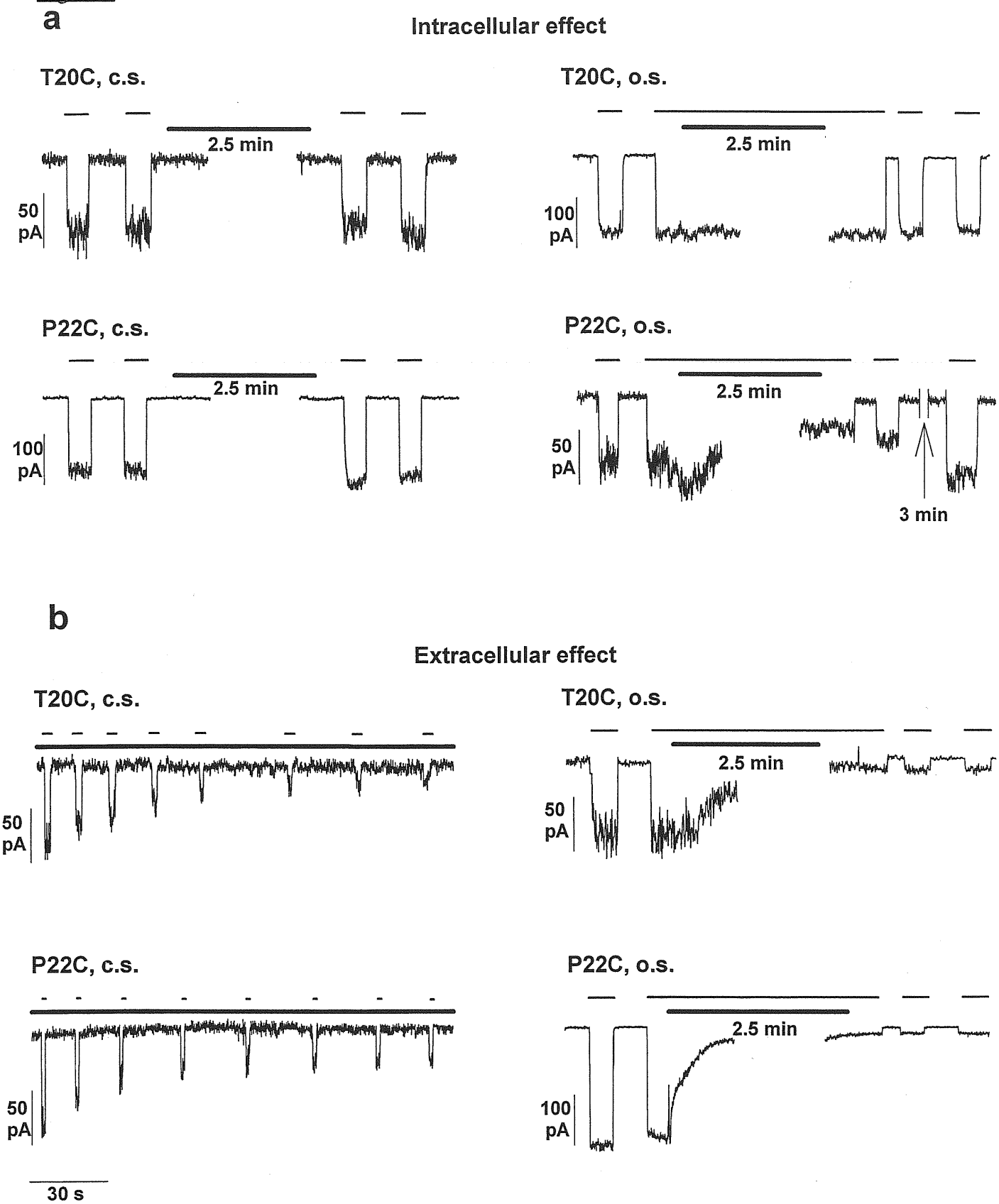
a
Intracellular effect
T20C, c.s.
2.5 min
50 pA
T20C, o.s.
2.5 min
100 pA
P22C, c.s.
2.5 min
100 pA
P22C, o.s.
2.5 min
50 pA
3 min
b
Extracellular effect
T20C, c.s.
50 pA
T20C, o.s.
2.5 min
50 pA
P22C, c.s.
50 pA
30 s
P22C, o.s.
2.5 min
100 pA

Fig. 20 : MTSET effect on T20C and P22C mutant channels

a) MTSET application on the inner side of membrane patches. Upper panel: MTSET effect on T20C mutant in the closed state (c.s.) and in the open state (o.s.). Lower panel: MTSET effect on P22C mutant in the closed state (c.s.) and in the open state (o.s.). b) MTSET application on the outer side of membrane patches. Upper panel: MTSET effect on T20C mutant in the closed state (c.s.) and in the open state (o.s.). Lower panel: MTSET effect on P22C mutant in the closed state (c.s.) and in the open state (o.s.).

Fig. 21 :

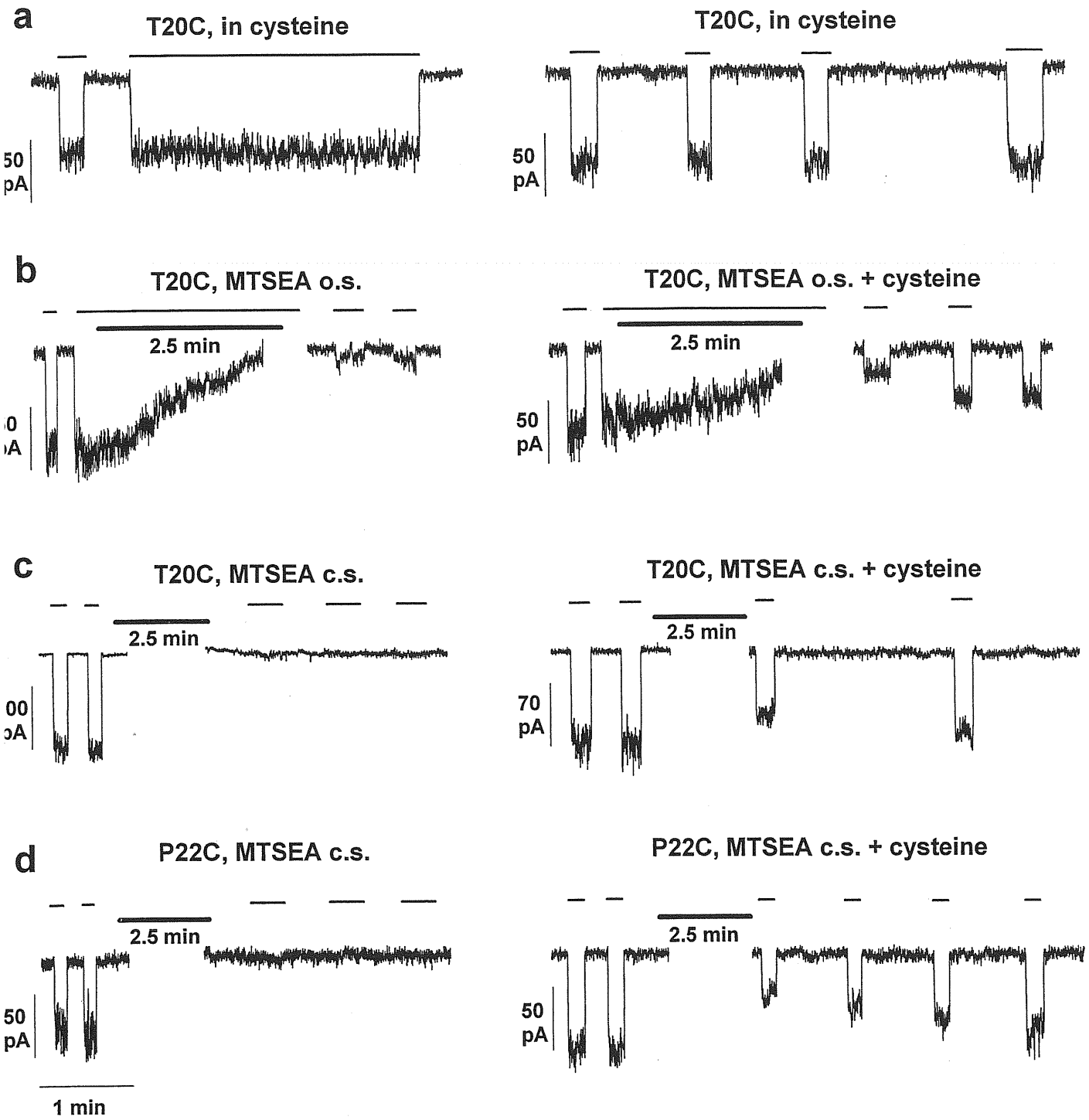
a
T20C, in cysteine
50
pA
T20C, in cysteine
50
pA
b
T20C, MTSEA o.s.
2.5 min
T20C, MTSEA o.s. + cysteine
2.5 min
50
pA
c
T20C, MTSEA c.s.
2.5 min
T20C, MTSEA c.s. + cysteine
2.5 min
70
pA
d
P22C, MTSEA c.s.
2.5 min
P22C, MTSEA c.s. + cysteine
2.5 min
50
pA
1 min

Fig. 21 : Cysteine prevented MTSEA effect on T20C and P22C channels

a) 10 mM cysteine applied to the outer side of membrane patches had no effect on T20C currents. Left panel: cysteine applied in the open state. Right panel: cysteine applied in the absence of cGMP. b) Effect of MTSEA applied to the inner side of patches containing T20C channels, in the open state (o.s.). Left panel: MTSEA irreversibly inhibited T20C current. Right panel: 10 mM cysteine on the outer side of the patch prevented the irreversible block produced by MTSEA applied to the patch inner side. c) Effect of MTSEA applied to the inner side of patches containing T20C channels, in the closed state (c.s.). Left panel: MTSEA irreversibly inhibited T20C current. Right panel: 10 mM cysteine on the outer side of the patch prevented the irreversible block produced by MTSEA applied to the patch inner side. d) Effect of MTSEA applied to the inner side of patches containing P22C channels, in the closed state (c.s.). Left panel: MTSEA irreversibly inhibited P22C current. Right panel: 10 mM cysteine on the outer side of the patch prevented the irreversible block produced by MTSEA applied to the patch inner side.

Fig. 22 :

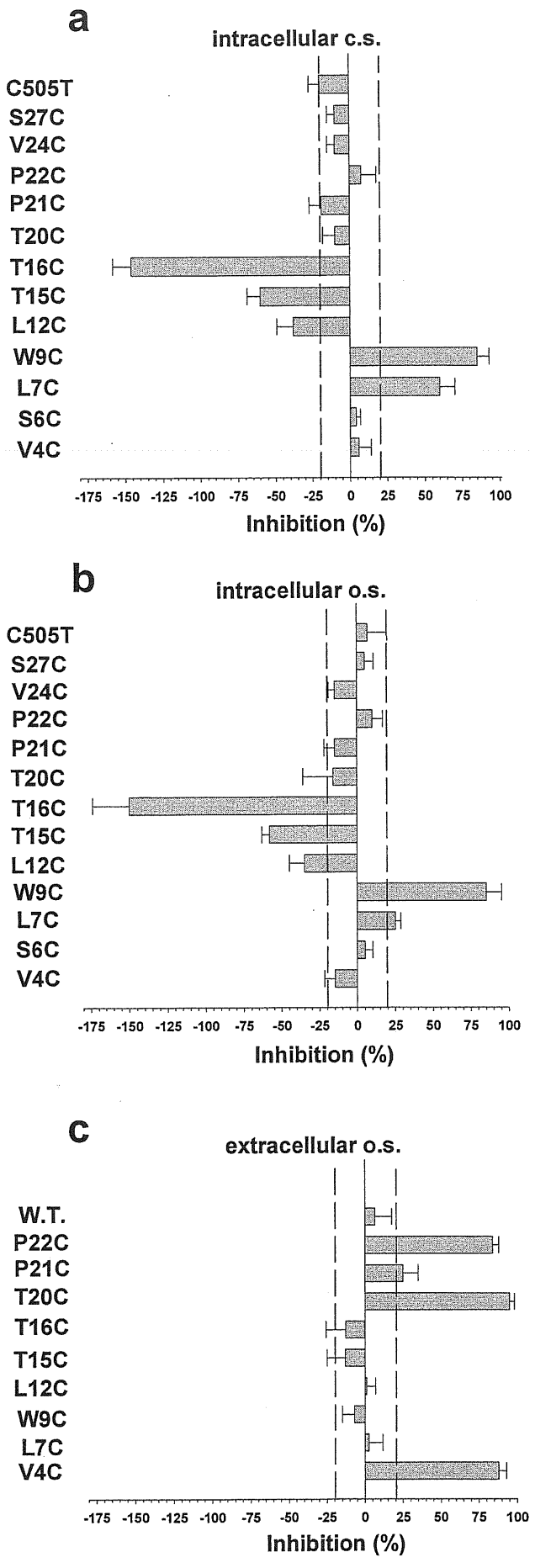
a
intracellular c.s.
C505T
S27C
V24C
P22C
P21C
T20C
T16C
T15C
L12C
W9C
L7C
S6C
V4C
-175 -150 -125 -100 -75 -50 -25 0 25 50 75 100
Inhibition (%)
b
intracellular o.s.
C505T
S27C
V24C
P22C
P21C
T20C
T16C
T15C
L12C
W9C
L7C
S6C
V4C
-175 -150 -125 -100 -75 -50 -25 0 25 50 75 100
Inhibition (%)
c
extracellular o.s.
W.T.
P22C
P21C
T20C
T16C
T15C
L12C
W9C
L7C
V4C
-175 -150 -125 -100 -75 -50 -25 0 25 50 75 100
Inhibition (%)

Fig. 22 : Summary of MTSET effects on mutant channels, on the indicated mutants

a) Intracellular MTSET effect, in the absence of cGMP. b) Intracellular MTSET effect, in the presence of cGMP. c) Extracellular MTSET effect, in the presence of cGMP.
The experimental procedure was explained in Fig. 15. The dashed lines mark the 20% level of inhibition or potentiation, which we considered significant for inferences about residue accessibility (see text).

III.A.3 INTERACTION OF Na^+ AND K^+ IN THE PORE OF THE CNG CHANNEL

The pore region of CNG channels is characterised by a loop of three prolines which is not present in voltage-gated channels (Fig. 23). These three prolines are found in all known α subunits of CNG channels; they are at positions 365 to 367 in the sequence of the α subunit from bovine rod. In all β subunits of CNG channels the second proline of the motif is replaced by an aspartate. Previous studies localised this proline loop near a glutamate residue known to play an essential role in ionic permeation (Root and MacKinnon, 1993; Eismann *et al.*, 1994; Sesti *et al.*, 1995; Park and MacKinnon, 1995). The results described in section III.A.2.5. concerning MTS compounds applied to the residues P21C (i.e. P365C) and P22C (i.e. P366C) strongly suggest that these residues belong to the external vestibule of CNG channels. In this part of the thesis it is shown that mutation of proline 365 of the α subunit of the CNG channel from bovine rod into a threonine, a cysteine or an alanine, leads to mutant channels with unusual properties. Therefore this proline loop is likely to be a distinct feature of CNG channels.

III.A.3.1. PROPERTIES OF MUTANT P365T

The cRNA of channel mutants was injected into oocytes and after two or three days it was possible to record currents activated by small amounts of cGMP added to the medium bathing the cytoplasmic side of the oocyte membrane (see Materials and Methods). Fig. 24 reproduces current recordings measured in voltage clamp mode obtained from membrane patches excised from oocytes injected with the cRNA of mutant P365T. The voltage commands were changed from 0 mV to + or -180 mV in steps of 20 mV. The current activated in the steady state by 500 μM cGMP exhibited a significant outward rectification (see Fig. 24a), which was observed also in the presence of 100 and 1000 μM cGMP (see Fig. 24c).

Fig. 23 :

BovRod CNG	K	Y	V	Y	S	L	Y	W	S	T	L	T	L	T	T	I	G	_	_	E	T	**P**	**P**	_	**P**	V	R	D	S		
	346																														371
RatRod CNG	K	Y	V	Y	S	L	Y	W	S	T	L	T	L	T	T	I	G	_	_	E	T	**P**	**P**	_	**P**	V	L	D	S		
	339																														364
ChiCone CNG	K	Y	I	Y	S	L	Y	W	S	T	L	T	L	T	T	I	G	_	_	E	T	**P**	**P**	_	**P**	V	K	D	E		
	393																														418
RabOlf CNG	E	Y	I	Y	C	L	Y	W	S	T	L	T	L	T	T	I	G	_	_	E	T	**P**	**P**	_	**P**	V	K	D	E		
	323																														348
Hum β	_	Y	I	R	C	Y	Y	F	A	V	K	T	L	I	T	I	G	_	_	G	L	**P**	**D**	_	**P**	K	T	L	F		
	826																														850
Bov β	_	Y	I	R	C	Y	Y	W	A	V	K	T	L	I	T	I	G	_	_	G	L	**P**	**D**	_	**P**	R	T	L	F		
	946																														970
Rat β	_	Y	I	R	C	Y	Y	W	A	V	K	T	L	I	T	I	G	_	_	G	L	**P**	**D**	_	**P**	Q	T	L	F		
	928																														952
Rat OCNC2	Q	Y	L	Y	S	F	Y	F	S	T	L	I	L	T	T	V	G	_	_	D	T	**P**	**L**	_	**P**	D	_	_	_		
	217																									239					
Shaker	S	I	P	D	A	F	W	W	A	V	V	T	M	T	T	V	G	Y	G	D	M	**T**	_	_	**P**	V	G	F	W		
	428																														454
Herg	K	Y	V	T	A	L	Y	F	T	F	S	S	L	T	S	V	G	F	G	N	V	**S**	_	_	**P**	N	T	N	S		
	610																														636
Romk	G	M	T	S	A	F	L	F	S	L	E	T	Q	V	T	I	G	Y	G	F	R	**F**	**V**	T	**E**	Q	C	A	T		
	127																														155
KcsA	T	Y	P	R	A	L	W	W	S	V	E	T	A	T	T	V	G	Y	G	D	L	**Y**	_	_	**P**	V	T	L	W		
	61																														87
Kv2.1	S	I	P	A	S	F	W	W	A	T	I	T	M	T	T	V	G	Y	G	D	I	**Y**	_	_	**P**	K	T	L	L		
	359																														385
Na I	T	F	S	W	A	F	L	S	L	F	R	L	M	T	_	_	_	_	Q	D	F	**W**	_	_	**E**	N	L	Y	Q		
	367																														389
Na II	D	F	F	H	S	F	L	I	V	F	R	V	L	C	_	_	_	_	G	E	W	**I**	_	_	**E**	T	M	W	D		
	936																														958
Na III	N	V	G	F	G	Y	L	S	L	L	Q	V	A	T	_	_	_	_	F	K	G	**W**	_	_	**M**	D	I	M	Y		
	1417																														1439
Na IV	T	F	G	N	S	M	I	C	L	F	Q	I	T	T	_	_	_	_	S	A	G	**W**	_	_	**D**	G	L	L	A		
	1709																														1731

Fig. 23 : Sequence alignment of the pore-forming regions of α and β subunits of CNG channels with selected K^+ channels and the four domains of a Na^+ channel.

The sequences are from top to bottom: CNG α subunit from bovine rods (BovRod CNG, *Bos taurus*, accession number (acc) Swissprot Q00194); CNG α subunit from rat rods (RatRod CNG, *Rattus norvegicus*, acc Swissprot Q62927); CNG α subunit from chick cones (ChiCone CNG, *Gallus gallus*, acc PIR I50630); CNG α subunit from rabbit olfactory sensory neurons (RabOlf CNG, *Oryctolagus cuniculus*, acc Swissprot Q28718); CNG β subunit from human rods (Hum β , *Homo sapiens*, acc Genbank AF042498); CNG β subunit from bovine rods (Bov β, B. taurus, acc EMBL x89626); CNG β subunit from rat rods (Rat β, *R. Norvegicus*, acc Genbank AJ000496); CNG OCNC2 β subunit from rat olfactory sensory neurons (Rat OCNC2, *R. norvegicus*, acc Swissprot Q64359); K^+ channel Shaker (*Drosophila melanogaster*, acc Swissprot P08510); K^+ channel Herg (*H. sapiens*, acc PIR I38465); K^+ channel Romk (*R. norvegicus*, acc Swissprot P35560); K^+ channel KcsA (*Streptomyces lividans*, acc PIR S60172); K^+ channel Kv2.1 (*R. norvegicus*, acc Swissprot P15387); Na^+ channel domains I, II, III, IV (*R. norvegicus*, acc Swissprot P04774).The sequences of the CNG channels were aligned to the sequences of the potassium channels as suggested in Doyle *et al.*, 1998. The alignment of the four domains of the Na^+ channels was that proposed by Guy and Durell, 1995.

The currents activated by 500 and 1000 μM cGMP were almost identical and therefore 500 μM cGMP can be considered as a saturating cGMP concentration. The concentration activating half of the maximal current was about 200 μM for the mutants P365A, P365T and P365C and was larger than the value measured in the w.t. channel, ranging between 50 and 100 μM. The ratio between the current flowing in the steady state at +100 and -100 mV was about 3 and at the higher voltage of +180 mV it was about 5. The w.t. channel displays a smaller voltage-dependence of gating : the current flowing in the steady-state at positive voltage is about 1.5x higher than at negative one (Karpen *et al.*, 1988).

When Na^+ ions present in the bathing medium were substituted by an equimolar amount of K^+ ions, no appreciable outward current was observed, even at membrane voltages larger than +100 mV (see Fig. 24b). The steady-state I-V relation in the presence of K^+ in the bathing medium, as shown in Fig. 24d, is flat at positive voltages between 0 and +120 mV. In some patches a very small outward current of 1 or 2 pA was observed at membrane voltages larger than +140 mV.

An other remarkable feature of current recordings shown in Fig. 24b, is the presence of a large current transient, when the voltage command was stepped from 0 mV to membrane voltages more negative than -120 mV. This current transient was reduced or almost absent when K^+ ions were replaced by Na^+ ions in the bathing medium. This current is therefore referred as the transient K^+-dependent current (tKdc). At voltages more negative than –100 mV, the time constant characterising the decay of this tKdc was calculated for three different patches (see Fig. 24e). The more negative was the pulse applied to the patch, the more rapid was the decay; its values were comprised between 0.8 and 0.3ms.

Mutant P365T

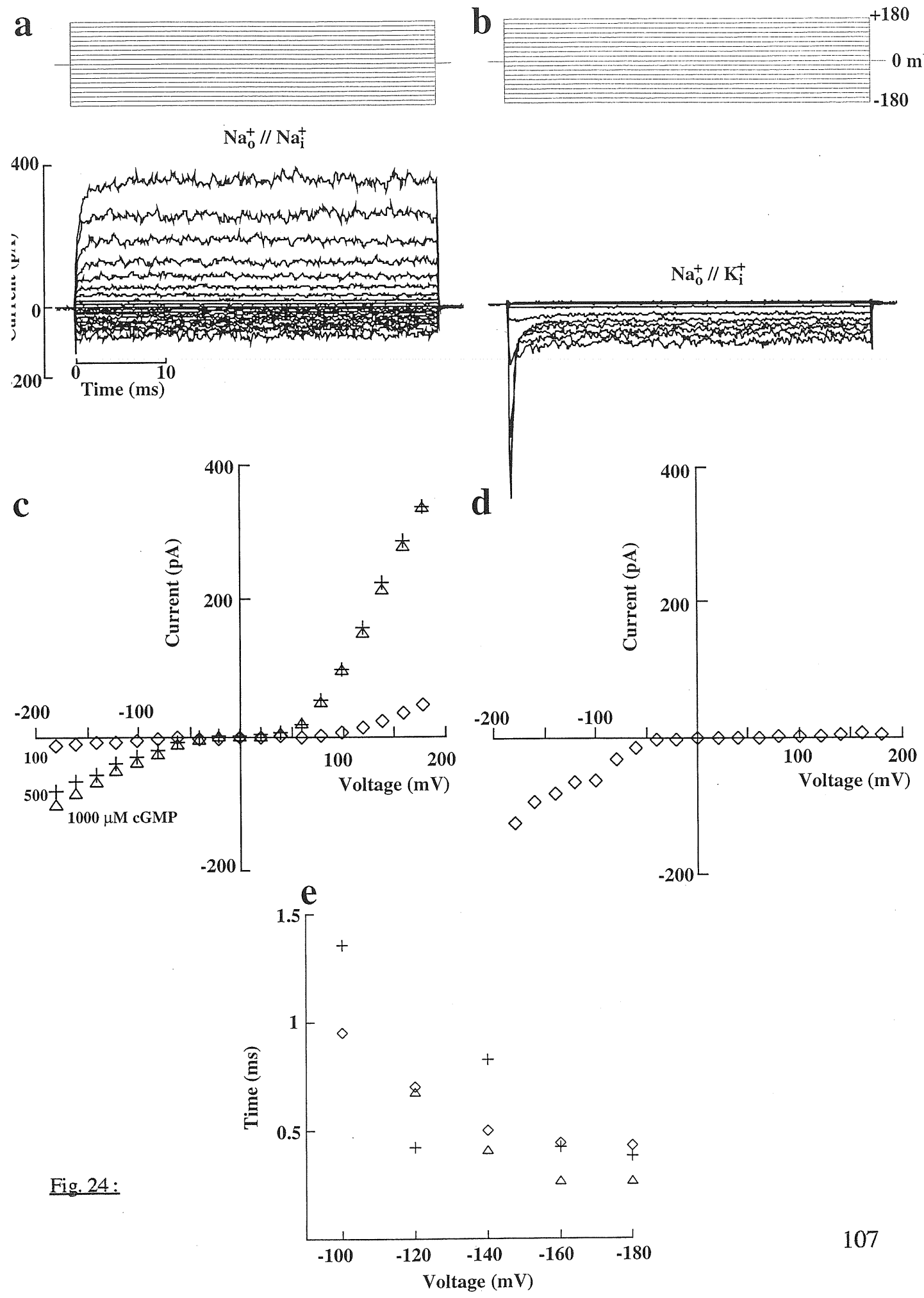

Fig. 24 :

Fig. 24 : Current-voltage relation of mutant P365T

a) and b): Current traces recorded in voltage clamp conditions in the presence of 500 μM cGMP, 110 mM NaCl in the patch pipette and 110 mM NaCl (a) KCl (b) in the bathing medium. Holding voltage 0 mV, pulses from -180 to 180 mV in steps of 20 mV. Traces obtained by averaging 20 different trials. c): I-V relations in the steady state in the presence of 100 (◇), 500 (+) and 1000 μM (Δ) cGMP with 110 mM NaCl on both side of the patch. d): I-V relations in the presence of 500 μM cGMP with 110 mM KCl in the bathing medium. Data from the experiment illustrated in b. e): dependence of the time constant of the current relaxation to its steady state value on membrane voltage in the presence of KCl in the bathing medium. Data from three different patches.

III.A.3.2. SINGLE CHANNEL PROPERTIES OF MUTANT P365T

In order to understand the origin of this outward rectification single channel properties at positive and negative voltages were analysed. Fig. 25a illustrates current recordings obtained at +/-100, +/-140 and +/-180 mV from a patch containing a limited number of mutant channels P365T. The analysis of amplitude histograms (b) obtained at positive voltages indicates the presence of well resolved peaks corresponding to the close state and to current levels with one, two, three and four open channels. At negative voltages the probability of observing two channels open simultaneously was very small, indicating that the open probability increases with the voltage.

Fig. 25c reproduces the current-voltage relation corresponding to the single channel recordings from the experiment shown in Fig. 25a. A straight line provides a good fit of the data, indicating a single channel conductance of about 18 pS between -160 and +160 mV. As a consequence, the origin of the outward rectification of the macroscopic current shown in Fig. 24 is likely to be due to a voltage-dependent gating.

When intracellular Na^+ was replaced by K^+ no outward macroscopic current was detected (see Fig. 24b) and at 0 mV no net inward current carried by Na^+ ions was observed. This last observation suggests a blockade of the Na^+ influx by intracellular K^+. As the traces shown in Fig. 24b were averaged and the leak current - measured in the absence of cGMP - was substracted, a very small current of less than 1 pA carried by K^+ ions would not be reliably detected. In order to test the hypothesis of a K^+ blockade of the Na^+ current and to examine if a very small outward current may be carried by K^+ ions at membrane voltages between 0 and 120 mV, current fluctuations of membrane patches containing very few channels were studied (Fig. 26a,b,c). At -40 mV current fluctuations carried by Na^+ ions were almost completely blocked by the presence of intracellular K^+.

Fig. 25 :

Mutant P365T

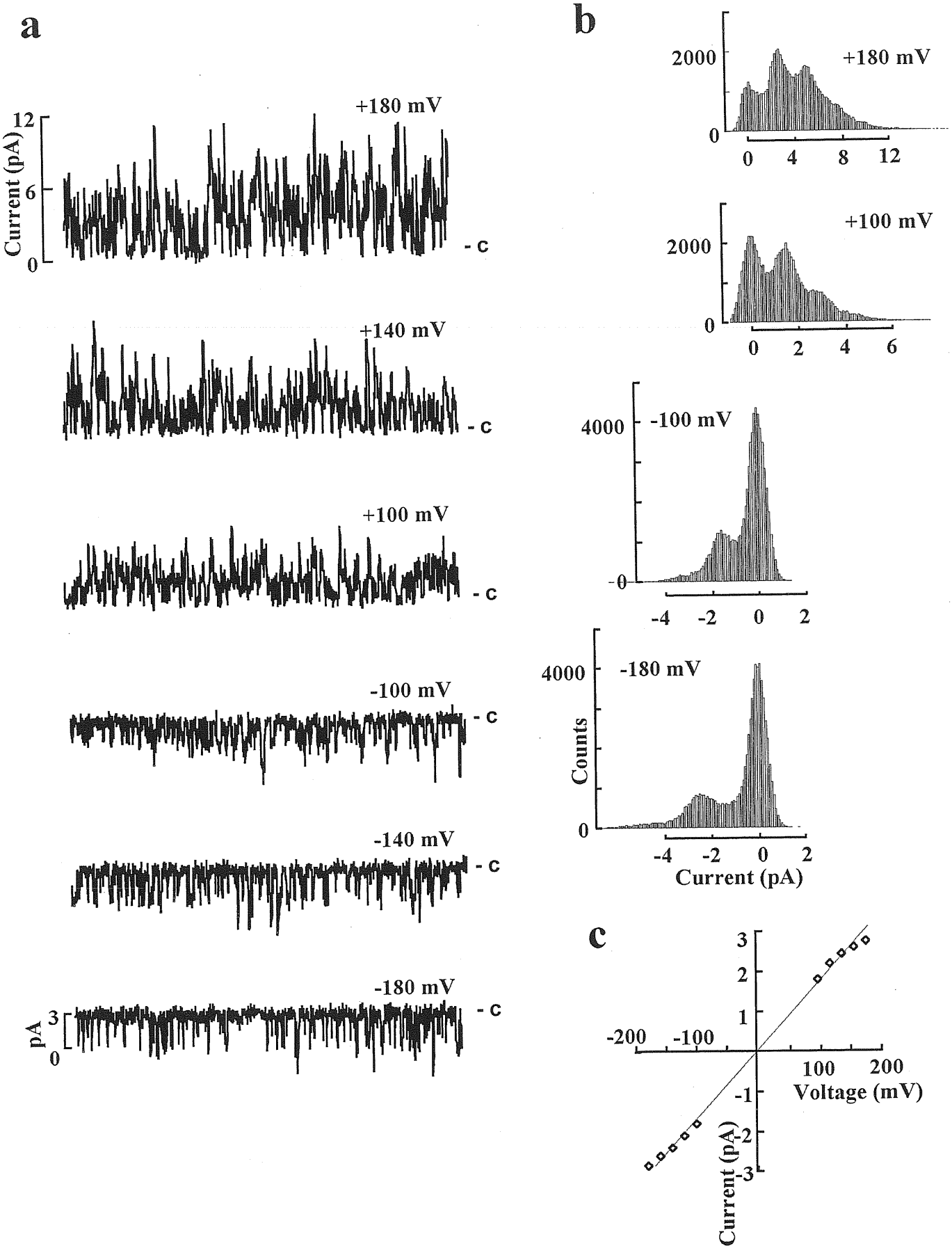

Fig. 25 : a) Single channel current recordings obtained at +180, +140, +100, -100, -140, -180 mV from a patch containing at least four channels of mutant P365T. 500 μM cGMP was present in the intracellular medium. b) Amplitude histograms of current fluctuations shown in a at +180, +100, -100 and -180 mV. Histograms obtained from 5 seconds of continuous recording. The amplitude of the single channel current was obtained by measuring the distance between successive peaks in the amplitude histogram. c) I-V relation of a single channel of mutant P365T. The straight line was computed by assuming a single channel conductance of 18 pS.

This blockade progressively decreased at more negative membrane voltages, such as -80 mV and was almost absent at membrane voltages more negative than -120 mV. These results show that intracellular K^+ ions block the influx of Na^+ ions in a voltage dependent way.

At membrane voltages comprised between 0 and +100 mV current recordings obtained with K^+ in the bathing medium in the presence of cGMP were indistinguishable from those obtained in the absence of ligand. At +120 mV and at more positive voltages some brief and small outward transients carried by K^+ ions were observed (Fig. 26). In order to have a better measurement of these outward transients a patch containing many P365T-channels was analysed at a high gain and in the presence of K^+ in the intracellular medium. In the absence of cGMP the current trace at +120 mV was quiet with a root mean square (rms) of 0.31 pA (Fig. 26d). When 500 μM cGMP was added to the medium bathing the intracellular side of the membrane brief current transients were detected. These current transients never lasted longer than 1 msec and had a variable amplitude up to 3 pA. Their shape is reminiscent of single channel openings, as those shown in Fig. 25.

The amplitude histogram of the current recording in the presence of cGMP (Fig. 26e) indicates that the probability of observing these openings was less than 0.03 and that the net average current carried by K^+ ions was about 0.08 pA. Large single channel currents which are observed at a very low probability is a phenomenon generally identified as a change in gating. As the macroscopic current carried by Na^+ in the same patch at the same voltage was 25 pA, the ratio between the current carried by Na^+ and K^+ was about 300. The same experiment was repeated in other four patches and the ratio between the current carried by Na^+ and by K^+ varied between 150 and 310.

Single channel analysis of these current transients failed to identify a unitary event, but their properties are consistent with the openings of a limited number of channels. It is concluded that K^+ ions permeate through mutant channels P365T at membrane voltages more positive than 100 mV with an altered gating, i.e. with a much lower open probability and with very brief channel openings.

Fig. 26 :

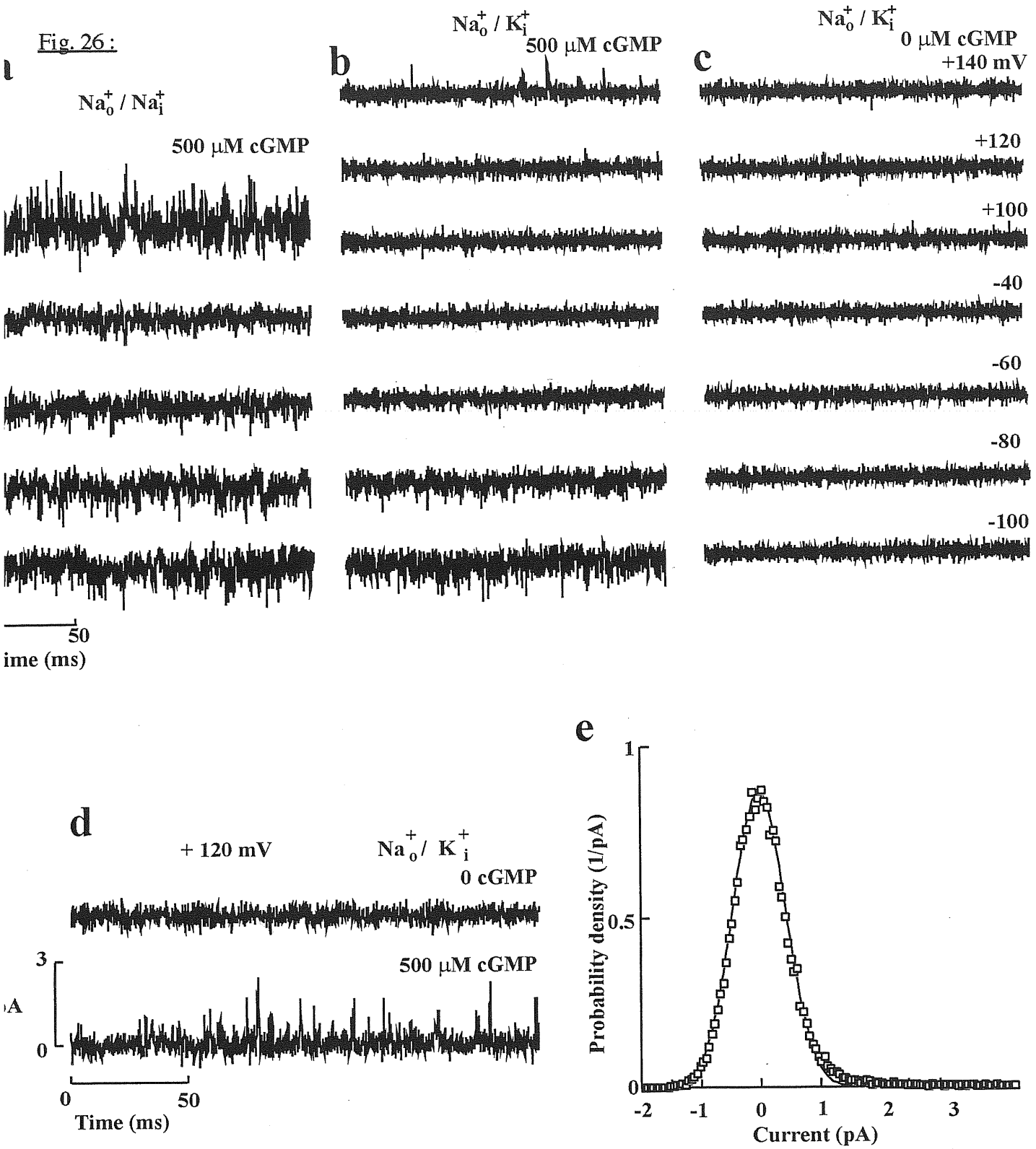
Mutant P365T
a
Na_o^+ / Na_i^+
500 µM cGMP
50
ime (ms)
b
Na_o^+ / K_i^+
500 µM cGMP
c
Na_o^+ / K_i^+
0 µM cGMP
+140 mV
+120
+100
-40
-60
-80
-100
d
+ 120 mV
Na_o^+ / K_i^+
0 cGMP
500 µM cGMP
3
0
0
50
Time (ms)
e
Probability density (1/pA)
1
0.5
0
-2
-1
0
1
2
3
Current (pA)

Fig. 26 : K^+ blockade and permeation

a), b) and c) : Current recordings obtained in the presence of 110 mM Na^+ in the patch pipette and in the presence of 110 mM Na^+ (a), 110 mM K^+ (b and c) in the intracellular medium at the membrane voltages indicated on the right. Recordings in a and b were obtained in the presence of 500 µM cGMP, while those in c in the absence of cGMP. d) A current recording from a membrane patch containing mutant channels P365T at + 120 mV in the presence of 110 mM Na^+ in the extracellular medium and 110 mM K^+ in the intracellular medium in the absence (upper trace) and in the presence of 500 µM cGMP (lower trace) in the intracellular medium. In the presence of 110 mM Na^+ in the extracellular medium a macroscopic current of about 55 pA was observed at +120 mV. e) Amplitude histogram of current fluctuations during 5 seconds of recording in the presence of 110 mM K^+ and 500 µM cGMP in the intracellular medium at + 120 mV. The solid line is a Gaussian distribution with a rms of 0.3 pA corresponding to the noise observed in the absence of cGMP. The area of the histogram corresponding to channel openings was about 0.03, providing a net mean current of 0.06 pA carried by K^+.

III.A.3.3. THE EFFECT OF Ni^{2+} ON MUTANT P365T

The rectification of the I-V relations of mutant channel P365T reported in Fig. 24 and 25, may be caused by a voltage dependence, similar to that of usual voltage-gated channels (Hille 1992), acquired by the mutant channel or by a partial activation of the mutant channel by saturating cGMP concentrations (Li *et al.*, 1997). This last possibility is consistent with the observation that the degree of rectification and the time constant of current activation in the presence of saturating cGMP concentrations in mutant P365T (see Figs. 24 and 34a) is similar to what observed in native CNG channels but in the presence of a subsaturating cGMP concentrations (Karpen *et al.*, 1988).

In the aim of understanding the origin of the rectification observed in Fig. 24, Ni^{2+} ions were added to the bathing medium. Indeed this compound is known to fully activate CNG channels in the presence of a partial agonist (Gordon and Zagotta, 1995a). Its use should allow to discriminate between a rectification phenomenon effectively due to a conformational change and a rectification originating simply from a partial activation of the mutated channel.

10 μM of Ni^{2+} was added to the bathing medium, during the experiment in which current recordings shown in Fig. 24 were obtained. In the presence of Ni^{2+} current recordings presented in Fig. 27a and b were measured. As shown by the I-V relations in Fig. 27c, the addition of Ni^{2+} abolished the outward rectification previously observed. At membrane voltages between 0 and +100 mV the addition of Ni^{2+} led to a 3- to 4- fold increase of the outward current carried by intracellular Na^+ ions. In contrast, even in the presence of Ni^{2+}, no clear outward current carried by intracellular K^+ ions (Fig. 27b and d) could be detected. Ni^{2+} had a different effect on the inward current carried by Na^+ ions at the peak and at the steady state: on average the peak and the steady state current increased by about 3 and 12 times respectively. Therefore the amplitude of the tKdc previously described in the absence of Ni^{2+} (see Fig. 24b) was significantly reduced when Ni^{2+} was added.

The results reported in Fig. 27 offer some explanations for understanding the properties of the mutant P365T. First, the rectification observed in mutant P365T (see Fig. 24a and c) is due to the fact that the cGMP does not fully activate the P365T-mutant but behaves like a partial agonist for this channel. As a consequence in the presence of a saturating cGMP concentration, the maximal open probability of the mutant channel P365T is significantly less than 1. As the potentiation induced by Ni^{2+}

at the steady state is about 12, the maximal open probability of mutant P365T is not larger than 0.09. Second, the K^+ permeation in this mutant is significantly altered. This is strongly suggested by the absence of an outward current carried by K^+ ions at positive voltages even in the presence of Ni^{2+} potentiation (Fig. 27d). Third, the amplitude of the tKdc at very negative membrane voltages in the absence of potentiation is slightly smaller than the peak observed in the presence of Ni^{2+}. Thus the tKdc is likely to represent a transient potentiation of the current carried by the Na^+ ions, due to the presence of K^+ in the bathing medium.

Fig. 27:

Mutant P365T

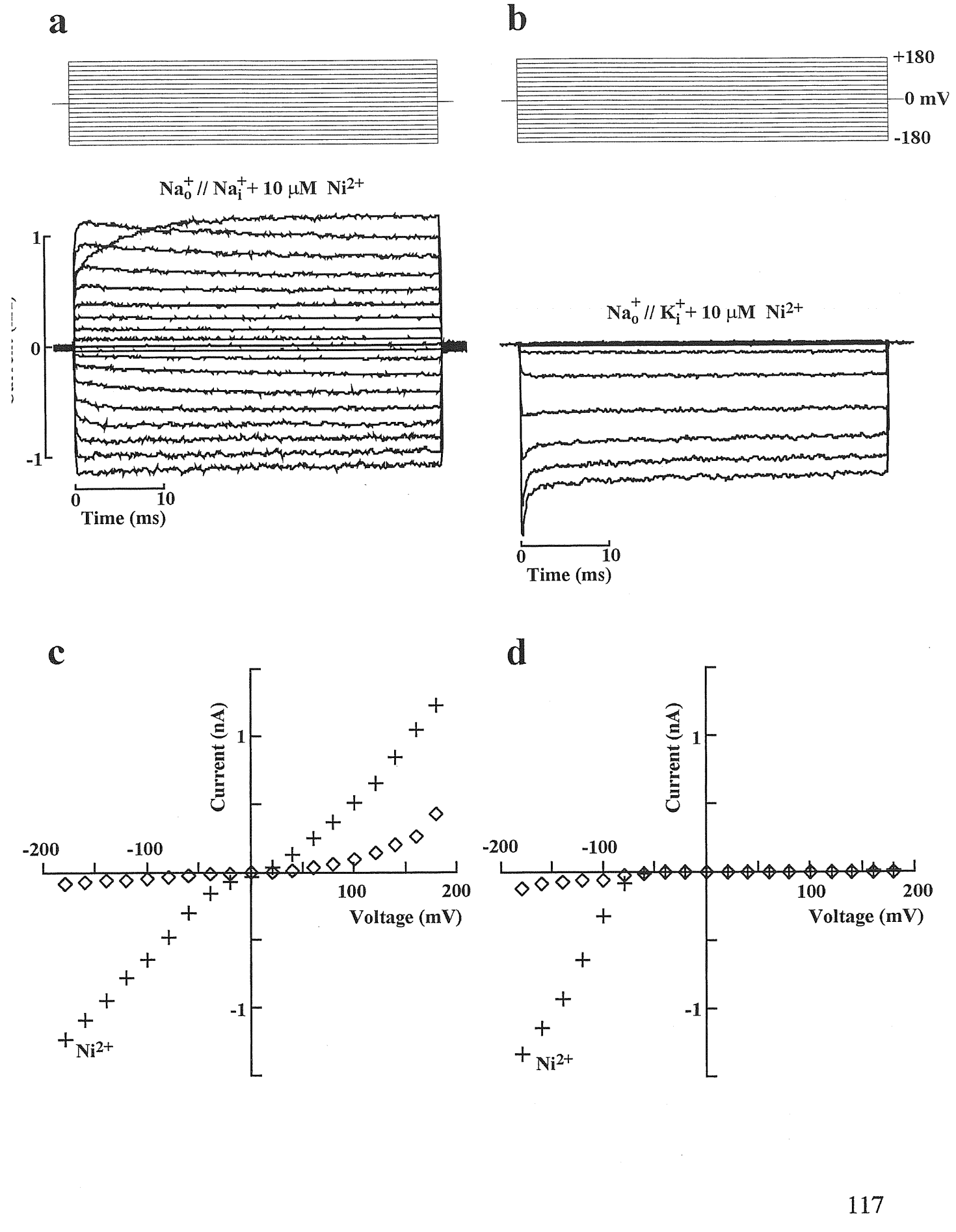

Fig. 27 : Current-voltage relation of mutant P365T in the presence of 10 μM Ni^{2+}

a) and b): Current traces recorded in voltage clamp conditions in the presence of 500 μM cGMP. 110 mM NaCl in the patch pipette and 110 mM NaCl (a) KCl (b) in the bathing medium. Voltage pulses as in Fig. 24. Traces obtained by averaging 20 different trials. c) and d) : I-V relations in the steady state from the experiments shown in a and b respectively. Data from the same patch illustrated in Fig. 24.

III.A.3.4. PROPERTIES OF THE TRANSIENT K^+-DEPENDENT CURRENT IN MUTANT P365T

In order to explore the origin of the tKdc seen in Fig. 24b, different voltage protocols were applied to excised patches containing the mutant channel P365T in the presence of Na^+ or K^+ in the bathing medium. In Fig. 28 results of experiments in which the voltage command V_C to -180 mV, was preceeded by different voltage prepulses V_{pre}, are shown. In the presence of Na^+ ions on both sides of the patch, the current recordings obtained when the voltage command was stepped at - 180 mV led to a minor transient (Fig. 28a). In contrast, this transient was much larger in the presence of K^+ ions in the bathing medium (Fig. 28b). These current recordings are shown on an expanded time scale in panels c and d respectively. The amplitude of tKdc was modulated by the voltage prepulse V_{pre} and was largest when V_{pre} was around 0 mV. The dependence of the ratio I_{peak}/I_{ss}, where I_{peak} and I_{ss} stand respectively for the amplitude of the peak current and for the one of the steady-state, on the value of V_{pre} is shown in Fig. 28e and f. In the presence of K^+ in the bathing medium (panel f), this ratio was maximal around 0 mV and decreased both at very positive and very negative voltages.

The effect of the cGMP concentration on tKdc is analysed in Fig. 29. The experiments described in this figure consisted in stepping the voltage command from 0 to –180 mV using different concentrations of cGMP. Panel a reproduce current recordings obtained in presence of either Na^+ or K^+ in the bathing medium. In the presence of 20 μM cGMP no appreciable current was observed in the presence of intracellular Na^+, but in the presence of intracellular K^+ a very brief and very large transient preceeded the steady-state. Increasing the cGMP concentration led to the appearance of a steady state current which was always larger in the presence of K^+ in the intracellular medium. The dependence of Ipeak on the cGMP concentration for the experiment shown in a is reproduced in panel b. The dependence of $I_{peak}/I_{peak,sat}$ and of $I_{ss}/I_{ss,sat}$ on cGMP concentration is shown in Fig. 29c and d respectively in the presence of intracellular K^+ (filled symbols) and Na^+ (open symbols). The continuous line in panel c is fit to equation (1) with n equal to 2 and Kd equal to 50 μM cGMP (line through the filled symbols) and 150 μM cGMP (line through the open symbols). The data at the steady state (panel d) were fitted to the same equation, with n equal to 2 and Kd of 150 and 240 μM cGMP for the filled and open symbols respectively. These results indicate that the tKdc is more sensitive to cGMP than the current at the steady state or the peak current in the presence of symmetrical Na^+ solution.

Fig. 28:

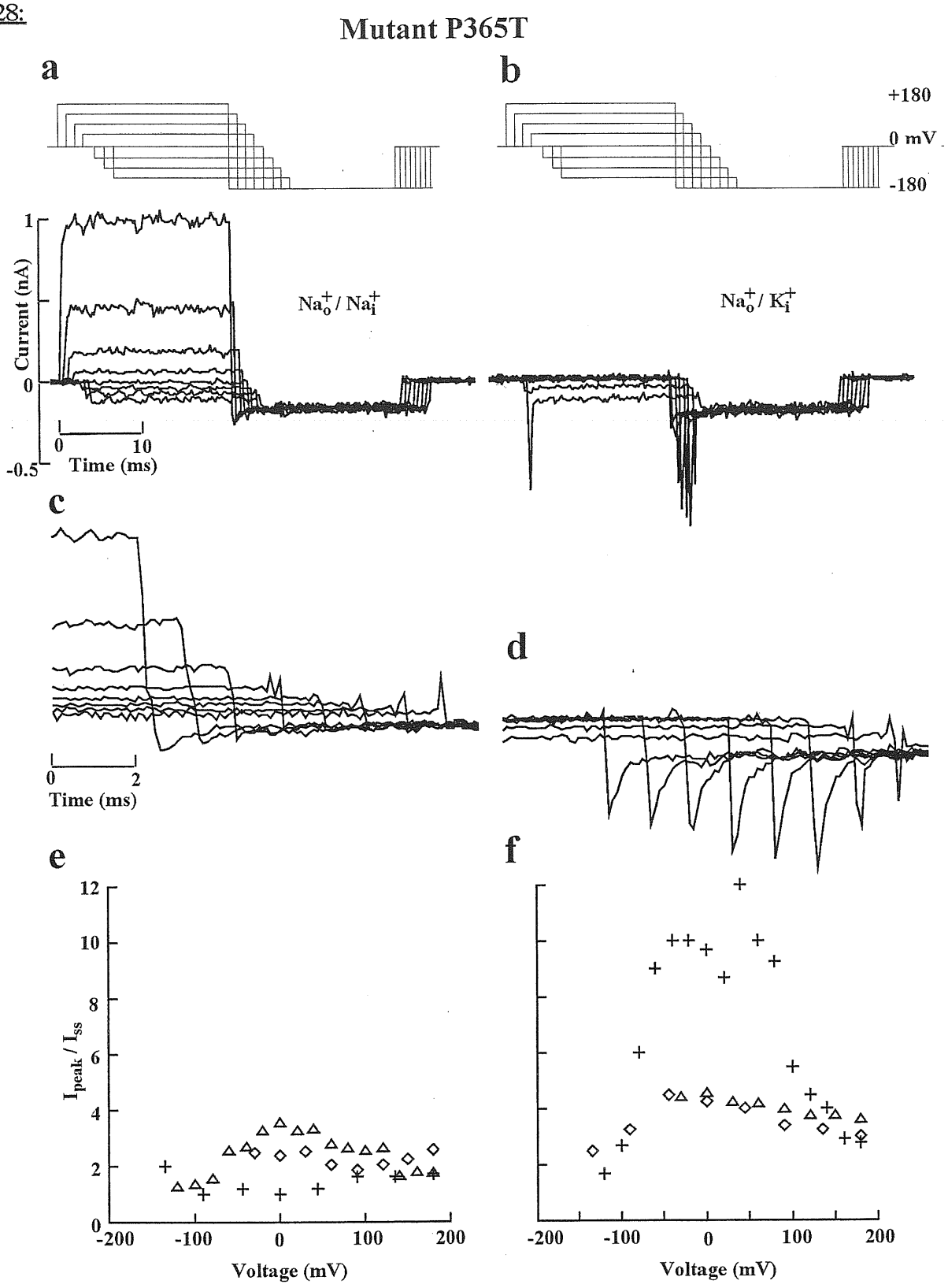
Mutant P365T
a
b
+180
0 mV
-180
1
0
-0.5
Current (nA)
0
10
Time (ms)
Na_o^+ / Na_i^+
Na_o^+ / K_i^+
c
d
0
2
Time (ms)
e
f
12
10
8
6
4
2
0
I_{peak} / I_{ss}
-200
-100
0
100
200
Voltage (mV)

Fig. 28 : Transient K^+-dependent potentiation in mutant P365T

a) and b): current recordings obtained with the voltage protocol shown in the upper part of the panel in the presence of 500 µM cGMP and 110 mM NaCl (a) and KCl (b) in the bathing medium. 110 mM NaCl in the patch pipette. c) and d) : current recordings obtained when switching the voltage command to -180 mV shown in a and b reproduced in greater details. e) and f) : Dependence of I_{peak}/I_{ss} on voltage V_{pre} in the presence of 110 mM NaCl (e) and KCl (f) in the bathing medium and 110 mM NaCl in the patch pipette. The voltage V_{pre} is indicated in the voltage protocol shown in the upper part of panel a. I_{peak} is the amplitude of the current transient observed at voltage V_c and I_{ss} is the steady state current at voltage V_c. Data from three different patches.

Fig. 29 :

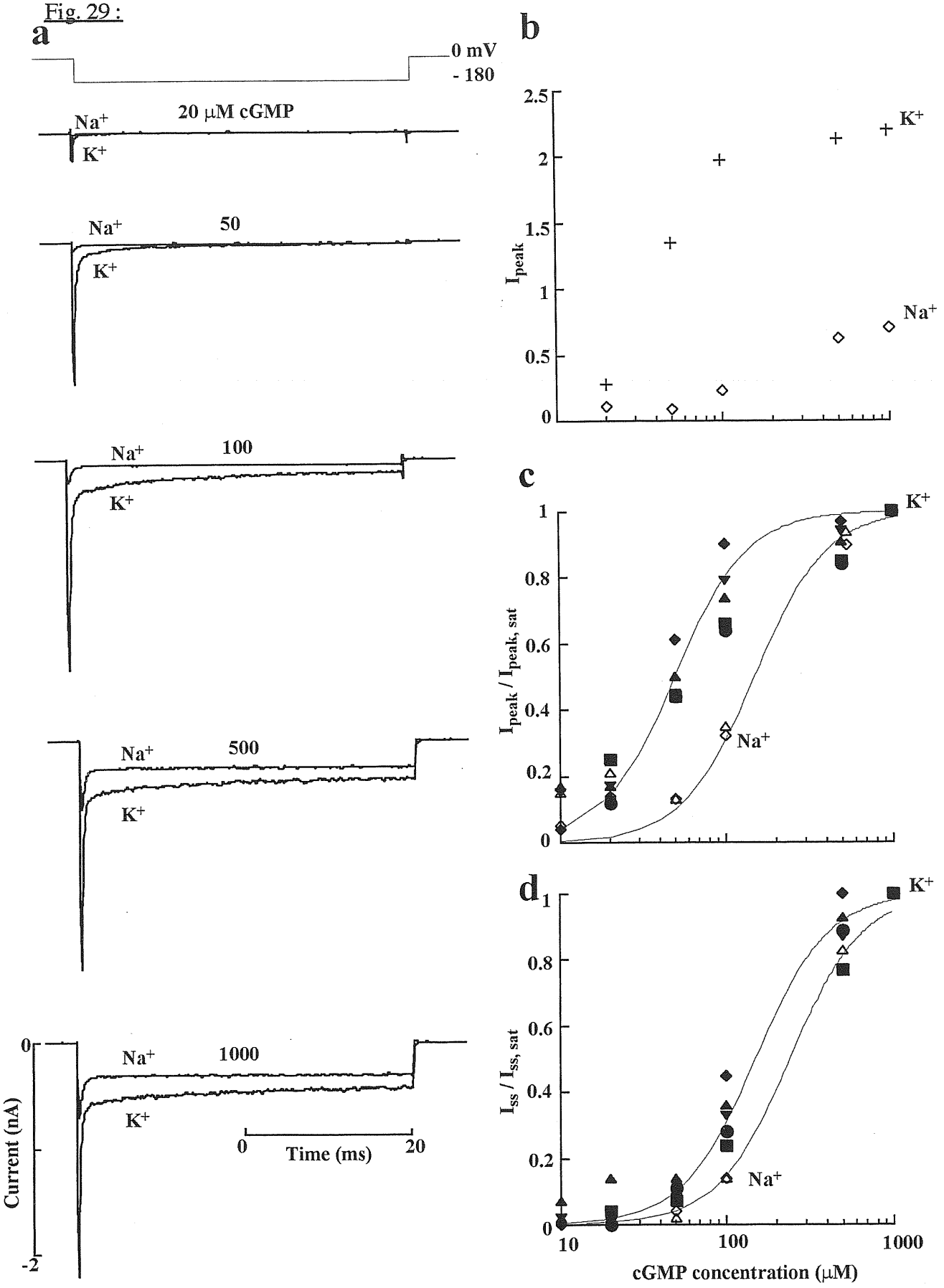
a
0 mV
- 180
Na+
20 μM cGMP
K+
Na+
50
K+
Na+
100
K+
Na+
500
K+
0
Na+
1000
K+
0
Time (ms)
20
Current (nA)
-2
b
2.5
2
1.5
1
0.5
0
I_{peak}
K+
Na+
c
1
0.8
0.6
0.4
0.2
0
I_{peak} / $I_{peak, sat}$
K+
Na+
d
1
0.8
0.6
0.4
0.2
0
I_{ss} / $I_{ss, sat}$
K+
Na+
10
100
1000
cGMP concentration (μM)

Fig. 29 : The effect of cGMP concentration on the transient K^+ dependent current in mutant P365T

a): current recordings in the presence of Na^+ and K^+ in the bathing medium in the presence of different cGMP concentrations. 110 mM NaCl was present in the patch pipette. Voltage command from 0 to -180 mV. b): dependence of I_{pk} and I_{ss} on cGMP concentration in the presence of K^+ in the bathing medium. Data from the experiments shown in panel a. c) : dependence of $I_{pk}/I_{pk,sat}$ on cGMP concentration. Open and filled symbols obtained in the presence of Na^+ and K^+ respectively in the bathing medium. $I_{pk,sat}$ is the peak current recorded in the presence of a saturating cGMP concentration. Data from five different patches. d): dependence of $I_{ss}/I_{ss,sat}$ on cGMP concentration. Open and filled symbols obtained in the presence of Na^+ and K^+ respectively in the bathing medium. $I_{ss,sat}$ is the steady state current recorded in the presence of a saturating cGMP concentration. Data from five different patches.

When the patch pipette was filled with a solution containing K^+ instead of Na^+, current recordings shown in Fig. 30a were obtained. Under these conditions when Na^+ was present at the intracellular side only a macroscopic outward current was observed and no macroscopic inward current was detected. In the presence of 20 μM cGMP only transient outward currents were measured. The current carried by Na^+ at positive voltages increased steeply with voltage and the current flowing at +120 mV was about 10 times the current flowing at + 60 mV. At 0 mV, no appreciable net inward current was observed. In the presence of K^+ on both sides of the patch no appreciable macroscopic current was flowing in either direction (data not shown).
The dependence of I_{peak} and I_{ss} measured at +180 mV on the cGMP concentration is shown in Fig. 30b. The graph shown in panel c represents the ratio I/I_{max} calculated for the peak current (open symbols) as well as for the steady-state current (filled symbols) plotted in function of the cGMP concentration. The solid line through the open and filled symbols were obtained from equation (1) with n equal to 1.8 and Kd of 57 μM cGMP and 120 μM cGMP respectively. The concentration activating half of the maximal current was larger at the steady state than at the peak. The time constant measuring the decay of the peak current at +180 mV was evaluated and plotted as a function of the cGMP concentration (Fig. 30d). The value of the time constant was not dependent on the cGMP concentration and was in general around 1.5 ms (values obtained for three different patches).

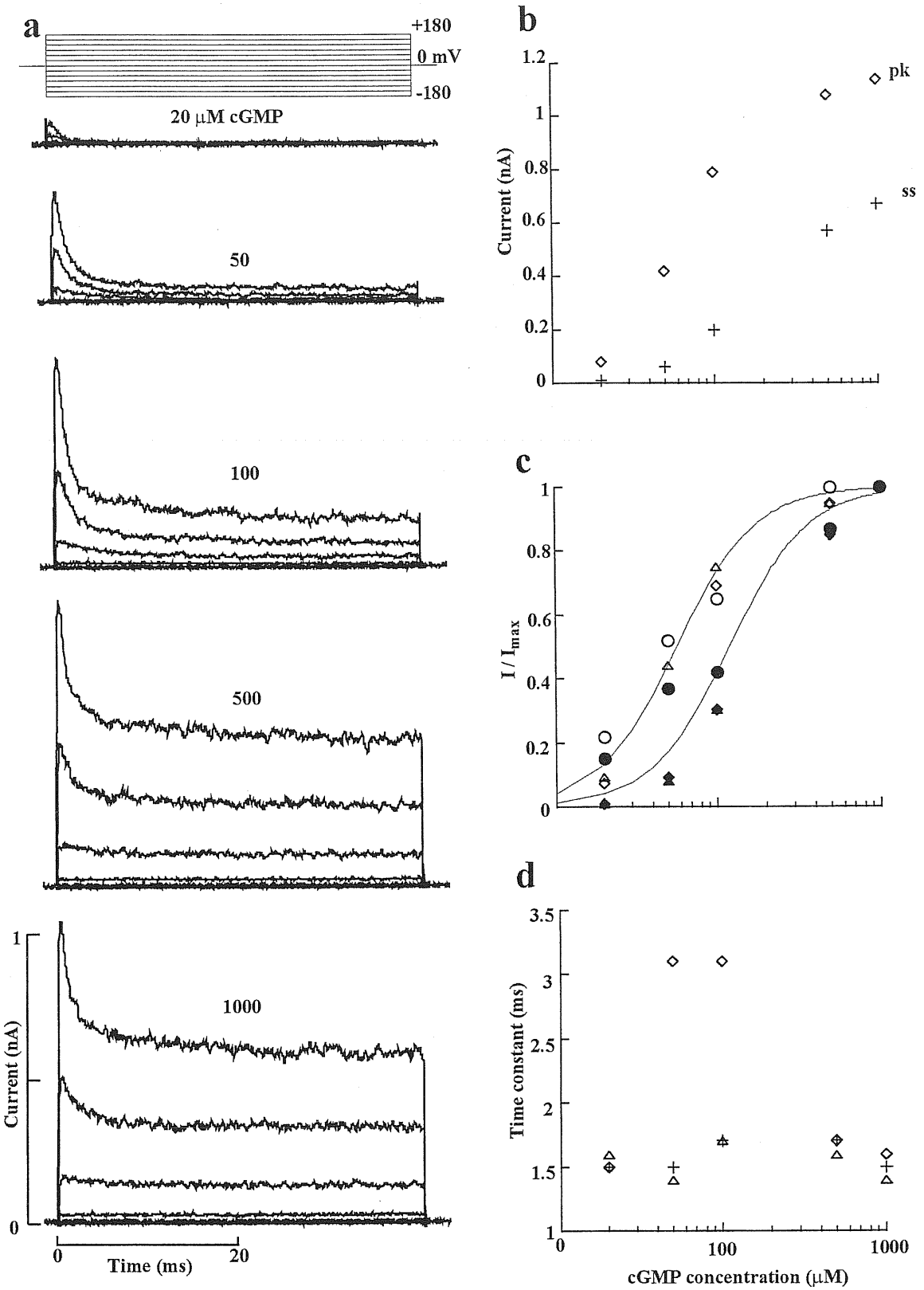
a
+180
0 mV
-180
20 μM cGMP
50
100
500
1000
Current (nA)
Time (ms)
b
pk
ss
Current (nA)
c
I / I max
d
Time constant (ms)
cGMP concentration (μM)

Fig. 30 :

Fig. 30 : Current recordings in the presence of K^+ in the extracellular medium

a): Current traces recorded in voltage clamp conditions in the presence of different cGMP concentrations. 110 mM KCl in the patch pipette and 110 mM NaCl in the bathing medium. Holding voltage 0 mV, pulses from -180 to 180 mV in steps of 30 mV. Traces obtained by averaging 10 different trials. b): dependence of Ipk and Iss measured at + 180 mV on cGMP concentration. Data from the experiments shown in panel a. c): dependence of $I_{pk}/I_{pk,sat}$ (open symbols) and $I_{ss}/I_{ss,sat}$ (filled symbols) on cGMP concentration. Data from three different patches. Solid lines computed from equation 1 with n=1.8 and Kd=57 and 120 μM cGMP. d): dependence of the time constant measuring the decay of the peak current at +180 mV on cGMP concentration. Data from three different patches.

III.A.3.5. MIXTURES OF Na^+ AND K^+

In the presence of two permeating ions, it is interesting to study an effect termed anomalous mole fraction. This phenomenon is studied using solutions containing different proportions of two permeating ions. If x is the fraction of the permeating ion X and (1-x) the fraction of the permeating ion Y, then the total current carried by the two ions is an increasing or a decreasing function of the fraction x in the case of a single ion binding site. Deviations from this behaviour is called anomalous mole fraction effect and indicates simultaneous binding of the two ion species in the pore of the channel studied. Therefore, in order to characterise the nature of the interaction between Na^+ and K^+ in mutant channels P365T the current flowing in the presence of mixtures of Na^+ and K^+ was analysed.

Fig. 31a shows current traces recorded in voltage clamp conditions in the presence of different ratios of Na^+ and K^+ in the intracellular medium with 110 mM NaCl in the patch pipette and in the presence of 100 μM cGMP in the intracellular medium. In the absence of K^+, current recordings do not have a significant transient when the voltage command was turned to very negative voltages. When the K^+ concentration in the bathing medium was increased, the outward current at positive voltages decreased and the amplitude of the tKdc increased. The I-V relations in the presence of different Na^+/K^+ ratios are shown in Fig. 31b. The inward current at -180 mV increases and the net outward current at + 180 mV decreases as the K^+ concentration is increased in the intracellular medium. This former observation is consistent with a K^+ dependent potentiation of the Na^+ current also at the steady state (see also Fig. 31a). The latter observation is consistent with a poor permeation of K^+ ions through mutant channels P365T (see also Fig. 26). Another explanation may be that, during the brief current transient, K^+ goes inside the channel pore. Then, it is as if a profound decrease in the open probability of opening would result from the occupacy of the pore by K^+ ions. Immediately after that K^+ is driven out, a brief potentiation of the gating is observed. Fig. 31c illustrates the dependence of $I_{peak}/I_{peak,\,max}$ measured at -180 mV on the mole fraction from three different patches. The presence of 1/6 K^+ (=18 mM) in the intracellular medium evoked almost about half of the maximal tKdc. A similar tKdc was observed in the presence of 1/2 K^+ (= 55 mM) and with K^+ only (110 mM).

When the patch pipette was filled with 110 mM KCl in the presence of different ratios of Na^+ and K^+ in the intracellular medium current recordings shown in Fig. 31d were obtained. In these conditions only outward currents were measured and the large tKdc

observed in the absence of K^+ in the intracellular medium, was halved by the presence of only 1/6 K^+ (=18 mM) in the intracellular medium. The dependence of $I_{peak}/I_{peak,max}$ measured at 180 mV on the mole fraction for two different patches is illustrated in Fig. 31e. A study of the dependence of $I_{peak}/I_{peak,max}$ on the mole fraction at + 180 and -180 mV indicates a different sensitivity of the tKdc to positive and negative voltages. these results as well as those shown in Figs. 28-30 indicate a complex interaction between Na^+ and K^+ ions in the pore of mutant P365T.

Fig. 31 :

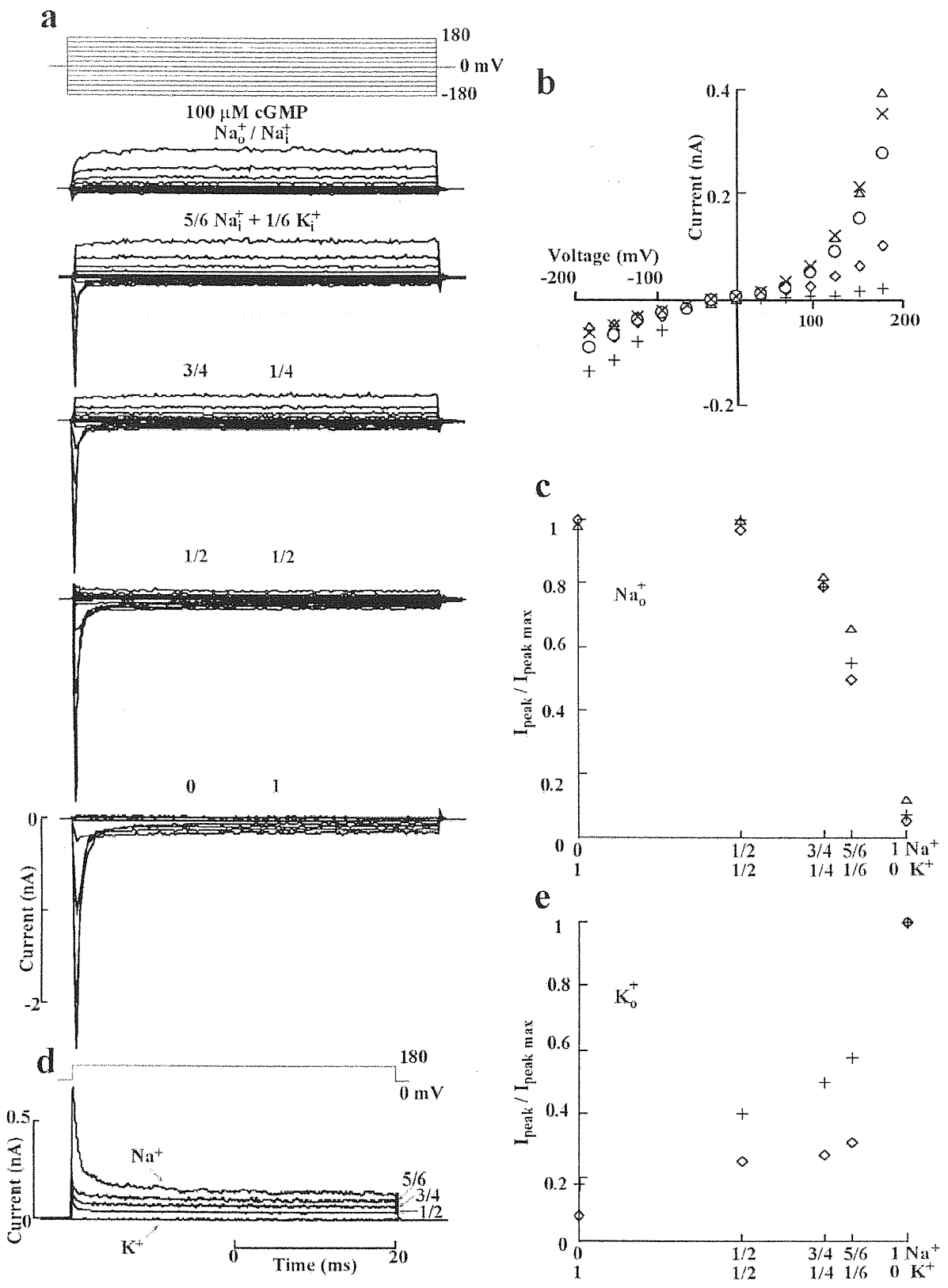
a
180
0 mV
-180
100 µM cGMP
Na_o^+ / Na_i^+
5/6 Na_i^+ + 1/6 K_i^+
3/4
1/4
1/2
1/2
0
1
0
Current (nA)
-2
b
0.4
0.2
-0.2
Current (nA)
Voltage (mV)
-200
-100
100
200
c
1
0.8
0.6
0.4
0.2
0
Na_o^+
I_{peak} / $I_{peak\ max}$
0 1/2 3/4 5/6 1 Na^+
1 1/2 1/4 1/6 0 K^+
d
180
0 mV
0.5
0
Current (nA)
Na^+
5/6
3/4
1/2
K^+
0
20
Time (ms)
e
1
0.8
0.6
0.4
0.2
0
K_o^+
I_{peak} / $I_{peak\ max}$
0 1/2 3/4 5/6 1 Na^+
1 1/2 1/4 1/6 0 K^+

Fig. 31 : Current recordings in the presence of mixtures of Na^+ and K^+

a): Current traces recorded in voltage clamp conditions in the presence of different ratios of Na^+ and K^+ in the intracellular medium. 110 mM NaCl in the patch pipette and in the presence of 100 mM cGMP in the intracellular medium. Holding voltage 0 mV, pulses from -180 to 180 mV in steps of 30 mV. Traces obtained by averaging 10 different trials. b): I-V relations in different ratios of Na^+ and K^+ : 1 Na^+, 0 K^+ (Δ); 5/6 Na^+, 1/6 K^+ (X), 3/4 Na^+, 1/4 K^+ (O); 1/2 Na^+, 1/2 K^+ ($\diamond$), 0 Na^+, 1 K^+ (+). c): dependence of $I_{pk}/I_{pk,max}$ measured at - 180 mV on the mole fraction. Data from three different patches. d): Current traces recorded in voltage clamp conditions in the presence of different ratios of Na^+ and K^+ in the intracellular medium. 110 mM KCl in the patch pipette and in the presence of 100 μM cGMP in the intracellular medium. Holding voltage 0 mV, voltage pulses to 180 mV. Traces obtained by averaging 10 different trials. e): dependence of $I_{pk}/I_{pk,max}$ measured at 180 mV on the mole fraction. Data from two different patches.

III.A.3.6. SINGLE CHANNEL PROPERTIES DURING THE TRANSIENT K^+-DEPENDENT CURRENT

The large tKdc described in Figs. 28 and 31 may originate either from a transient increase of the open probability or from a transient increase of the single channel current. In membrane patches containing a small number of channels, such as those described in Figs. 25 and 26, current openings at –140 mV were analysed.
The average current obtained from 20 different sweeps is reproduced in Fig. 32a. This average current has a clear peak at the onset of the voltage pulse indicated by the dashed line. Channel openings in individual sweeps were analysed (Fig. 32b). As shown in Fig. 32b channel openings observed during the peak of the average current (see the dashed line) had an amplitude very similar to those observed during the steady state. In some sweeps in correspondence of the peak of the average current, double openings (indicated by the arrow) were observed, as in the bottom trace of Fig. 32b.
These results indicate that the tKdc is caused by a transient potentiation of the current carried by Na^+ ions, i.e. an increase of the open probability and not by a transient increase of the single channel current. This conclusion favors the hypothesis mentioned before of a change in gating due to the presence of K^+ ions in the channel pore. Therefore, in CNG channels the complex mechanisms of gating and permeation are likely to be coupled.

Fig. 32 :

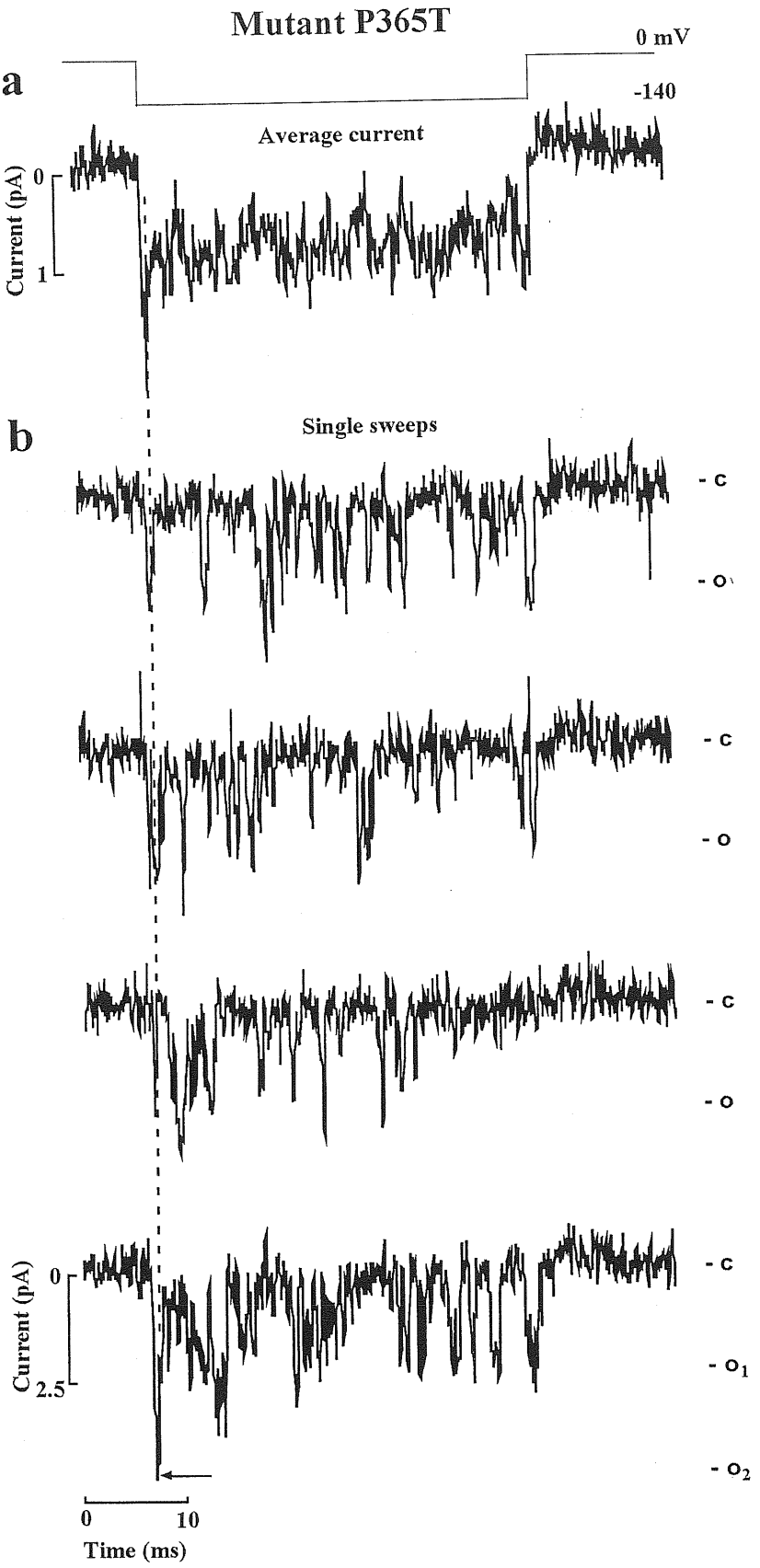
Mutant P365T
0 mV
-140
a
Average current
Current (pA)
0
1
b
Single sweeps
- C
- O
- C
- O
- C
- O
- C
- O1
- O2
Current (pA)
0
2.5
0
10
Time (ms)

Fig. 32 : Single channel properties during the tKdc in mutant P365T

a): average current obtained from 20 consecutive sweeps. b): current recordings from individual sweeps. Voltage pulses of 40 msec duration from 0 to -140 mV. 500 μM cGMP and 110 mM KCl were present in the bathing medium. 110 mM NaCl was present in the patch pipette. The average current shown in a was obtained as the difference of the average of 20 recordings in the presence and absence of cGMP. Recordings shown in b were obtained as the difference of an individual sweep and the average of 20 recordings obtained in the absence of cGMP, in order to remove the artifact caused by the voltage command.

III.A.3.7. IONIC SELECTIVITY OF MUTANTS P365T AND P365A

The ionic selectivity of mutant channels P365T, P365A and P365C to alkali monovalent cations was investigated by measuring the reversal potential V_{rev} of the macroscopic current under biionic conditions. The patch pipette was filled with 110 mM NaCl and currents activated by 500μM cGMP were studied in the presence of equimolar amounts of Na^+ (Fig. 33a), Li^+ (b), K^+ (c), Rb^+ (d) and Cs^+ (e) in the bathing medium. As shown in Fig. 33, an outward current was measured in the mutant P365T only in the presence of either Li^+ or Na^+ at the intracellular side of the membrane. In the presence of Rb^+ and Cs^+ no outward macroscopic current was ever seen even at membrane voltages up to +100 mV. In two patches a small transient outward current of 1-2 pA carried by large alkali cations such as Rb^+ and Cs^+ was observed at +160 mV (data not shown). The reversal potential in the presence of Li^+ was +9.5 mV, 16.2 mV and 14.5 mV for mutants P365A, P365T and P365C, respectively, indicating a permeability ratio P_{Li}/P_{Na} equal to 0.7, 0.54 and 0.6 for the three mutants respectively. In the presence of Rb^+ and Cs^+ a transient current, very similar to tKdc, was observed when the voltage command was turned to very negative values. The value of the reversal potential in the presence of K^+, Rb^+, Cs^+ in the intracellular medium could not be reliably determined, as the I/V relations were flat between -20 and +100 mV. Therefore, the ion permeation is different in the mutant channels with respect to the w.t.'s but no conclusion can be drawn concerning their selectivity sequence. The behaviour of Rb^+ and Cs^+ is similar to the one of K^+ ions. As a consequence, the permeation changes observed for these two ions are likely to be due to interference with channel gating as it has been previously proposed for the permeation of K^+ (see sections III.A.3.5. and 6.).

Fig. 33 :

Mutant P365T

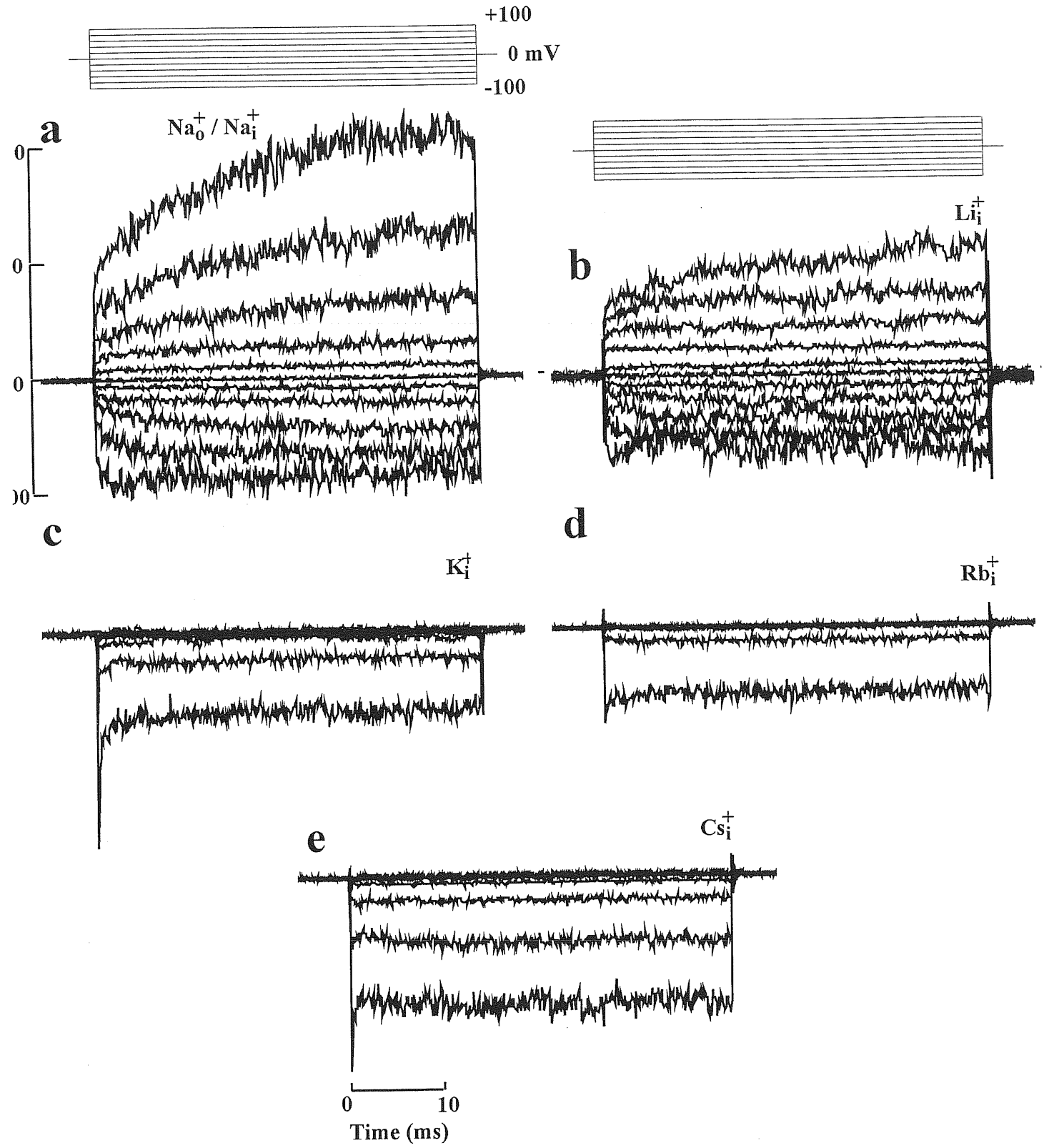

Fig. 33 : Ionic selectivity of mutant P365T to alkali monovalent cations

Current recordings in the presence of 110 mM Na^+ (a), Li^+ (b), K^+ (c), Rb^+ (d) and Cs^+ (e) at the intracellular side of the membrane. 110 mM Na^+ was present in the extracellular medium. Voltage commands as in Fig. 24a-c. The reversal potential for Li^+ was 16 mV.

The selectivity to organic monovalent cations was analysed in the experiments shown in Fig. 34. The mutant channel P365T was permeable to formamidinium (b), guanidinium (c), aminoguanidinium (d) and ammonium ions (e). Some methyl derivatives of ammonium such as methylammonium (f) and dimethylammonium (g) were permeant also. As shown in Table 4 the reversal potential for ammonium was slightly negative, as in wild type CNG channels (Picco and Menini, 1993). Ammonium, however, carried a rather small outward current; rather unexpectedly methylammonium carried a current larger than ammonium at positive voltages, indicating a larger chord conductance for methylammonium.
As shown in Fig. 34e, when the voltage command was stepped to a negative voltage in the presence of intracellular ammonium, a large inward current very similar to the tKdc previously described in the presence of K^+, was observed. This current rapidly declined to a smaller level within a few milliseconds. This result was consistently observed in all patches and in both mutants P365T and P365A.

Table 4 summarises the data collected on reversal potentials and on permeability ratios between different cations and Na^+. Permeability ratios of mutants P365T and P365A were almost identical for monovalent alkali cations and similar for organic cations. For organic cations, the permeability of mutant P365A was very similar to that of CNG channels while the permeability of mutant P365T to the same cations was intermediate between that of CNG channels and that of Na^+ channels. The selectivity of mutant P365C to organic compounds was not determined.

Fig. 34 :

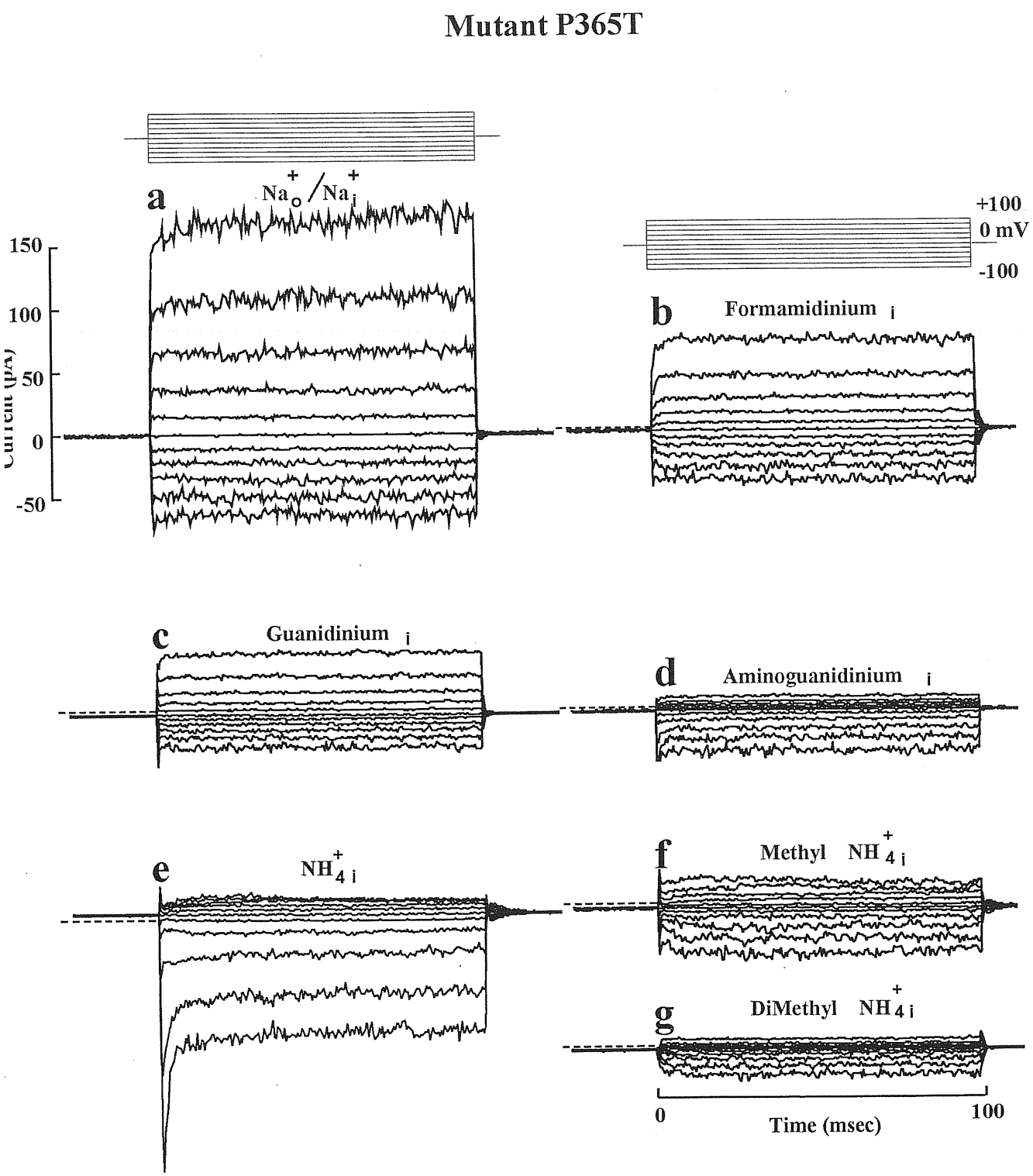
Mutant P365T
a
Na^+_o / Na^+_i
+100
0 mV
-100
150
100
50
0
-50
b
Formamidinium i
c
Guanidinium i
d
Aminoguanidinium i
e
$NH^+_{4\,i}$
f
Methyl $NH^+_{4\,i}$
g
DiMethyl $NH^+_{4\,i}$
0
100
Time (msec)

Fig. 34 : Ionic selectivity of mutant P365T to organic cations

Current recordings in the presence of 110 mM Na^+ (a), formamidinium (b), guanidinium (c), aminoguanidinium (d), ammonium (e), methylammonium (f) and dimethylammonium (g) at the intracellular side of the membrane. 110 mM Na^+ was present in the extracellular medium. Holding voltage 0 mV and voltage commands from -100 to 100 mV in steps of 20 mV. All data obtained in the presence of 500 μM cGMP in the bathing medium.

Cation	Sphere of radius crystal (Angström)	P365T		P365A		cGMP	Na^+
		V_{rev} (mV)	P_X/P_{Na}	V_{rev} (mV)	P_X/P_{Na}	P_X/P_{Na}	P_X/P_{Na}
Ammonium	0.90	-6	1.20	-16	1.80	2.8	0.16
Guanidinium	1.70	8	0.74	- 6	1.20	1.12	0.13
Formamidinium	1.70	8	0.74	- 2	1.08	1	0.14
Aminoguanidinium	1.90	20	0.46	10	0.68	0.63	0.006
Methylammonium	1.30	22	0.40	13	0.60	0.6	<0.007
Dimethylammonium	1.60	50	0.14	45	0.18	0.14	<0.007
Li^+	0.70	16	0.54	9	0.70	1.14	0.93
Na^+	1.00		1		1	1	1
K^+	1.3		n.d.		n.d.	0.98	0.086
Rb^+	1.54		n.d.		n.d.	0.84	<0.012
Cs^+	1.69		n.d.		n.d.	0.54	<0.013

Table 4 : Permeability ratios (P_X/P_{Na}) of mutant channels P365T and P365A.

First and second columns give the nature of the cation X and its sphere of radius crystal. Third and fourth columns reproduce the value of the reversal potential V_{rev} and of the permeability ratio computed from eqn. (2). V_{rev} was measured under biionic conditions with 110 mM Na^+ in the patch pipette and 110 mM cation X in the medium bathing the cytoplasmic side of the membrane. The last columns report the permeability ratios of the native cGMP channel from tiger salamander rods (Menini, 1990; Picco and Menini, 1993) and of the Na^+ channel (Hille, 1992).

III.A.3.8. PROPERTIES OF OTHER MUTANTS NEAR THE PROLINE LOOP

A variety of mutants around the proline loop were also analysed namely: P366T, P366C, P367V, P367C, P365T & P367V; ΔP mutants where one proline of the loop was deleted; YG mutants where the two amino-acids tyrosine and glycine were added between residues 362 and 363. The "YG" containing mutants (YG, YG+P365T, YG+P365A, YG+ΔP, YG+P365T+ΔP) were designed because an alignment of sequences from the pore region of most K^+ channels showed the presence of a YG motif located between the corresponding residues 362 and 363 of the CNG channels (Heginbotham *et al.*, 1992; see Fig. 23). In agreement with Heginbotham *et al.* (1992), the addition of the YG motif into the CNG channel sequence was fatal in all tested mutants. This result suggests that the YG addition disrupts the organisation of the pore in CNG channels.

The alignment of the pore region sequences from both the K^+ channels and the CNG channels indicates that the third proline (P367) of the proline loop in CNG channels is highly conserved also in the K^+ channels. Indeed, all mutants with the P367C or P367V mutation were not functional. When the proline 366 was mutated to a cysteine or to a threonine, the mutant channels had a voltage sensitivity and an ionic conductance very similar to those of the w.t.

The deletion of one proline in the mutants named "ΔP" and "P365T & ΔP" led to interesting results. Deleting one proline from the P365T mutant surprisingly conferred to the resulting mutant P365T & ΔP a clear permeability to K^+. As shown in Fig. 35a in this double mutant similar outward currents were observed in the presence of Na^+ and K^+ in the intracellular medium. In addition the outward rectification present in the single mutant P365T disappeared in the double mutant P365T & ΔP (Fig. 35). These ΔP mutants produced very small macroscopic currents, never exceeding 10 pA at +100 mV in an inside out excised patch. In most of the patches it was possible to record a small cGMP-activated current, where single channel openings could be seen Fig. 35b and c). These openings were rather small and of similar size at +100 and at -100 mV for both mutants P365T & ΔP (Fig. 35b) and ΔP (Fig. 35c). Channel openings at +100 mV in the presence of Na^+ or K^+ in the bathing medium were very similar, in agreement with the observation that in the double mutant P365T & ΔP, Na^+ and K^+ permeate in a similar way.

Fig. 35 :

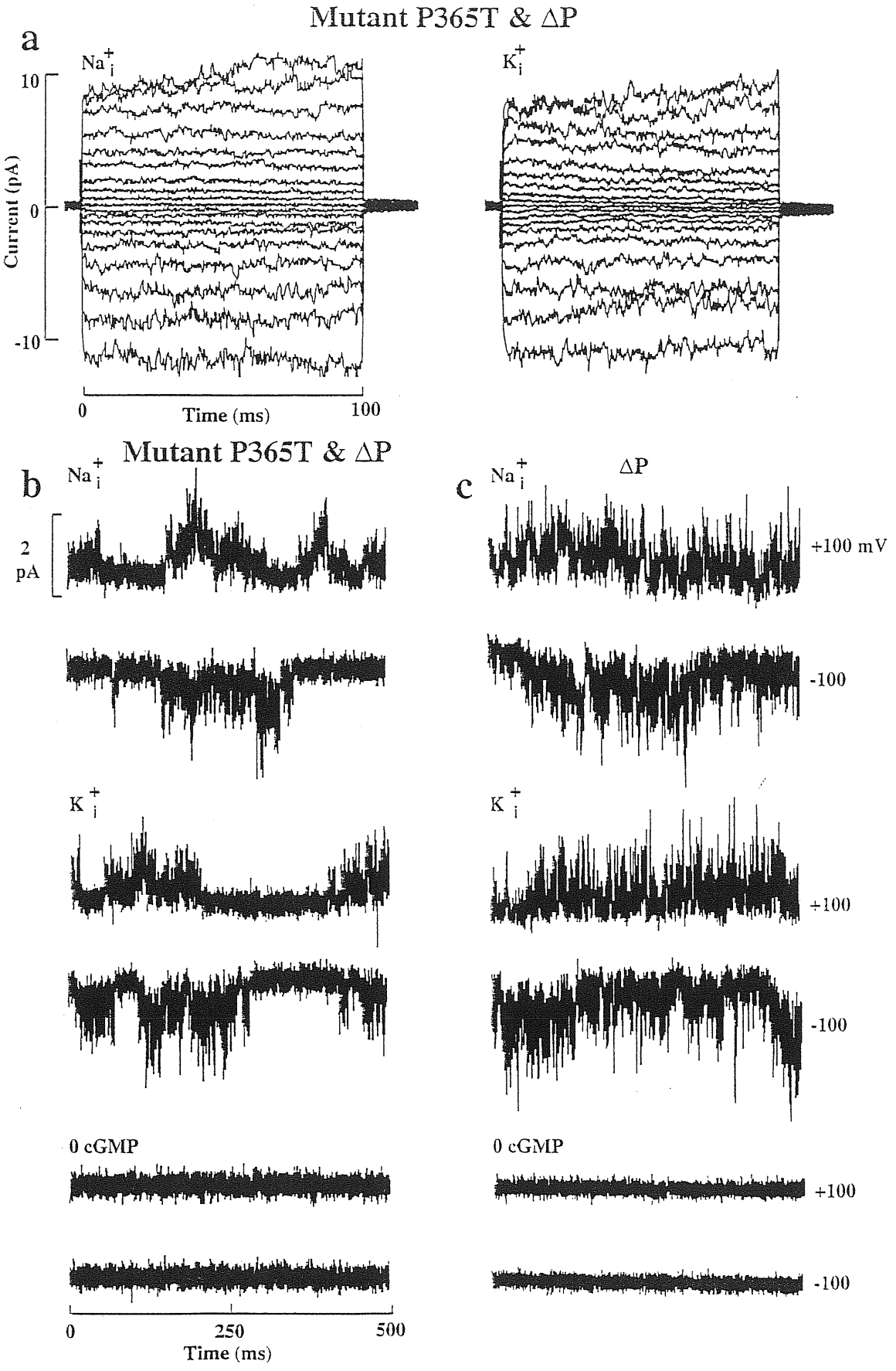
Mutant P365T & ΔP
a
Na^+_i
K^+_i
10
0
-10
Current (pA)
0
Time (ms)
100
Mutant P365T & ΔP
b
c
Na^+_i
ΔP
2 pA
+100 mV
-100
K^+_i
+100
-100
0 cGMP
0 cGMP
+100
-100
0
250
500
Time (ms)

Fig. 35 : Properties of other mutants in the proline loop

a): Current recordings from the double mutant ΔP& P365T in the presence of 110 mM Na^+ (left) and 110 mM K^+ (right) in the intracellular medium. 110 mM Na^+ was present in the extracellular medium. Voltage commands as in Fig. 24a-c. Data averaged over 20 different trials. b) and c): Current recordings from double mutant ΔP & P365T (b) and mutant ΔP (c) at +100 (upper trace) and -100 mV (lower trace). 110 mM Na^+ was present in the extracellular medium and 110 mM Na^+ was present in the intracellular medium when the first and third sets of two recordings were obtained. The second set of two recordings was obtained in the presence of 110 mM K^+ in the intracellular medium. All recordings (with the exception of the bottom two in b and c were obtained in the presence of 500 μM cGMP in the bathing medium.

III.A.3.9. TRANSIENT K^+-DEPENDENT POTENTIATION IN THE W.T. CHANNEL

The observation of a large tKdc in mutant P365T raises the possibility of the existence of a similar current also in the w.t. channel. Such a current has not been described so far and therefore is likely to be small and visible only under particular conditions. Hidden behind such an hypothesis is the possibility of a complex interaction between Na^+ and K^+ ions in the pore of the w.t. CNG channel.

The voltage protocol previously used in the experiment shown in Fig. 28, was applied to a patch excised from an oocyte expressing w.t. CNG channels. When the patch pipette was filled with 110 mM NaCl, the current recordings shown in Fig. 36 were obtained. In the presence of Na^+ on both sides of the membrane, the currents recorded when the voltage command was turned to -180 mV were flat both in the presence of 100 (a) and 500 μM (c) cGMP. When K^+ replaced Na^+ in the bathing medium, the steady state inward current carried by Na^+ at -180 mV was identical, but it was preceeded by a clear transient current, which was larger in the presence of 100 (b) than 500 μM (d) cGMP. This transient current declined with two time constants, one fast of about 1 msec and a slower one of about 10 msec. The dependence of the ratio I_{peak}/I_{ss} on membrane voltage for three different patches in the presence of intracellular K^+ is reproduced in Fig. 36e for 100 (open symbols) and 500 (filled symbols) μM cGMP. Each symbol in Fig. 36f reproduces the value of I_{peak}/I_{ss} at -180 mV calculated for the same patch. The amplitude of the ratio I_{peak}/I_{ss} varied among different patches but at voltages higher than +50 mV, it was always bigger with 100 μM cGMP than with 500 μM cGMP. The ratios I_{peak}/I_{ss} for intracellular Na^+ were plotted in function of the ones obtained for intracellular K^+ in the presence of four different cGMP concentration -50, 100, 500 and 1000 μM- and in three different patches (see panel f). From visual inspection of these collected data it is evident that in no patch a larger value of I_{peak}/I_{ss} was measured in the presence of Na^+. Therefore the differential effect of Na^+ and K^+ on this transient current indicates that it is the equivalent current in the w.t. of the tKdc observed in the mutant P365T.

When the patch pipette was filled with 110 mM KCl and the voltage protocol used in Fig. 36 had opposite polarities current recordings shown in Fig. 37 were obtained.

The inward current carried by K^+ did not show any significant current transient when the voltage was stepped to negative voltages, neither in the presence of Na^+ nor K^+ in the bathing medium, whatever the cGMP concentration used (100 or 500 μM).

Contrary to what was observed in the presence of Na^+ in the patch pipette (see Fig. 14), the outward current carried by Na^+ at +180 mV decayed with a time constant of about 11 msec both in the presence of 100 (a) and 500 μM (c) cGMP. The peak of the outward current at +180 mV dependended on V_{pre} and it was larger for very negative prepulses, i.e. when K^+ ions enter into the channel. The outward current carried by K^+ at +180 mV had a different kinetics than that carried by Na^+. Indeed its peak was smaller but its steady state was larger, leading to a clear crossing of the current traces carried by Na^+ and K^+. The dependence of the ratio $(I_{peak}-I_{ss})/I_{ss}$ at +180 mV on voltage prepulses in the presence of Na^+ and K^+ is shown in Fig. 37e and f respectively. It is evident that the ratio $(I_{pk}-I_{ss})/I_{ss}$ was consistently larger in the presence of intracellular Na^+. The results shown in Figs. 36 and 37 show that the permeation of Na^+ and K^+ through the w.t. CNG channel is not identical and that Na^+ and K^+ interact in a complex way.

In this part of the thesis it has been shown that mutation of proline 365 of the BRET into a threonine, a cysteine or an alanine, leads to mutant channels with unusual properties. First the ionic permeation of the mutant channel is altered. Indeed the presence of K^+, Rb^+ or Cs^+ in the pore of those mutants block the current carried by Na^+ ions. It has also been shown that in mutant P365T, the presence of K^+ in the bathing medium activates a transient current carried by Na^+ when the voltage command is quickly moved to values more negative than -80 mV. This current, here referred as the transient K^+ -dependent current (tKdc) is caused by a transient potentiation, i.e. a transient increase in the open probability of the mutant P365T. It is as if, during the brief transient, K^+ is having no trouble passing through the channel. But, there is a profound decrease in the probability of opening while K^+ is occupying the pore, and a potentiation of gating immediately after it is driven out. A small tKdc was also observed in w.t. CNG channels with properties very similar to those observed in mutant P365T. The deletion of one proline from the loop in the mutant P365T restores the usual permeation of monovalent alkali cations of the w.t. CNG channel. The mutation of the proline in position 366, into a cysteine or a threonine does not alter significantly neither selectivity nor gating. The replacement of the proline in position 367 is a fatal mutation as no cGMP-gated current was observed. These results indicate that: i - K^+ and Na^+ ions do not permeate through CNG channels in the same way and that K^+ ions influence the channel gating; ii - the proline loop is an essential feature of ion permeation in CNG channels.

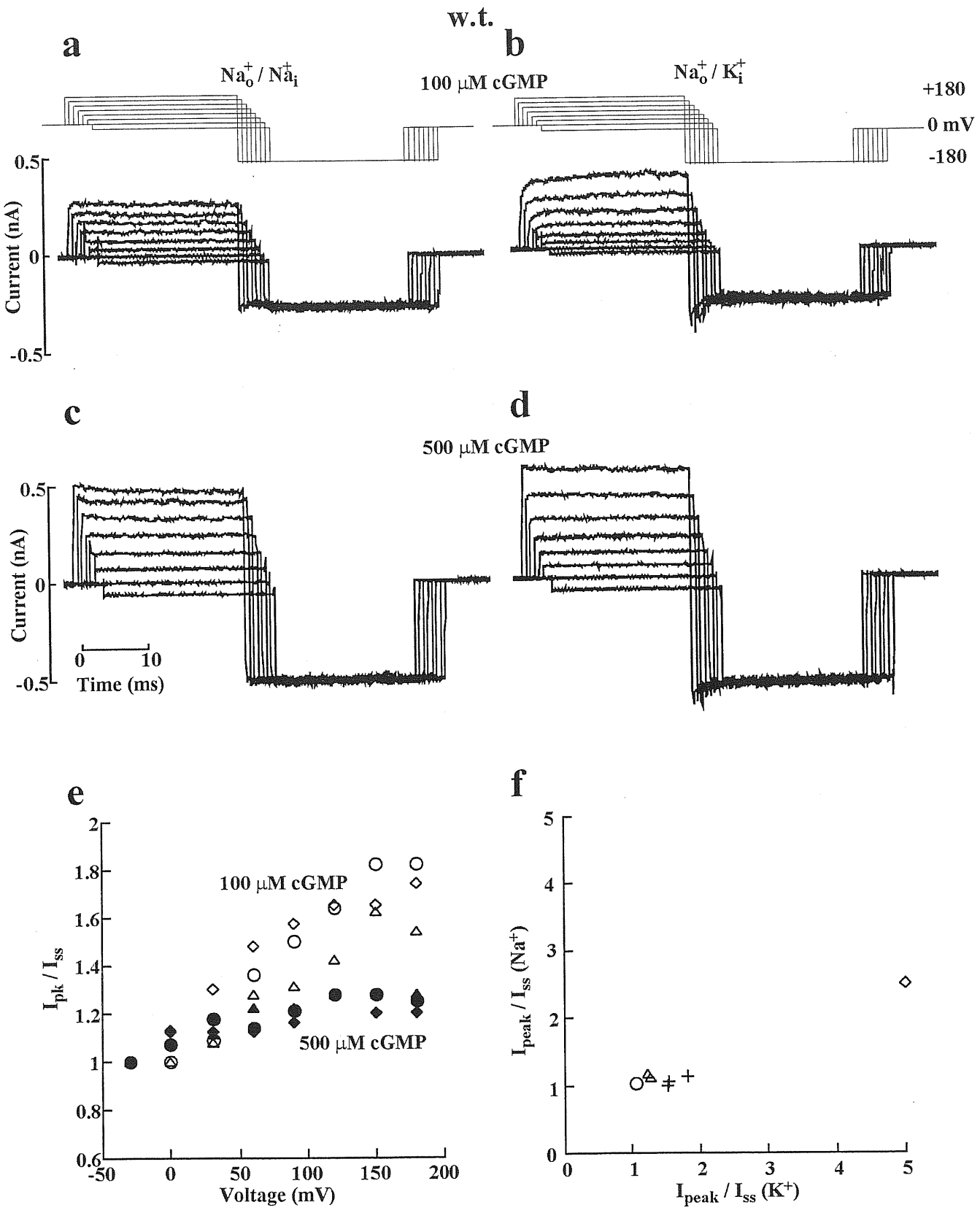
w.t.
a
b
Na_o^+ / Na_i^+
100 μM cGMP
Na_o^+ / K_i^+
+180
0 mV
-180
0.5
0
-0.5
Current (nA)
c
d
500 μM cGMP
0
10
Time (ms)
e
f
100 μM cGMP
500 μM cGMP
I_{pk} / I_{ss}
Voltage (mV)
I_{peak} / I_{ss} (Na^+)
I_{peak} / I_{ss} (K^+)

Fig. 36 :

Fig. 36 : Transient K^+-dependent potentiation in w.t. channel in the presence of Na^+ in the patch pipette

Current recordings obtained with the voltage protocol shown in the upper part of the panel in the presence of 100 (a and b) 500 μM (c and d) cGMP and 110 mM NaCl (a and c) and KCl (b and d) in the bathing medium. 110 mM NaCl in the patch pipette. e): dependence of the ratio Ipk/Iss on membrane voltage in the presence of 100 μM cGMP (open symbols) and 500 μM cGMP (filled symbols) with Na^+ and K^+ ions in the extracellular and intracellular medium. Data from three different patches. f): Comparison of the ratio Ipk/Iss at - 180 mV in the presence of Na^+ versus Ipk/Iss at - 180 mV in the presence of K^+ in the intracellular medium. 110 mM NaCl in the patch pipette. Data from four different patches and in the presence of different cGMP concentrations.

Fig. 37 :

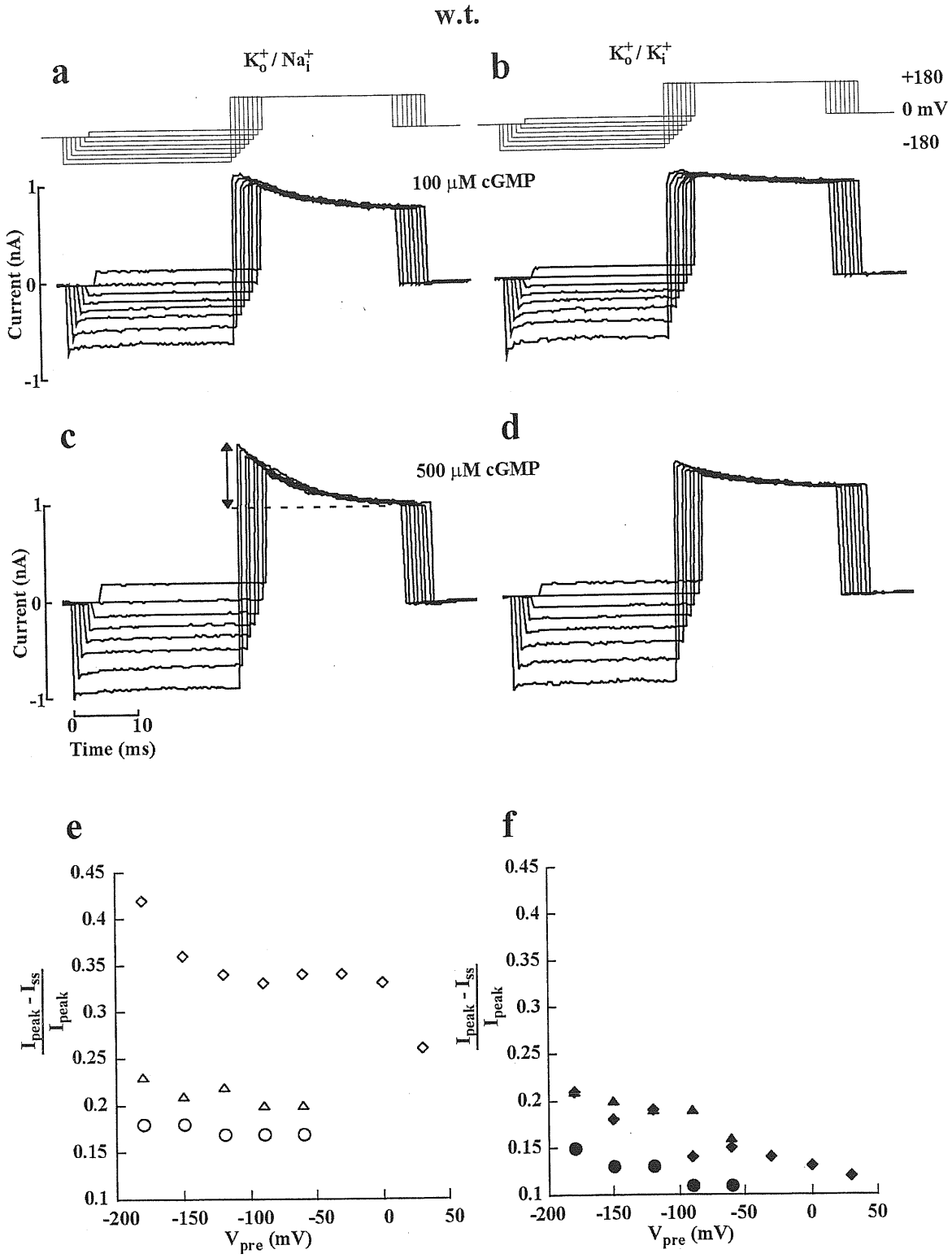
w.t.
a
K_o^+ / Na_i^+
b
K_o^+ / K_i^+
+180
0 mV
-180
100 µM cGMP
Current (nA)
1
0
-1
c
d
500 µM cGMP
Current (nA)
1
0
-1
0
10
Time (ms)
e
f
$\frac{I_{peak} - I_{ss}}{I_{peak}}$
0.45
0.4
0.35
0.3
0.25
0.2
0.15
0.1
-200
-150
-100
-50
0
50
V_{pre} (mV)

Fig. 37 : Na^+ and K^+ interaction in the w.t. CNG channel

Current recordings obtained with the voltage protocol shown in the upper part of the panel in the presence of 100 (a and b) 500 μM (c and d) cGMP and 110 mM NaCl (a and c) and KCl (b and d) in the bathing medium. 110 mM KCl in the patch pipette. e) and f): dependence of the ratio $(I_{pk}-I_{ss})/I_{ss}$ at + 180 mV on voltage prepulse in the presence of 500 or 1000 μM cGMP and in the presence of Na^+ (e) and K^+ (f) in the intracellular medium. 110 mM NaCl in the patch pipette. Data from three different patches.

III.B. CLONING, EXPRESSION AND PURIFICATION OF THE C-TERMINAL PART OF THE BRET

The major part of the thesis is dedicated to the study of the pore which is one of the most important motif present in ionic channels. Because CNG channels are functionally gated by the binding of ligand, a more complete picture of the relationship between structure and function in these channels required a chapter dedicated to the C-terminal part, i.e. the part containing the cyclic nucleotide binding site.

III.B.1. CLONING, EXPRESSION AND PURIFICATION

The aim of this project was to overexpress the C-terminal part of BRET, purify it and obtain a sufficient quantity of extremely pure protein in order to perform crystallisation trials to determine the structure of the cGMP binding site. The prerequisite for crystallisation trials are extremely difficult to be reached. Indeed, the quantity of protein needed is around 10 mg of pure protein obtained in a single batch to maximally avoid the problems of heterogeneity of the protein solution. The purity of the protein must be around 97% as a minimum. The population of the protein molecules present in the solution must be as homogeneous as possible, correctly folded and considering our final goal, the capacity of binding the cGMP molecule had to be checked.

III.B.1.1. CLONING AND PILOT EXPRESSION

For cloning purposes a *Pst* I site was introduced using the QuikChange™ Site-Directed Mutagenesis procedure changing the second base of the codon encoding for the amino acid 478 located in the hydrophobic segment of the cytoplasmic C-terminal part of the BRET. After the mutagenesis, pGEM-HEcG was double digested with *Pst* I and *EcoR* I and the DNA fragment corresponding to the C-terminal part of the BRET starting at the amino acid 480 was isolated and cloned into the pTrcHis B vector (Invitrogen). The success of the cloning was confirmed by the complete sequencing of the cloned C-terminal part of BRET -termed "cyto". The pTrcHis B-cyto plasmid was then propagated in E. coli cells in 50 ml of culture medium (LB + amp) at 37°C until an OD_{600} = 0.6. Once the mid-log phase was reached, the expression of the recombinant protein was induced by IPTG (final concentration of 1 mM) and the expression was stopped after either 1, 2, 3 or 4 hours of incubation. This same protocol was also

applied to the pTrcHis B and to the pTrcHisCAT (a pTrcHis containing the chloramphenicol acetyl transferase gene) as controls. Samples were collected at each time point and obviously also just before incubation (control sample). The bacterial cells were broken by a series of freeze-thaw and the membrane were separated from the cytoplasm by centrifugation. Samples of these pilot expression were loaded on a 10% SDS-PAGE. A myriad of bands were detected both in the cytoplasmic fractions and in the pellet ones (see Fig. 38a). However, a band migrating at about 30 kDa which was absent in the control samples started to appear after 1 hour of expression in the pTrcHis-cyto membrane fractions. The intensity of this band raised up with the time of expression. The result of the pilot expression allowed to envisage to stop the expression after 2 hours (a significant quantity of cyto was already present at this time point and by limiting the time of expression one limits obviously the number of contaminant proteins). At this point the temperature of expression was switched down to 30°C in order to limit the production of contaminant proteins and to try to inhibit the possible formation of inclusion bodies. This temperature was then adopted for every subsequent expression protocol (see the Flow-chart in Fig. 39).

III.B.1.2. EXPRESSION

As the protein was always blocked in the bacterial membrane, a series of solubilization trials were performed by treating the bacterial cells with two different detergents (either 5 or 10 mM NP40 or 46 mM octyl-βD-glucopyranoside "BOG"); these treatments were obviously performed in cold room and using proteases inhibitors (aprotinin, PMSF, antipapain). Steps of sonication were also tried for getting the protein in a soluble form. None of these treatments gave satisfactory results. Then always in the aim of reducing the production of contaminant proteins, different quantities of IPTG were tested and 0.5 mM IPTG seemed to be sufficient to induce the production of cyto. In addition to the traditional Coomassie blue staining of the SDS-PAGE, Western blots were performed to confirm the nature of the band migrating at 30 kDa as well as to see if a fraction of cyto might be present in the cytoplasmic fractions. After the protein transfer on nitrocellulose membrane, an incubation with the AntiXpress™ antibody was performed and followed by an incubation with the Antimouse IgG-HRP complex for ECL detection. The nature of the 30 kDa band was confirmed and a fraction of cyto was indeed present in the cytoplasmic fractions (data not shown). Unfortunately, the quantity of soluble cyto was definitely too low and subsequent trials of purification under native conditions led to quantity as low as 150 ng of pure protein (starting from 50 ml of culture). As a consequence, the purification

of cyto was done under denaturing conditions (see section III.B.1.3. and Fig. 39).

III.B.1.3. PURIFICATION

At the end of the purification process, fractions of 1ml were manually collected and the elution was monitored measuring the OD_{280}. The fractions containing the peak of absorbency were submitted to the Bradford test (Sambrook *et al.*, 1989) for determining the quantity of protein(s) present. From 1 to 3 mg of cyto protein pure at about 90% could be obtained starting from 50 ml of culture (Fig. 38b). The protein was not pure enough as a series of very thin bands were present between 50 and 70 kDa (not visible on the photo). The stability of the protein was tested loading a 10% SDS-polyacrylamide gel with 1 µg of cyto after having left the protein 2 days either at 4°C or at room temperature. Absolutely no degradation was observed, the protein was very stable and no precipitate was ever detected. To improve the purification and get rid of the contaminants some trials using the Centricon 50 (Amicon) were performed but the loss of protein during this treatment was too high. Therefore 10 mM imidazole were added into the binding and the various wash buffers to enhance the stringency and forbid the binding of contaminants to the nickel resin. When preparing the columns, an additional resuspension step of the resin into the imidazole-containing binding buffer was achieved. This method seemed very promising as when running about 2 µg of protein on a 10% SDS-PAGE no more contaminants were visible. When proteins are purified under denaturing conditions, renaturation is necessary and the refolding protocol for each protein must be determined empirically. In order to help the refolding of cyto, the urea was slowly removed by o/n dialysis at 4°C. The dialysis buffer was a Tris 10 mM pH8 supplemented with 0.1% Triton X-100 as very low concentration of detergents may be used in refolding protocols. Nevertheless, for crystallisation purposes a less concentrated Tris buffer (i.e.5 mM) should be preferred (Pr. M. Bolognesi, personal communication). The fractions of purified protein I obtained were then tested for assessing the binding capability of the recombinant protein. The purification strategy is summarised in the flow-chart in Fig. 39.

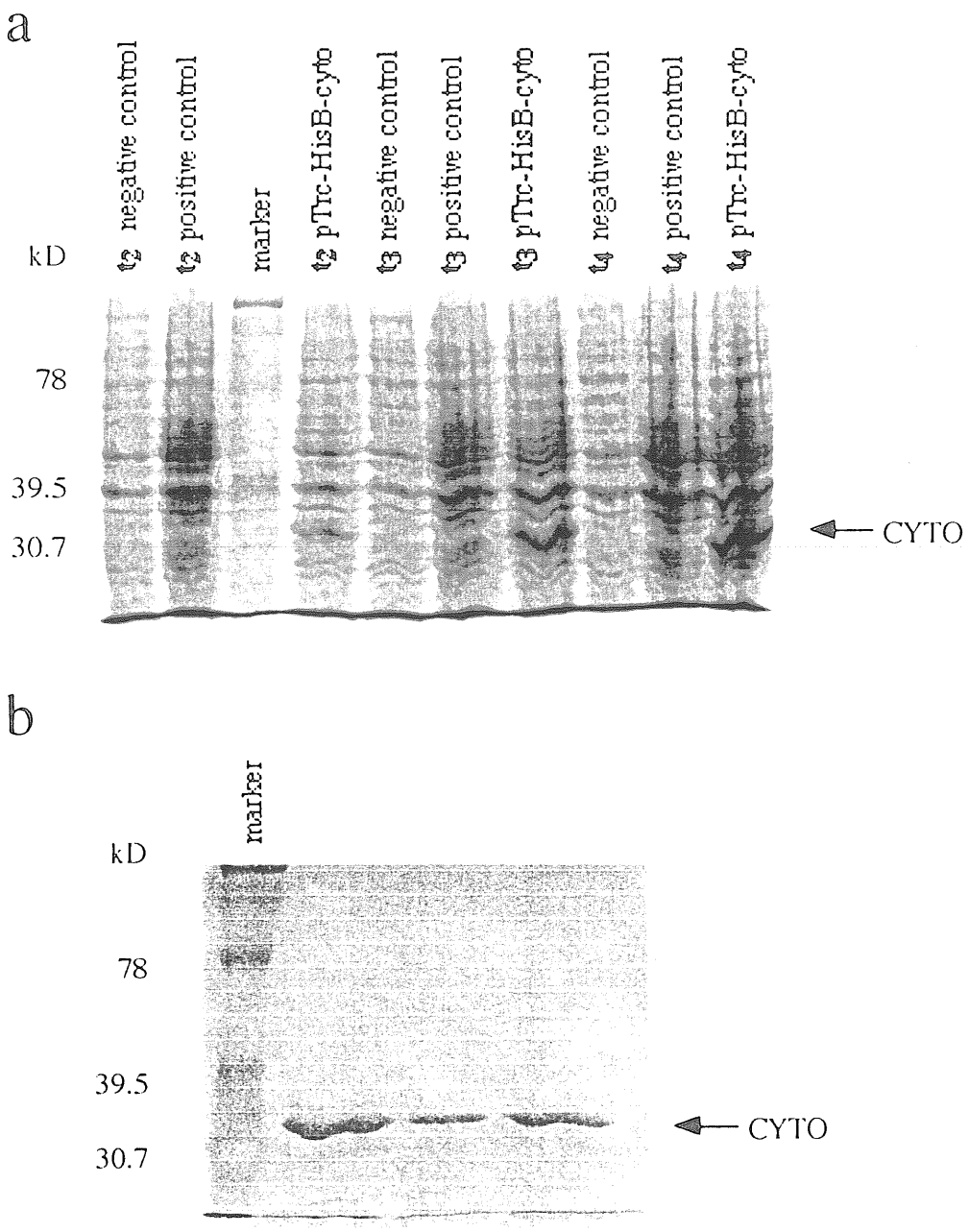

38 : 10% SDS-polyacrylamide gels loaded with pilot expression products (a) and purified cyto samples (b)

Pilot expression. The gel was loaded with the insoluble fractions collected after 2 (t_2), 3 (t_3) or 4 (t_4) hours of pression. The negative control represents the mock expression of pTrcHis vector alone. pTrcHis-CAT is the sitive control but CAT is not visible here as it was expressed in the soluble fraction. pTrc-HisB-cyto is the ctor expressing the cyto protein. Cyto migrates around 30 kD.

Results of the purification. Insoluble fractions obtained after 3 hours of pTrc-HisB-cyto expression were purified der denaturing conditions (see text). The quantity of the purified samples loaded here was estimated at 3µg, 1.5 µg d 2.3 µg respectively for the three successive wells after the marker. The marker is the Kaleidoscope (BioRad).

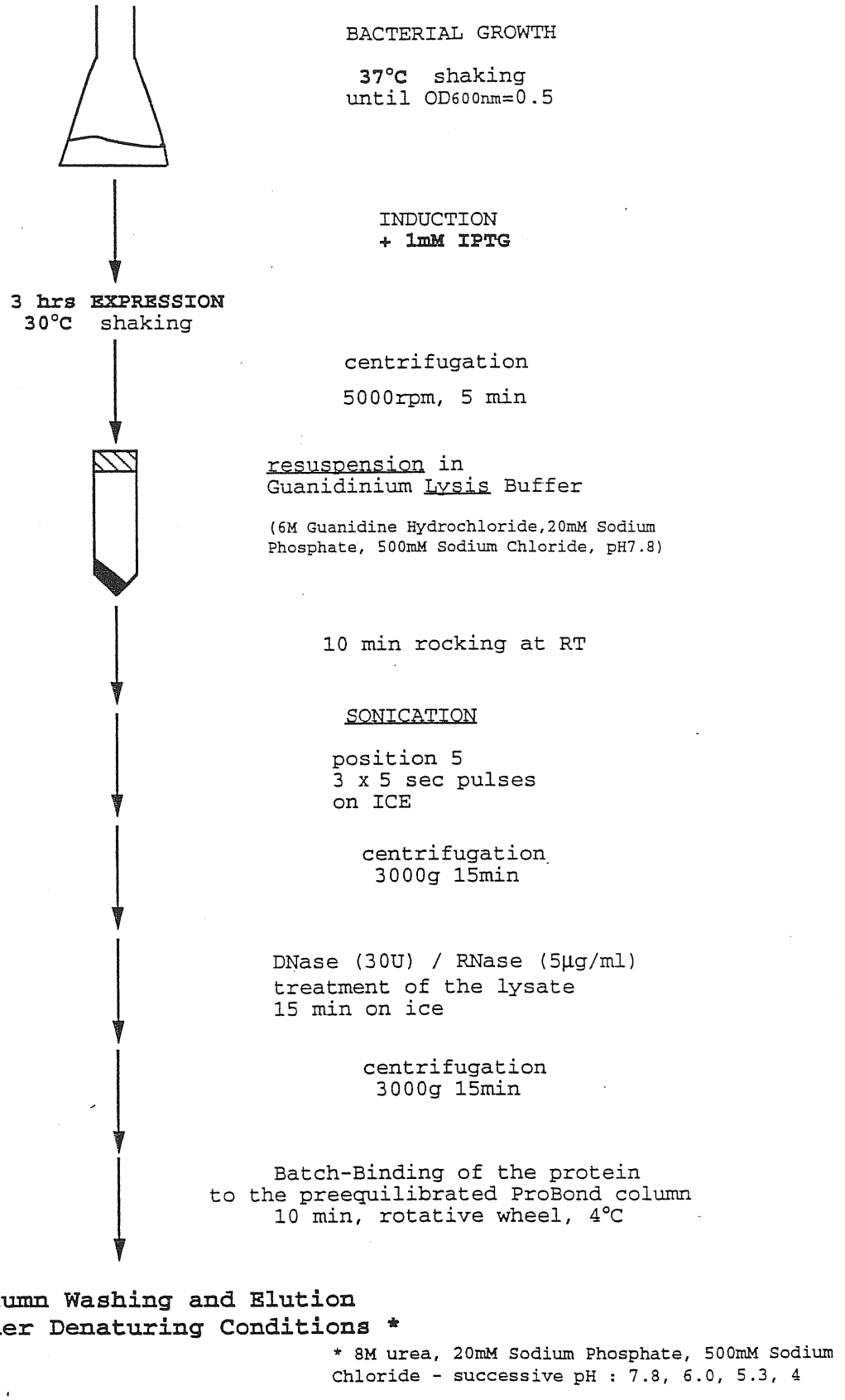

Fig. 39 : Expression and purification of the C-terminal part of the BRET CNG channel.

III.B.2. RESULTS OF THE BINDING EXPERIMENTS

In order to test if the purification protocol chosen allowed to get a solution of pure protein sufficiently homogeneous to envisage a project of crystallisation, the fractions of pure cyto were then used to test its ability to bind the cGMP and thus to confirm its correct refolding.
In all the experiments done before the equilibrium dialysis a clear problem of radioactivity background was consistently present and probably due to the scintillation analyzer. This device was then substituted with a new one, allowing a better estimation of the binding capacity of cyto to cGMP.

III.B.2.1. PEG PRECIPITATION

In this method PEG 6000 is used to selectively precipitate the cGMP-cyto complex. Gamma globulin was added to act as a carrier for the precipitation reaction. A pH of 7.5 was chosen as it has been observed that if the pH of the buffer containing the gamma globulin is >8 or <7, the complex is less effectively precipitated (El-Refai, 1980). 1 pmol of cyto was incubated with 6 pmol of [^{3}H]cGMP for 10 min on ice in a total volume of 100 µl in a Tris-HCl 20 mM pH7.5 supplemented with 200 mM NaCl and 10 mM EDTA with or without 1 mM DTT and 0.5 mg/ml BSA. Following incubation, 100 µl of precipitation buffer was added (Tris-HCl 20 mM pH7.5 + 200 mM NaCl + 10 mM EDTA + 0.1 % γ-globuline + 10% PEG). The samples were then centrifuged for 20 min at 10 000 rpm. The quantity of radioactivity present in the supernatants and pellets was estimated after transferring the samples in vials containing the scintillation fluid. The measures made on the pellet fractions were inconsistent. The counts obtained on the supernatants suggested to proceed without BSA : about 47000 cpm were measured in the control vials without cyto and about 35000 cpm were measured in vials containing cyto previously incubated in buffer containing DTT but no BSA. The quantity of protein was then varied from 1 to 10 pmol without improving the results. The quantity of PEG was also varied from 10% to 4 and 8 % and a step of incubation of the protein / ligand mix together with the precipitation buffer was added (5 min on ice before the centrifugation step). The 8% PEG precipitation (experiment done using 1 pmol of cyto and 6 pmol of [^{3}H]cGMP) seemed promising : about 42000 cpm in control vial and 22000 cpm in the cyto containing vial were measured for the supernatant fractions; the measures on pellet were still unclear. The same experiment was repeated adding or not 3 nmol of cold cGMP but no specificity was detected and the results were totally inconsistent. In

addition to a clear problem of background the lack of reproducibility in these series of trials was perhaps due to the buffer used as Tris buffers appeared to interfere with PEG precipitation (Hollenberg, 1990).

III.B.2.2. $(NH_4)_2SO_4$ PRECIPITATION

Saturating levels of $(NH_4)_2SO_4$ (70%) are known to favour the precipitation of ligand/receptor complexes and as for PEG precipitation the use of γ-globuline as a carrier is essential. The precipitated complexes are separated from the assay mixture by filtration or centrifugation. 1 pmol of cyto protein was incubated with 2 pmol of [^{3}H]cGMP with or without 100 nmol cold cGMP in the presence of 1 mM DTT and 0.1 % γ-globuline in a total volume of 200 µl. The buffer of incubation was Tris-HCl 20 mM pH7.4 + 200 mM NaCl + 1 mM EDTA and the time of incubation was varied from 5 min to 1 hour. The filtration was then performed directly after adding 200 µl of precipitation buffer [Tris-HCl 20 mM pH7.4 + 1 mM EDTA + 1 mM DTT + 0.1 % γ-globuline + saturated $(NH4)_2SO_4$] or after a period of 2 to 5 min incubation with the precipitation buffer using either GF/B or nitrocellulose filters, pretreated or not with 0.1% polyethylenamine. The filtration process was performed with a Manifold Vacuum Filtration system (Millipore, Milan, Italy) and the filters were washed twice with 2 ml of precipitation buffer. None of those trials gave any consistent result.

III.B.2.3. CENTRIFUGATION METHODS

Cyto was incubated at 4°C with the radiolabelled cGMP with or without an excess of cold ligand. Incubation times were varied from 15 min to 2 hours. In order to separate the free cGMP from the cyto-[^{3}H]cGMP complex, centrifugation trials using Microcon-10 columns (Amicon) were performed. The centrifugation was done at 4°C for 50 min. No clear data were obtained.

III.C.2.4. EQUILIBRIUM DIALYSIS

The method consists of dialysing the protein against a large volume of buffer containing the radioligand (see Fig. 8). The protein and the radioligand are separated by an hemipermeable membrane whose cut-off is chosen in the way that it can only be crossed by the radioligand. At the equilibrium, there are a concentration g_{free} of free radioligand in the compartment of the ligand and a concentration $g_{tot} = g_{free} + g_{bound}$

in the compartment of the protein. A binding is observed when $g_{tot} > g_{free}$. In Pyrex tubes 200 pmol of radioligand were put into 100 ml of buffer (Tris 20 mM pH7.5, 200 mM NaCl, 10 mM EDTA, 1 mM DTT) and dialysis tubes containing 500 µl of the same buffer supplemented with either 0 (negative control), 100 pmol of cyto protein were subsequently immersed inside the radioactive mixture and incubated o/n at 4°C. The radioactivity was measured on 100 µl aliquots. In the negative control 3534 cpm (= g_{free}) were measured whereas in the cyto containing tube 4389 cpm (= g_{tot}) were detected. A difference of 855 cpm was obtained on 1/5 of the dialysis tube content. Considering that $1.8x10^4$ cpm corresponded to 1 pmol of [^{3}H]cGMP, 855x5=4275 cpm corresponded to 0.24 pmol. Therefore, 100 pmol of cyto were in this case able to bind 0.24 pmol of [^{3}H]cGMP (855 cpm = g_{tot} - g_{free}). The binding capacity of cyto was then estimated at 855 / 4389 = 19%. This experiment was repeated using 0, 10, 50 and 100 pmol of cyto in the same conditions as described above and the results were reproduced. So the next step was to try to increase the quantity of protein in order to reach a plateau and calculate the Kd. These saturation experiments never worked. Thus another equilibrium dialysis experiment was done with the protein 10x in excess compared to the radioligand quantity : 500 pmol of cyto were put together with 50 pmol of [^{3}H]cGMP in the dialysis bag. A negative control without protein as well as a control of specificity (500 pmol of cyto + 50 pmol of [^{3}H]cGMP + 50 nmol of cold cGMP) were also performed. The negative control led to 4518 cpm (g_{free}), the cyto sample gave 7688 cpm (gtot) so that the binding capacity was estimated at 3170 / 7688 = 41%. The test of specificity gave the following results : 10880 cpm for the negative control and 11166 cpm for the cyto sample. These values being similar, the binding was specific. I subsequently tried to repeat this experiment, adding also a real negative control (i.e. a tube containing a protein different from cyto without known affinity for the cGMP; the BSA was tried), but the trials were not successful.

The variability obtained from one binding experiment to the other is attributed first to the difficulties encountered when trying to find at by trial and error the right conditions of such assays. Moreover, the fractions of cyto were coming from different batches of purification (as all those purification experiments were in fact performed in order to find the right procedure and valuate the size of the scale-up which would have been necessary for crystallisation purposes) and might be *per se* of different nature. Some insights in the expression and purification procedure were nevertheless acquired during this generally unachieved study. No thorough discussion on this topic will be done in this thesis manuscript.

IV. DISCUSSION

In this part of the thesis, the experimental results obtained regarding two fundamental aspects of CNG channels structure and function are discussed. First, a new model for the structural organization of the pore is proposed : the residues forming the pore of CNG channels are arranged like a cone structure resembling the tridimensional organization of the pore of potassium channels. Second, two major functional aspects of CNG channels are analysed : ion permeation and gating properties. In particular, the results obtained in this thesis suggest a complex permeation of Na^+ and K^+ ions which are likely to interact in the pore of CNG channels. Moreover, the permeation of K^+ modifies the gating features of the channels. Therefore, permeation and gating which are two major aspects of ion channel function are linked. Some particular proline residues localized at the outer vestibule of CNG channels play a major role for controlling these two principal properties.

IV.A. THE PORE STRUCTURE

The results of the SCAM study made on the α-subunit of the bovine rod CNG channel revealed that the accessibility of several residues in the P loop to MTSEA and MTSET is significantly different. The results obtained are not in accordance with those reported by Sun *et al.* (1996). Therefore, the accessibility map of the residues tested with MTS compounds (Fig. 22) is consistent with a topological structure of the pore region different from the one previously proposed (Sun *et al.*, 1996). The primary sequence of the pore region of the CNG channels is highly similar to the one of voltage-gated K^+ channels (Fig. 23). Considering our results of the SCAM, also the tertiary organisation of the pore of the CNG channel seem to be similar to that of voltage-dependent K^+ channels (Lu and Miller, 1995; Kurtz *et al.*, 1995; Pascual *et al.*, 1995; Durell and Guy, 1996; Doyle *et al.*, 1998).

IV.A.1. EXTERNAL RESIDUES

The MTSEA and MTSET effects on cysteine mutant channels were different from one another. Residues T20C, P22C and, to a lesser extent, P21C were accessible to MTSET only from the outer side of the plasma membrane whereas MTSEA was able to block the current from T20C and P22C even when applied from the inner side of

the membrane independently of the gating state of the channel (see also Sun *et al.*, 1996). When external cysteine where added to these patches, MTSEA block from the inner side was prevented (Fig. 21). Therefore, the blocks observed whether MTSEA was applied from the inner or outer side of the membrane were in reality due to the fact that MTSEA - but not MTSET - partly permeates through the plasma membrane as a charged amine (Holmgren *et al.* 1996; Wilson and Karlin, 1998). This control using external cysteine was not done in the study made by Sun and coworkers who consequently misinterpretated their results of double MTSEA accessibility for T20C and P22C mutants. Thus, T20, P21 and P22 are in reality extracellular residues; in agreement with the strong current inhibition produced by external MTSET on T20C and P22C mutants, T20, P21, P22 are likely to form the extracellular pore vestibule. This strategic position of the residue P21 is also confirmed by the surprising results obtained by mutating this amino acid into either Thr, Ala, or Cys (see section III.A.3.). The block produced by extracellular MTSET on V4C suggests that V4, too, is an extracellular residue (Fig. 15). Data are consistent both with a location of V4 within the extracellular pore vestibule and with a possible crucial involvement of V4 in the gating process, not necessarily involving the channel vestibule.

IV.A.2. INTRACELLULAR RESIDUES LOCATED AT THE NARROWEST PART OF THE PORE

Current activated by cGMP from I17C mutant spontaneously decayed in inside-out patches (Fig. 19). This decay is slowed down by intracellular DTT (see III.A.1.5.), suggesting that current rundown is due to the formation of disulphide bridges, in inside-out patches. It is likely that the formation of disulphide bridges is prevented in the intact oocyte, because of the reducing intracellular environment (Creighton, 1993). As shown in Fig. 19, intracellular MTS compounds decreased the half-time of current decay. The time course of current rundown is slower in the absence of cGMP, suggesting that this residue may move slightly towards the pore axis, during channel opening. These results suggest that I17C residue is intracellular. In addition, when the adjacent residues G18 and E19 were replaced by a cysteine, no functional channels were observed. In this case also, the lack of expression may be due to the formation of disulphide bridges, since E19 residue is thought to line the channel pore. Indeed, previous studies showed that this residue is accessible to extracellular divalent cations (Root and MacKinnon, 1993; Eismann *et al.*, 1994), to intracellular monovalent cations (Sesti *et al.*, 1995), and is a strong determinant of CNG channel permeation (Root and MacKinnon, 1993; Eismann *et al.*, 1994; Sesti *et al.*, 1995). Hence, we

suggest that I17 residue is intracellular and located within the channel pore, and that G18 and E19 form the narrowest section of the pore itself.

IV.A.3. OTHER INTRACELLULAR RESIDUES

Within the segment L7-T16, only mutants L7C, W9C, L12C, T15C and T16C produced functional channels, in *Xenopus* oocytes. None of these mutants was affected by external MTSET, whereas all were sensitive to intracellular application of MTSET, to different degrees though. cGMP-gated currents from L7C and W9C were inhibited, indicating directly that residues L7C and W9C are accessible from the intracellular side. On the contrary, currents from L12C, T15C and T16C were potentiated. It should be noted that, in these mutants, single-channel recordings showed a decrease in open probability with respect to the w.t. channels, in saturating cGMP (Fig. 13). Therefore, we can not exclude that cysteine substitution of these residues makes cGMP a partial agonist. In this case, the potentiation exerted by intracellular MTSET may be caused by an aspecific interaction between the cationic MTSET and channel portions different from the substituted cysteine, as for instance the residue H420, responsible for cGMP-gated current potentiation, at submaximal cGMP concentrations (Gordon and Zagotta, 1995a). However, since intracellular MTSET had a partial irreversible inhibitory effect on T16C after the quick initial potentiation, and the residues L7, W9 and I17, which bracket the L12-T16 segment, were inhibited by intracellular treatment, L12, T15 and T16 must face the inner side of the plasma membrane.

IV.A.4. STRUCTURAL MODEL OF THE PORE LOOP

In the light of the results the model shown in Fig. 40 is proposed for the pore loop topology in CNG channels. Residues accessible to MTSET from the external side of the plasma membrane were coloured in red; residues accessible from the internal side were coloured in blue; white residues were either not accessible to MTS compounds or were not studied because cysteine substitution on these positions did not yield functional channels. The arrows indicate suggested displacements occurring during channel opening. Residues I17, G18 and E19 form the narrowest portion of the pore, whereas residues T20, P21, P22 and P23 form the extracellular vestibule of the channel. The three prolines 21-23 may form a polyproline loop (Creighton, 1993). The diameter of extracellular vestibule lumen, lined by residues T20, P21 and P22, is likely to be wider than the diameter of the pore lumen at the level of the residues G18-E19,

for two reasons. First, the large thiol reagent MTSET can readily reach all these residues. Second, in mutant channels T20C, P21C and P22C cysteines of neighbouring subunits are not likely to become so close to each other to form disulphide bonds, leading to channel occlusion. In fact, cGMP-gated currents from mutants T20C, P21C and P22C, in symmetrical sodium and in saturating cGMP, usually have amplitudes comparable to those of w.t. currents, with no evidence of rundown (see sections III.A.1. and III.A.3.). Residue G18 may cause a turn in the P region, so that the adjacent I17 residues belonging to the different subunits are still sufficiently close to form disulphide bridges, when substituted with cysteines, while the following residues towards the amino-terminal do not line the pore lumen.
Residues in the segment from L7 to T16 are intracellular. In particular, residues L7 to T13 have a significant homology with residues L66 to T72 forming the final portion of the pore outer helix in KcsA potassium channel (Doyle *et al.*, 1998). Therefore, residues L7 to T13 in CNG channels may form an alpha helix. Residues from V4 to L7 span the plasma membrane and residue V4 is extracellular, possibly being part of the outer pore vestibule. It should be recalled here that the residues which form the segment 321-339, towards the amino-terminal with respect to V4 (which is the valine at position 348) , were shown to be extracellular by immunocytochemistry (Wolfhart *et al.*, 1992).

IV.A.5. STRUCTURAL CHANGES DURING CHANNEL GATING

The accessibility to MTSET of most of the tested residues was similar irrespective of whether MTSET was applied in the presence or in the absence of cGMP. In mutants whose open probabilities were 0.8 or larger, in saturating cGMP (as is also the case for w.t. channels), the presence or absence of cGMP was a tool to study the accessibility in the open or in the closed state, respectively. In mutants whose open probabilities were smaller (all mutants between W9C and T16C; see section III.A.1.), the distinction between accessibility in the open and closed state was not clear-cut, since even in the presence of saturating cGMP the channels remained in the closed state for a considerable fraction of time. MTSET inhibition of L7C channels (Fig. 15) was slightly larger in the closed state, suggesting that, in the open state, L7 residue either moves towards the extracellular side of the plasma membrane, or becomes less accessible. On the contrary, the accessibilities of residues T20, P21 and P22 were almost identical in the closed and in the open state, indicating that the outer vestibule does not undergo any large conformational rearrangement during gating. The faster rundown of cGMP-

activated current in mutant I17C in the open state (Fig. 19) may be taken as an indication that residues I17 are closer to each other in the open state than in the closed state. These results suggest, although do not prove, that the opening of the CNG channel is primarily mediated by a widening of the channel lumen near residues 18 and 19, which is accompanied by a movement of I17 residues towards the pore axis. This is in agreement with reports that residue E19 is accessible to internal tetracaine in the closed but not open configuration (Fodor *et al.*, 1997). As a consequence, I17 may directly contribute to the partial obstruction of the intracellular pathway leading to E19, in the open state. Overall, these data suggest that channel closing is not caused by the occlusion of the pore lumen by a different channel domain but argue in favour of a gating mechanism involving portions of the P region. In other terms, a "pinching-shut" of the selectivity filter (Liu *et al.*, 1997), i. e. a movement of translation of some internal residues of the P region along the central axis of the pore, may account as a gating mechanism (Sun *et al.*, 1996; Liu *et al.*, 1997; Fodor *et al.*, 1997). Therefore, the CNG channel activation is likely to occur through a mechanism different from the one proposed for the related Shaker-type K^+ channels, involving the movement of an intracellular gate, distinct from the selectivity filter (Liu *et al.*, 1997).

Fig. 40 :

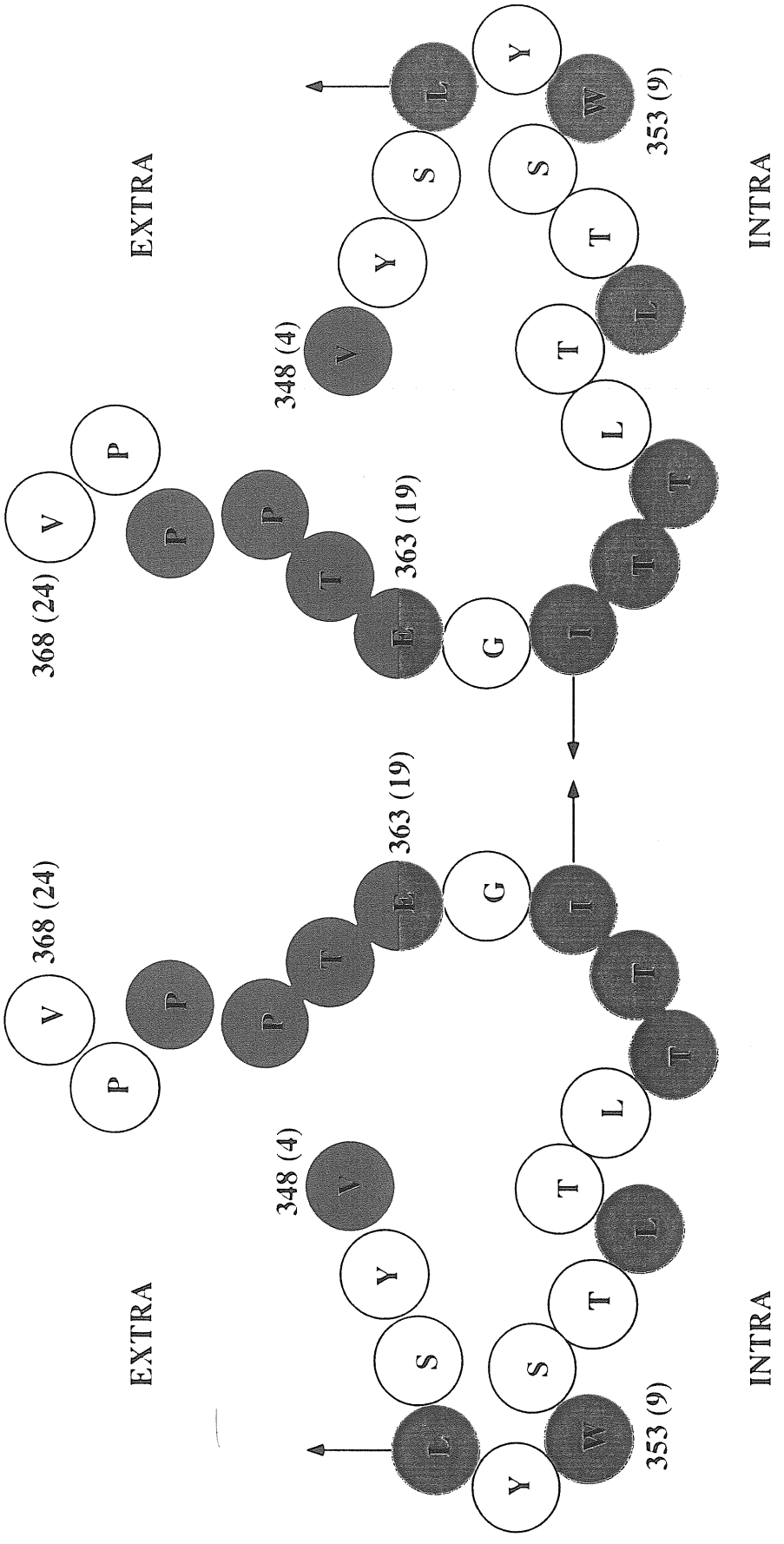
EXTRA
EXTRA
INTRA
INTRA
368 (24)
348 (4)
363 (19)
353 (9)
368 (24)
348 (4)
363 (19)
353 (9)

Fig. 41 : Model of the proposed topology of two adjacent P loops in CNG channels

Arrows indicate the suggested displacements occurring during channel opening. Red circles represent proposed extracellular residues. Blue circles represent proposed intracellular residues. White circles represent residues not accessible to MTS compounds or residues which, when substituted with cysteine, prevented the expression of functional channels. Residues are numbered according to their position in the CNG channel protein (Kaupp *et al.*, 1989). The residue position corresponding the conventional numbering R1-S27 used in this paper is given within brackets. Extra = extracellular side, Intra = intracellular side.

IV.A.6. COMPARISON TO THE PORE LOOP OF VG POTASSIUM CHANNELS

SCAM has been applied to the study of the pore loop topology of voltage-dependent Kv2.1 delayed rectifying channels from rat brain (Kurtz *et al.*, 1995; Pascual *et al.*, 1995). In Kv2.1 channels, current inhibition produced by MTSET identifies two distinct pore loop segments whose residues are accessible either from the outer or from the inner side of the plasma membrane. In particular, residues D378 to K382, corresponding to G18-P22 in CNG channels (Fig. 23), were mostly accessible to external MTSET and Cd^{2+} (Kurtz *et al.*, 1995; Pascual *et al.*, 1995). On the other hand, residues T370 to V374, corresponding to T13-I17 in CNG channels were mostly accessible to intracellular MTSET (Pascual *et al.*, 1995). Furthermore, residue P361 in Kv2.1 channels, corresponding to V4 in CNG channels was only accessible to extracellular MTSET and Cd^{2+} (Kurtz *et al.*, 1995). On the whole, available data from Kv2.1 potassium channel are analogous to the results obtained with MTSET presented in this paper. A similar topology of the pore region was proposed for a Shaker voltage-dependent potassium channel, based on accessibility of substituted cysteines to silver ions (Lu and Miller, 1995). The comparison of SCAM data obtained from CNG channels and voltage-dependent potassium channels suggest that the pore topology is similar in these families of channels. Recently, the pore structure of the KcsA K^+ channel has been resolved by X-ray crystallography (see Fig. 41 and Doyle *et al.*, 1998). All known K^+- as well as CNG- channels share some homologies with the KcsA channel whose crystal structure thus represents a precious source of information. The X-ray analysis revealed that four identical subunits create an inverted teepee, or cone, bearing the selectivity filter at its outer end. The selectivity filter in the KcsA channel is made of the residues of the K^+ channels signature sequence (T75-G79). The sequence alignment of this channel with the α-subunit of CNG channels strictly corresponds to residues T16, I17, G18 and two gaps. Indeed, the results of our SCAM analysis places the selectivity filter at residues I17-E19. The localisation of the outer vestibule of CNG channels revealed by our SCAM (T20 + the proline loop) fits with the position of the outer segment of the KcsA channel. The first proline of the proline loop (P365 = P21) corresponds to Y82 of the KcsA channel. According to the X-ray study, Y82 is located at the entrance of the channel pore. This strategic position nicely reinforces the importance of residue P21 in ionic selectivity of CNG channels. Residues L7 to T13 have a significant homology with residues L66 to T72 forming the C-terminal portion of the pore outer helix in KcsA potassium channel (Doyle *et al.*,

1998). Therefore, residues L7 to T13 in CNG channels may form an alpha helix. The data on accessibility place them in the intracellular side of the CNG channel pore.

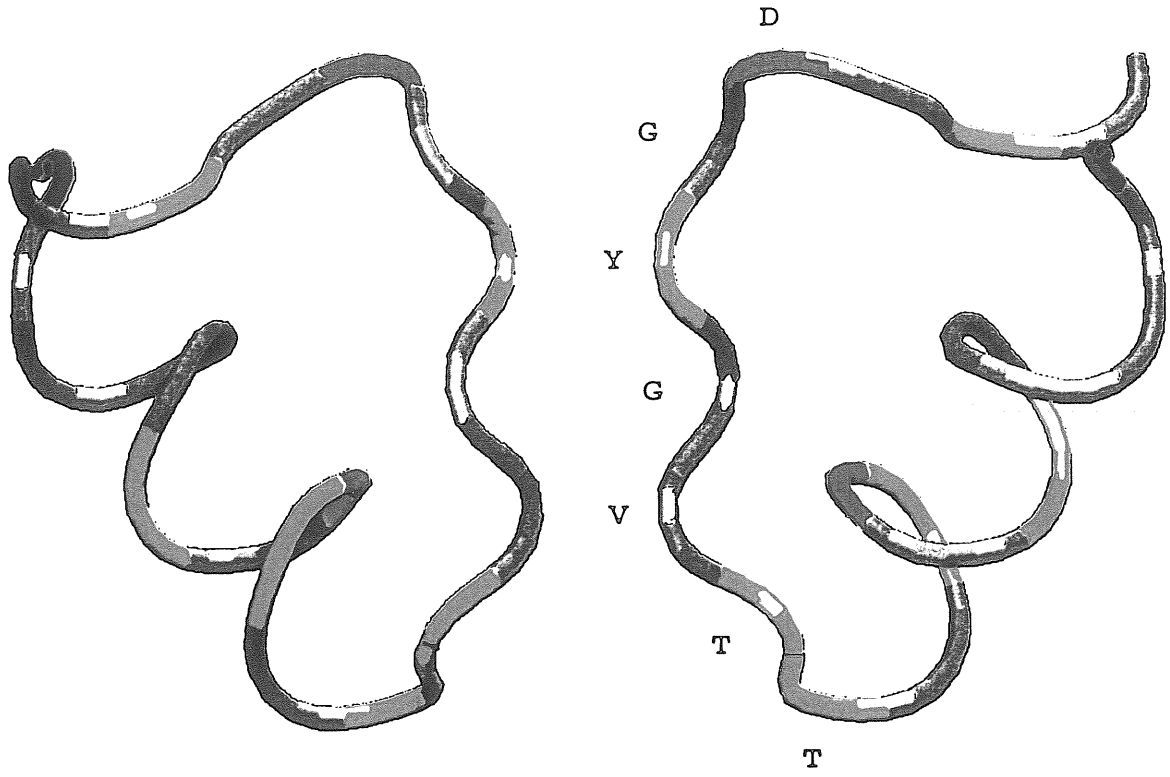

Fig. 41 : Structure of the KcsA channel pore.

This figure shows the KcsA selectivity filter which is comprised of the signature sequence amino acids T, V, G, Y, G (residues 75 to 79, running from bottom to top). This scheme has been realised taking into consideration the results obtained by Doyle *et al.* (1998) by X-ray analysis of the KcsA crystal.

IV.B. A NEW CONCEPT OF IONIC PERMEATION AND GATING

The major part of this thesis which is untitled "Interaction of Na^+ and K^+ in the pore of the CNG channel" describes unexpected properties of CNG channels and relates in particular the features presented by a mutant channel obtained changing the proline in position 365 of the α subunit of bovine rods into a threonine, an alanine or a cysteine. Proline 365 is the first proline of a loop of three consecutive prolines conserved in all known α subunits of CNG channels (Fig. 23). In mutants P365T, P365C and P365A, K^+ ions permeation is modified. In these mutant channels and in the presence of Na^+ and K^+ on opposite sides of the membrane a transient K^+ dependent current (tKdc) was observed. This tKdc is caused by a transient potentiation of the channel, i.e. a transient increase of the open probability. A similar but smaller tKdc was also found in the w.t. CNG channel.

These results show that: i - the gating of the Na^+ current is significantly affected by the presence of K^+ ; ii - permeation and gating in CNG channels are coupled; iii - Na^+ and K^+ ions permeate differently through the pore of CNG channels.

IV.B.1. IONIC PERMEATION IN MUTANTS P365T, P365C AND P365A

The w.t. CNG channel is poorly selective among monovalent alkali cations (Kaupp *et al.*, 1989; Menini, 1990; Sesti *et al.*, 1996), but channel mutants P365T, P365A and P365C are significantly permeable only to Na^+ and Li^+. As shown in Fig. 33, the permeation of alkali monovalent cations with a radius larger than 1.3 Å (i.e. K^+, Rb^+ and Cs^+) is modified in the P365T mutant. Similar results were obtained with mutants P365C and P365A. A recent theory of ionic selectivity for monovalent alkali cations (Laio and Torre, 1998) suggests that the different selectivity among Na^+ channels and CNG channels can be ascribed to a larger flexibility of the pore of CNG channels. As a consequence the change of permeation observed in mutants P365T and P365A can be explained as caused by a reduced flexibility of the pore of mutant channels. In the presence of 110 mM Na^+ and K^+ respectively in the extracellular and intracellular medium, brief transient outward currents carried by K^+ ions was observed for potentials larger than +100 mV (Fig. 26). In these ionic conditions at membrane

voltages between -30 and + 100 mV neither inward nor outward current gated by cGMP was detected (see I-V relations in Fig. 24d and 27d). When large cations such as Rb^+ and Cs^+ were present in the intracellular medium no appreciable inward current was observed at 0 mV, indicating that these cations blocked the permeation of Na^+. These large ions seem to reach the inner core of the channel but then they remain trapped in the pore and block it (Fig. 26). An explanation for this apparent block can be that large cations have no trouble to enter the channel pore but then the modified flexibility of the pore of the mutant channels either reduces the probability of opening or slowers its kinetic. The steady-state I-V relations in the presence of Na^+ and K^+ respectively in the extracellular and intracellular medium, are reminiscent of those observed in the inward K^+ rectifier (Hagiwara et al 1976). In these channels the inward rectification is caused by a voltage dependent block of internal spermine (Fakler *et al.*, 1995; Oliver *et al.*, 1998; Lee *et al.*, 1999). In mutant P365T the rectification is caused by the block of Na^+ ions by intracellular K^+.

Contrary to Na^+ channels but similarly to the w.t. CNG channel (Picco and Menini, 1993; Goulding *et al.*, 1993; Sesti *et al.*, 1996), mutant channels P365T and P365A are significantly permeable to methyl compounds such as methylammonium and dimethylammonium (Table 4). This observation is surprising considering the radius of these ions (respectively 1.3 and 1.6 Å). This results indicate that the molecular mechanisms controlling the permeation of monovalent alkali and organic cations are distinct. Indeed replacing the first proline from the proline loop alters the permeation of alkali cations but not of organic cations. Therefore the molecular mechanisms allowing the permeation of methyl compounds through the w.t. CNG channels are still functional in mutant channels where the proline loop was altered.

IV.B.2. **ORIGIN OF THE tKdc**

In the presence of biionic conditions, with Na^+ ions in the extracellular medium and K^+ ions in the intracellular medium a large transient current (tKdc) carried by Na^+ ions was observed in mutant P365T at membrane voltages more negative than -80 mV. This tKdc is attributed to a transient potentiation, i.e. to a transient increase of the open probability of mutant channels P365T for three reasons : i - the cGMP concentration evoking half of maximal tKdc is between 20 and 50 μM, when about 200 μM cGMP is nececessary to evoke half of the maximal current at the steady state (Fig. 29), ii - when the channel opening was potentiated by the addition of Ni^{2+}

(Gordon and Zagotta, 1995a), the ratio Ipeak/Iss became close to 1, thus showing that once CNG channels are mostly in the open state the tKdc is significantly reduced (Fig. 27), iii - during tKdc and at the steady state the single channel conductance is unchanged (Fig. 32). All these observations strongly argue that the origin of tKdc is a transient potentiation of CNG channels caused by the presence of K^+ ions inside the channel pore.

IV.B.3. K^+ IONS IN THE PORE OF MUTANT P365T INFLUENCE CHANNEL GATING

CNG channels open following the binding of cyclic nucleotides to a domain near the C-terminus (Kaupp *et al.*, 1989; Finn *et al.*, 1996; Zagotta and Siegelbaum, 1996;). When the channel binds at least two cyclic nucleotides, it undergoes a conformational transition to open states with different conductances (Ruiz and Karpen, 1997, 1999). When four cyclic nucleotides are bound, the channel opens preferentially to a high conductance state (Ruiz and Karpen, 1997, 1999). Several kinetics schemes have been proposed to describe the channel opening and allosteric models have been considered (Gordon and Zagotta, 1995b; Liu *et al.*, 1996, 1998; Li *et al.*, 1997; Ruiz and Karpen, 1999; Varnum and Zagotta, 1996, 1997). In allosteric models it is assumed that the liganded state and the open state are in a thermodynamic equilibrium with an equilibrium constant L (Goulding *et al.*, 1994; Sunderman and Zagotta, 1999b). The value of L controls the maximal open probability pmax in the presence of a saturating cyclic nucleotide concentration and $p_{max} = L/(L+1)$. Different domains of CNG channels control L in a complex and subtle way (Bucossi *et al.*, 1997, Sunderman and Zagotta, 1999a). The analysis of single channels current shown in Fig. 25 and of the effect of Ni^{2+} shown in Fig. 27, indicate that p_{max} of mutant P365T in the presence of a saturating concentration of cGMP is not larger than 0.09, when in the wild type channel is between 0.8 and 0.9 (Nizzari *et al.*, 1993). Therefore L is about 0.08 and 6 for mutant P365T and the w.t. channel respectively. As a consequence in mutant P365T the equilibrium constant L is displaced towards the liganded state. As shown in Figs. 33 and 34 a significant transient current at negative voltages is observed in the presence of K^+, Rb^+, Cs^+ and NH_4^+ but not in the presence of organic cations. Parallel to the modifications of ionic permeation, the gating properties of the mutant channel P365T in presence of K^+, Rb^+, Cs^+ and NH_4^+ ions have been modified.

IV.B.4. ADDITIONAL PROPERTIES OF THE tKdc

The tKdc decayed with a time constant dependent on membrane potential: at –100 mV the time constant was of about 1 msec and at -180 mV it was reduced to 0.5 msec. When the biionic conditions were inverted with Na^+ present in the intracellular medium and K^+ in the extracellular medium, a tKdc was also observed at positive voltages. However, the current carried by Na^+ ions at +180 mV decayed with a longer time constant of a few msec (Fig. 30). As shown in Fig. 31 a few mM K^+ in the intracellular medium are sufficient to evoke half of the maximal tKdc. When biionic conditions were inverted 1/6 (=18 mM) K^+ in the intracellular medium are sufficient to powerfully block the tKdc carried by Na^+ at + 180 mV.

These observations are consistent with several distinct molecular schemes, two of which deserves consideration. In the first scheme the channel exists in a liganded state C_l, in a potentiated state C_p and in an open state C_o. In this scheme the equilibrium constant between C_p and C_o, L_p, is much larger than L, (i.e. the equilibrium constant between C_l and C_o) and the presence of K^+ inside the channel favours the conversion of C_l into C_p. In order to explain the dependence on membrane voltage of the decay of tKdc, the rate of reaction from C_p to C_l should be less than 1 second at –180 mV and some msec at + 180 mV. In the second scheme the channel exists only in the liganded and open state C_l and C_o and there is not distinct state C_p, intermediate between C_l and C_o. In this scheme the rates between C_l and C_o are controlled in a complex way by the cGMP concentration, K^+ ions and membrane voltage V. The analysis of ligand locked channels P365T , similar to that performed in w.t. channels (Ruiz and Karpen, 1997, 1999) could distinguish between these two possibilities and other more complex schemes.

IV.B.5. Na^+ AND K^+ INTERACTIONS IN THE W.T. CNG CHANNEL

As shown in Fig. 34 a tKdc is also observed in the w.t. CNG channel. This tKdc is smaller than the one observed in mutant P365T and at –180 mV in the wild type the ratio Ipeak/Iss is about 1.3 and 1.6 in the presence of 100 and 500 μM respectively. The tKdc current decayed at -180 mV with a similar time constant of about 0.5-1

IV.B.4. ADDITIONAL PROPERTIES OF THE tKdc

The tKdc decayed with a time constant dependent on membrane potential: at –100 mV the time constant was of about 1 msec and at -180 mV it was reduced to 0.5 msec. When the biionic conditions were inverted with Na^+ present in the intracellular medium and K^+ in the extracellular medium, a tKdc was also observed at positive voltages. However, the current carried by Na^+ ions at +180 mV decayed with a longer time constant of a few msec (Fig. 30). As shown in Fig. 31 a few mM K^+ in the intracellular medium are sufficient to evoke half of the maximal tKdc. When biionic conditions were inverted 1/6 (=18 mM) K^+ in the intracellular medium are sufficient to powerfully block the tKdc carried by Na^+ at + 180 mV.

These observations are consistent with several distinct molecular schemes, two of which deserves consideration. In the first scheme the channel exists in a liganded state C_l, in a potentiated state C_p and in an open state C_o. In this scheme the equilibrium constant between C_p and C_o, L_p, is much larger than L, (i.e. the equilibrium constant between C_l and C_o) and the presence of K^+ inside the channel favours the conversion of C_l into C_p. In order to explain the dependence on membrane voltage of the decay of tKdc, the rate of reaction from C_p to C_l should be less than 1 second at –180 mV and some msec at + 180 mV. In the second scheme the channel exists only in the liganded and open state C_l and C_o and there is not distinct state C_p, intermediate between C_l and C_o. In this scheme the rates between C_l and C_o are controlled in a complex way by the cGMP concentration, K^+ ions and membrane voltage V. The analysis of ligand locked channels P365T , similar to that performed in w.t. channels (Ruiz and Karpen, 1997, 1999) could distinguish between these two possibilities and other more complex schemes.

IV.B.5. Na^+ AND K^+ INTERACTIONS IN THE W.T. CNG CHANNEL

As shown in Fig. 34 a tKdc is also observed in the w.t. CNG channel. This tKdc is smaller than the one observed in mutant P365T and at –180 mV in the wild type the ratio Ipeak/Iss is about 1.3 and 1.6 in the presence of 100 and 500 μM respectively. The tKdc current decayed at -180 mV with a similar time constant of about 0.5-1

msec (Fig. 36). In the w.t. channel the inward current carried by extracellular Na^+ is influenced by the presence of K^+ (Fig. 36), but the inward current carried by extracellular K^+ is not significantly different in the presence of Na^+ or K^+ in the intracellular medium (Fig. 37). Thus the interaction between Na^+ and K^+ in the w.t. channel is asymmetric : K^+ ions seem to influence the gating of the current carried by Na^+, but Na^+ ions do not affect significantly the current carried by K^+.
These results indicate that although the permeability ratio P_K/P_{Na} is close to 1 (Kaupp *et al.*, 1989, Picco and Menini, 1993) and the single channel conductance of Na^+ and K^+ is almost identical in the w.t. CNG channel (Nizzari *et al.*, 1993) Na^+ and K^+ ions do not permeate exactly in the same way. This conclusion is not really surprising given the significant differences of their hydration thermodynamics (Hille, 1992; Laio and Torre, 1999). It is possible that Na^+ and K^+ have the same permeability and single channel conductance through CNG channels as the result of two distinct mechanisms : their different hydration thermodynamics and a complex interaction between permeating ions and the channel itself. This possibility is reminiscent of a recent theory of ionic selectivity (Laio and Torre, 1999) through CNG channels. In order to explain the low selectivity of CNG channels it is necessary to assume that the pore walls are flexible. In this view large alkali cations, such as K^+, Rb^+ and Cs^+ permeate only when the pore becomes wider, while small alkali cations such Li^+ and Na^+ do not need a larger pore for their permeation. The flexibility necessary to explain ionic selectivity and permeation may originate from the interaction of permeating ions with the channel pore. Such information about the flexibility of a selectivity filter may be obtained using MDM simulations. Indeed, it has been recently found using this technique that the residues lining the selectivity filter in the KcsA potassium channel were relatively stable (Guidoni *et al.*, 1999). Thus, one could expect that a similar study of the pore of a CNG channel would lead to the opposite results, i. e. larger fluctuations in the regions involved in ionic selectivity.

IV.B.6. THE PROLINE LOOP OF CNG CHANNELS

The mutation substantially altering the K^+ permeability and dramatically enhancing the tKdc affects the first proline of a loop of three prolines located at position 365 to 367 in the α subunit of the bovine rod CNG channel. These three residues are certainly localised in the extracellular vestibule very close to the narrowest section of the CNG pore which plays the role of selectivity filter. The localisation of prolines in the

extracellular vestibule, i. e. in a typical hydrophilic region is not surprising. Indeed it is known that a proline residue excels in making turns, a property that makes a proline almost absent in the interior of proteins and thus almost always in contact with the protein surface or with a region having hydrophilic properties. The three prolines of the pore region of CNG channels α-subunits may be arranged in a Polyproline II helix (Creighton, 1993; Adzhubei and Sternberg, 1993), leading to a rigid stick of 9.3 A which has few main chain hydrogen bonds with the rest of the protein (Adzhubei and Sternberg, 1993). This rigid stick is likely to confer very unusual structural properties to the pore of CNG channels : the reduction in hydrogen bonds in this region may be a reason for explaining the properties of fluctuation which seem to be required for ion permeation in CNG channels. Indeed, several mutants affecting the proline loop have been engineered and tested in this thesis. The w.t channel, which contains three prolines is not selective among monovalent alkali cations which permeate easily. The ΔP mutant, i.e. a mutant bearing only two prolines, displays the same type of behaviour. On the contrary, every mutation tested which changed the first proline of the loop and thus, similarly to the ΔP mutant, led to a channel bearing two remaining prolines displayed however drastic changes in ion permeation. Therefore, it is likely that in the ΔP mutant, the prolines are still organised in a conformation, perhaps a polyproline structure, which is the same as the one of the w.t. channel. On the contrary, the polyproline structure must have been disrupted in the P365T/A/C mutants. Thus, the precise point in which the first β-turn occurs must have its importance, the sequence preceding this structure as well. The fact that the P21T-ΔP mutant displays the same properties as the w.t. channel is surprising. In this case, only one proline of the proline loop is remaining. Because two prolines in a row are needed to make a polyproline structure, this conformation is certainly absent in this mutant. In order to understand the origins of these discrepancies and to find out the molecular mechanisms involved in ionic permeation, MDM simulations may be useful meanwhile the crystal structure of the CNG channel pore is resolved. The fact that mutations affecting the third proline of the loop always led to nonfunctional channels can be explained by its high conservation in the sequence of both subunits of CNG channels and in the sequence of several K^+ channels. This information is useful for making correct sequence alignments between the different VG- and CNG- channels.

V. CONCLUSIONS AND PERSPECTIVES

Some important features of the relationship between the structure and the function of CNG channels have been revealed in this thesis. First, using the SCAM technique, a tertiary structure has been proposed for the CNG channel pore. Our results are consistent with a structural organisation of the P loop which resembles the one of usual VG K^+ channels. The second important finding in this thesis is related to the function of the pore region. Site-directed mutagenesis applied to the proline loop of the CNG channel pore allowed to get several interesting information concerning ionic selectivity as well as gating properties of this channel. Indeed, it has been found that : i - Na^+ and K^+ do not permeate in the same way; ii - the molecular mechanisms regulating the permeation of monovalent alkali cations are different from the ones involved in the permeation of organic cation; iii - the gating of the Na^+ current is significantly affected by the presence of K^+; iv - permeation and gating in CNG channels are coupled.

X-ray analysis on a CNG channel crystal would provide a definitive picture of the organisation of the CNG channel pore. Such a crystallographic study has been recently carried out for the KcsA K^+ channel (Doyle *et al.*, 1998). The KcsA channel is constituted of two transmembrane domains linked by the P loop, whereas CNG channels always bear six transmembrane regions with the pore linking the fifth to the sixth membrane-spanning domains. This complicate transmembrane organisation makes it almost impossible to obtain crystals. Thus, the only method one can envisage in the aim of crystallising the CNG channel is to clone transmembrane domains 5 and 6 with the pore region in between and to reproduce the work made by the group of MacKinnon on the KcsA channel. Until the crystal structure is revealed, some other methods providing structural information may be envisaged. The technique of MDM simulations is a powerful mean of computer science that can be used to predict the tridimensional structure of proteins. In collaboration with the sector of Condensed Matter at SISSA, such a prediction has been made for the CNG channel. The method used was based on the crystal structure of the KcsA channel and takes into consideration the biophysical parameters of the residues of the CNG channel sequence from BRET. A preliminary result has been obtained and is shown in Fig. 42. The organisation of the CNG channel pore revealed by MDM simulations confirms the results obtained by the SCAM analysis. The most surprising result concerns the spatial disposition adopted by the three prolines of the P loop. Indeed, they are effectively forming a helical structure as previously suggested. A consequence of their position

and helical organisation is that they contribute to a significant enlargement of the CNG channel outer vestibule with respect to the same portion of the K^+ channel. This wider entrance of the channel pore may be associated to the different properties of ion selectivity displayed by these two groups of channels.

To conclude, the results obtained during this thesis represent a solid base for future scientific investigation in the field of CNG channels. Associated to the preliminary results of the MDM simulations, our findings will be useful to precise the tridimensional organisation of the CNG channel pore. In addition, the results presented here will be helpful to understand the molecular mechanisms of gating as well as the ones regulating ion permeation and selectivity. Further studies using MDM simulations will certainly be useful to these aims.

Another project of this thesis concerned the crystallisation of the CNG binding domain. The C-terminal portion bearing the ligand binding site has been cloned, overexpressed in bacteria and purified using an affinity chromatography. The correct folding of the protein could not be proven. Experiments of limited proteolysis and mass-spectrometry are currently achieved by our collaborators at EMBL to characterise the nature of our solution of protein. The protocol described in this thesis represent a preliminary result. Additional modification of this protocol will be necessary in order to obtain a suitable solution of pure protein for crystallisation purposes.

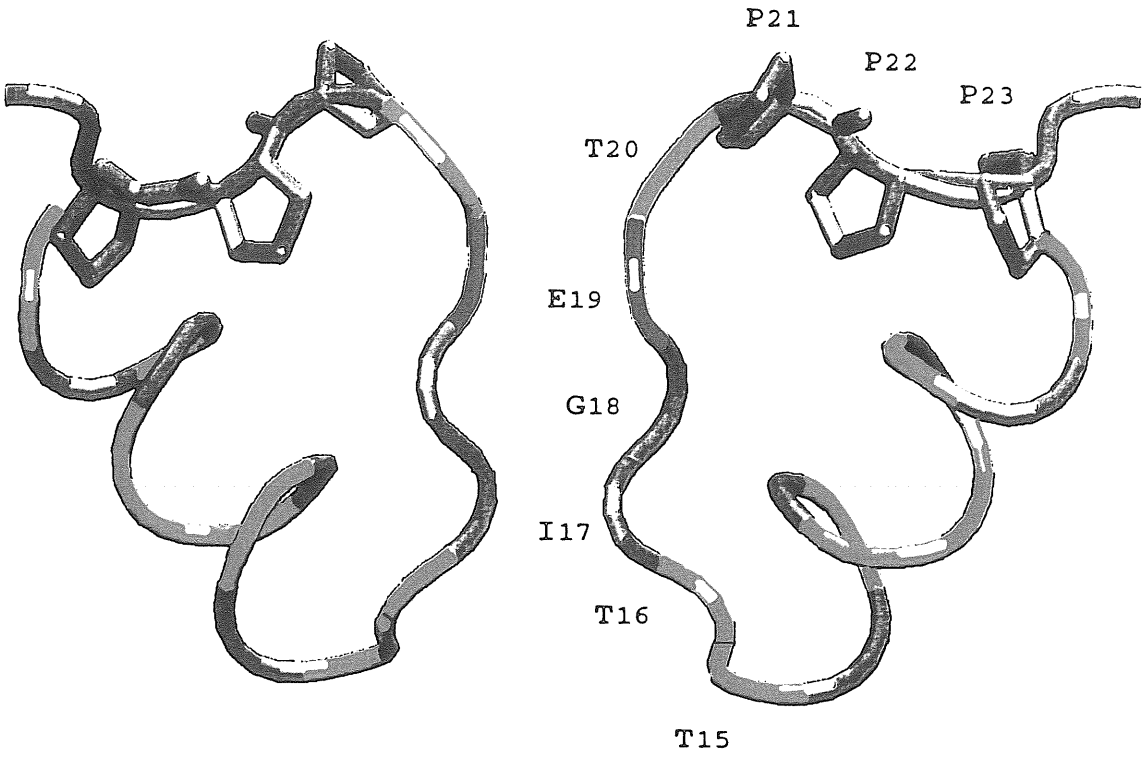

Fig. 42 : Structure of the CNG channel pore.

This figure shows the organisation of the pore from the cGMP-activated channel from bovine rod. The selectivity filter is comprised of the amino acid sequence T, I, G, E, T (residues 360 to 364, running from bottom to top). This scheme shows also that the three prolines P365-P367 are forming a helical structure localised at the outer vestibule of the channel. The presence of these prolines leads to an enlargement of the entrance to the CNG channel pore (for comparison with the VG outer vestibule, see Fig. 41). This representation has been made by MDM simulations (courtesy of the Condensed Matter Sector, SISSA).

Annex A

DNA sequence from the α subunit of the bovine rod cGMP-activated channel

```
   1 atgaagaaag tgattatcaa tacatggcac tcttttgtaa atattcccaa tgtggttgga ccagatgttg aaaaggaaat
  81 aacaaggatg gaaaatggag catgcagctc cttttctggt gatgatgacg acagtgcctc tatgtttgaa gaatcagaga
 161 ctgagaaccc ccacgcaagg gattccttta gaagtaatac acacggaagc ggacaaccat cacagaggga gcaatacctg
 241 cctggagcca ttgcactttt taatgttaac aacagcagca ataaggagca agaaccaaag gaaaagaaga aaaagaaaaa
 321 agaaaagaag agcaagccag atgataaaaa tgaaaataaa aaggacccag aaaagaaaaa gaagaaagaa aaggacaaag
 401 acaagaaaaa gaaagaggag aaaggcaaag ataagaaaga ggaagagaag aaggaagtcg tggttattga tccctcagga
 481 aatacgtatt acaactggct gttctgcatc accttacctg ttatgtataa ctggaccatg attattgcaa gagcatgttt
 561 tgatgaactt cagtctgatt acctagaata ctggcttgct tttgattact tatcagatgt agtctatctt cttgatatgt
 641 ttgtacgaac aaggacaggt tacctagaaca aggactact ggtgaaggaa gagcgtaaac tcatagacaa gtataaatca
 721 acctttcaat ttaaacttga tgttctatca gtgatcccaa ctgatctgct gtatattaag tttggctgga attatccaga
 801 aattagatta aacagattgt taaggatctc tcgaatgttt gagttcttcc agagaacaga aacacggaca aactacccaa
 881 acatcttcag gatctctaac cttgtcatgt acatcatcat catcatccac tggaatgcgt gtgtgtactt ctctatttcc
 921 aaagctattg ggtttggaaa tgacacatgg gtctatcctg atgttaatga tcctgatttt ggccgtttgg ctagaaaata
1041 tgtgtacagt ctttactggt ctacactgac tttgaccact attggcgaaa caccacctcc tgtgagggat tctgagtatt
1121 tctttgtggt ggctgatttc ctcattggag tgttaatttt tgccaccatt gtcggtaaca taggttctat gatttccaac
1201 atgaatgcgg ccagggcaga atttcaagca agaattgatg caatcaagca atacatgcat tttcgaaatg taagcaaaga
1281 tatggagaag cgagtcatta aatggtttga ctatctgtgg accaacaaaa aaacagtgga tgagagagaa gtcttgaagt
1361 atctacctga taaactaaga gcagagatcg ccatcaatgt tcatttagac acattaaaaa aggtgcgcat ttttgcagac
1441 tgtgaagctg gtctgttggt ggagttggtc ttgaaattac aaccccaagt ctacagtcct ggagattaca tttgcaagaa
1521 aggggacatt ggccgagaga tgtacatcat caaggaaggc aaactcgccg tggtggctga tgacgggatc actcagtttg
1601 tagtattgag tgatggcagc tactttggtg aaatcagtat ccttaatatt aaaggtagca aagctggcaa tcgaagaaca
1681 gccaatatta aaagcattgg ctactcagat ctattctgtc tctcaaaaga tgacctcatg gaagctctaa ctgagtaccc
1761 agatgccaaa ggtatgctag aagagaaagg gaagcaaatt ttgatgaaag atggtctatt ggacataaac attgcaaatg
1841 ctggaagtga tcctaaagat cttgaagaga aggtcacccg aatggagagc tcagtagacc tcctgcaaac aaggtttgct
1921 cggatcctgg ctgagtatga gtcaatgcag cagaaactga agcagaggct aaccaaggtt gagaaattcc tgaaaccact
2001 tattgacaca gaattttcag ctattgaagg atctggaact gaaagtgggc ccacagactc tacacaggac tga
```

Aminoacids sequence from the α subunit of the bovine rod cGMP-activated channel

```
   1 MKKVIINTWH SFVNIPNVVG PDVEKEITRM ENGACSSFSG DDDDSASMFE ESETENPHAR
  61 DSFRSNTHGS GQPSQREQYL PGAIALFNVN NSSNKEQEPK EKKKKKKEKK SKPDDKNENK
 121 KDPEKKKKKE KDKDKKKKEE KGKDKKEEEK KEVVVIDPSG NTYYNWLFCI TLPVMYNWTM
 181 IIARACFDEL QSDYLEYWLA FDYLSDVVYL LDMFVRTRTG YLEQGLLVKE ERKLIDKYKS
 241 TFQFKLDVLS VIPTDLLYIK FGWNYPEIRL NRLLRISRMF EFFQRTETRT NYPNIFRISN
 301 LVMYIIIIIH WNACVYFSIS KAIGFGNDTW VYPDVNDPDF GRLARKYVYS LYWSTLTLTT
 361 IGETPPPVRD SEYFFVVADF LIGVLIFATI VGNIGSMISN MNAARAEFQA RIDAIKQYMH
 421 FRNVSKDMEK RVIKWFDYLW TNKKTVDERE VLKYLPDKLR AEIAINVHLD TLKKVRIFAD
 481 CEAGLLVELV LKLQPQVYSP GDYICKKGDI GREMYIIKEG KLAVVADDGI TQFVVLSDGS
 541 YFGEISILNI KGSKAGNRRT ANIKSIGYSD LFCLSKDDLM EALTEYPDAK GMLEEKGKQI
 601 LMKDGLLDIN IANAGSDPKD LEEKVTRMES SVDLLQTRFA RILAEYESMQ QKLKQRLTKV
 661 EKFLKPLIDT EFSAIEGSGT ESGPTDSTQD
```

Annex C

MTS Reagents

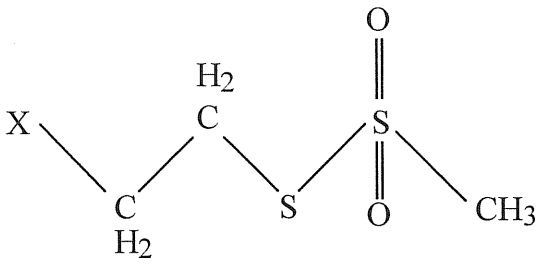

X = NH_3^+ for MTSEA

X= $(CH_3)_3N^+$ for MTSET

Cyclic-Nucleotides

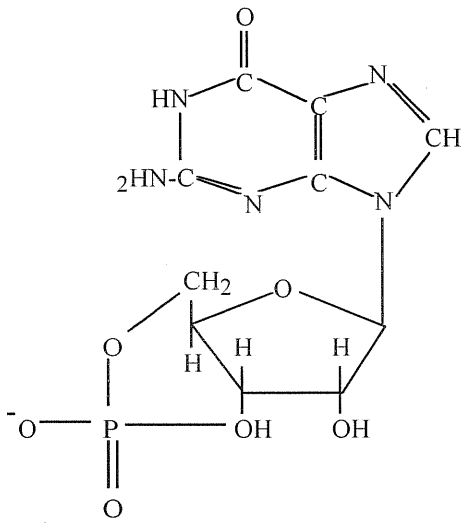

cGMP

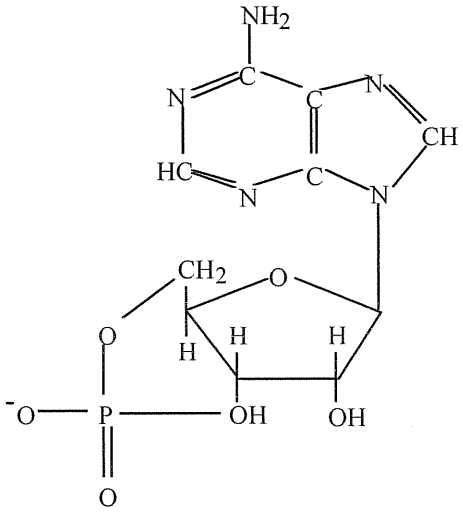

cAMP

VI. REFERENCES

Ache, B.W. and A. Zhainarov. 1995. Dual second-messenger pathways in olfctory transduction. *Curr. Opin. Neurobiol.* 5:461-466.

Adzhubei, A.A., and M.J.E. Sternberg. 1993. Left-handed Polyproline II Helices Commonly occur in Globular Protein. *J. Mol. Biol.* 229:472493.

Aggarwal, S. K., and R. MacKinnon. 1996. Contribution of the S4 segment to the gating charge in the Shaker K^+channel. *Neuron* 16:1169-1177.

Ahmad, I., L.J. Redmond and C.J. Barnstable. 1990. Developmental and tissue specific expression of the rod photoreceptor cGMP-gated ion channel. *Biochem. Biophys. Res. Commun.* 173:463-470.

Almers, W. and E.W. McCleskey. 1984. Nonselective conductance in calcium channels of frog muscle: calcium selectivity in a single-file pore. *J. Physiol.* 353:585-608.

Altenhofen, W., J. Ludwig, E. Eismann, W. Kraus, W. Bönigk and U.B. Kaupp. 1991. Control of ligand specificity in cyclic nucleotide-gated channels from rod photoreceptors and olfactory epithelium. *Proc. Natl. Acad. Sci. USA 88:9868-9872.*

Armstrong, C.M. and J. Neyton. 1992. Ion permeation through calcium channels. *Ann. NY Acad. Sci.* 635:18-25.

Balasubramanian, S., J.W. Lynch and P.H. Barry. 1996. Calcium-dependent modulation of the agonist affinity of the mammalian olfactory cyclic nucleotide-gated channel by calmodulin and a novel endogenous factor. *J. Membr. Biol.* 152:13-23.

Barnard, E.A. 1992. Subunits of $GABA_A$, glycine and glutamate receptors. In "Receptor subunits and complexes"(Burgen, A.S.V. and E.A. Barnard), Cambridge University Press, 163-187.

Barnstable, C.J. and J.-Y. Wei. 1995. Isolation and characterization of the alpha-subunit of rod photoreceptor cGMP-gated cation channel. *J. Molec. Neurosci.* 6:289-302.

Bauer P.J. 1996. Cyclic GMP-gated channels of bovine rod photoreceptors: affinity, density and stoichiometry of Ca^{2+}-calmodulin binding sites. *J. Physiol.* 494:675-85.

Baumann, A., S. Frings, M. Godde, R. Seifert and U.B. Kaupp. 1994. Primary structure and functional expression of a *Drosophila* cyclic nucleotide-gated channel present in eyes and antennae. *EMBO J.* 13:5040-5050.

Baylor, D., T.D. Lamb and K.-W. Yau. 1979. The membrane current of single rod outer segments. *J. Physiol. London* 288:589-611.

Baylor, D. 1996. How photons start vison. *Proc. Natl. Acad. Sci. USA* 93:560-565.

Belluscio, L., G.H. Gold, A. Nemes and R. Axel. 1998. Mice deficient in G_{olf} are anosmic. *Neuron* 20:69-81.

Benitah, J.P., Ranjan, R., Yamagishi, T., Janecki, M., Tomaselli, G.F., and E. Marban. 1997. Molecular motions within the pore of voltage-dependent sodium channels. *Biophys. J.* 73:603-613.

Berghard, A., L.B. Buck and E.R. Liman. 1996. Evidence for distinct signalling mechanisms in two mammalian olfactory sense organs. *Proc. Natl. Acad. Sci. USA* 93:2365-2369.

Biel, M., W. Altenhofen, R. Hullin, J. Ludwig, M. Freichel, V. Flockerzi, N. Dascal, U.B. Kaupp and

F. Hofmann. 1993. Primary structure and functionnal expression of a cyclic nucleotide-gated channel from rabbit aorta. *FEBS Lett.* 329:134-138.

Biel, M., X. Zong, M. Distler, E. Bosse, N. Klugbauer, M. Murakami, V. Flockerzi and F. Hoffmann. 1994. Another member of cyclic nucleotide-gated channels family expressed in testis, kidney, and heart. *Proc. Natl. Acad. Sci. U.S.A.* 91:3505-3509.

Biel, M., X. Zong, and F. Hofmann. 1995. Molecular diversity of cyclic nucleotide-gated cation channels. *Naunyn Schmiedebergs Arch. Pharmacol.* 353(1):1-10.

Boekhoff, I., E. Tareilus, J. Strotmann and H. Breer. 1990. Rapid activation of alternative second messenger pathways in olfactory cilia by different odorants. *EMBO J.* 9:2453-2458.

Boekhoff, I. and H. Breer. 1992. Termination of second messenger signaling in olfaction. *Proc. Natl. Acad. Sci. U.S.A.* 89:471-474.

Boekhoff, I., S. Schleicher, J. Strotmann and H. Breer, 1992. Odor-induced phosphorylation of olfactory cilia proteins. *Proc. Natl. Acad. Sci. U.S.A.* 89:11983-11987.

Bönigk, W., W. Altenhofen, F. Müller, A. Dose, M. Illing, R.S. Molday and U.B. Kaupp. 1993. Rod and cone photoreceptor cells express distinct genes for cGMP-gated channels. *Neuron* 10:865-877.

Bönigk, W., J. Bradley, F. Müller, F. Sesti, I. Boekhoff, G.V. Ronnett, U.B. Kaupp and S. Frings. 1999. The native rat olfactory cyclic nucleotide-gated channel is composed of three distinct subunits. *J. Neurosci.* 19:5332-5347.

Borisy, F.F., G.V. Ronnett, A.M. Cunningham, D. Juifs, J. Beavo and S.H. Snyder. 1992. Calcium/calmodulin-activated phosphodiesterase expressed in olfactory receptor neurons. *J.Neurosci.* 12:915-923.

Bradley, J., J. Li, N. Davidson, H.A. Lester and K. Zinn. 1994. Heteromeric olfactory cyclic nucleotide-gated channels: a subunit that confers increased sensitivity to cAMP. *Proc. Natl. Acad. Sci. USA.* 91:8890-8894.

Bradley, J., Y. Zhang, R. Bakin, H.A. Lester, G.V. Ronett and K. Zinn. 1997. Functional expression of the heteromeric "olfactory" cyclic nucleotide-gated channel in the hippocampus : a potential effector of synaptic plasticity in brain neurons. *J. Neurosci.* 17:1993-2005.

Breer, H. and I. Boekhoff. 1991. Odorants of the same class activate different second messenger pathways. *Chem. Senses* 16:19-29.

Broillet, M.-C. and S. Firestein. 1996. Direct activation of the olfactory cyclic nucleotide-gated channel through modification of sulfhydryl groups by NO compounds. *Neuron* 16:377-385.

Broillet, M.-C. and S. Firestein. 1997. β subunits of the olfactory cyclic nucleotide-gated channel form a nitric oxide activated Ca^{2+} channel. *Neuron* 18:951-958.

Brown, L.R., R. Gramling, R.J. Bert and J.W. Karpen. 1995. Cyclic-GMP contact points within the 63 kDa subunit and the 240 kDa associated protein of retinal rod cGMP-activated channels. *Biochemistry* 34:8365-8370.

Brüne, B. and V. Ullrich. 1987. Inhibition of platelet aggregation by carbon monoxide is mediated by activation of guanylyl cyclase. *Mol. Pharmacol.* 32:497-504.

Brunet, L.J., G.H. Gold and J. Ngai. 1996. General anosmia caused by a targeted disruption of the mouse olfactory cyclic nucleotide-gated cation channel. Neuron 17:681-693.

Bucossi, G., E. Eismann, F. Sesti, M. Nizzari, M. Seri, U.B. Kaupp and V. Torre. 1996. Time

dependent current decline in cyclic GMP gated channels caused by point mutations in the pore region. *J. Physiol.* 493: 409-418.

Bucossi, G., M. Nizzari and V. Torre. 1997. Single-channel properties of ionic channels gated by cyclic nucleotides. *Biophys. J.* 72: 1165-1181.

Capovilla, M., A. Caretta, L. Cervetto and V. Torre. 1983. Ionic movements through light-sensitive channels of toad rods. *J. Physiol.* 343:295-310.

Chen, F.H., M. Ukhanova, D. Thomas, G. Afshar, S. Tanda, B.A. Battelle and R Payne. 1999. Molecular cloning of a putative cyclic nucleotide-gated ion channel cDNA from *Limulus polyphemus*. *J. Neurochem.* 72:461-471.

Chen, T.Y., Y.W. Peng, R.S. Dhallan, B. Ahamed, R.R. Reed and K.-W. Yau. 1993. A new subunit of the cyclic nucleotide-gated cation channel in retinal rods. *Nature* 362:764-767.

Chen T.Y., M. Illing, L.L. Molday, Y.T. Hsu, K.-W. Yau and R.S. Molday. 1994. Subunit 2 (or beta) of retinal rod cGMP-gated cation channel is a component of the 240-kDa channel-associated protein and mediates Ca^{2+}-calmodulin modulation. *Proc. Natl. Acad. Sci. USA* 91:11757-11761.

Chen T.Y. and K.-W. Yau. 1994. Direct modulation by Ca^{2+}-calmodulin of cyclic nucleotide-activated channel of rat olfactory receptor neurons. *Nature* 368:545-548.

Cobbs, W.H., A.E.III Barkdoll and E.N.Jr. Pugh. 1985. Cyclic GMP increases photocurrent and light sensitivity of retinal cones. *Nature* 317:585-587.

Coburn, C.M. and C. Bargmann. 1996. A putative cyclic nucleotide-gated channel is required for sensory development and function in *C. elegans*. *Neuron* 17:695-706.

Colamartino, G., A. Menini, and V. Torre. 1991. Blockage and permeation of divalent cations through the cyclic GMP-activated channel from tiger salamander retinal rods. *J. Physiol. (Camb.)* 440:189-206.

Cook, N.J., W. Hanke and U.B. Kaupp. 1987. Identification, purification, and functional reconstitution of the cyclic GMP-dependent channel from rod photoreceptors. *Proc. Natl. Acad. Sci. USA*. 84:585-589.

Creighton, T.E. 1993. Proteins. Structures and Molecular Properties. 2nd ed. W.H. Freeman and Company, New York. NY. 507 pp.

Dhallan, R.S., K.W. Yau, K.A. Schrader and R.R. Reed. 1990. Primary structure and functional expression of a cyclic nucleotide-activated channel from olfactory neurons. *Nature* 347:184-187.

Dhallan, R.S., J.P. Macke, R.L. Eddy, T.B. Shows and R.R. Reed. 1992. Human rod photoreceptor cGMP-gated channel: amino acid sequence, gene structure, and functional expression. *J. Neurosci.* 12:3248-3256.

DiFrancesco, D. 1993. Pacemaker mechanisms in cardiac tissue. *Annu. Rev. Physiol.* 55:455-472.

Doyle, D.A., J.M. Cabral, R.A. Pfuetzner, A. Kuo, J.M. Gulbis, S.L. Cohen, B.T. Chait, and R. MacKinnon. 1998. The structure of the potassium channel: molecular basis of K^+ conduction and selectivity. *Science*. 280: 69-77.

Durell, S.R., and H.R. Guy. 1992. Atomic scale structure and functional models of voltage-gated potassium channels. *Biophys. J.* 62:238-250.

Durell, S.R., and H.R. Guy. 1996. Structural model of the outer vestibule and selectivity filter of the *Shaker* voltage-gated K^+ channel. *Neuropharmacology.* 35:761-773.

Eismann, E.F., W. Bönigk and U.B. Kaupp. 1993. Structural features of cyclic nucleotide-gated channels. *Cell. Physiol. Biochem.* 3:332-351.

Eismann, E., F. Muller, S.H. Heinemann and U.B. Kaupp. 1994. A single negative charge within the pore region of a cGMP-gated channel controls rectification, Ca^{2+} blockage, and ionic selectivity. *Proc. Natl. Acad. Sci. USA.* 91:1109-1113.

El-Refai. 1980. Assay of soluble receptors. In "Membranes, detergents and receptor solubilization" (J.C. Venter and L.C. Harrison). Alan R., Liss, Inc., NY.

Emeis, D., H. Kuhn, J. Reichert and K.P. Hofmann. 1982. Complex formation between metarhodopsin II and GTP-binding protein in bovine photoreceptor membranes leads to a shift of the photoproduct equilibrium. *FEBS Lett.* 143, 29-34.

Fain, G.L., H.R. Matthews and W.C. Cornwall. 1996. Dark adaptation in vertebrate photoreceptors. *Trends Neurosci.* 19:502-507.

Fakler, B., U. Brandle, E. Glowatzki, S. Weidemann, H.P. Zenner and J.P. Ruppersberg. 1995. Strong voltage-dependent inward rectification of inward rectifier K^+ channels is caused by intracellular spermine. *Cell* 80:149-154.

Fesenko, E. E., Kolesnikov, S. S., Lyubarsky, A. L. 1985. Induction by cyclic GMP of cationic conductance in plasma membrane of retinal rod outer segment. *Nature* 313: 310-13.

Filatov, G.N., A.B. Jainazarov, S.S. Kolesnikov, A.L. Lyubarsky and E.E. Fesenko. 1989. The effect of ATP, GTP and cAMP on the cGMP-dependent conductance of the fragments from frog rod plasma membrane. *FEBS Lett.* 245:185-188.

Finn, J.T., M.E. Grunwald, and K-W. Yau. 1996. Cyclic nucleotide-gated ion channels: an extended family with diverse functions. *Annu. Rev. Physiol.* 58:395-426.

Finn, J.T., E.C. Solessio and K.W. Yau. 1997. A cGMP-gated cation channel in depolarizing photoreceptors of the lizard parietal eye. *Nature* 385:815-819.

Fodor, A.A., S.E. Gordon, and W. Zagotta. 1997. Mechanism of tetracaine block of cyclic nucleotide-gated channels. *J. Gen. Physiol.* 109: 3-14.

Frings, S., J.W. Lynch and B. Lindemann. 1992. Properties of cyclic nucleotide-gated channels mediating olfactory transduction: activation, selectivity and blockage. *J. Gen. Physiol.* 100:45-67.

Frings, S., R. Seifert, M. Godde and U.B. Kaupp. 1995. Profoundly different calcium permeation and blockage determine the specific function of distinct cyclic nucleotide-gated channels. *Neuron* 15:169-179.

Furchgott, R.F. and D. Jothianandan. 1991. Endothelium-dependent and -independent vasodilatation involving cyclic GMP: relaxation induced by nitric oxide, carbon monoxide and light. *Blood Vessels* 28:52-61.

Furman, R.E. and J.C. Tanaka. 1990. Monovalent selectivity of the cyclic guanosine monophosphatactivated ion channel. *J. Gen. Physiol.* 96:57-82.

Gold, G.H. 1999. Controversial issues in vertebrate olfactory transduction. *Annu. Rev. Physiol.* 61:857-871.

Gong, L.and N. Kraus. 1998. Molecular cloning of cDNA encoding the alpha subunit of CNGC gene from human fetal heart. *Life Sci.* 63:1555-1562.

Gorczyca, W.A., M.P. Gray-Keller, P.B. Detwiler and K. Palczewski. 1994. Purification and physiological identification of a guanylate cyclase activating protein from retinal rods. *Proc. Natl. Acad. Sci. USA.* 91:4014-4018.

Gordon, S.E., D.L. Brautigan and A.L. Zimmerman. 1992. Protein phosphatases modulate the apparent agonist affinity of the light-regulated ion channel in retinal rods. 1992. *Neuron* 9:739-748.

Gordon, S.E., and W. N. Zagotta. 1995a. A histidine residue associated with the gate of the cyclic nucleotide-activated channels in rod photoreceptors. *Neuron.* 14: 177-183.

Gordon, S.E., and W. N. Zagotta. 1995b. Localization of regions affecting an allosteric transition in cyclic nucleotide-activated channels. *Neuron.* 14:857-864

Gordon, S.E., and W. N. Zagotta. 1995c. Subunit interactions in coordination of Ni^{2+} in cyclic nucleotide-gated channels. *Proc. Natl. Acad. Sci. USA.* 92:10222-10226.

Gordon, S.E., J. Downing-Park, B. Tam and A.L. Zimmerman. 1995. Diacylglycerol analogs inhibit the rod cGMP-gated channel by a phosphorylation-independent mechanism. *Biophys. J.* 69:409-417.

Gordon, S.E., J.C. Oakley, M.D. Varnum, and W. N. Zagotta. 1996. Altered ligand specificity by protonation in the ligand binding domain of cyclic-nucleotide gated channels. *Biochemistry* 35:3994-4001.

Gordon, S.E., M.D. Varnum, and W. N. Zagotta. 1997. Direct interaction between amino- and carboxyl-terminal domains of cyclic-nucleotide-gated channels. *Neuron* 19:431-441.

Goulding, E.H., J. Ngai, R.H. Kramer, S. Colicos, R. Axel, S.A. Siegelbaum and A. Chess. 1992. Molecular cloning and single-channel properties of the cyclic-nucleotide-gated channel from catfish olfactory neurons. *Neuron.* 8:45-58.

Goulding, E.H., G.R. Tibbs, D. Liu and S.A. Siegelbaum. 1993. Role of H5 domain in determining pore diameter and ionic permeation through cyclic nucleotide-gated channels. *Nature* 364: 61-64.

Goulding, E.H., G.R. Tibbs and S.A. Siegelbaum. 1994. Molecular mechanism of cyclic nucleotide-gated channel activation. *Nature* 372: 369-374.

Gray-Keller, M., A. Polans, K. Palczewski and P. Detwiler. 1993. The effect of recoverin-like calcium-binding proteins on the photoresponse of retinal rods. *Neuron* 10:523-531.

Guidoni, L, V. Torre and P. Carloni. 1999. Potassium and sodium binding to the outer mouth of the K^+ channel. *Biochemistry* 38:8599-8604.

Guy, H.R. and F. Conti. 1990. Pursuing the structure and function of voltage-gated channels. *TINS* 13:201-206.

Guy, H.R. and S.R. Durell. 1995. Structural models of Na^+, Ca^{2+}, and K^+ channels. In "Ion channels and genetic diseases". The Rockefeller University Press: 1-16.

Hagins, W.A., R.D. Penn and S. Yoshikami. 1970. Dark current and photocurrent in retinal rods. *Biophys. J.* 10:380-412.

Hagiwara, S., S. Miyazaki and N.P. Rosenthal. 1976. Potassium current and the effect of cesium on this current during anomalous rectification of the egg cell membrane of a starfish. *J. Gen. Physiol.*

67:621-638.

Hamill, O.P., A. Marty, E. Neher, B. Sakmann, and F.J. Sigworth. 1981. Improved patch-clamp technique for high resolution current recording from cells and cell-free membrane patches. *Pflugers Arch.* 391:85-100.

Haynes, L.W. and K.W. Yau. 1985. Cyclic GMP-sensitive conductance in outer segment membrane of catfish cones. *Nature* 317:61-64.

Haynes, L.W., A.R. Kay and K.W. Yau. 1986. Single cyclic GMP-activated channel activity in excised patches of rod outer segment membrane. *Nature* 321:66-70.

Haynes, L.W. 1992. Block of the cyclic GMP-gated channel of vertebrate rod and cone photoreceptors by *l-cis*-diltiazem. *J.Gen.Physiol.* 100:783-801.

Haynes, L.W. 1995. Permeation and block by internal and external divalent cations of the catfish cone photoreceptor cGMP-gated channel. *J. Gen. Physiol.* 106:507-523.

Heginbotham L., T. Abramson and R. McKinnon. 1992. A functional connection between the pores of distantly related ion channels as revealed by mutant K^+ channels. *Science* 258: 1152-1155.

Heginbotham L., Z. Lu, T. Abramson and R. McKinnon. 1994. Mutations in the K^+ channel signature sequence. *Biophys. J.* 66:1061-1067.

Heinemann, S.H., H. Terlau, W. Stuhmer, K. Imoto and S. Numa. 1992. Calcium channel characteristics conferred on the sodium channel by single mutations. *Nature* 356: 441-443.

Henn, D.K., A. Baumann, and U.B. Kaupp. 1995. Probing the transmembrane topology of cyclic nucleotide-gated ion channels with a gene fusion approach. *Proc. Natl. Acad. Sci. USA.* 92: 7425-7429.

Hess, P. and R.W. Tsien. 1984. Mechanism of ion permeation through calcium channels. *Nature* 309:453-456.

Hille, B. 1992. Ionic Channels of Exitable Membranes. Sinauer Associates, Sunderlands, MA, USA.

Hollenberg, M. D. 1990. Receptor solubilization, characterization, and isolation. In "Methods in neurotransmitter receptor analysis" (by H.I. Yamamura *et al.*) Raven Press, Ltd., NY. 111-145.

Holmgren, M., Y. Liu, Y. Xu, and G. Yellen. 1996. On the use of thiol-modifying agents to determine channel topology. *Neuropharmacology.* 35:797-804.

Horn, R. 1991. Estimating the number of channels in patch recordings. *Biophys. J.* 60: 433-439.

Hsu, Y.-T. and R.S. Molday. 1993. Modulation of the cGMP-gated channel of rod photoreceptor by calmodulin. *Nature* 361:76-79.

Ildefonse, M., and N. Bennett. 1991. Single-channel study of the cGMP-dependent conductance of retinal rods from incorporation of native vesicles into planar lipid bilayers *J. Memb. Biol.* 123: 133-147.

Ildefonse, M., S. Crouzy, and N. Bennett. 1992. Gating of retinal rod cation channel by different nucleotides: comparative study of unitary currents. *J. Membrane Biol.* 130:91-104.

Jan, L.Y. and Y.N. Jan. 1990. A superfamily of ion channels. *Nature* 345:672.

Jan, L.Y., and Y.N. Jan, Y.N. 1992. Tracing the roots of ion channels. *Cell* 69:715-718.

Kaplan, W.D. and W.E. Trout. 1969. The behaviour of four neurological mutants of *Drosophila*. *Genetics*. 61:399.

Karlin, A., and M.H. Akabas. 1998. Substituted-cysteine-accessibility method. In "Methods in Enzymology". (P.M. Conn, editor) Academic Press, Inc. San Diego, CA. 293:123-136.

Karpen, J.W., A.L. Zimmerman, L. Stryer and D.A. Baylor. 1988. Gating kinetics of the cyclic-cGMP-activated channel of retinal rods: flash photolysis and voltage-jump studies. *Proc Natl Acad Sci USA* 85: 1287-1291.

Karpen, J.W., D.A. Loney and D.A. Baylor. 1992. Cyclic GMP-activated channels of salamander retinal rods : spatial distribution and variation of responsiveness. *J. Physiol.* 448:257-274.

Karpen, J.W., R. L. Brown, L. Stryer, and D.A. Baylor. 1993. Interactions between divalent cations and the gating machinery of cyclic GMP-activated channels in salamander retinal rods. *J.Gen.Physiol.* 101:1-25.

Kaupp, U.B., T. Niidome, T. Tanabe, S. Terada, W. Bonigk,W. Stuhmer, N.J. Cook, K. Kangawa, H. Matsuo, T. Hirose, T. Miyata, and S. Numa. 1989. Primary structure and functional expression from complementary DNA of the rod photoreceptor cyclic GMP-gated channel. *Nature (Lond.)*. 342:762-766.

Kaupp, U.B. 1995. Family of cyclic nucleotide gated ion channels. *Curr. Opin. Neurobiol.* 5:434-442.

Kharitonov, V.G., V.S. Sharma, R.B. Pilz, D. Magde and D. Koesling. 1995. Basis of guanylate cyclase activation by carbon monoxide. *Proc. Natl. Acad. Sci. USA* 92:2568-2571.

Kingston, P.A., F. Zufall and C.J. Barnstable. 1996. Rat hippocampal neurons express genes for both rod retinal and olfactory cyclic nucleotide-gated channels: novel targets for cAMP/cGMP function. *Proc. Natl. Acad. Sci. USA* 93:10440-10445.

Kleene, S.J. 1995. Block by external calcium and magnesium of the cyclic nucleotide-activated current in olfactory cilia. *Neurosci.* 66:1001-1008.

Koch and Kaupp, 1985. Cyclic GMP directly regulates a cation conductance in membranes of bovine rods by a cooperative mechanism. *J. Biol. Chem.* 260:6788-6800.

Koch, W.-H. and L. Stryer. 1988. Highly cooperative feedback control of retinal rod guanylate cyclase by calcium ions. *Nature* 334:64-66.

Kolesnikov, S.S., A.B. Zhainazarov and A.V. Kosolapov. 1990. Cyclic-nucleotide-activated channel in the frog olfactory receptor plasma membrane. *FEBS Lett.* 266:96-98.

Komatsu, H., I. Mori, J.-S. Rhee, N. Akaike and Y. Ohshima. 1996. Mutations in a cyclic nucleotide-gated channel lead to abnormal thermosensation and chemosensation in *C. elegans*. *Neuron* 17:707-718.

Körschen, H.G., M. Illing, R. Seifert, F. Sesti, A. Williams, S. Gotzes, C. Colville, F. Müller, A. Dosé, M. Godde, L. Molday, U.B. Kaupp and R.S. Molday. 1995. A 240 kDa protein represents the complete β-subunit of the cyclic-nucleotide-gated channel from rod photoreceptor. *Neuron* 15:627-636.

Körschen, H.G., M. Beyermann, F. Müller, M. Heck, M. Vantler, K.-W. Koch, R. Kellner, U. Wolfrum, C. Bode, K.P. Hofmann and U.B. Kaupp. 1999. Interaction of glutamic-acid-rich proteins with the cGMP signalling pathway in rod photoreceptors. *Nature*. 400:761-766.

Koutalos, Y. and K.W. Yau. 1996. Sensitivity regulation in rod photoreceptors by calcium. *Trends Neurosci.* 19:73-81.

Kramer, R.H. and S.A. Siegelbaum. 1992. Intracellular Ca^{2+} regulates the sensitivity of cyclic nucleotide-gated channels in olfactory receptor neurons. *Neuron* 9:897-906.

Kramer, R.H., E. Goulding and S.A. Siegelbaum. 1994. Potassium channel inactivation peptide blocks cyclic nucleotide-gated channels by binding to the conserved pore domain. *Neuron* 12:655-662.

Kumar, V.D. and I.T. Weber. 1992. Molecular model of the cyclic GMP-binding domain of the cyclic GMP-gated ion channel. *Biochemistry* 31:4643-4649.

Kuner, T., L.P. Wollmuth, A. Karlin, P.H. Seeburg, and B. Sakmann. 1996. Structure of the NMDA receptor channel M2 segment inferred from the accessibility of substituted cysteines. *Neuron.* 17:343-352.

Kurtz L.L., R.D. Zuhlke, H.-J. Zhang, and R. Joho. 1995. Side-chain accessibilities in the pore of a K^+ channel probed by sulfhydryl-specific reagents after cysteine-scanning mutagenesis. *Biophys. J.* 68:900-905.

Lagnado, L. and D.A. Baylor. 1994. Calcium controls light-triggered formation of catalytically active rhodopsin. *Nature* 367:273-277.

Lander, H.M. 1997. An essential role for free radicals and derived species in signal transduction. *FASEB J.* 11:118-124.

Laio, A., and V. Torre. 1999. Physical Origin of selectivity in ionic channels of biological membranes. *Biophys. J.* 76:129-148.

Lee, J.-K., S.A. Scott and J.N. Weiss. 1999. Novel gating mechanism of polyamine block in the strong inward rectifier K+ channel Kir 2.1. *J. Gen. Physiol.* 113:555-563.

Leinders-Zufall, T., H. Rosenboom, C.J., Barnstable, G.M. Shepherd and F. Zufall. 1995. A calcium permeable cGMP-activated cation conductance in hippocampal neurons. *Neuroreport* 6:1761-1765.

Levitan, I.B. 1985. Phosphorylation of ion channels. *J. Memb. Biol.* 87:177-190.

Levitan, I.B. 1994. Modulation of ion channels by protein phosphorylation and dephosphorylation. *Annu. Rev. Physiol.* 56:193-212.

Li, J., W.N. Zagotta and H.A. Lester. 1997. Cyclic nucleotide-gated channels: structural basis of ligand efficacy and allosteric modulation. *Q. Rev. Biophys.* 30:177-193.

Li, J. and H.A. Lester. 1999. Functional roles of aromatic residues in the ligand-binding domain of cyclic nucleotide-gated channels. *Mol. Pharmacol.* 55:873-882.

Light, D.B., F.V. McCann, T.M. Keller and B.A. Stanton. 1988. Amiloride-sensitive cation channel in apical membrane of inner medullary collecting duct. *Am. J. Physiol.* 255:F278.

Liman, E.R. and L.B. Buck. 1994. A second subunit of the olfactory cyclic nucleotide-gated channel confers high sensitivity to cAMP. *Neuron* 13:611-621.

Liu, M., T.-Y. Chen, B. Ahamed, J. Li and K.-W. Yau. 1994. Calcium-modulation of the olfactory cyclic nucleotide-gated cation channel. *Science* 266:1348-1354.

Liu D.T., G.R. Tibbs and S.A. Siegelbaum. 1996. Subunit stoichiometry of cyclic nucleotide-gated channels and effects of subunit order on channel function. *Neuron* 16:983-990.

Liu, Y., M. Holmgren, M.E. Jurman, and G. Yellen. 1997. Gated access to the pore of a voltage-dependent K^+ channel. *Neuron* 19:175-184.

Liu, D.T., G.R. Tibbs, P. Paoletti and S.A. Siegelbaum. 1998. Constraining ligand-binding site stoichiometry suggests that a cyclic nucleotide-gated channel is composed of two functional dimers. *Neuron* 21:235-248.

Lolley, R.N. and E. Racz. 1982. Calcium modulation of cyclic GMP synthesis in rat visual cells. *Vision Res.* 22:1481-1486.

Lowe, G., T. Nakamura, G.H. Gold. 1989. Adenylate cyclase mediates olfactory transduction for a wide variety of odorants. *Proc. Natl. Acad. Sci. USA.* 86:5641-5645.

Lu, Q., and C. Miller. 1995. Silver as a probe of pore-forming residues in a potassium channel. *Science* 268: 304-307.

Lu, Z. and L. Ding. 1999. Blockade of a retinal cGMP-gated channel by polyamines. *J. Gen. Physiol.* 113:35-43.

Ludwig, J., T. Margalit, E. Eismann, D. Lancet and U.B. Kaupp. 1990. Primary structure of cAMP-gated channel from bovine olfactory epithelium. *FEBS Lett.* 270:24-29.

Ludwig, A., X. Zong, J. Stieber, R. Hullin, F. Hofmann and M. Biel. 1999. Two pacemaker channels from human heart with profoundly different activation kinetics. *EMBO J.* 18:2323-2329.

Luehring, H., W. Hanke, R. Simmoteit and U.B. Kaupp. 1990. Cation selectivity of the cyclic GMP-gated channel of mammalian rod photoreceptors. In "Sensory transduction"(Borselino, L., L. Cervetto and V. Torre). Plenum Press, N-Y 169-174.

Lynch, J.W. and B. Lindemann. 1994. Cyclic nucleotide-gated channels of rat olfactory receptor cells: divalent cations control the sensitivity to cAMP. *J. Gen. Physiol. 103:87-106.*

Lynch, J.W. 1998. Nitric oxide inhibition of the rat olfactory cyclic nucleotide-gated cation channel. *J. Memb. Biol.* 165: 227-234.

Matthews, G. and S.-I. Watanabe. 1987. Properties of ion channels closed by light and opened by 3',5'-cyclic monophosphate in toad retinal rods. *J. Physiol.* 389:691-715.

Matthews, G. and S.-I. Watanabe. 1988. Activation of single ions channels from toad retinal rod inner segments by cyclic GMP: concentration dependence. *J.Physiol. London* 403:389-405.

McGeoch, J.E.M., M.W. McGeoch and G. Guidotti. 1995. Eye CNG channel is modulated by nicotine. *Biochem. Biophys. Res. Commun.* 214:879-887.

McKay, D.B. and T.A. Steitz. 1981. Structure of catabolite gene activator protein at 2.9 Angström resolution suggests binding to left-handed B-DNA. *Nature* 290:744-749.

McLatchie, L.M. and H.R. Matthews. 1992. Voltage-dependent block by *l-cis*-diltiazem of the cyclic GMP-activated conductance of salamander rods. *Proc. R. Soc. Lond. (B)* 247:113-119.

Menini, A., G. Rispoli and V. Torre. 1988. The ion selectivity of the light-sensitive current in isolated rods of the tiger salamander. *J. Physiol.* 402:279-300.

Menini, A. and B.J. Nunn. 1990. The effect of pH on the cyclic-GMP-activated conductance in retinal rods. In "Sensory Transduction" Plenum Press 175-181.

Menini A. 1990. Currents carried by monovalent cations through cyclic GMP-activated channels in excised patches from salamander rods. *J Physiol* 424: 167-185.

Misaka, T., Y. Kusakabe, Y. Emori, T. Gonoi, S. Arai and K. Abe. 1997. Taste buds have a cyclic nucleotide-activated channel, CNGgust. *J. Biol. Chem.* 272:22623-22629.

Molday, R.S. 1996. Calmodulin regulation of cyclic-nucleotide-gated channels. *Curr Opin Neurobiol* 6:445-452.

Molokanova, E., B. Trivedi, A. Savchenko and R.H. Kramer. 1997. Modulation of rod photoreceptor cyclic nucleotide-gated channels by tyrosine phosphorylation. *J. Neurosci.* 17:9068-9076.

Molokanova, E., F. Maddox, C.W. Luetje and R.H. Kramer. 1999a. Activity dependent modulation of rod photoreceptor cyclic nucleotide-gated channels mediated by phosphorylation of a specific tyrosine residue. *J. Neurosci.* 19:4786-4795.

Molokanova, E., A. Savchenko and R.H. Kramer. 1999b. Noncatalytic inhibition of cyclic nucleotide-gated channels by tyrosine kinase induced by genistein. *J. Gen. Physiol.* 113:45-56.

Muller, F., W. Bonigk, F. Sesti and S. Frings. 1998. Phosphorylation of mammalian olfactory cyclic nucleotide-gated channels increases ligand sensitivity. *J. Neurosci.* 18:164-173.

Nakamura, T. and G.H. Gold. 1987. A cyclic nucleotide-gated conductance in olfactory receptor cilia. *Nature* 325:442-444.

Nakatani, K. and K.-W. Yau. 1988. Calcium and magnesium fluxes across the plasma membrane of the toad rod outer segment. *J. Physiol.* 395:695-729.

Nakatani, K., Y. Koutalos and K.-W. Yau. 1995. Ca^{2+} modulation of the cGMP-gated channel of bullfrog retinal rod photoreceptors. *J. Physiol.* 484:69-76.

Nicol, G.D. 1993. The calcium channel antagonist, pimozide, blocks the cyclic GMP-activated current in rod photoreceptors. *J. Pharmac. exp. Ther.* 265:626-632.

Nizzari, M., F. Sesti, M.T. Giraudo, C. Virginio, A. Cattaneo, and V. Torre. 1993. Single-channel properties of cloned cGMP-activated channels from retinal rods. *Proc. Roy. Soc. Lond. B* 254:69-74.

North, A. 1995. Hanbook of receptors and channels. CRC Press. 1-151.

Nunn, B.J. 1987. Ionic permeability ratios of the cyclic GMP-activated conductance in the outer segment membrane of salamander rods. *J. Physiol.* 394, 17P.

Oda, Y., L.C. Timpe, R.C. McKenzie, D.N. Sauder, C. Largman and T. Mauro. 1997. Alternatively spliced forms of the cGMP-gated channel in human keratinocytes. *FEBS Lett.* 414:140-145.

O'Dell, T.J., R.D. Hawkins, E.R. Kandel and O. Arancio. 1991. Tests on the roles of two diffusible substances in long-term potentiation: evidence for nitric oxide as a possible early retrograde messenger. *Proc. Natl. Acad. Sci. USA* 88:11285-11289.

Oliver, D., H. Hahn, C. Antz, J.P. Ruppersberg and B. Fakler. 1998. Interaction of permeant and blocking ions in cloned inward-rectifier K^+ channels. *Biophys. J.* 74:2318-2326.

Paoletti, P., E.C. Young and S.A. Siegelbaum. 1999. C-linker of cyclic nucleotide-gated channels controls coupling of ligand binding to channel gating. *J.Gen.Physiol.* 113:17-33.

Park, C.S. and R. MacKinnon. 1995. Divalent cation selectivity of an ionbinding site in the pore of a cyclic nucleotide-gated channel. *Biochemistry* 34:13328-13333.

Pascual, J.M., C.-C. Shieh, G.E. Kirsch, and A.M. Brown. 1995. K^+ pore structure revealed by reporter cysteines at inner and outer surfaces. *Neuron.* 14:1055-1063.

Picco, C., and A. Menini. 1993. The permeability of the cGMP-activated channel to organic cations in retinal rods of the tiger salamander. *J. Physiol. (Camb.)* 460:741-758.

Picones, A. and J.I. Korenbrot. 1995a. Permeability and interaction of Ca^{++} with cGMP-gated ion channels differ in retinal rod and cone photoreceptors. *Biophys. J.* 69:120-127.

Picones, A. and J.I. Korenbrot. 1995b. Spontaneous, ligand-independent activity of the cGMP-gated ion channels in cone photoreceptors of fish. *J. Physiol.* 485:699-714.

Pittler, S.J., A.K. Lee, M.R. Altherr, T.A. Howard, M.F. Seldin, R.L. Hurwitz, J.J. Wasmuth and W. Baehr. 1992. Primary structure and chromosomal localization of human and mouse rod photoreceptor cGMP-gated cation channel. *J. Biol. Chem.* 267:6257-6262.

Quandt, F.N., G.D. Nicol and P.P.M. Schnetkamp. 1991. Voltage-dependent gating and block of the cyclic-GMP-dependent current in bovine rod outer segments. *Neurosci.* 42:629-638.

Rieke, F. and E.A. Schwartz. 1994. A cGMP-gated current can control exocytosis at cone synapses. *Neuron* 13:863-873.

Root, M.J., and R. MacKinnon. 1993. Identification of an external divalent cation-binding site in the pore of a cGMP-activated channel. *Neuron.* 11:459-466.

Root, M.J., and R. MacKinnon. 1994. Two identical noninteracting sites in an ion channel revealed by proton transfer. *Science* 265:1852-1856.

Ruiz, M.L., B. London and B. Nadal-Ginard. 1996. Cloning and characterization of an olfactory cyclic nucleotide-gated channel expressed in mouse heart. *J. Molec. Cell. Cardiol.* 2828:1453-1461.

Ruiz, M.L. and J.W. Karpen. 1997. Single cyclic nucleotide-gated channels locked in different ligand-bound states. *Nature* 389:389-392.

Ruiz, M.L. and J.W. Karpen. 1999. Opening mechanism of a cyclic nucleotide-gated channel based on analysis of single channels locked in each liganded state. *J. Gen. Physiol.* 113:873-895.

Sambrook J., E.F. Fritsch and T. Maniatis. 1989. Molecular Cloning: A Laboratory Manual. 2nd ed. Cold Spring Harbor Laboratory Press, Cold Spring Harbor, New York.

Sautter, A., M. Biel and F. Hofmann. 1997. Molecular cloning of cyclic nucleotide-gated cation channel channel subunits from rat pineal gland. *Brain Res. Mol. Brain Res.* 48:171-175.

Sautter, A., X. Zong, F. Hoffmann and M. Biel. 1998. An isoform of the rod photoreceptor cyclic nucleotide-gated channel β-subunit expressed in olfactory neurons. *Proc. Natl. Acad. Sci. USA.* 95:4696-4701.

Savchenko, A., S. Barnes and R.H. Kramer. 1997.Cyclic-nucleotide-gated channels mediate synaptic feedback by nitric oxide. *Nature* 390:694-698.

Schuman, E.M. and D.V. Madison. 1994. Nitric oxide and synaptic function. *Annu. Rev. Neurosci.* 17:153-183.

Scott, S.P., R.W. Harrison, I.T. Weber and J.C. Tanaka. 1996. Predicted ligand interactions for 3', 5'-cyclic nucleotide gated channel binding sites: comparison of retina and olfactory binding site models. *Protein Eng* 9:333-344.

Seifert, R., E. Eismann, J. Ludwig, A. Baumann and U.B. Kaupp. 1999. Molecular determinants of a Ca^{2+}-binding site in the pore of cyclic nucleotide gated channels: S5/S6 segments control affinity of intrapore glutamates. *EMBO J.* 18:119-130.

Sesti, F., M. Straforini, T.D. Lamb and V. Torre. 1994. Properties of single channels activated by cyclic GMP in retinal rods of the tiger salamander. *J. Physiol. (Lond.)* 474:203-222.

Sesti, F., E. Eismann, U.B. Kaupp, M. Nizzari, and V. Torre. 1995. The multi-ion nature of the cGMP-gated channel from vertebrate rods. *J. Physiol. (Camb.)* 487:17-36.

Sesti, F., M. Nizzari, and V. Torre. 1996. Effect of changing temperature on the ionic permeation through the cyclic GMP-gated channel from vertebrate photoreceptors. *Biophys. J.* 70:2616-2639.

Shabb, J.B., L. Ng and J.D. Corbin. 1990. One amino acid change produces a high affinity cGMP-binding site in cAMP-dependent protein kinase. *J. Biol. Chem.* 265:16031-16034.

Shabb, J.B., and J.D. Corbin. 1992. Cyclic nucleotide binding domains in proteins having diverse functions. *J. Biol. Chem.* 267:5723-5726.

Shapiro, M.S. and W.N. Zagotta. 1998. Stoichiometry arrangement of heteromeric olfactory cyclic-nucleotide-gated ion channels. *Proc. Natl. Acad. Sci. USA.* 95:14546-14551.

Sklar, P.B., R.R.H. Anholt and S.H. Snyder. 1986. The odorant-sensitive adenylate cyclase of olfactory receptor cells. Differential stimulation by distinct classes of odorants. *J. Biol. Chem.* 261:15538-15543.

Stern, J.H., U.B. Kaupp and P.R. MacLeish. 1986. Control of the light regulated current in rod photoreceptors by cyclic GMP, calcium and *l-cis*-diltiazem. *Proc. Natl. Acad. Sci. USA.* 83:1163-1167.

Stevens, C.F. and Y. Wang. 1993. Reversal of long-term potentiation by inhibitors of heme oxygenase. Nature 364:147-149.

Stryer, L. 1987.Visual transduction: design and recurring motifs. *Chem. Scr.* 27B:161-71.

Stuhmer, W. 1992. Electrophysiological recording from *Xenopus* oocytes. In "Methods in Enzymology" (B. Rudy and L. Iverson, editors). Academic Press, Inc. San Diego, CA. 319-339.

Su, Y., W.R. Dostmann, F.W. Herberg, K. Durick, N.H. Xuong, L. Ten Eyck, S.S. Taylor and K.I. Varughese. 1995. Regulatory subunit of protein kinase A: structure of deletion mutant with cAMP binding domains. *Science* 269:807-813.

Sudlow, L.C., R.-C. Huang, D.J. Green and R. Gilette. 1993. cAMP-activated Na^+ current of molluscan neurons is resistant to kinase inhibitors and is gated by cAMP in the isolated patch. *J. Neurosci.* 13:5188-5193.

Sun, Z.-P., M.H. Akabas, E.H. Goulding, A. Karlin, and S.A.D. Siegelbaum. 1996. Exposure of residues in the cyclic nucleotide-gated channel pore: P region structure and function in gating. *Neuron.* 16:141-149.

Sunderman, E.R. and W.N. Zagotta. 1999a. Sequence of events underlying the allosteric transition of rod cyclic nucleotide-gated channels. *J. Gen. Physiol.* 113:621-640.

Sunderman, E.R. and W.N. Zagotta. 1999b. Mechanism of allosteric modulation of rod cyclic nucleotide-gated channels. *J. Gen. Physiol.* 113:601-619.

Tanaka, J.C. 1993. The effects of protons on 3', 5' -cGMP-activated currents in photoreceptor patches. *Biophys. J.* 65:2517-2523.

Tang C.-Y. and D.M. Papazian. 1997. Transfer of voltage independence from a rat olfactory channel to the *Drosophila* ether-a-go-go K^+ channel. *J Gen Physiol* 109: 301-311.

Torre, V., M. Straforini, F. Sesti and T.D. Lamb. 1992. Different channel-gating properties of two classes of cyclic GMP-activated channel in vertebrate photoreceptors. *Proc. R. Soc. B* 250:209-215.

Torre, V. and A. Menini. 1994. Selectivity and single channel properties of the cGMP-activated channel in amphibian retinal rods. Handbook of membrane channels.

Varnum, M.D., K.D. Black and W.N. Zagotta. 1995. Molecular mechanism for ligand discrimination of cyclic nucleotide-gated channels. *Neuron* 15:619-625.

Varnum, M.D. and W.N. Zagotta. 1996. Subunit interactions in the activation of cyclic nucleotide-gated ion channels. *Biophys J.* 70:2667-79.

Varnum, M.D. and W.N. Zagotta. 1997. Interdomain interactions underlying activation of cyclic nucleotide-gated channels. *Science* 278:110-113.

Watanabe, S.-I. and G. Matthews. 1988. Regional distribution of cGMP-activated ion channels in the plasma membrane of the rod photoreceptor. *J. Neurosci.* 8:2334-2337.

Watanabe, S.-I. and J. Shen. 1997. Two opposite effects of ATP on the apparent sensitivity of the cGMP-gated channel of the carp retinal cone. *Vis. Neurosci.* 14:609-615.

Weber, I.T. and T.A. Steitz. 1987. Structure of a complex of catabolite gene activator protein and cyclic AMP refined at 2.5 Angström resolution. *J.Mol. Biol.* 198:311-326.

Weber, I., J. Shabb and J. Corbin. 1989. Predicted structures of cGMP-binding domains of the cGMP-dependent protein kinase: a key alanine/threonine difference in evolutionary divergence of cAMP and cGMP binding sites. *Biochemistry* 28:6122-6127.

Wei, J.Y., D.S. Roy, L. Leconte and C.J. Barnstable. 1998. Molecular and pharmacological analysis of cyclic nucleotide-gated channel function in the central nervous system. *Prog. in Neurobiol.* 56:37-64.

Weitz, D., M. Zoche, F. Müller, M. Beyermann, H.G. Körschen, U.B. Kaupp and K.-W. Koch. 1998. Calmodulin controls the rod photoreceptor CNG channel through an unconventional binding site in the N-terminus of the β-subunit. *EMBO J.* 17:2273-2284.

Weyand, I., M. Godde, S. Frings, J. Weiner, F. Muller, W. Altenhofen, H. Hatt and U.B. Kaupp. 1994. Cloning and functional expression of a cyclic nucleotide-gated channel from mammalian sperm. *Nature* 368:859-863.

Wilson, G.G., and A. Karlin. 1998. The location of the gate in the acetylcholine receptor channel. *Neuron.* 20:1269-1281.

Wolfhart, P., W. Haase, R.S. Molday, and N.J. Cook. 1992. Antibodies against synthetic peptides used to determine the topology and site of glycosylation of the cGMP-gated channel from bovine rod photoreceptors. *J. Biol. Chem.* 267:644-648.

Yang, J., P.T. Ellinor, W.A. Sather, J.-F. Zhang and R.W. Tsien. 1993. Molecular determinants of Ca^{2+} selectivity and ion permeation in L-type Ca^{2+} channels. *Nature* 366:158-161.

Yang, N., and R. Horn. 1995. Evidence for voltage-dependent S4 movement in sodium channels. *Neuron* 15:213-218.

Yang, N., A.L.Jr. George and R. Horn. 1996. Molecular basis of charge movement in voltage-gated sodium channels. *Neuron* 16:113-122.

Yau, K.-W. and K. Nakatani. 1984. Cation selectivity of light-sensitive conductance in retinal rods. *Nature* 309:352-354.

Yau, K.-W. and K. Nakatani. 1985a. Light-suppressible, cyclic GMP-sensitive conductance in the plasma membrane of a truncated rod outer segment. *Nature* 317:252-255.

Yau, K.-W. and K. Nakatani. 1985b. Light-induced reduction of cytoplasmic free calcium in retinal rod outer segment. Nature 313:579-582.

Yau, K.-W. and D. Baylor. 1989. Cyclic GMP-activated conductance of retinal photoreceptor cells. *Annu. Rev. Neurosci.* 12:289-327.

Yoshizawa, T. and G. Wald. 1963. *Nature* 197:1279-1286.

Yusaf, S.P., D. Wray and A. Sivaprasadarao. 1996. Measurement of the movement of the S4 segment during the activation of a voltage-gated potassium channel. *Eur. J. Physiol.* 433:91-97.

Zagotta, W. N., and S.A. Siegelbaum. 1996. Structure and function of cyclic nucleotide-gated channels. *Annu. Rev. Neurosci.* 19:235-263.

Zhang, Q., S. Pearce-Kelling, G.M. Acland, G.D. Aguirre and K. Ray. 1997. Canine rod photoreceptor cGMP-gated channel protein α-subunit: studies on the expression of the gene and characterization of the cDNA. *Exp. Eye Res.* 65:301-309.

Zhuo, M., A.S. Scott, R.R. Kandel and R.D. Hawkins. 1993. Nitric oxide and carbon monoxide produce activity-dependent long-term synaptic enhancement in hippocampus. *Science* 260:1946-1950.

Zimmerman, A.L. and D.A. Baylor. 1986. Cyclic GMP-sensitive conductance of retinal rods consists of aqueous pores. *Nature* 321:70-72.

Zimmerman, A.L. and D.A. Baylor. 1992. Cation interactions within the cyclic GMP-activated channel of retinal rods from the tiger salamander. *J. Physiol.* 449:759-783.

Zong, X., H. Zucker, F. Hofmann and M. Biel. 1998. Three amino acids in the C-linker are major determinants of gating in cyclic nucleotide-gated channels. *EMBO J.* 17:353-362.

Zufall, F. and S. Firestein. 1993. Divalent cations block the cyclic nucleotide-gated channels of olfactory receptor neurons. *J. Neurophys.* 69:1758-1768.

Zufall, F., H. Hatt, and S. Firestein. 1993. Rapid application and removal of second messengers to cyclic nucleotide-gated channels from olfactory epithelium. *Proc. Natl. Acad. Sci. USA.* 90:9335-9339.

Zufall, F., S. Firestein and G.M. Shepherd. 1994. Cyclic nucleotide-gated ion channels and sensory transduction in olfactory receptor neurons. *Annu. Rev. Biophys. Biomol. Struct.* 23:577-607.

Zufall, F. and T. Leinders-Zufall. 1997. Identification of a long-lasting form of odor adaptation that depends on the carbon monoxide/cGMP second messenger system. *J. Neurosci.* 17:2703-2712.